V.I. Il`icev Pacific Oceanological Institute
Far East Branch, Academy of Sciences of Russia
Vladivostok, Russian Federation

Acoustic & Hydrographic Studies on the North East Sakhalin Shelf 3 July to 15 September, 2007 Sakhalin, Russian Federation

S.V. Borisov
A.V. Gritsenko
D.G. Kovzel
R.A Korotchenko
M.V. Kruglov
A.N. Rutenko
A.A. Solovyev
V.A. Sosnin
V.G. Ushipovsky
F.F. Khrapchenkov

Prepared for

Exxon Neftegas Limited
&
Sakhalin Energy Investment Company,

Yuzhno-Sakhalinsk, Sakhalin,
Russian Federation

March 2008

V.I. Il`icev Pacific Oceanological Institute
Far East Branch, Academy of Sciences of Russia
Vladivostok, Russian Federation

'Approved'
POI FEB RAS Director
Academic V.A. Akulichev

_____
Date: _____2007

Acoustic & Hydrographic Studies on the North East Sakhalin Shelf 3 July to 15 September, 2007 Sakhalin, Russian Federation

S.V. Borisov
A.V. Gritsenko
D.G. Kovzel
R.A. Korotchenko
M.V. Kruglov
A.N. Rutenko
A.A. Solovyev
V.A. Sosnin
V.G. Ushipovsky
F.F. Khrapchenkov

Prepared for
Exxon Neftegas Limited
&
Sakhalin Energy Investment Company,

Yuzhno-Sakhalinsk, Sakhalin,
Russian Federation

March 2008

V.I. Il`icev Pacific Oceanological Institute
Far East Branch, Academy of Sciences of Russia
Vladivostok, Russian Federation

'Approved'
POI FEB RAS Director
Academic V.A. Akulichev

Date: 09.04.2008

Acoustic & Hydrographic Studies on the North East Sakhalin Shelf 22 June to 15 September, 2007 Sakhalin, Russian Federation

S.V. Borisov
A.V. Gritsenko
D.G. Kovzel
R.A. Korotchenko
M.V. Kruglov
A.N. Rutenko
A.A. Solovyev
V.A. Sosnin
V.G. Ushipovsky
F.F. Khrapchenkov

Prepared for
Exxon Neftegas Limited
&
Sakhalin Energy Investment Company,

Yuzhno-Sakhalinsk, Sakhalin,
Russian Federation

March, 2008

Table of Contents

LIST OF TABLES

LIST OF FIGURES

Executive Summary

In 2007 the Pacific Oceanological Institute (POI) deployed 22 Autonomous Underwater Acoustic Recorders (AUARs), four analog and two digital sonobuoys, low-frequency (LF) resonant electromagnetic acoustic and seismo-acoustic sources, and high-frequency (HF) broadband piezoelectric sources. The Mollusk-07 vertical autonomous acoustic and hydrologic recording array, developed by POI, was used for the first time. The goal of the program was to measure key acoustic and hydrologic data, and to estimate sound propagation to the Korean-Okhotsk gray whale (*Eschrichtius robustus*)[1] feeding areas.

The 2007 acoustic program measured anthropogenic and ambient noise levels, conducted bathymetric and hydrologic surveys and made Transmission Loss (TL) measurements along profiles from the proposed facilities locations to the edges of the Piltun and offshore feeding areas. LF TL studies from the Odoptu-FSP out to sea were also conducted. These TL measurements will be used to calibrate acoustic models that, in conjunction with the recorded spectra of noise sources will be used to predict the sound levels received in the gray whale feeding areas. The model predictions of the acoustic footprint will be used to plan construction and development operations and will aid in determining the appropriate mitigation measures to be applied. These measurements showed that for profiles extending from deep water to shallow water the bathymetry and velocity field significantly affects the received acoustic field. The spatial and temporal parameters of the sound velocity field vary significantly over the summer-fall season and under the influence of wind. For long shallow profiles, such as those parallel to the coast, reflections from the bottom and sea surface have a greater impact than the sound velocity field on acoustic propagation.

Three full-scale hydrological surveys and 15 individual transects were acquired in 2007, both parallel and perpendicular to the shore. During work on the TL profiles 183 vertical hydrologic profiles were conducted. During storms, the *Professor Bogorov* sheltered beyond the northern tip of the island and six more transects were performed in Severny and Sakhalin bays, daily hydrology observations were also made while at anchor in Severny Bay. A total of 634 hydrology measurements were made. A station with two (POI) Potok autonomous current and water temperature recorders was deployed in the offshore feeding

[1] The Korean Okhotsk (western) gray whale population is listed as endangered in the Russian Red Book and critically endangered by the International Union for the Conservation of Nature (IUCN).

area in 43 m of water, and was operational from 23 July to 5 September. The Mollusk-07 vertical autonomous acoustic and hydrologic recording array and an autonomous 320 Hz CW transducer were used to acquire substantial data on the characteristics of the internal waves typical of the summer hydrologic conditions in the region, and their effect on low frequency TL. Seven thousand two hundred (7,200) km of bathymetry data was acquired in 2007; this data was used to build a bathymetric map of the area and to study the spatial and temporal variation of hydro-physical parameters under the influence of winds, tides and storms. The relationship between benthos development and the hydrology of the area was also analyzed.

1 Introduction

The shallow water (6 - 15 m) part of the NE Sakhalin shelf, starting south of the mouth of Piltun Bay and extending northwards up the Sakhalin coast, is the most important known summer and fall feeding area for Korean-Okhotsk (western) gray whales. Mother-calf pairs have been seen in water depths of less than 10 m in the Piltun feeding area. Acoustic studies have been conducted in the area since 1999 since some of the planned oil and gas developments are near the Piltun feeding area. In 2001 a second gray whale feeding area (the offshore feeding area) was discovered in deeper water (30-60 m), approximately 20 km South East of the mouth of Chayvo Bay.

The acoustic program conducted on the NE shelf of Sakhalin Island in 2007 had two distinct components which were conducted simultaneously for much of the field season. These components were:

- A real-time acoustic monitoring program designed to monitor the anthropogenic sound levels at the eastern edge of the Piltun feeding area during construction operations near the PA-B platform (topsides installation and pipeline tie-in).
- An extension to the long-term acoustic monitoring program initiated in 2003. This acoustic program was designed to study temporal and spatial variations in the amplitude and frequency characteristics of ambient and anthropogenic sound at the edges of the Piltun and offshore gray whale feeding areas. In addition to the program monitoring the background acoustic environment, detailed studies of sound propagation characteristics and Transmission Loss (TL) were conducted between current and proposed ENL and SEIC facilities, both onshore and offshore, and defined locations at the edge of the gray whale feeding areas. In conjunction with these measurements a comprehensive grid of bathymetric and hydrologic data was acquired across the study area. This data was also used to investigate the spatial and temporal variations in the hydrology due to weather events (e.g. typhoons). Two joint studies were initiated in 2005 in conjunction with the behavioral and benthic teams; these studies were continued in 2007. The first study analyzed the data recorded near the behavioral monitoring stations; the spectral density of the data in the frequency range from 20 Hz to 20 kHz was analyzed in 1-minute windows and converted to one octave bands. The second, conducted jointly with the benthic team, investigated the relationship between the distribution of benthos and the bathymetry and hydrology of the study area [Fadeev 2007].

This report describes the objectives of the 2007 program, the operational (including real time acoustic data acquisition) strategy and methodology; the equipment used during the 2007 field season (both new and upgraded [Borisov et. al. 2006]), its testing and calibration as well as the data processing and analysis methodology. This report also includes a listing of the data acquired during the 2007 field season and a DVD containing the sonograms in

24-hour segments for all the acoustic data recorded in 2007 as well as the bathymetric and hydrologic data acquired during the 2004 to 2007 field seasons.

This report is mainly dedicated to analysis of the data, and includes conclusions and recommendations for future work. This data analysis includes the following components:

Acoustic Monitoring

1. An analysis of the acoustic monitoring data recorded at four stations during the 2007 construction operations and correlation of the acoustic data with construction operations.

Western gray whale research program – Acoustic studies

2. Quantitative spectral analysis of the variation in the ambient acoustic noise level with weather conditions (including cyclones).
3. The results of experiments designed to study the sound propagation characteristics and spectral TL (over the frequency range from 15 Hz to 15 kHz) along profiles between the major current and future facilities and defined locations at the edge of the gray whale feeding areas.
4. A temporal, spectral and spectral-temporal analysis of the acoustic data recorded at different locations on the Sakhalin shelf[2].
5. A temporal analysis of the variation of the spectral density (one-third octave bands) of acoustic data recorded inside and at the edge of the Piltun feeding area for correlation with behavioral monitoring data.
6. Analysis of the hydrologic data (sound velocity, temperature, and salinity) recorded between 2004 and 2007.
7. An experimental study of the relationship between the distribution of benthos and the hydrology and bathymetry of the study area, conducted jointly with the benthic team, [Fadeev 2007].

The acoustic measurements were conducted using 16 digital Autonomous Underwater Acoustic Recorders (AUARs) developed at POI FEB RAS[3] (POI) (Figure 1.1), five of these AUARs were Telemetry-AUARs (T-AUARs) having an additional radio-telemetry channel (Figure 1.2)[4]. Six smaller mini-AUARs with reduced (72 hours) endurance were used for TL and source level measurements (Figure 1.3). The AUARs were designed to accurately

[2] The use of Autonomous Underwater Acoustic recorders (AUARs) for the 2007 program allowed an unprecedented characterization of the ambient sound levels at the Sakhalin monitoring stations. However, since the vessels used to house the scientists (*Professor Bogorov and Academik Oparin*) were often a significant distance from the AUAR the identification and specific location of any transient anthropogenic sound source is generally unknown.
[3] POI FEB RAS – V.I Il`ichev Pacific Oceanological Institute, Far East Branch of the Russian Academy of Sciences.
[4] The T-AUARs were equipped with a radio channel and were capable of simultaneously recording data on the AUAR hard drive and transmitting data (bandwidth 10 Hz to 5 kHz) to a receiving radio station. The transmission can be continuous or on a pre-programmed schedule.

record frequencies between 1-15,000 Hz and enable accurate, synchronous acoustic measurements over a broad range of frequencies (including infrasounds[5]).

Figure 1.1 – Autonomous Underwater acoustic recorder (AUAR).

[5] Infrasounds are sounds with a frequency of less than 20 Hz.

Figure 1.2 – T-AUAR being prepared for deployment (note the radio transmission unit connected by cable to the AUAR container).

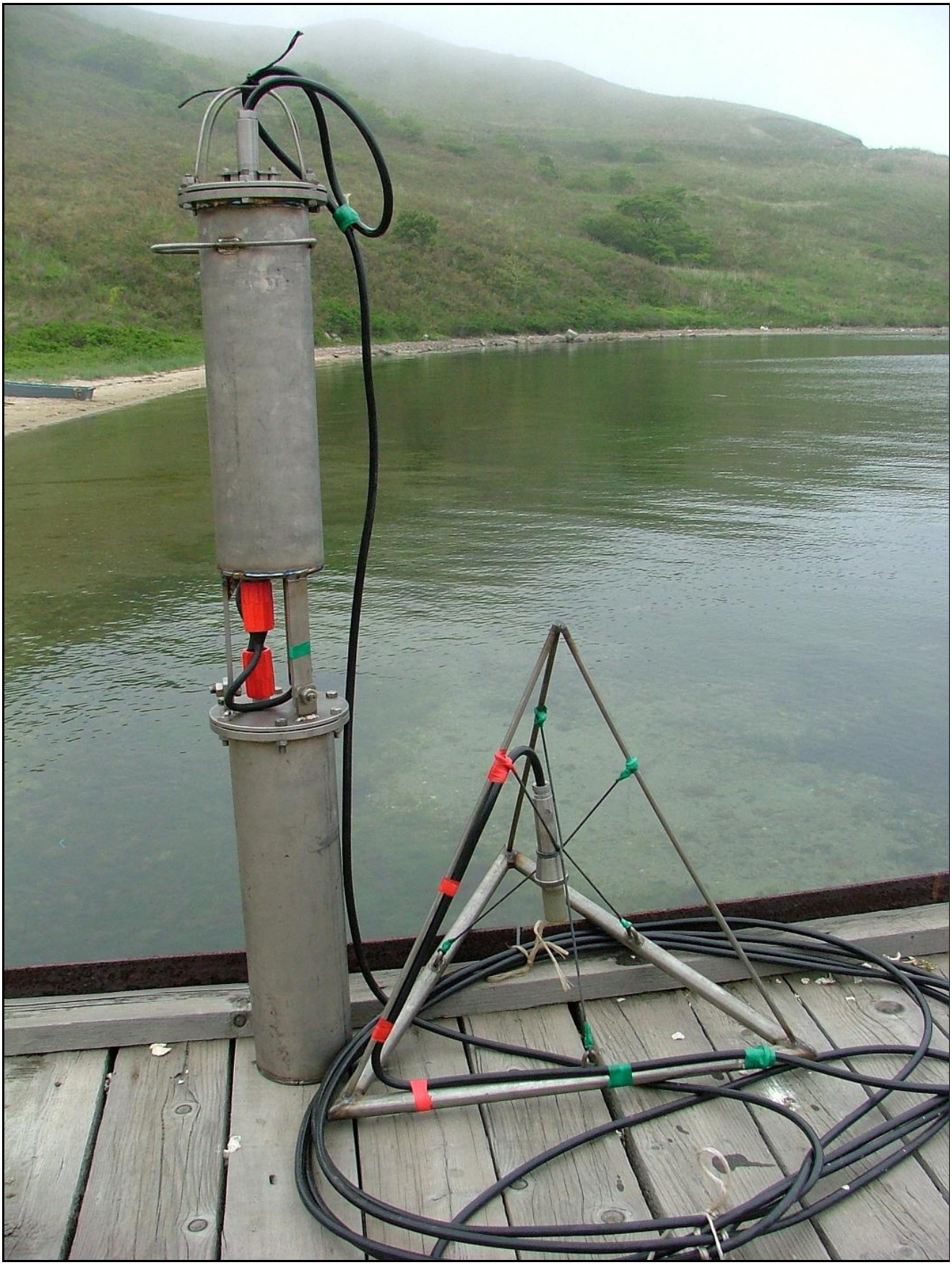

Figure 1.3 – Mini-AUAR used for short-term source or TL measurements.

In addition, two digital and four analog acoustic sonobuoys, also developed at POI, were used during the 2007 field season to measure acoustic signals and to transmit them to a receiving station in real time. The analog sonobuoys (Figure 1.4) were used to record frequencies from 10 Hz to 10 kHz and the digital sonobuoys from 1 Hz to 2.6 kHz. When used together an analog and digital sonobuoy pair can record acoustic data from 1 Hz to 10 kHz[6]. A detailed description of this equipment was given in [Borisov et. al. 2006]. In addition, the Mollusk-07 autonomous vertical acoustic and hydrologic recorder was used in the field for the first time in 2007. This system was specially developed at POI for stationary measurements in a 31.5 m water layer of the vertical structure (eight depths) of the acoustic field in the frequency range from 10 Hz to 5 kHz, and of the temperature field (resolution 0.006°C). The data from the Mollusk-07 can be used to evaluate the accuracy of experimental TL estimates which can vary due to refraction and scattering on three-dimensional inhomogeneities in the sound velocity field at the thermocline generated by internal waves. Figure 1.5 shows the major components of the Mollusk-07.

The radio signals from the analog and digital sonobuoys and the T-AUARs were received either at a recording station at Piltun lighthouse (Figure 1.6) or the Odoptu-07 onshore camp as well as the vessel *Professor Bogorov*. The range of the digital radio channel was over 5 km when received by the non-directional antenna at the Odoptu-07 camp and over 7 km when received at Piltun Lighthouse. The reception range of the analog radio channel depended on the frequency range of the transmitted data. Broadband (10-10,000 Hz) signals could be transmitted up to 12 km; narrowband (10-5000 Hz) signals could be transmitted more than 20 km if received by the station at Piltun lighthouse.

During the 2007 field season (22 June to 15 September), AUARs and sonobuoys were deployed from the research vessel *Professor Bogorov* (Figure 1.7). Synchronous acoustic measurements were made at stations ranging from north of the Odoptu license area to the southern edge of the offshore feeding area (Figure 1.8), an area whose western edge extends 180 km along the NE Sakhalin shelf.

[6] In 2007 a bandwidth of 10 Hz to 5 kHz was used to improve reception reliability.

Figure 1.4 – Digital sonobuoy (DSB); the container and hydrophone are standardized for analog (ASB) or digital (DSB) sonobuoys.

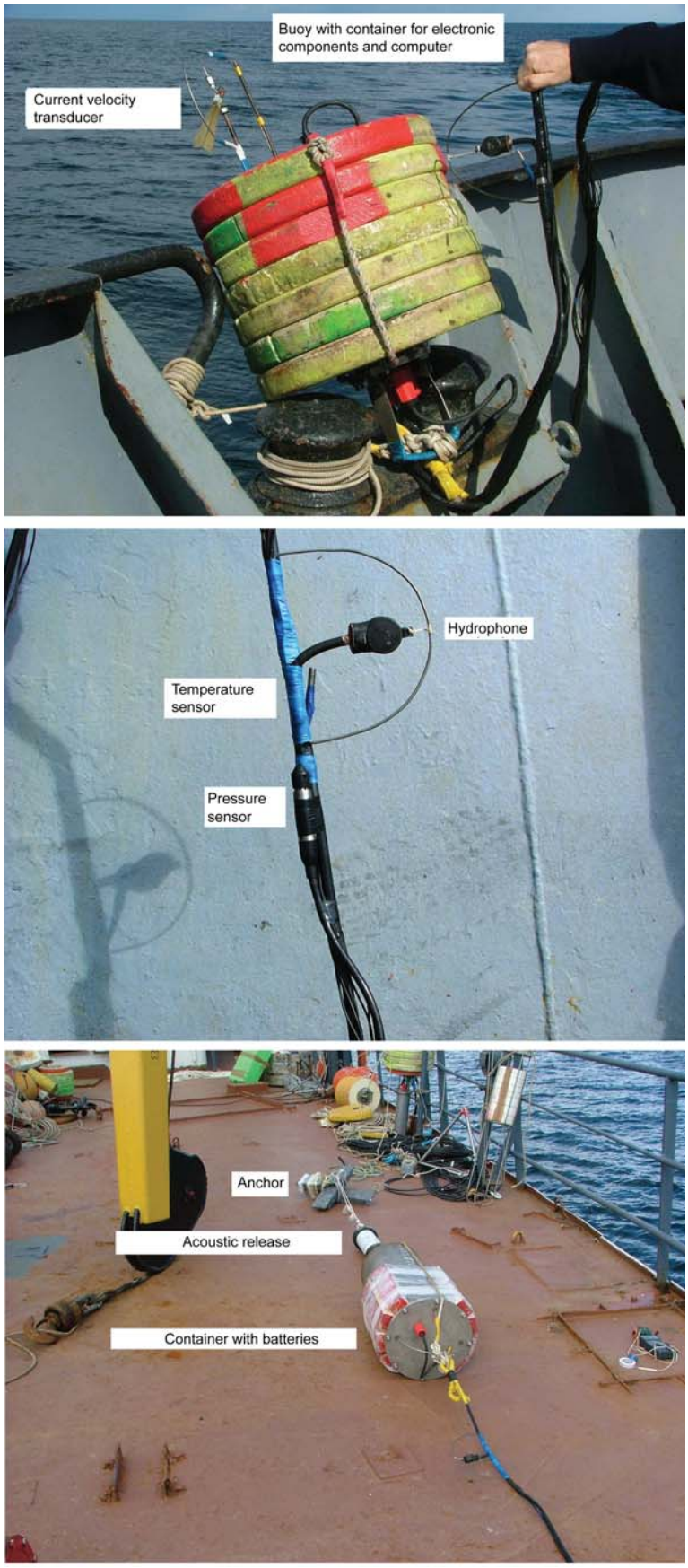

Figure 1.5 – Mollusk-07 autonomous vertical acoustic and hydrologic recording array.

Figure 1.6 – Top: Directional and whip antennas on the top of Piltun lighthouse; Bottom: radio-telemetry receiving station also at the top of Piltun lighthouse.

Figure 1.7 - The research vessel *Professor Bogorov*.

Previous work has shown that the results from acoustic modeling are very sensitive to the hydrologic, bathymetric and elastic properties of the sea bottom along the profile of interest. A comprehensive suite of bathymetric and hydrologic measurements were therefore acquired using the sonar on the *Professor Bogorov* and a hydrologic sonde. During the expedition 634 vertical hydrologic profiles[7] (comprising sound velocity, temperature and salinity), and approximately 7,200 km of bathymetry data were acquired by the *Professor Bogorov*. Figure 1.9 includes two maps showing the extent of the bathymetric grid and the points at which vertical hydrologic profiles were acquired. This plot shows the combined 2004 (323 vertical hydrologic profiles and 8,400 km of bathymetry data), 2005 (354 profiles and 7,788 km), 2006 (372 profiles and 12,147 km) and 2007 data.

[7] Of the 634 vertical hydrologic profiles acquired in 2007, 238 were acquired in July, 329 in August and 67 in September.

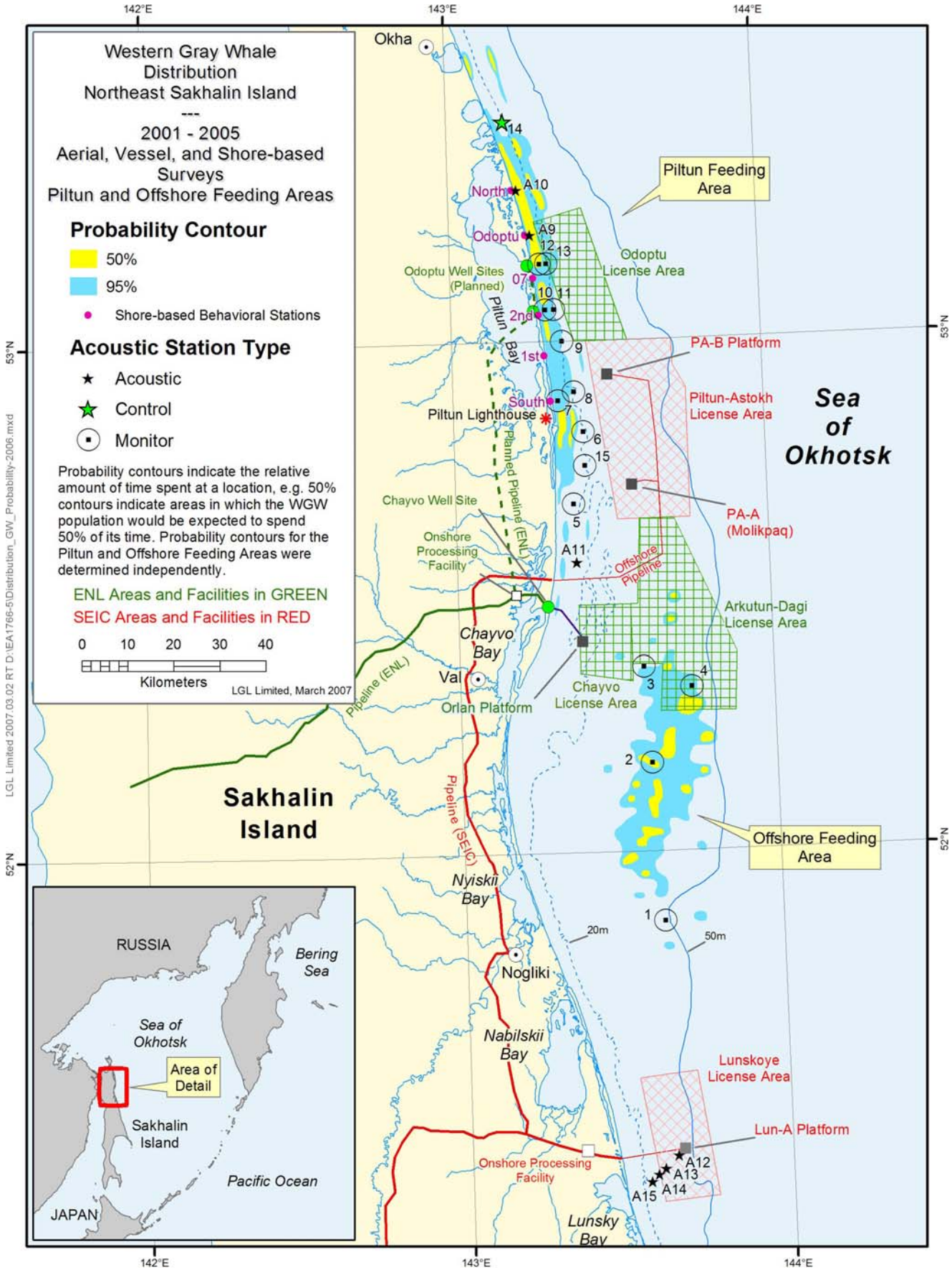

Figure 1.8 - Map of the NE Sakhalin Shelf showing the locations of the LUN-A, Molikpaq, Orlan and PA-B platforms as well as the AUAR deployment locations.

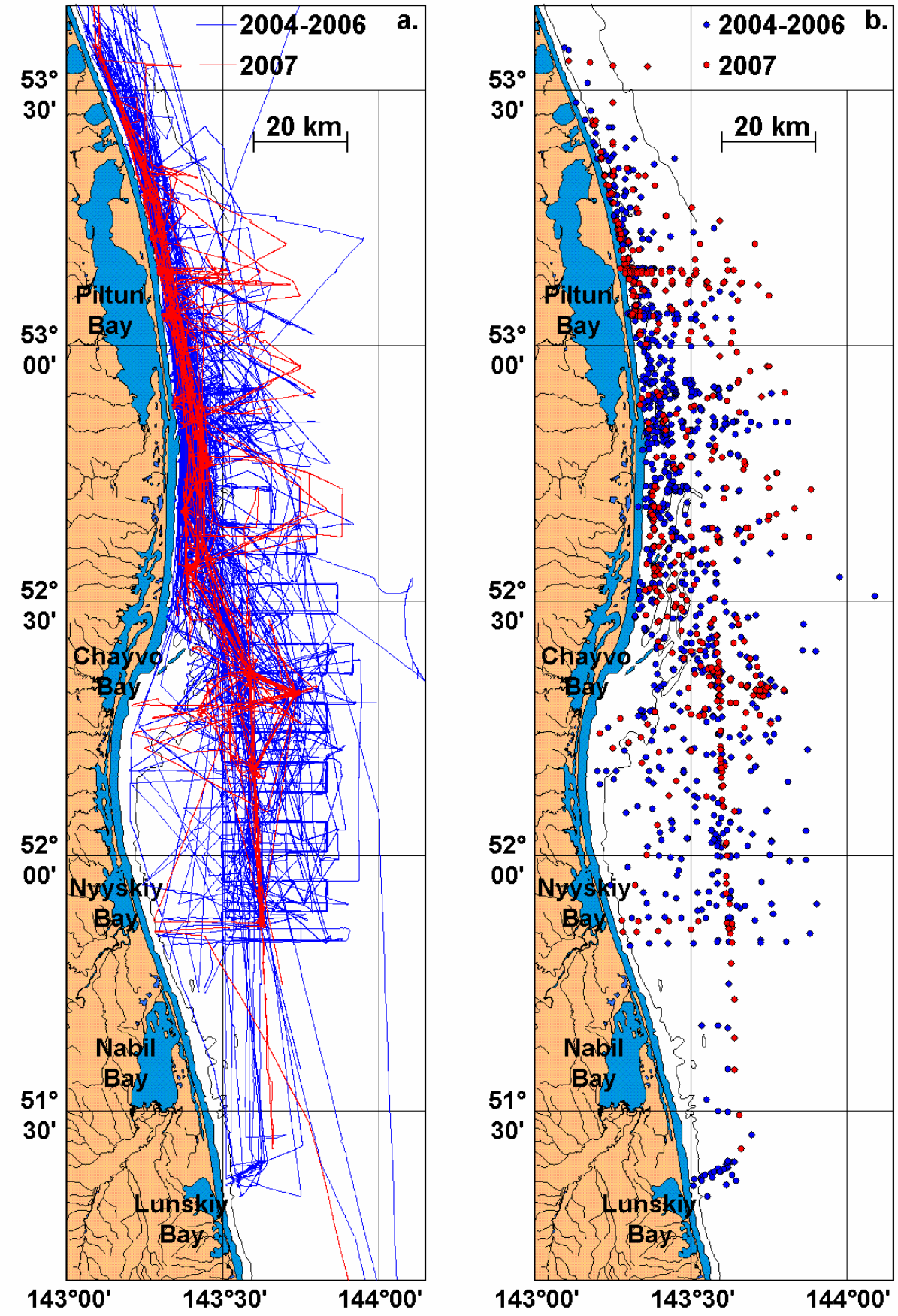

Figure 1.9 - Map of the NE Sakhalin Shelf showing (a) the 2004 to 2007 bathymetric grids and (b) the locations where vertical hydrologic profiles were acquired in 2004 to 2007.

1.1 Objectives of the acoustic program

The acoustic program conducted on the NE shelf of Sakhalin Island in 2006 had seven main objectives:

1. The first was monitor sound propagating from construction operations and engineering work associated with the PA-B platform. This real-time monitoring was designed to allow the construction operations to be conducted so as to minimize the impact on the western gray whale population.
2. The second objective was to study both temporal and spatial variations in the amplitude and frequency characteristics of ambient and anthropogenic sound at a series of monitoring stations located throughout the development area. These monitoring stations were positioned to be at the nearest outside edge of a gray whale feeding area to a proposed facility. The goal of this annual acoustic monitoring program is to estimate any change in the acoustic levels in the gray whale feeding areas due to the oil development and production activities.
3. The third objective was to study sound propagation and the variation in frequency dependent TL along a series of TL profiles from current or proposed facilities and pipelines to the nearest gray whale feeding area. The results of these TL studies can be used to predict the potential acoustic footprint from a facility with a defined acoustic signature, installed at the proposed location.
4. The fourth objective was to acquire a comprehensive grid of bathymetric and hydrologic data across the study area, and to investigate the spatial and temporal variations in the hydrology due to weather events (e.g. typhoons). This data will be integrated with the 677 vertical hydrologic profiles and 16,188 km of bathymetry data acquired between 2004 & 2006.
5. The sixth objective was to estimate the one-third octave spectral density over the frequency range from 20 Hz to 15 kHz in 1 minute windows for all the monitoring AUARs in the Piltun feeding area.
6. The final objective was to study the relationship between the distribution and development of benthos and the hydrology and bathymetry of the study area [Fadeev, 2007].

1.2 Operational strategy and methodology

The shallow water (5 - 15 m) part of the NE Sakhalin shelf starting south of the mouth of Piltun Bay and extending northwards up the Sakhalin coast is one of the most important summer feeding areas for western gray whales. For this reason acoustic studies have been conducted in the area since 1999.

In 2007, as in the previous three years, the main acoustic program was operated from a vessel and was led by Dr. Alexander Rutenko; the vessel used in 2007 was the *Professor*

Bogorov. The plan was that the acoustics program would be operated from the *Professor Bogorov* and the vessel-based biology programs (Photo-ID, benthic, MMO) from the *Academik Oparin* with Dr. Yuri Yakovlev as the expedition leader for the biology expedition on the *Academik Oparin*.

In 2007 16 AUARs designed and developed by POI were used to capitalize on the enhanced flexibility of a vessel-based program and to allow synchronous acoustic measurements to be conducted over a greatly enlarged spatial area. Fourteen (14) of these AUARs could be deployed at depths up to 50 m (two to 100 m), could record continuously for greater than 18 days and could measure the absolute acoustic amplitude of a signal over a frequency band from 1-15000 Hz. The expedition also had 6 mini-AUARs with similar recording characteristics, but only three days recording duration. A detailed description of this equipment was given in [Borisov et. al. 2006]. The Mollusk-07 vertical autonomous acoustic and hydrologic recording array was used for the first time in 2007. This equipment was developed by POI for experimental studies of the modal composition of internal waves and low-frequency sound propagating in offshore areas. The Mollusk-07 can make stationary synchronous measurements in a 31.5 m water layer of the vertical structure (eight depths) of the acoustic field in the frequency range from 10 Hz to 5 kHz, and of the temperature field (resolution 0.006 °C). Two pressure sensors are used to confirm the depth of the upper and middle hydrophones. The Mollusk-07 is designed to be deployed in water depths up to 100 m, using an anchor with an acoustic release. An onboard computer allows program control of the data acquisition and storage schedules. The system can operate autonomously for at least 7 days.

One of the operational advantages of the *Professor Bogorov* is that it can operate in water depths as shallow as 10 m. The AUARs were deployed from the stern of the *Professor Bogorov* as the vessel sailed slowly along its course (Figure 1.10). AUARs were retrieved manually using a zodiac deployed from the *Professor Bogorov*. After each AUAR was pulled to the surface it was towed to the vessel by a zodiac (Figure 1.11) and transferred to the *Professor Bogorov* using its crane (Figure 1.12).

Figure 1.10 - Deployment of an AUAR from the stern of the *Professor Bogorov.*

Figure 1.11 – Retrieval of the AUAR using a Zodiac, and towing it to the stern crane of the *Professor Bogorov.*

Figure 1.12 – Transferring an AUAR from a Zodiac to the *Professor Bogorov.*

1.3 Ambient noise studies and Western gray whale core areas[8]

One of the key goals of the acoustic studies in the western gray whale research program is to measure and characterize the ambient noise field on the NE Sakhalin shelf. This long-term program commenced in 2003, and is currently ongoing. These data, in conjunction with the measurement of the acoustic signature of present and future facilities will allow the cumulative effect of oil development and production operations on the acoustic background in the area, as well as on the gray whale population, to be more effectively estimated.

In order to strategically plan the location of the monitoring stations for the 2003 to 2006 and future programs it was critical to estimate the core areas for the gray whales on the NE Sakhalin shelf. In 2003 the core areas were estimated and the acoustic monitoring locations selected using the sightings from all of the 2001 and 2002 aerial surveys [Borisov et. al. 2004], however in 2001 many more aerial surveys were acquired and they were concentrated in a reduced seasonal range. Further, no correction was made for survey effort. For 2004 the core areas were determined using whale densities estimated from the 2003 and 2004 aerial survey data taking the survey effort into account[9].

In these analyses, probability contours are used to visualize areas with the greatest likelihood of encountering gray whales, and to examine shifts in the 'centers of activity' of gray whales over time[10]. Cumulative probability contours of 50% and 95% were generated to visualize the distribution of gray whales. The 50% contour represents the area within which 50% of the whales sighted are expected to be found. In 2003 the probability contours were estimated using a conventional kernel density method[11]. This kernel density method employed a square-gridding process, which is robust for small sample sizes unless the variances of the north-south and east-west components of the distribution are very different, which is the case for the Piltun feeding area.

---

[8] This section is based on work performed by LGL Limited (Robin Tamasi, Peter Wainwright, Judy Muir, Sergei Yazvenko, Sonya Meier, and Steve Johnson).

[9] Density is the number of whales per unit area; multiple surveys over a grid cell result in larger densities within that cell if densities are not compensated for survey effort and average densities computed.

[10] Cumulative probability contours were computed independently for the Piltun and offshore feeding areas.

[11] The kernel density contours were mapped using the ArcView© 3.1 extension Animal Movement 2.04 [Hooge et. al., 1997]. Kernel density contours are an estimator that assesses an animal's probability of occurrence at each point in space based on a utilization distribution.

For the Piltun feeding area the distribution of whale sightings is oriented parallel to the coast with significantly greater variance in the along-shore direction than in the perpendicular-to-shore direction. For this reason, in 2004, a spatial grid was constructed for the Piltun feeding area that was oriented along-shore and with an along-shore grid cell dimension greater than the perpendicular-to-shore dimension, (i.e. each cell was 4 km by 0.5 km). Density was then computed for each cell as the number of observed whales divided by the cumulative area surveyed within the cell. The same methodology was employed for the offshore feeding area except that, in this case, the conventional assumptions about distribution were satisfied and a spatial grid of 1 km by 1 km cells was employed.

There was significant variation among the 2003, 2004, 2005 and 2006 estimates of the western gray whale core areas. Consequently, this analysis was updated in 2007 using all available systematic survey data. These included data from the 2001 to 2005 aerial surveys, 2002 to 2006 vessel-based surveys, 2001 to 2006 shore-based behavior scan surveys, and the 2004 to 2006 shore-based vehicle scan surveys. Appendix C gives details of this analysis.

1.3.1 Monitor, control and acoustic station locations

A systematic acoustic monitoring framework was developed in 2003 and extended from 2004 to 2006. The goal is to monitor changes in the acoustic field on the NE Sakhalin shelf and most importantly those changes in the anthropogenic sound level that could cause a significant increase in the Received Level (RL) in either the Piltun or offshore feeding areas.

Three types of stations for recording acoustic data were designated:

- **Monitor stations** - These are locations that will be systematically monitored to gain an understanding of the changes in the acoustic field over time. They will be reoccupied multiple times in a season and over multiple seasons. The monitor stations will generally be located at the edge of a gray whale feeding area nearest to a proposed facility or in a location where the greatest cumulative impact from multiple facilities could be expected.
- **Control station(s)** - Dr. John Richardson (LGL Limited) recommended that a control station or stations be set up far enough away from the proposed development operations that the anthropogenic acoustic field would not be expected to increase. This station would reflect any changes to the ambient noise field unrelated to the oil development activities.
- **Acoustic stations** - These locations will be infrequently monitored; their purpose is to gain an understanding of the anthropogenic sound field from a known location at a specific time related to development activities or to conduct TL experiments.

Eleven stations were designated prior to the start of the 2003 field season; seven were monitor stations, three were acoustic stations and one was a control station. For the 2004 season a further six monitor stations and seven acoustic stations were designated. In 2005 one additional acoustic station was designated. In 2006 one additional monitor station and four acoustic stations were designated. No new stations were designated in 2007. Table 1.1 gives the names, numbers and locations of these stations[12].

The locations of the monitor stations were determined with reference to the major gray whale concentrations in the area (Figure 1.13)[13]. For the offshore feeding area, the locations of the stations (except the OFA station) were chosen to be on the 95% probability contour at the point closest to a current or proposed facility. The location of the monitor stations remained constant between 2004 and 2007[14]. The western gray whale distribution in the Piltun feeding area varies with bathymetry, with most whales feeding in water depths between ~8-12 m. Mother-calf pairs have been seen in the Piltun feeding area, often in water depths of 5-10 m, and fewer whales have been seen outside the 20 m contour. Thus, the two key acoustic monitoring points are the 20 m and the 10 m bathymetry contour (regarded as the edge and center of the whale distribution).

The control station location has remained the same since 2003[15]. This location has a similar hydrology and bathymetric character to the Piltun feeding area, is far enough away to serve as an acoustic control point, but close enough for effective operational support. Stations A1 to A8 and A12 to A15 were not occupied in 2007. All the unused acoustic stations were previously used for TL experiments.

---

[12] Where possible in order to facilitate long term monitoring the numbers and names of the monitor stations will be maintained year to year.

[13] Various vessel-based (MMO, Photo-ID, Benthic) and land based (vehicle surveys, behavioral) biology programs were being conducted over the same seasonal range, so an evaluation of the effect of any changes in the acoustic field on the behavior or distribution of gray whales could be evaluated.

[14] 2004: The Orlan station is on the 95% cumulative probability contour (from 2003) closest to the proposed location of the Orlan platform, the Lunskoye station is at the southern edge of the offshore feeding area, the OFA (Offshore Feeding Area) station is approximately in the center of the offshore feeding area and the Arkutun-Dagi station is at the North Eastern edge of the offshore feeding area. 2005: The Odoptu-S-10, Odoptu-N-10, Odoptu-N-10 and Odoptu-S-10 stations were at the 10 m and 20 m bathymetry contours off the coast from the two proposed Odoptu well pads. The Piltun station is at the 20 m bathymetry contour between the Molikpaq platform and the major gray whale concentration off Piltun lighthouse. The PA-B stations were at the 10 m (PA-B-10) and 20 m (PA-B-20) bathymetry contours closest to the proposed PA-B location. The Piltun-S station is on the 95% cumulative probability contour at the southern bathymetry contour of the Piltun feeding area and the Odoptu-PA-B station at the 20 m bathymetry contour between the proposed locations of the Odoptu-S well pad and the PA-B platform. 2006: The Molikpaq station is at the 20 m bathymetry contour between the Molikpaq platform and the major gray whale concentration off Piltun lighthouse.

[15] The control station was located on the 20 m bathymetry contour approximately 40 km north of the Odoptu North pad site.

Table 1.1 - Numbers, names, locations and depths of the acoustic, monitoring and control stations.

#	Station		Latitude	Longitude	Depth
Monitor Stations:					
1	Lunskoye	Лунское	51° 51' 45" N	143° 37' 27.3" E	50 m
2	OFA (Offshore Feeding area)	ГЗК (Глубоководная зона кормления)	52° 10' 18" N	143° 36' 1.8" E	~40 m
3	Orlan	Орлан	52° 21.6' N	143° 35.0' E	32 m
4	Arkutun-Dagi	Аркутун-Даги	52° 19' 9.6" N	143° 44' 4.6" E	~40 m
5	Piltun-S	Пильтун-Ю	52° 40' 51" N	143° 22' 34" E	10 m
6	Piltun	Пильтун	52° 49.3' N	143° 24.9' E	20 m
7	PA-B-10	ПА-Б-10	52° 53' 2.1" N	143° 20' 10.6" E	10 m
8	PA-B-20	ПА-Б-20	52° 54' 00" N	143° 23' 20.5" E	20 m
9	Odoptu-PA-B	Одопту-ПА-Б	53° 00' 00" N	143° 21' 18" E	20 m
10	Odoptu-S-10	Одопту-Ю-10	53° 03.7' N	143° 18.3' E	10 m
11	Odoptu-S-20	Одопту-Ю-20	53° 03' 42" N	143° 19' 58" E	20 m
12	Odoptu-N-10	Одопту-С-10	53° 09.1' N	143° 17.4' E	10.5 m
13	Odoptu-N-20	Одопту-С-20	53° 09' 6" N	143° 18' 42' E	20 m
14	**Control**	**Контрольная**	**53° 25' 57' N**	**143° 11' 06' E**	**20 m**
15	Molikpaq	Моликпак	52° 45' 52" N	143° 26' 38" E	24 m
Acoustic Stations:					
A1	#1 (Chayvo-1)	#1 (Чайво-1)	52° 27.8' N	143° 19.0' E	11 m
A2	#2 (Chayvo-2)	#2 (Чайво-2)	52° 25.9' N	143° 20.6' E	11 m
A3	#3 (Chayvo-3)	#3 (Чайво-3)	52° 26.8' N	143° 24.6' E	17 m
A4	#4 (Piltun-1)	#4 (Пильтун-1)	52° 43' 14.4" N	143° 22' 26.7" E	10 m
A5	#5 (Piltun-2)	#5 (Пильтун-2)	52° 43' 48" N	143° 25' 49" E	20 m
A6	#6 (Piltun-3)	#6 (Пильтун-3)	52° 49.3' N	143° 24.9' E	20 m
A7	#7 (PA-B-1)	#7 (ПА-Б-1)	52° 55' 54" N	143° 19' 39" E	10 m
A8	#8 (PA-B-2)	#8 (ПА-Б-2)	52° 55' 54" N	143° 21' 42.4" E	20 m
A9	#9 (BEH-Odoptu)	#9 (Одопту (Пов))	53° 12' 33.1" N	143° 15' 51" E	10 m
A10	#10 (BEH-north)	#10 (Пов-север)	53° 17' 52.4" N	143° 13' 25.4" E	10 m
A11	#11 (Chayvo-4)	#11 (Чайво-4)	52° 34' 00" N	143° 23' 00" E	~18 m
A12	#12 (Lunskoye-1)	#12 (Лунское-1)	51° 24' 12" N	143° 38' 30" E	47 m
A13	#13 (Lunskoye-2)	#13 (Лунское-2)	51° 22' 42" N	143° 36' 00" E	37 m
A14	#14 (Lunskoye-3)	#14 (Лунское-3)	51° 22' 00" N	143° 34' 42" E	31 m
A15	#15 (Lunskoye-4)	#15 (Лунское-4)	51° 21' 12" N	143° 33' 24" E	24 m

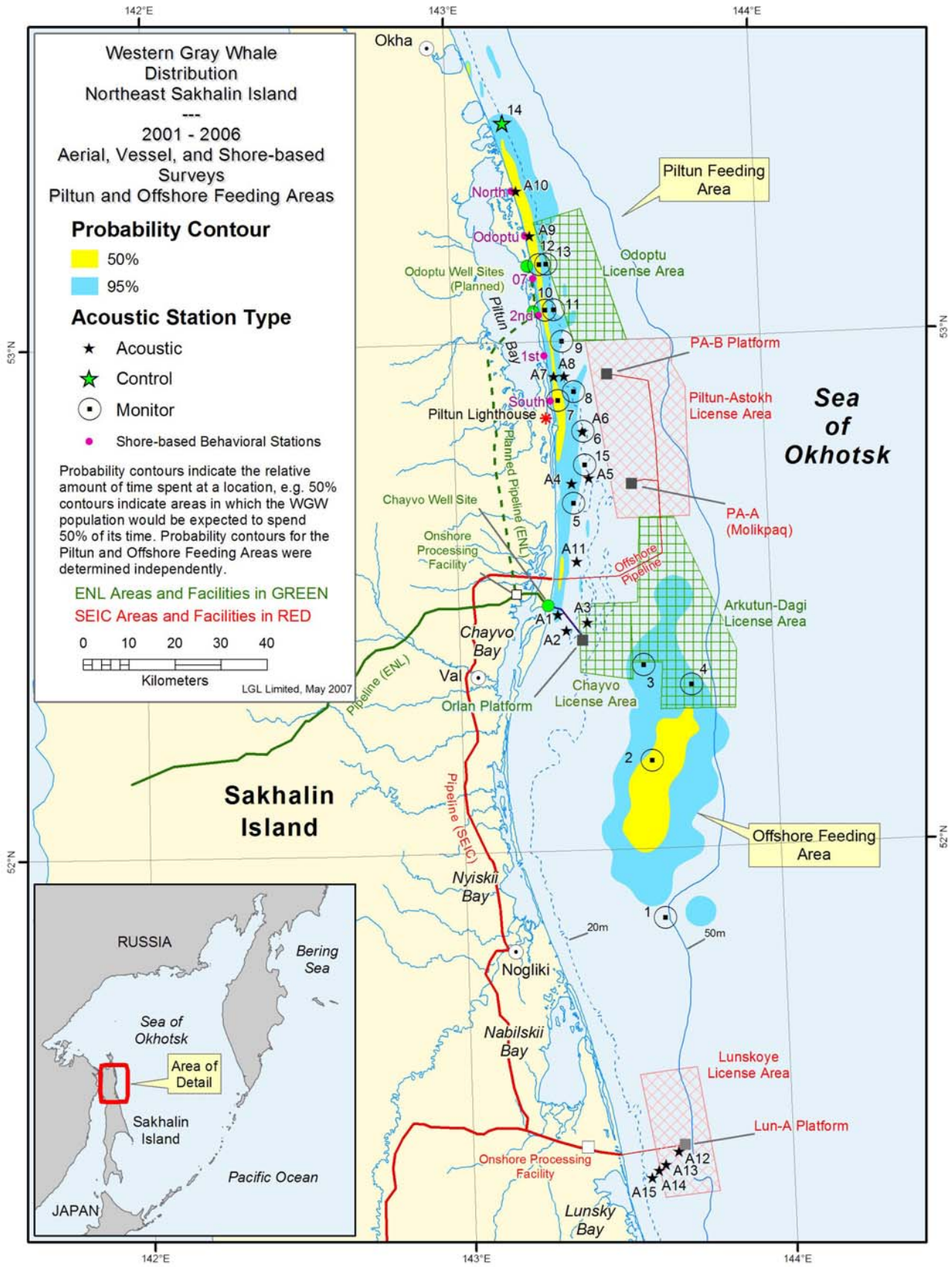

Figure 1.13 - Map showing the AUAR locations and cumulative probability contours showing the density distributions of western gray whales from the 2001 to 2005 aerial surveys, 2002 to 2006 vessel based surveys, 2001 to 2006 shore-based behavior scan surveys and the 2004 to 2006 shore-based vehicle scan surveys.

1.4 Data Recorded on the NE Sakhalin Shelf During the 2007 Field Season

During the 2007 expedition, as in 2006, AUARs were used to make synchronous acoustic measurements over a shelf area extending about 180 km from the northern boundary of the Odoptu license area to the Lunskoye platform (Figure 1.13). This section discusses the data recorded on the NE Sakhalin shelf during the 2007 field season. It describes the deployment dates, recording times, hydrophone depths and locations of the AUARs as well as their operational characteristics. Table 1.2 gives these details for the 16 AUARs used in the study.

All the acoustic data from the 2007 field program will be presented as sonograms[16], where the spectral density values *G(f,t)* are represented by different colors[17], one sonogram representing the acoustic data for one AUAR for one day. These daily sonograms also include plots of the variation in sound pressure level $D(\Delta f,t)$ with time over the annotated bandwidth. The sonograms *G(f,t)* cover a broad frequency band (2 Hz to 15 kHz) and are plotted with a logarithmic frequency axis to aid in the visual analysis of the data (e.g. Figure 1.14). The logarithmic scale on the frequency axis clearly shows the pseudo-noise signals below 15 Hz. This is flow noise caused by a tidal current with a velocity exceeding 1 m/s and is recorded twice a day. The acoustic data for the infrasonic band should therefore be analyzed during slack tide periods when flow noise is absent (approximately 4 hours). These sonograms *G(f,t)* show the variation in the spectral levels of ambient and anthropogenic sound with frequency and time due to changing meteorological conditions, vessel movements and industrial activity. All sonograms *G(f,t)* will be in absolute amplitude (dB re 1 μPa^2/Hz), all instrument and sensor corrections having been applied to the data. Appendix A shows the days on which data was acquired at each station, sonograms for all the data are available on a DVD at the back of this report.

Analysis of the acoustic data recorded by the monitor stations deployed in the offshore feeding area (Orlan, Arkutun-Dagi, OFA and Lunskoye) showed occasional strong acoustic signals from a nearby seismic vessel. These caused overloads in the high-sensitivity AUAR conditioning and recording channels, which are designed to record low amplitude signals.

[16] A sonogram is a plot showing the variation in acoustic power spectral density level with frequency and time.
[17] The scale of the sonograms varies from 37 to 120 dB re 1 μPa^2/Hz in 3 dB increments.

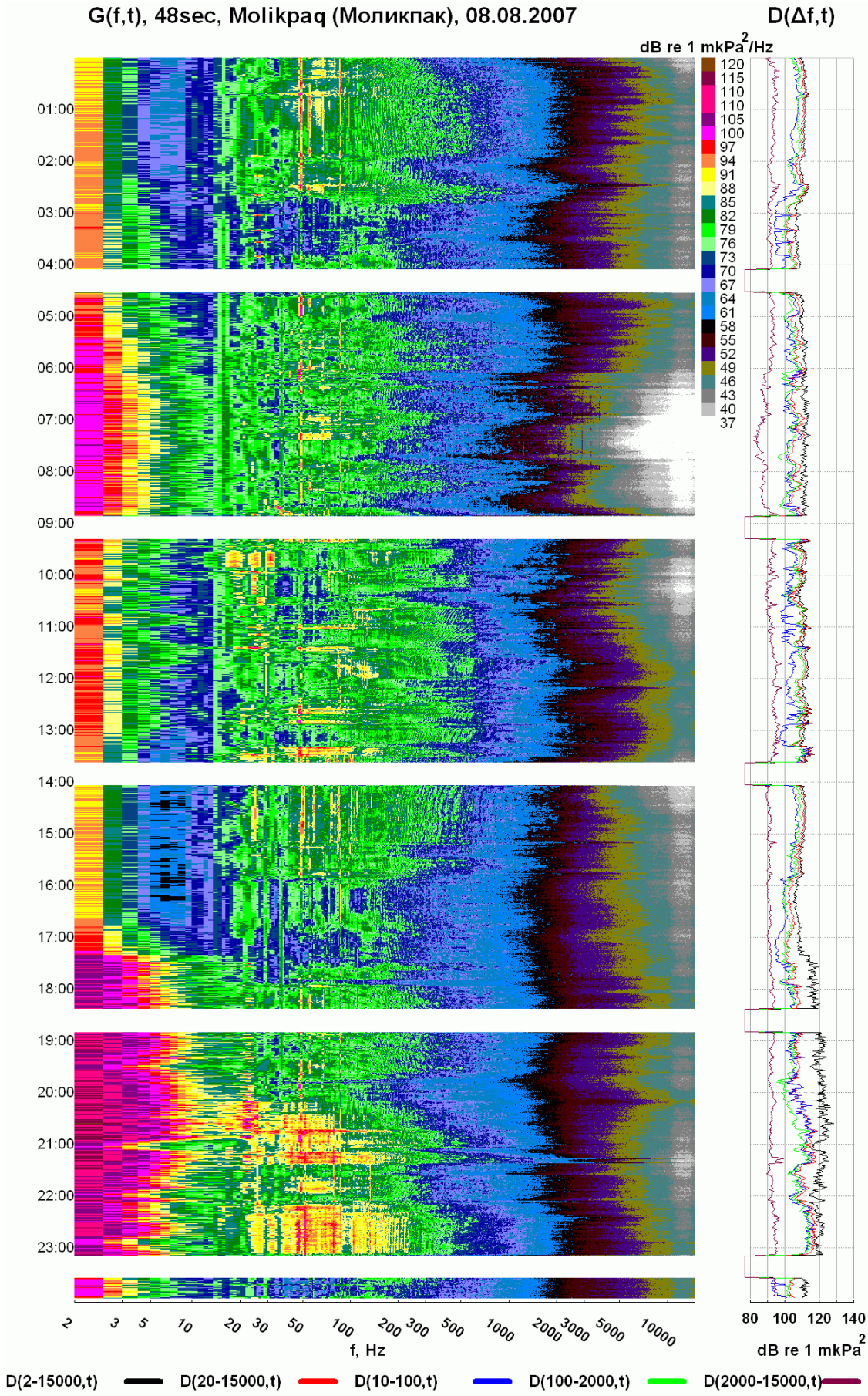

Figure 1.14 - Sonogram *G(f,t)* with plots of sound pressure level *D(Δf,t)* of acoustic energy recorded at the Molikpaq acoustic station on 8 August 2007.

Consequently the acoustic measurements for these time intervals were incorrect. These intervals clearly visible on the daily sonograms (Figure 1.15) and can therefore be disregarded during analysis.

1.5 Terminology and algorithms used in the report

Ambient and anthropogenic acoustic data recorded by an AUAR was written to the AUAR disc in a raw format and converted to microPascals (μPa)[18] after downloading to the computer on the *Professor Bogorov* (or during analysis). Acoustic spectra in decibels were used to describe the variation in acoustic power as a function of frequency. In this report sound pressure power density spectra *G(f)* ($\mu Pa^2/Hz$)[19] will be used when spectral data are plotted. The sonograms *G(f,t)* are plots of power spectral density vs. frequency and time and also include the variation in sound pressure level $D(\Delta f,t)$ (dB re 1 μPa^2) with time over the annotated bandwidth[20]. Figure 1.14 shows a sonogram; the color scales generally run from 37 to 120 dB re 1 $\mu Pa^2/Hz$ and the frequency range from 2 Hz to 15 kHz

The ***Spectral level*** of an acoustic signal relates to the level of acoustic power in a 1 Hz band. This term is only applied to sounds with continuous frequency spectra[21]. These spectra are often averaged over a number of one-second windows[22] to improve the statistical stability of the ambient noise data[23]; the number of one-second windows used in the averaging is given at the top of each plot (if the data is averaged over multiple windows).

A detailed description of the methodology used for normalizing and calculating both the amplitude and spectral data is given in Appendix F.

[18] The data was scaled (after incorporating hydrophone sensitivity, system instrument response and system gain (at 1 kHz), to convert the data to standard units of pressure (measured through an omni-directional hydrophone).
[19] Energy and power spectra are scaled to 1 Hz whatever the analysis length.
[20] Sound pressure level is the integral of the acoustic energy over the specified frequency band.
[21] A continuous frequency spectrum is a spectrum with signal present at all sampled frequencies.
[22] Average of X 1-second spectral estimates.
[23] Spectral averaging is used to obtain a lower variance spectral estimate.

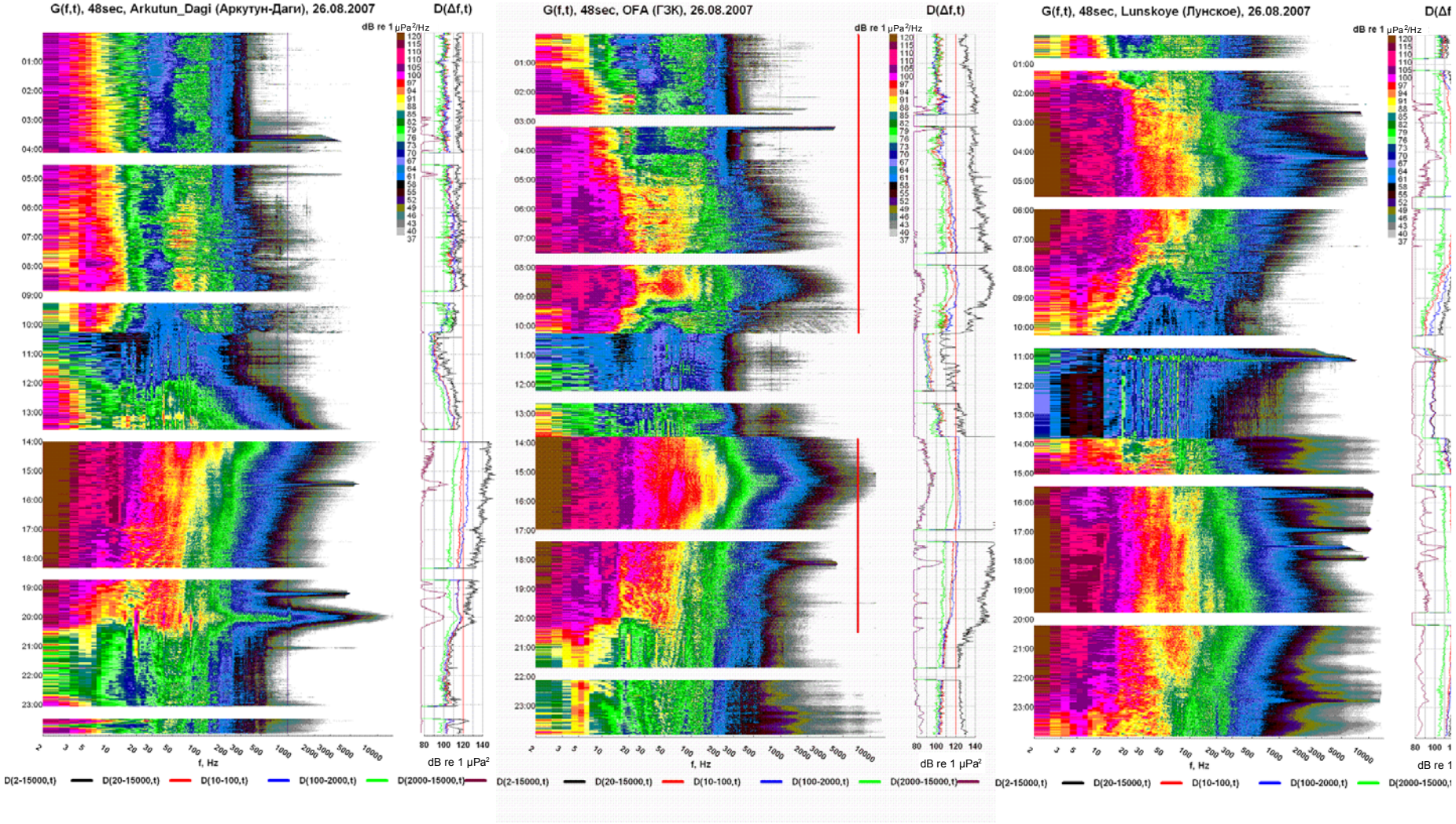

Figure 1.15 - Sonogram *G(f,t)* with plots of sound pressure level *D(Δf,t)* of acoustic energy recorded at three acoustic stations (Arkutun-Dagi, OFA and Lunskoye) on 26 August 2007. These sonograms illustrate the distortions caused by seismic exploration signals.

Table 1.2(a) - Operational times, parameters and locations of AUARs at monitor stations 1 to 9.

Station		Date		Time		Time	AUAR	Location		Depth	Gain	Sens.
Name	#	Start	End	Start	End	(hr)	#	Latitude	Longitude	(m)		(mV/Pa)
Lunskoye	1	09-Jul	7-Aug	09:50	15:05	701	№ 19	51°51.758	143°37.403	46	38	48.5
Lunskoye	1	14-Aug	8-Sep	17:25	20:15	603	№ 22	51°51.852	143°37.415	45	38	50
OFA	2	09-Jul	7-Aug	12:15	17:50	702	№ 21	52°10.318	143°36.040	42	38	49.7
OFA	2	14-Aug	07-Sep	13:40	08:30	571	№ 6	52°10.362	143°35.988	42	38	49.9
Orlan	3	09-Jul	04-Aug	18:00	03:45	610	№ 22	52°21.553	143°35.147	34	38	50
Orlan	3	15-Aug	09-Sep	11:15	09:50	599	№ 21	52°21.667	143°35.25	35	38	49.7
Arkutun-Dagi	4	09-Jul	07-Aug	17:05	20:39	700	№ 20	52°19.102	143°44.012	47	38	49.8
Arkutun-Dagi	4	15-Aug	08-Sep	09:50	15:30	582	№ 20	52°19.062	143°44.523	48	38	49.8
Piltun-S	5	22-Jul	17-Aug	20:55	08:15	611	№ 4	52°40.515	143°21.987	17	8	49.4
Piltun-S	5	19-Aug	07-Sep	17:55	12:50	451	№ 4	52°40.863	143°22.665	185	8	49.4
Piltun	6	03-Jul	21-Jul	15:00	07:30	425	№ 16	52°49.38	143°24.93	20	2	51.5
Piltun	6	23-Jul	18-Aug	17:30	06:15	613	№ 16	52°49.26	143°24.90	22	8	51.5
Piltun	6	19-Aug	07-Sep	18:55	18:50	456	№ 16	52°49.24	143°24.93	22	8	51.5
PA-B-10	7	10-Jul	08-Aug	14:15	20:51	703	№ 6	52°53.87	143°20.58	12	38	49.9
PA-B-10	7	15-Aug	07-Sep	18:30	17:00	551	№ 19	52°52.975	143°20.24	10	38	48.5
PA-B-20	8	03-Jul	22-Jul	14:20	13:40	455	№ 3	52°54.19	143°23.41	21	2	46.4
PA-B-20	8	23-Jul	18-Aug	14:30	03:11	613	№ 3	52°54.01	143°23.38	20	8	46.4
PA-B-20	8	19-Aug	07-Sep	19:20	18:00	473	№ 3	52°53.925	143°23.4	20	8	46.4
Odoptu-PA-	9	10-Jul	17-Jul	12:40	08:30	164	№ 17	53°00.03	143°21.29	21	2	49.6
Odoptu-PA-	9	22-Jul	05-Aug	11:15	08:55	347	№ 2	53°00.01	143°21.247	22	8	49
Odoptu-PA-	9	20-Aug	08-Sep	10:05	08:10	454	№ 2	53°00.13	143°21.255	22	8	49

Table 1.2(b) - Operational times, parameters and locations of AUARs at monitor stations 10 to 15, the control station, and acoustic stations A9 to A11.

Station		Date		Time		Time	AUAR	Location		Depth	Gain	Sens.
Name	#	Start	End	Start	End	(hr)	#	Latitude	Longitude	(m)		(mV/Pa)
Odoptu-S-10	10	29-Jul	16-Aug	16:30	08:00	424	№ 8	53°03.645	143°18.415	12	38	49.6
Odoptu-S-10	10	17-Aug	05-Sep	17:15	13:20	452	№ 8	53°03.603	143°18.415	12	38	44.5
Odoptu-S-20	11	11-Jul	27-Jul	14:50	12:55	382	№ 9	53°03.685	143°19.98	20	38	49
Odoptu-S-20	11	29-Jul	17-Aug	15:30	15:45	456	№ 9	53°03.752	143°19.942	20	38	49.5
Odoptu-S-20	11	18-Aug	05-Sep	17:30	13:00	428	№ 9	53°03.653	143°19.977	21	38	49.5
Odoptu-N-10	12	23-Jul	13-Aug	12:15	05:00	497	№ 5	53°09.078	143°17.413	12	38	49
Odoptu-N-10	12	17-Aug	05-Sep	13:00	11:00	454	№ 11	53°09.12	143°17.478	12	38	49.5
Odoptu-N-20	13	30-Jul	17-Aug	15:00	12:00	429	№ 7	53°09.162	143°18.672	19.5	38	49.2
Odoptu-N-20	13	18-Aug	05-Sep	16:50	11:55	427	№ 13	53°09.042	143°18.77	20	38	49.5
Molikpaq	15	22-Jul	16-Aug	18:00	23:52	606	№ 17	52°45.888	143°26.633	24	8	49.6
Molikpaq	15	19-Aug	07-Sep	18:30	13:55	451	№ 17	52°45.873	143°26.627	24	8	49.6
Control	14	11-Jul	27-Jul	10:50	08:17	381	№ 13	53°25.965	143°11.092	20	38	49.5
Control	14	30-Jul	17-Aug	12:10	10:00	430	№ 13	53°26.008	143°11.127	20	38	49.5
Control	14	17-Aug	05-Sep	10:35	09:10	455	№ 5	53°26.055	143°11.167	20	38	49
BEH-Odoptu	A.9	30-Jul	16-Aug	14:05	21:40	406	№ 11	53°12.573	143°16.418	12	38	49.5
BEH-north	A.10	11-Jul	29-Jul	12:50	17:30	437	№ 7	53°17.638	143°14.567	14	38	49.2
Chayvo-4	A.11	09-Jul	22-Jul	20:05	19:00	311	№ 5	52°34.090	143°23.145	17.5	38	49
Chayvo-4	A.11	18-Aug	05-Sep	09:55	16:55	439	№ 7	52°34.007	143°23.012	18	38	49.2

Table 1.3 – Plot showing the days when AUARs were active at each monitoring station (by station).

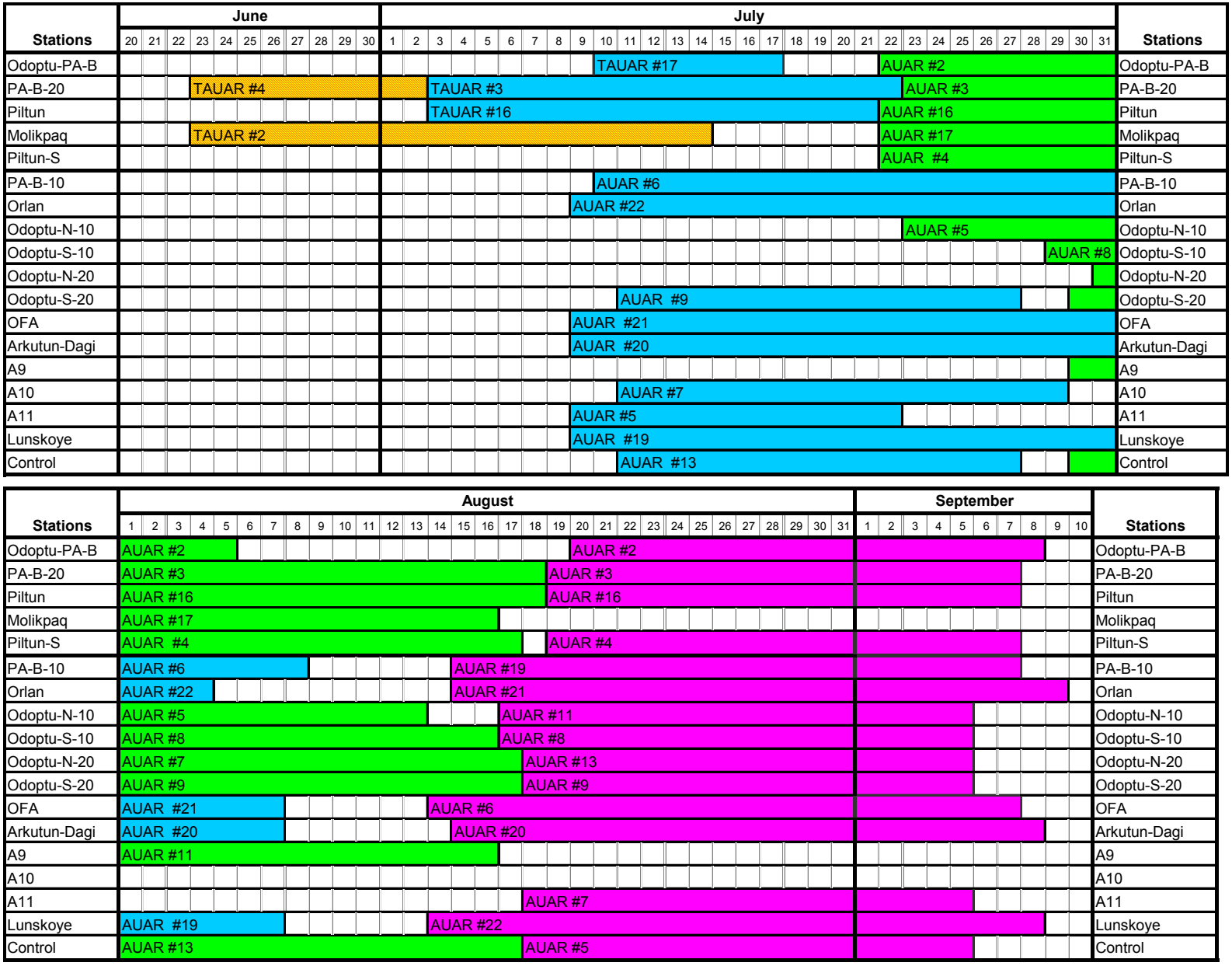

1.6 Units

During the course of this report a number of different unit notations have been used. This is due to differences in standard notation between different disciplines and nationalities[24]. For spectral density plots - although the units for power spectral density are $\mu Pa^2/(s\ Hz)$, $\mu Pa^2/s/Hz$ or μPa^2, the units for power spectral density are sometimes defined as $\mu Pa^2/Hz$ or $\mu Pa/\sqrt{Hz}$.

[24] The following are equivalent units using the different standard nomenclatures: 1 mkPa = 1 µPa and 1 mkV = 1 µV.

2 Acoustic recording and processing equipment

The acoustic measurements were conducted using 16 digital AUARs developed at POI. Five of these AUARs were Telemetry-AUARs[25] (Figure 1.2). Between 2005 and 2007 an additional six mini-AUARs were constructed; these were smaller with a reduced (72 hours) record time and were used for TL and source level measurements. The AUARs (all variants), were designed to enable accurate, autonomous, synchronous acoustic measurements over a broad range of frequencies (1 Hz to 15 kHz, including infrasounds[26]) to be recorded. Two digital sonobuoys (DSB) and four analog sonobuoys (ASB), also developed at POI, were used for real-time acoustic measurements. Analog sonobuoys can record frequencies from 10 Hz to 10 kHz and digital sonobuoys from 1 Hz to 2.6 kHz. When used together an analog and digital sonobuoy pair can record acoustic data from 1 Hz to 10 kHz. A detailed description of this equipment has been provided by Borisov [Borisov et. al. 2006].

2.1 Autonomous Underwater Acoustic Recorder (AUAR)

The AUARs[27] are made of welded titanium alloy and are rated to depths of up to 50 m (two are rated to 100 m) (Figure 1.1). Two external sensors (hydrophones, accelerometers or hydrologic measuring equipment) can be input to the AUAR electronics. Inside the AUAR there are batteries secured in a titanium frame and the AUAR electronics and power handling circuitry is attached to the lid. The capacity of the batteries depends on the AUAR design. The 10 AUARs fabricated in 2003, 2005, 2006 and 2007 have three sealed 115 ampere-hour batteries, enabling the AUAR to operate continuously for over 28 days, while the six AUARs produced in 2004 have three sealed 68 ampere-hour batteries providing continuous operation of the AUAR for over 18 days.

All of the AUARs and mini-AUARs use cylindrical hydrophones (model # GI-50 (ГИ-50)) (Figure 2.1(b)) with integrated pre-amplifiers designed specifically for use with the AUARs. Figure 2.1(a) shows the parallel charging of three AUAR batteries on the *Professor Bogorov.*

---

[25] The T-AUARs were equipped with a radio channel and were capable of simultaneously recording data on the AUAR hard drive and transmitting data (bandwidth 10 Hz to 5 kHz) to a receiving radio station. The transmission can be continuous or on a pre-programmed schedule.

[26] Infrasounds are sounds with a frequency of less than 20 Hz.

[27] 2003/2005/2006/2007 AUAR dimensions are length 0.8 m, diameter 0.38 m, weight in air ~155 kg. 2004 AUAR dimensions are length 1.2 m, diameter 0.32 m, weight in air ~105 kg.

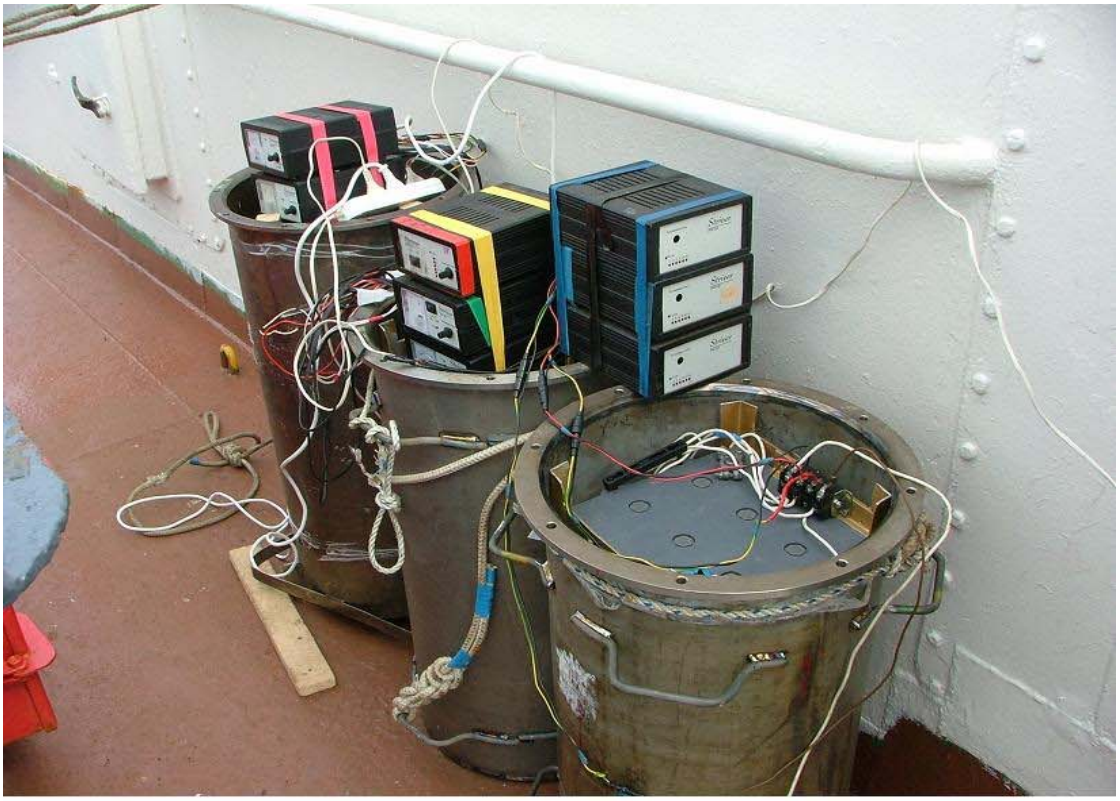

(a.)

(b.)

Figure 2.1 - (a) Charging AUAR batteries; (b) Hydrophone used in AUAR & mini-AUAR.

The AUARs digital recorder is based on the Prometheus single board computer, which has an integrated 16 bit analog to digital converter (ADC). In order to optimize the dynamic range of the 16 bit ADC the signal amplitudes should be approximately equal across the entire frequency range. However, ambient noise generally has an amplitude maximum at low frequencies and drops off with higher frequencies. The ADC does not always have the instantaneous dynamic range required to record ambient and anthropogenic noise at frequencies from 1 Hz to 15 kHz. Therefore, for all hydrophones, low-frequency amplitude correction is effected in the hydrophone preamplifier. These amplitude corrections ensure a consistent signal level across the entire frequency band for the analog channel of the AUARs with these hydrophones. An inverse correction is applied during spectral estimation.

The primary AUAR data storage is a 120-160 GB hard drive. To prevent electromagnetic and acoustic noise generated by the rotating hard drive from contaminating the data, and to conserve power, a 1 GB flash memory drive is used as a buffer. While data is being recorded on the flash drive the hard drive is in standby mode with its motor off. When the flash memory drive is full, the recording cycle is halted while the flash memory drive writes to the hard drive; the data therefore contains controlled gaps. The size of these gaps was approximately 22 minutes every 4:18 hours. Before each AUAR is deployed its computer is programmed for the desired recording schedule. The acoustic data on the AUAR hard drive was copied to DVDs and a removable hard drive before the files on the AUAR drive were deleted prior to redeployment.

In 2006, the resolution of the system timer in the QNX operating system was increased and periodic software corrections of the hardware clock were made to reduce the clock drift to less than one minute in a 19 day AUAR deployment. A tone was used to confirm that the AUAR computer was operating correctly prior to deployment. Prior to deployment of an AUAR a standard test signal was recorded (Figure 2.1); this signal is used to verify the AUAR gain and any other scaling factors.

In 2007 the analog channel was upgraded; RC circuits were installed at the output of the scale amplifier output and the input to the ADC to eliminate high-frequency crosstalk between the Prometheus motherboard and the DC/DC voltage converter are operating. The gain of the analog channel is set by jumpers near the scale amplifier chip. This switching is performed on jumpers outside the shielded housing of the analog channel.

The mechanical construction of the electronics unit was also modified in 2007. All of the electronic modules are now mounted in a single tray, and the connecting cables have been shortened where possible. The plug-and-socket connectors are equipped with catches to prevent them from shaking loose as a result of bumps and vibrations. The height of the electronics module was reduced to 6 cm, allowing an additional battery to be placed in the existing AUAR housings in 2007, extending their endurance to 28 days (Figure 1.1).

The AUARs and mini-AUARs employed during the 2007 field season utilized GI-50 hydrophones. The frequency response of these hydrophones is shown in Figure 2.2 (a, b, c). All of these hydrophones have a low-frequency amplitude correction accomplished by the hydrophone preamplifier. This eliminates the need for any additional low-frequency gain correction in the AUAR amplifier [Borisov et. al. 2006]. Calibration certificates for all the hydrophones used in the 2007 expedition are given in Appendix B.

Figure 2.3 shows the deployment of the three types of AUAR and how the AUAR and its hydrophone are anchored when deployed. Practical experience has shown that at shallow deployment depths (10-30 m), movement of any surface buoy due to wave action can be mechanically conducted down the rope or cable to the hydrophone, where this mechanical movement can be recorded as acoustic noise.

T-AUAR radio buoys and mini-AUAR surface buoys (Figure 2.3(a) and (c)) are deployed so as to reduce this noise by isolating the hydrophone from the surface buoy with an anchor, thus reducing the mechanical coupling between the surface buoy and the hydrophone. The hydrophone is also deployed 15 m from the AUAR to prevent distortion of the acoustic field by scattering or masking by the AUAR container at high frequencies. The hydrophone is deployed inside a pyramid shaped metal frame to which it is attached by rubber straps, isolating it to the best extent possible from the sea floor. In 2007, acoustic releases were

used in all AUARs deployments (Figure 2.4). Using acoustic releases (Figure 2.3(b)) virtually eliminates the possibility of unauthorized retrieval of the AUAR and 'isolates' the hydrophone as much as possible from surface waves.

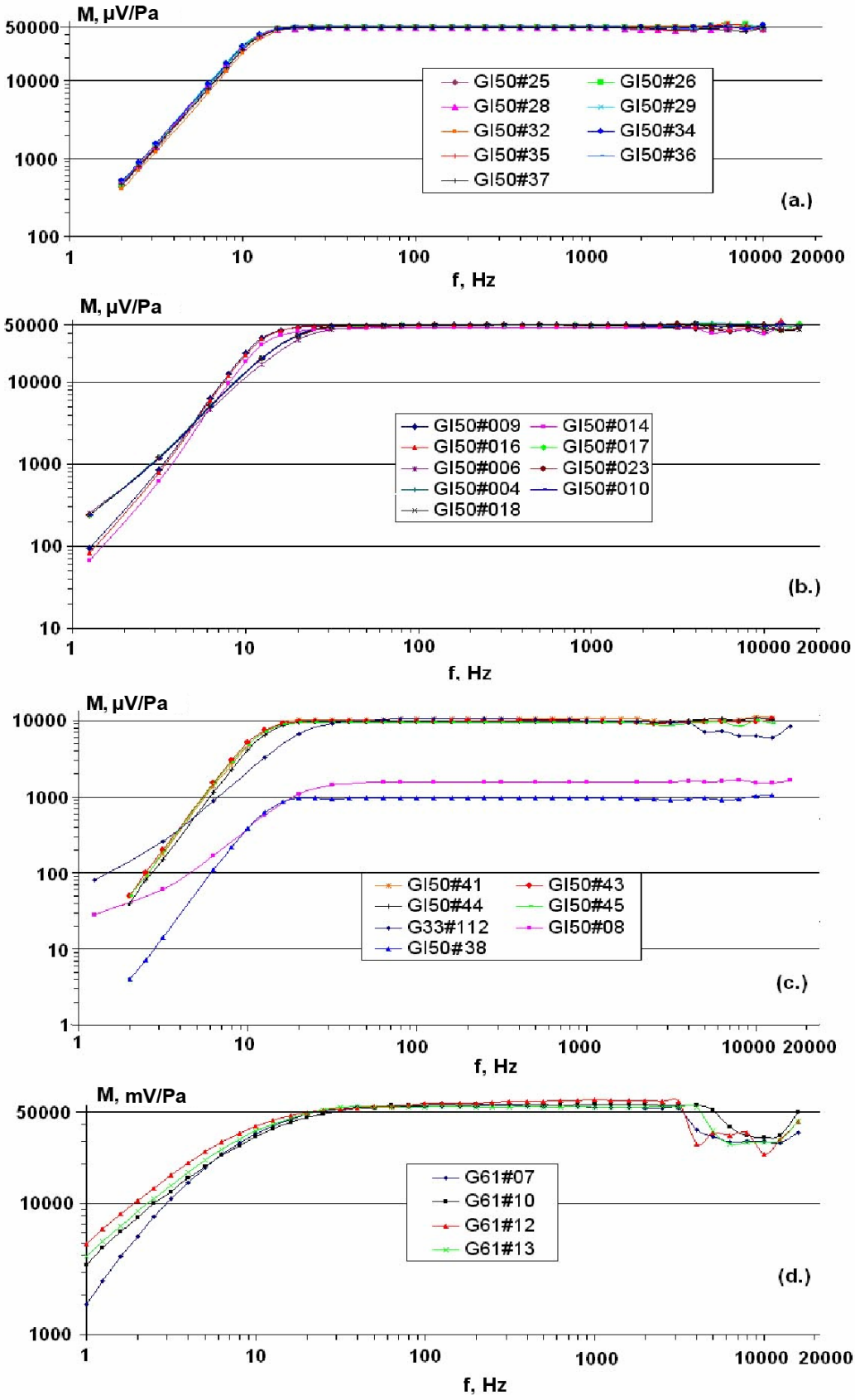

Figure 2.2 - Spectral characteristics of the hydrophones used during the 2007 field season: (a & b) Cylindrical (GI-50) hydrophones used by AUARs and T-AUARs; (c) GI-50 hydrophones (10mV/Pa sensitivity) used by mini-AUARs and as a transducer reference; and (d) Spherical (G-61) hydrophones used by ASBs and DSBs.

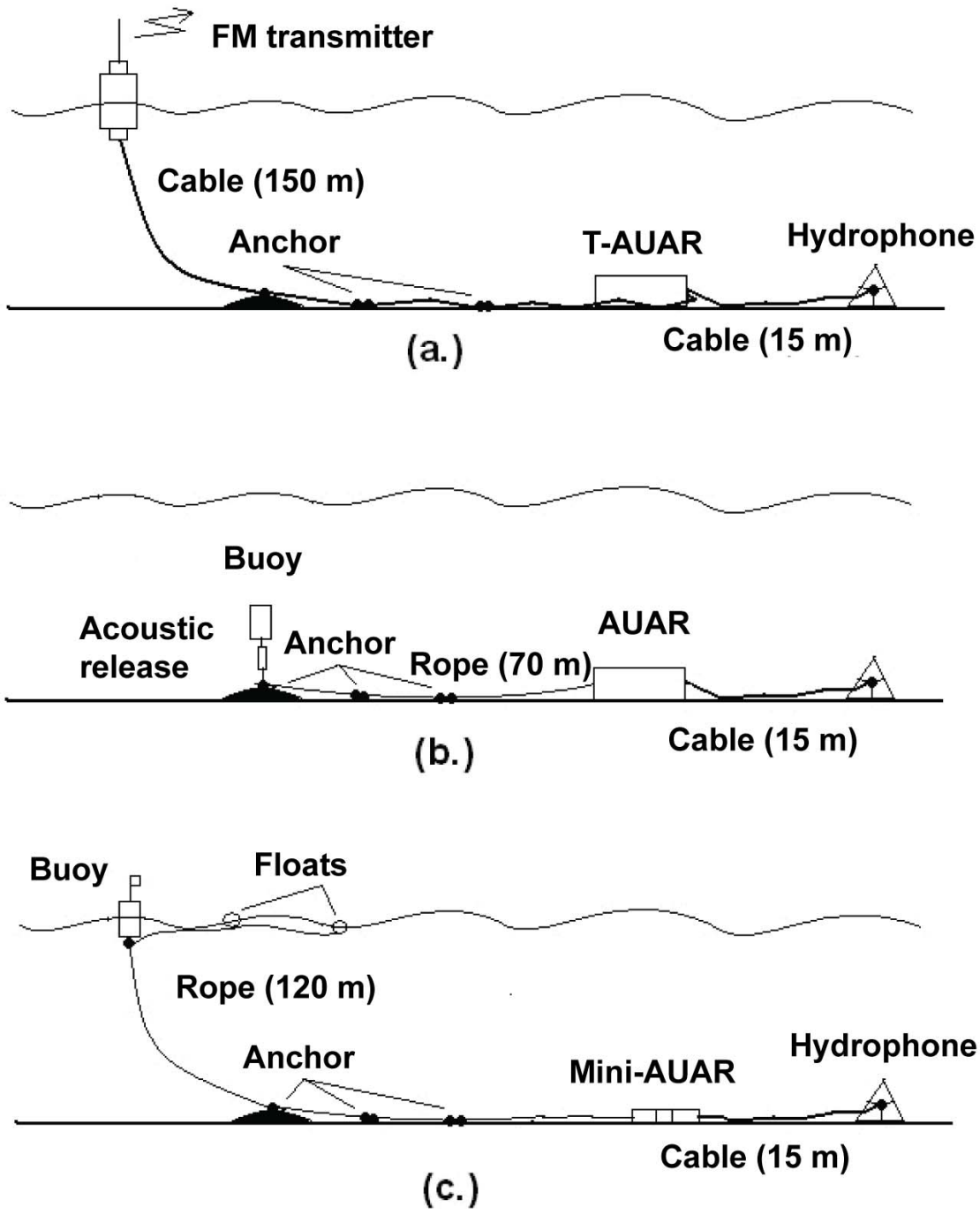

Figure 2.3 – Deployment schematics for (a) T- AUAR; (b) AUAR; and (c) Mini-AUAR.

To compute TL from acoustic measurements made by different AUARs, and to compare acoustic data over time, the data has to be calibrated to an absolute pressure standard. The hydrophones were manufactured with nominal sensitivities and the gains were set in the field (copies of the calibration certificates are given in Appendix B). Field cross-calibrations confirmed the absolute calibration of the data. Further details of the AUARs

used in 2007, their location, deployment depth and recording settings can be found in Table 1.2. A detailed description of the testing of the recording equipment is given in [Borisov et al., 2007].

Figure 2.4 – Acoustic release and buoy.

2.1.1 AUAR instrument test analysis

In order to ensure that all of the AUARs adhered to the design specifications, and that the AUARs recorded accurate absolute acoustic measurements, a set of instrument tests was created. These tests were designed to ensure that all the AUARs were operating within specifications and to generate an instrument response filter for the analog component of each AUAR. This estimate of the AUAR analog instrument response, measured in the laboratory prior to the field season *K(f)* and the hydrophone sensitivity *M(f)* was used to generate an inverse filter; this filter was subsequently applied to the analog voltage measurements to back out the system instrument response and generate absolute acoustic measurements. These frequency dependent responses correct the acoustic data over the range from 1 Hz - 15 kHz.

In 2007, measurements of the internal noise, dynamic range and analog channel system filter response of each AUAR were made using the procedure described by Borisov [Borisov et.al. 2007]. The following results quantitatively characterize the performance of the AUARs used during the 2007 field season.

2.1.2. AUAR internal noise

The AUAR internal noise was measured using a dummy GI-50 equivalent hydrophones constructed in 2005. The preamplifier electronics in the shielded housing of the equivalent hydrophone is identical to that of the corresponding hydrophone except that a piezoceramic capacitor with the same capacitance as the hydrophone piezoceramics is connected to its input. The internal noise measurements were performed using the procedure approved in 2006 and described in Borisov [Borisov et.al. 2007]. Figure 2.5 displays a spectral analysis of the results, showing the internal noise of the AUAR analog channels with a GI-50 hydrophone over the frequency ranges 0-15 kHz (top) and 0-300 Hz (bottom)[28].

2.1.3. AUAR dynamic range

Figure 2.6 displays spectra of the tonal signals recorded by the AUARs during the dynamic range measurements, with the gain factor set to its maximum value of 38. When the sound pressure level is close to the maximum input acoustic pressure level, the dynamic range is limited by non-linear distortion and is 60 dB (Figure 2.6 – Green curve). If the input signal level is decreased by 10 dB re 1 μPa^2/Hz (Figure 2.6 – Blue curve), the dynamic range of the AUAR increases to 76 dB. The red curve on Figure 2.6 shows that the internal instrument noise level of the AUAR recording channel with an equivalent GI-50 is approximately 27 dB re 1 μPa^2/Hz in the frequency band from 50 Hz to 15 kHz, increasing to 35 dB re 1 μPa^2/Hz at a frequency of 20 Hz. Since the instrument noise is below the distortion for most of the recorded frequency range, distortion limits the dynamic range of the AUAR.

2.1.4. Analog channel system filter response of the AUAR

The filter response of each AUAR analog channel was measured in laboratory conditions using a broadband white noise signal (*K(f)*), the results are used to estimate an analog instrument filter response for each AUAR, normalized to the gain at 1 kHz (Figure 2.7). The measurements were made for three scaling factors: 2, 8 and 38. Figure 2.7 shows that *K(f)*

[28] The results were not corrected by the amplitude-frequency response of the analog channel.

decreases with an increase in the gain factor at frequencies below 15 Hz, due to the presence of a 1μF separating capacitor at the output of the hydrophone preamplifier causing a corresponding decrease in the input resistance of the scale amplifier with an increase in gain.

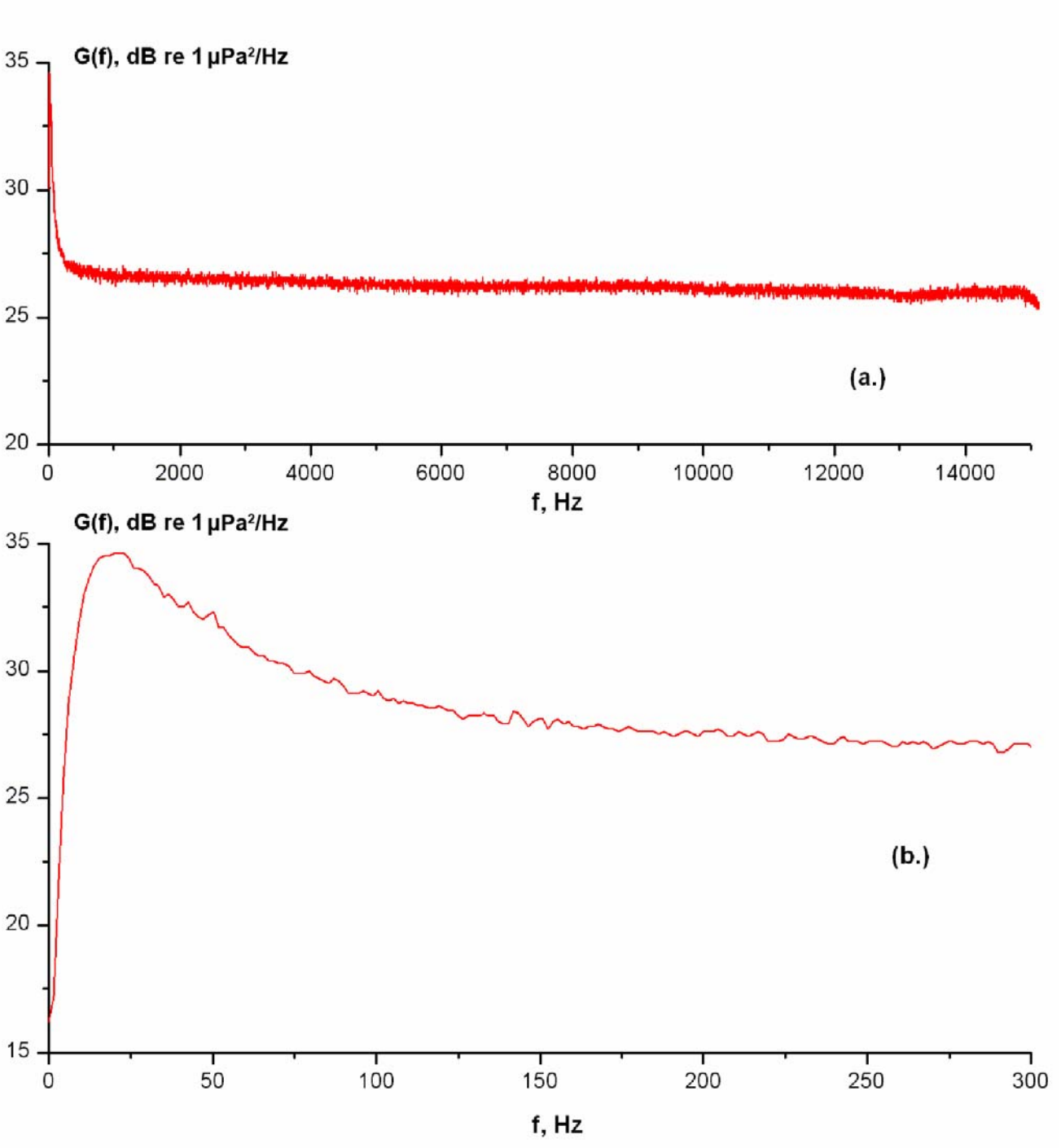

Figure 2.5 - Spectra showing the internal noise of the AUAR recording system: (a) 0-15 kHz and (b) 0-300 Hz.

This filter response, together with the frequency response of the hydrophone (*M(f)*) used in a given AUAR (Figure 2.2), is used to construct a system filter response. This is used to correct the data as it is processed, reducing the analog voltage measurements to absolute acoustic pressure for the frequency band from 1 Hz to 15 kHz.

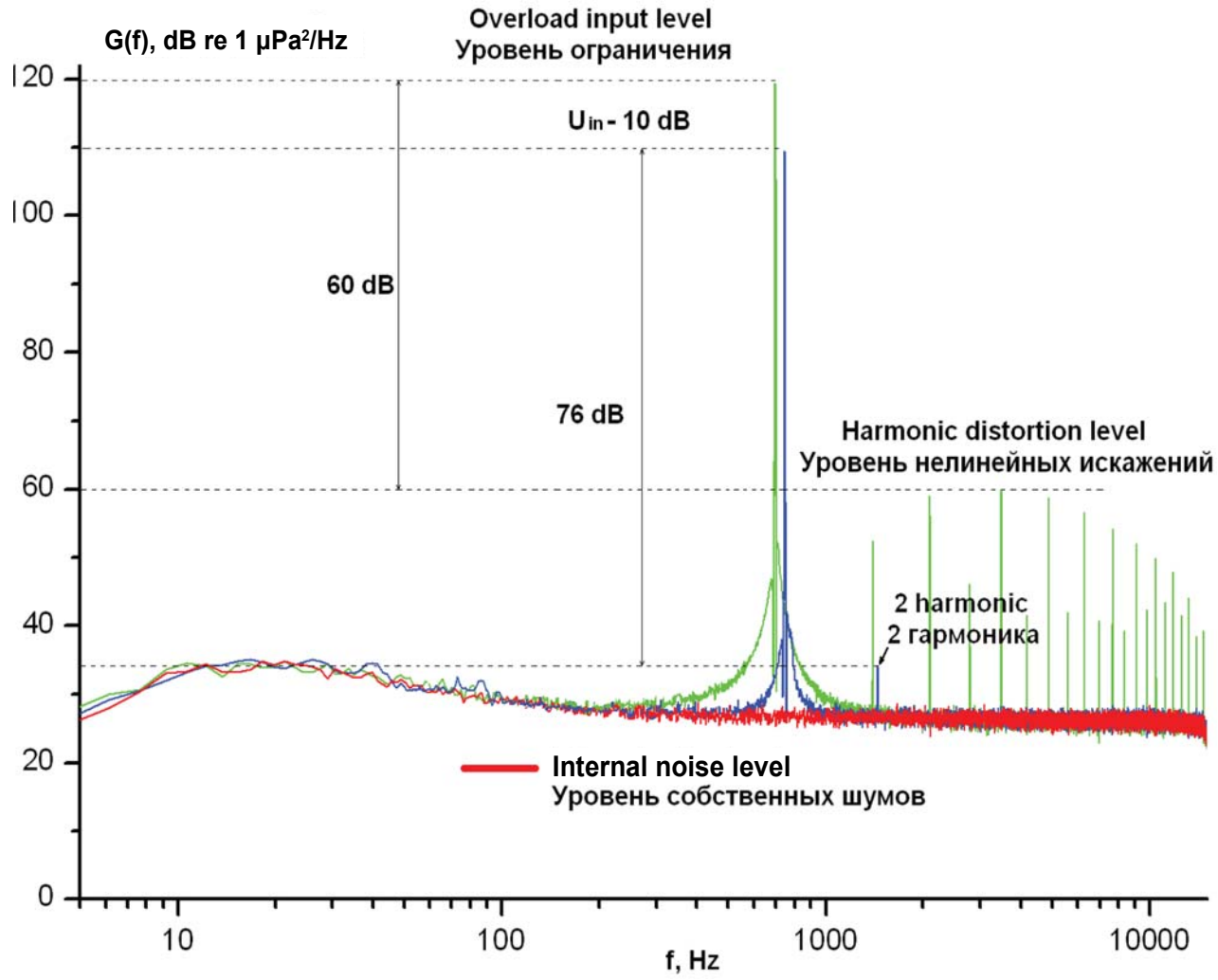

Figure 2.6 - Spectrum showing the internal noise and dynamic range of the AUAR recording system.

2.1.5 Results of the instrument tests

The unit to unit performance of all the AUARs was confirmed by regular testing. All the AUARs were subject to the tests listed in Borisov [Borisov et.al. 2007]; Table 2.1 gives the individual test results for all sixteen AUARs and six mini-AUARs performed in the laboratory. All AUARs performed within specifications.

Table 2.1 – Performance of AUARs on the instrument tests.

AUAR serial number										
02	**03**	**04**	**05**	**06**	**07**	**08**	**09**	**11**	**13**	**14**
Internal noise (dB re 1 μPa²/Hz) ***(1-200 Hz)***										
40.0	40.0	40.3	41.0	39.0	37.0	41.0	41.0	38.0	39.0	42.0
Internal noise (dB re 1 μPa²/Hz) ***(200 Hz - 15 kHz)***										
27.0	29.8	27.0	28.2	26.2	27.0	26.0	27.5	27.0	26.0	28.0
Dynamic range , dB										
76.0	76.0	77.0	78.0	78.0	75.0	77.0	75.0	77.0	76.0	77.0
AUAR serial number										
15	**16**	**17**	**18**	**19**	**20**	**21**	**22**	**23**	**24**	**25**
Internal noise (dB re 1 μPa²/Hz) ***(1-200 Hz)***										
43.0	38.3	43.0	39.0	36.0	39.0	41.0	40.0	40.5	41.0	39.0
Internal noise (dB re 1 μPa²/Hz) ***(200 Hz - 15 kHz)***										
28.0	28.0	27.0	30.0	26.5	250	27.0	27.0	27.5	28.0	29.1
Dynamic range , dB										
78.0	75.0	75.0	77.0	76.0	76.0	77.6	75.0	76.0	76.0	77.0

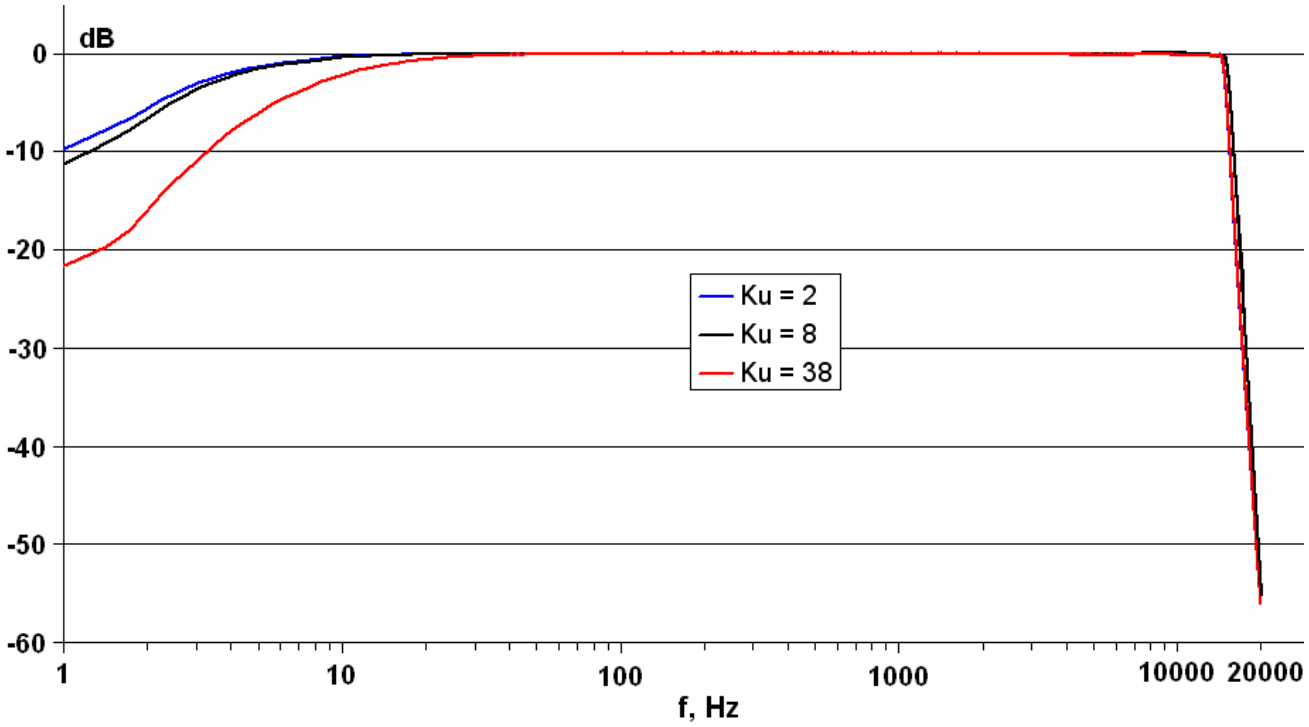

Figure 2.7 - Amplitude-frequency characteristics of an AUAR analog channel normalized to the gain at 1 kHz, measured using a broadband white noise signal and gain factors of 2, 8 and 38.

2.2 T-AUAR, Digital and analog sonobuoys

Figure 1.4 shows a digital sonobuoy. The flotation collar holds a steel (analog) or titanium (digital) cannister containing the sonobuoy electronics. The sonobuoy is powered by an external battery pack that can be changed at sea. The sonobuoy antenna is kept upright by a keel to which the batteries are attached. The surface unit is connected by a cable to a G61 (Г61) (spherical) or GI50 (ГИ50) (cylindrical) hydrophone with an integrated pre-amplifier designed specifically for the hydrophone. The hydrophone is suspended in a pyramid shaped metal frame and attached by rubber bands as with the AUAR hydrophone. The hydrophone pre-amplifier amplifies the signal prior to transmission along the 100 m cable to the surface sonobuoy module. The signal is then further filtered and amplified prior to radio transmission (analog sonobuoys) or low pass filtered to 2.6 kHz and digitized prior to encoding and radio transmission (digital sonobuoys). The analog and digital sonobuoys as well as the T-AUAR radio-telemetry channel are described in [Borisov et. al. 2006][2].

Analog and digital sonobuoys have both advantages and disadvantages. For the analog sonobuoys the advantages are greater measurement bandwidth and longer range (>10 km for a bandwidth of 10 Hz to 10 kHz and >20 km for 10 Hz to 5 kHz). However the dynamic range of an analog sonobuoy is much lower than that of a digital sonobuoy and is highly dependent on the quality of the radio channel. The digital sonobuoy (due to the 16-bit ADC) has a significantly greater dynamic range than the analog sonobuoy, is not susceptible to radio noise and has stable performance characteristics. Critically, the digital sonobuoy can also measure frequencies as low as 1 Hz accurately. The disadvantages of a digital sonobuoy are narrower measurement bandwidth and shorter range (≤ 8 km for a bandwidth of 1 Hz to 2.6 kHz).

2.2.1 T-AUAR, DSB and ASB instrument test analysis

The internal noise, dynamic range, and system filter response of the T-AUAR and ASB analog radio channels were measured using the procedure described in Borisov [Borisov et. al. 2007]. Figure 2.8 shows the measured total system filter response for the ASB, DSB and T-AUAR (both direct to AUAR disk and through the T-AUAR radio channel). These filter responses, together with the frequency response of the relevant hydrophone (*M(*f)), are used to construct system filter responses. These are used to correct the data as it is processed, reducing the analog voltage measurements to absolute acoustic pressure for

any given T-AUAR or ASB, for the frequency band from 10 Hz to 5 kHz (1 Hz to 15 kHz for the direct recording to disk).

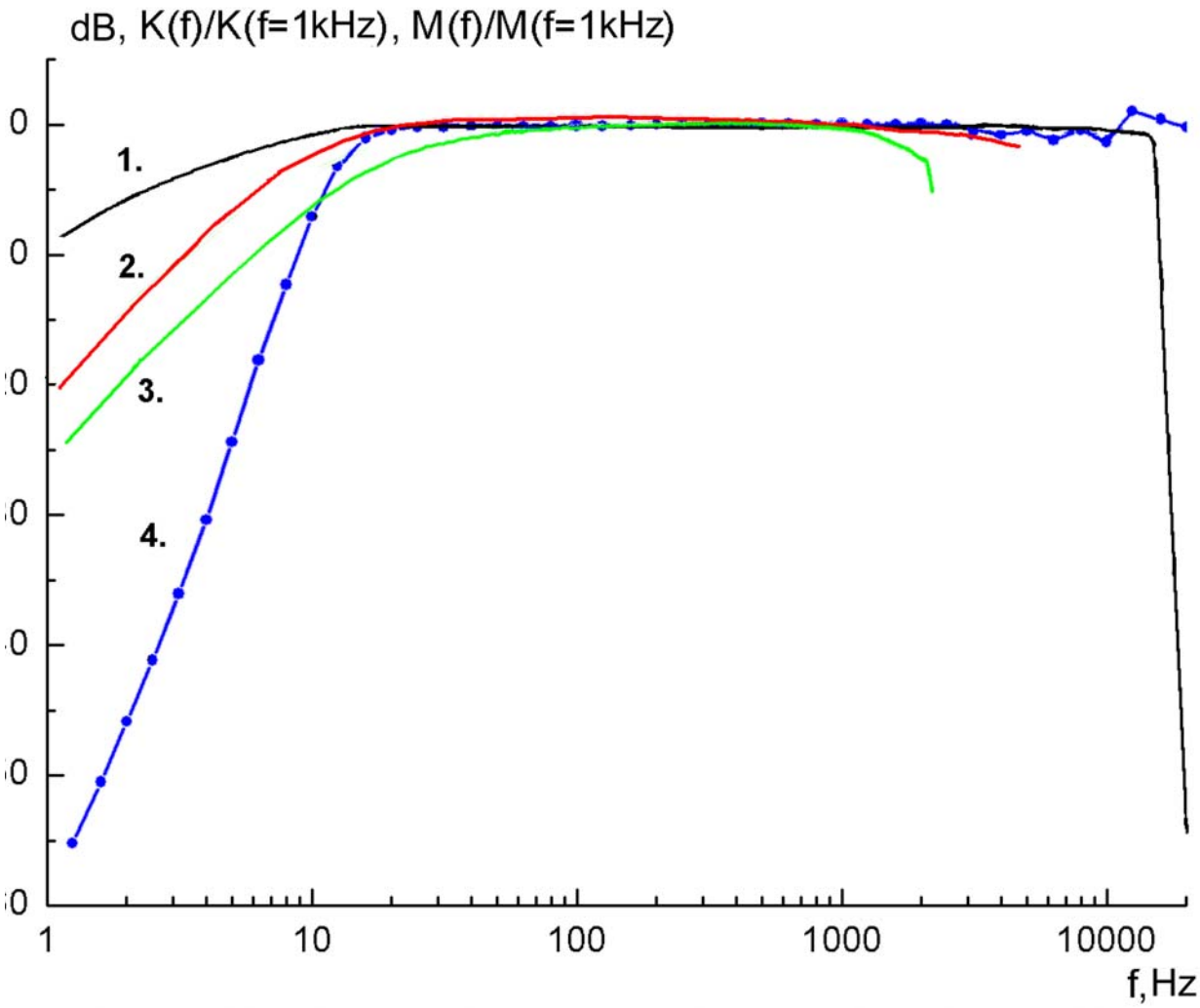

Figure 2.8 – Spectral characteristics of: (1-Black) The analog channel for data recorded to AUAR hard disk; (2-Red) Total system response for T-AUAR and ASB analog radio-telemetry channel; (3-Green) Total system response for DSB digital radio-telemetry channel; (4-Blue) Hydrophone sensitivity for GI-50 hydrophone.

Figure 2.9 shows the results of the system noise tests for the T-AUAR, ASB and DSB. Figure 2.10 shows typical results for dynamic range measurements on a T-AUAR, ASB and DSB, with a non-linear distortion level of -30 dB. Figure 2.10 shows that at high input signal levels (close to the maximum input level), the dynamic range of the ASB and T-AUAR radio channel is limited by nonlinear distortion and is 30 dB (ASB) and 40 dB (T-AUAR) for an input signal 15 dB down from the maximum. The dynamic range of the DSB exceeds 75 dB and is limited by non-linear distortion due to the second harmonic.

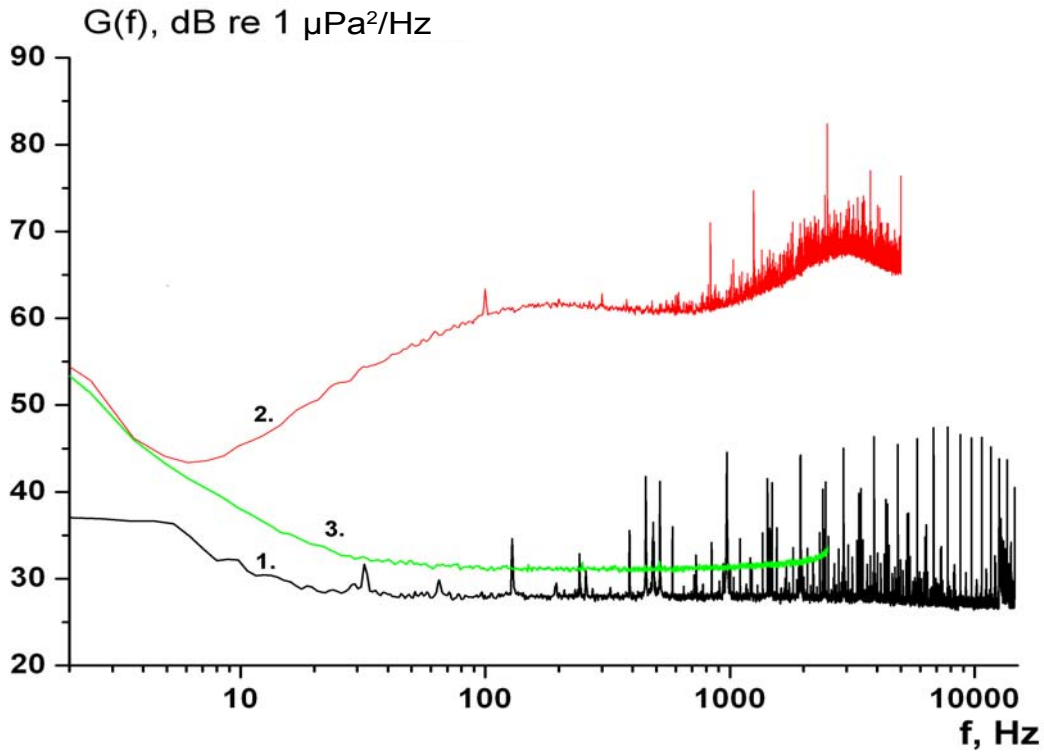

Figure 2.9 – Internal noise of: (1-Black) The analog channel for data recorded to AUAR hard disk; (2-Red) T-AUAR and ASB analog radio-telemetry channel; (3-Green) DSB digital radio-telemetry channel. All measurements were taken with a gain of 2.

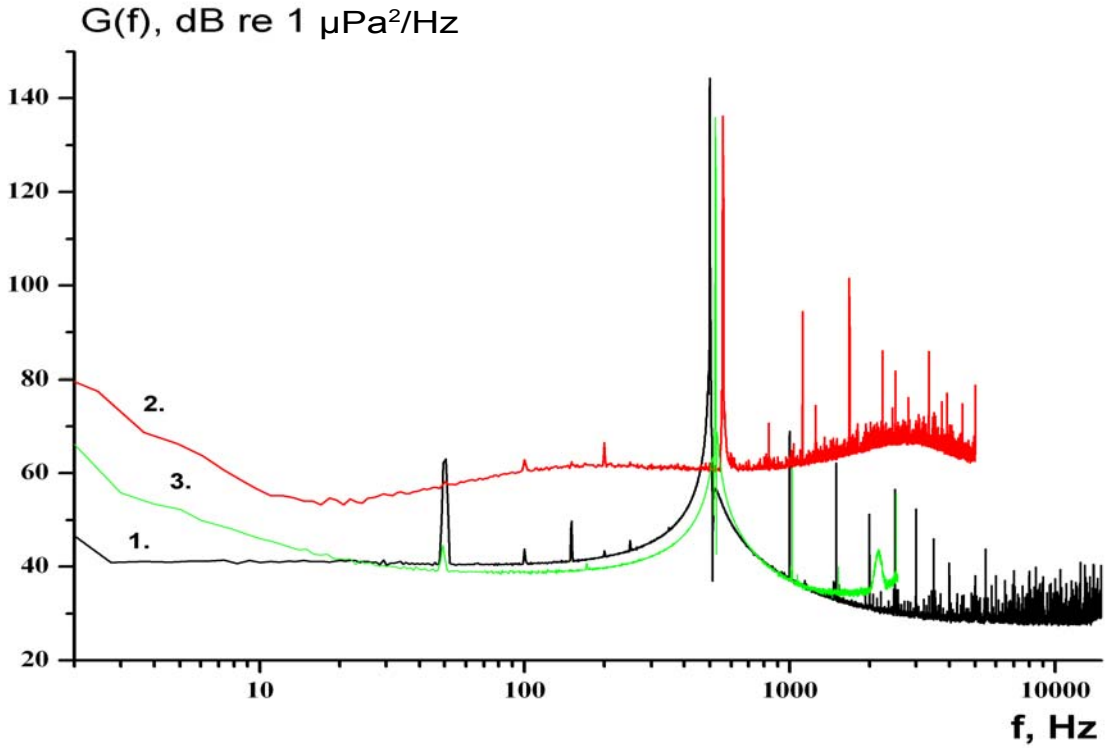

Figure 2.10 – Dynamic range measurements for: (1-Black) The analog channel for data recorded to AUAR hard disk; (2-Red) T-AUAR and ASB analog radio-telemetry channel; (3-Green) DSB digital radio-telemetry channel. All measurements were taken with a gain of 2.

The measured test results for all of the sonobuoys are presented in Table 2.2.

Table 2.2 - Performance of sonobuoys on the instrument tests.

Sonobuoy	Frequency band, Hz	Signal to Noise ratio not less than	Frequency band	Signal to Noise ratio not less than	Dynamic range , dB
DSB-1	1-2500	90			75
DSB-2	1-2500	87			75
ASB-1	10 - 500	60	500 - 5000	30	30
ASB-2	10 - 500	60	500 -5000	30	30
ASB-3	10 - 500	60	500 - 5000	30	30
ASB-4	10 - 500	60	500 - 5000	30	30

2.3 Mollusk-07 vertical autonomous acoustic and hydrologic recording array

The Mollusk-07 vertical autonomous acoustic and hydrologic recording array was developed by POI for experimental studies of the spatial and temporal heterogeneities in the sound velocity field generated by subsurface waves propagating along the seasonal thermocline and by other hydrodynamic sources. A vertical array of eight hydrophones and eight temperature sensors 4.5 m apart, allows the modal composition of subsurface waves and low-frequency sound propagating in offshore areas to be studied. The Mollusk-07 was tested in the Sea of Japan in May 2007, and during the field season was used successfully for experimental acoustic and hydrologic studies in the Sea of Okhotsk. One distinctive feature of the Mollusk-07 is its combination of coincident acoustic and water temperature measurements at each element, confirmation of the depth of the upper and middle hydrophones, as well as the use of an original digital data storage system based on an integrated computer. Development of the Mollusk-07 drew on many years of experience operating its predecessor, the Mollusk-97, in the Sea of Japan [Rutenko, 2006]. This initial version of the system was linked to an onshore monitoring station by a two-wire cable. The Mollusk-07 has no known analogues, since it allows autonomous, extended duration (more

than 7 days), broadband (up to 5 kHz) measurements of sound pressure at 8 depths with coincident, synchronous measurements of water temperature at each hydrophone. This allows the position and characteristics of the seasonal thermocline to be monitored, as well as any internal waves propagating along it. The operational control of the system can be programmed in accordance with the experimental requirements developed for each experiment using the integrated on-board computer. The basic components of the Mollusk-07 are described below along with their technical characteristics, which have been confirmed by instrument tests and field measurements. Figure 1.5 shows photographs of the basic components of the Mollusk-07, and Figure 2.11 is a schematic of the deployment of the Mollusk-07 at sea.

The initial design of the Mollusk-07 includes eight hydrophones, eight temperature sensors, two depth sensors (hydrostatic pressure transducers), one current velocity transducer and one service channel for checking the power supply voltage. In 2008 POI plan to upgrade the Mollusk-07 with two fast-response current velocity meters including orientation sensors. The mechanical structure of the Mollusk-07 is based on a standard surface buoy container and a shortened (2004) AUAR container (Figure 1.5).

Two gel batteries each with a capacity of 65 ampere-hours are used to power the unit. The vertical 'streamer' with the sensors is constructed from geophysical cable with steel strength members and copper conductors in PVC insulation. Power is supplied from the bottom container to the top hardware container with an identical cable to a T-AUAR; this provides the strength necessary for the entire vertical acoustic and hydrologic array. The Mollusk-07 is deployed using a 75-kg disposable anchor, which separates from the Mollusk-07 using an acoustic release when the system is recovered.

Figure 2.12 shows a photograph of the basic electronic components of the Mollusk-07 and a system schematic. The system uses a 16-bit ADC, which gives a theoretical dynamic range of the analog voltage measurement of 96 dB relative to its maximum value of $\pm$5 V. Eight channels are used to condition, digitize and record the eight acoustic signals, and a ninth is used for the hydrologic and service data. Data from the eight temperature sensors is input to a multiplexer and then to a buffer amplifier with a gain of 10, reducing the relative error between the sensors. This multiplexed and amplified channel is then multiplexed with the

two depth channels and the current velocity channel and input to the ADC of the ninth channel. Multiplexing the channels in this way allows the output from all the sensors to be recorded using the same analog and digital channel.

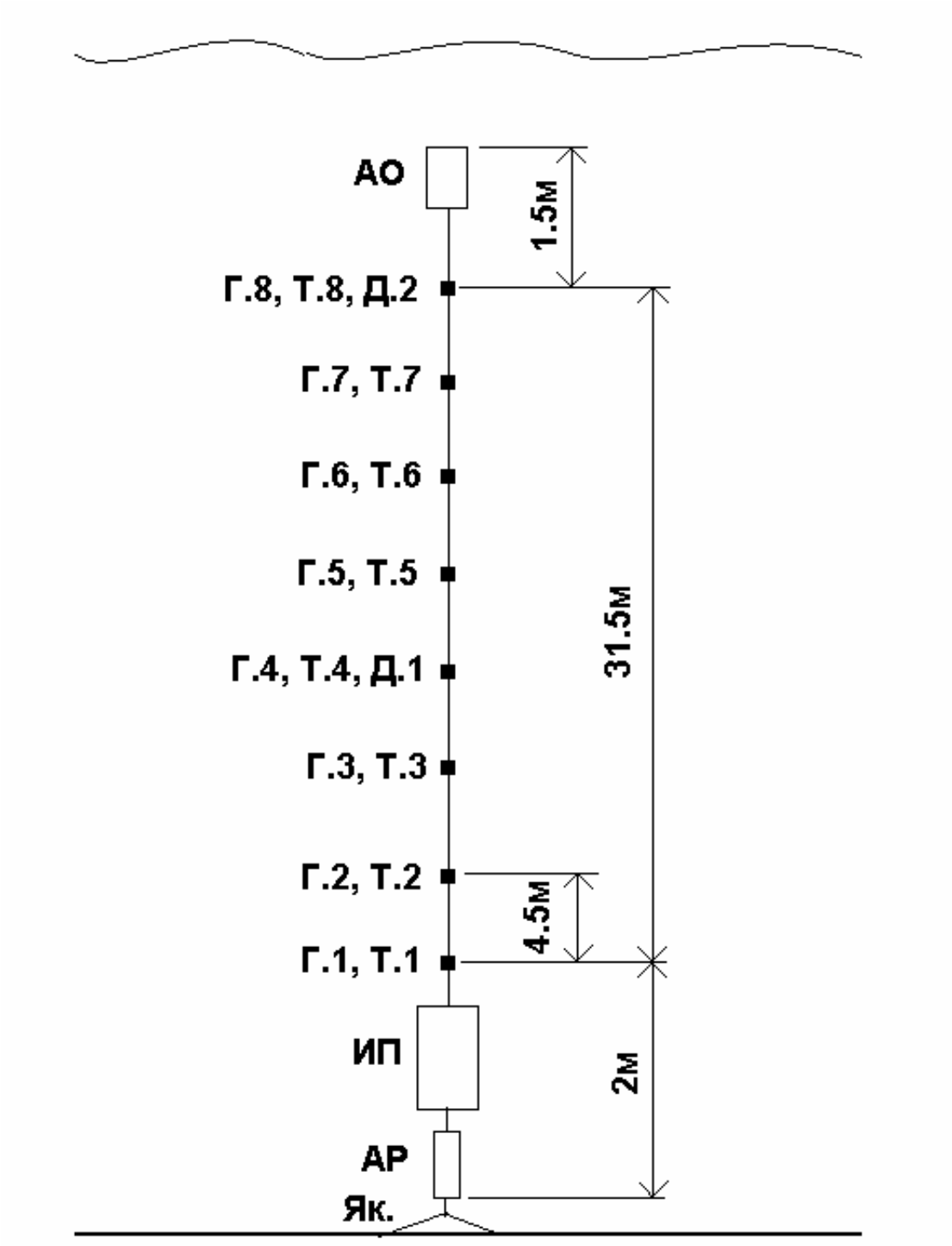

Figure 2.11 – Diagram showing deployment of the Mollusk-07 at sea. Notations: АО - hardware container; Г.1-Г.8 - hydrophones; Т.1-Т.8 - temperature sensors; Д.1, Д.2 – depth (pressure) sensors, ИП - sealed battery container; АР - acoustic release, Як. – anchor.

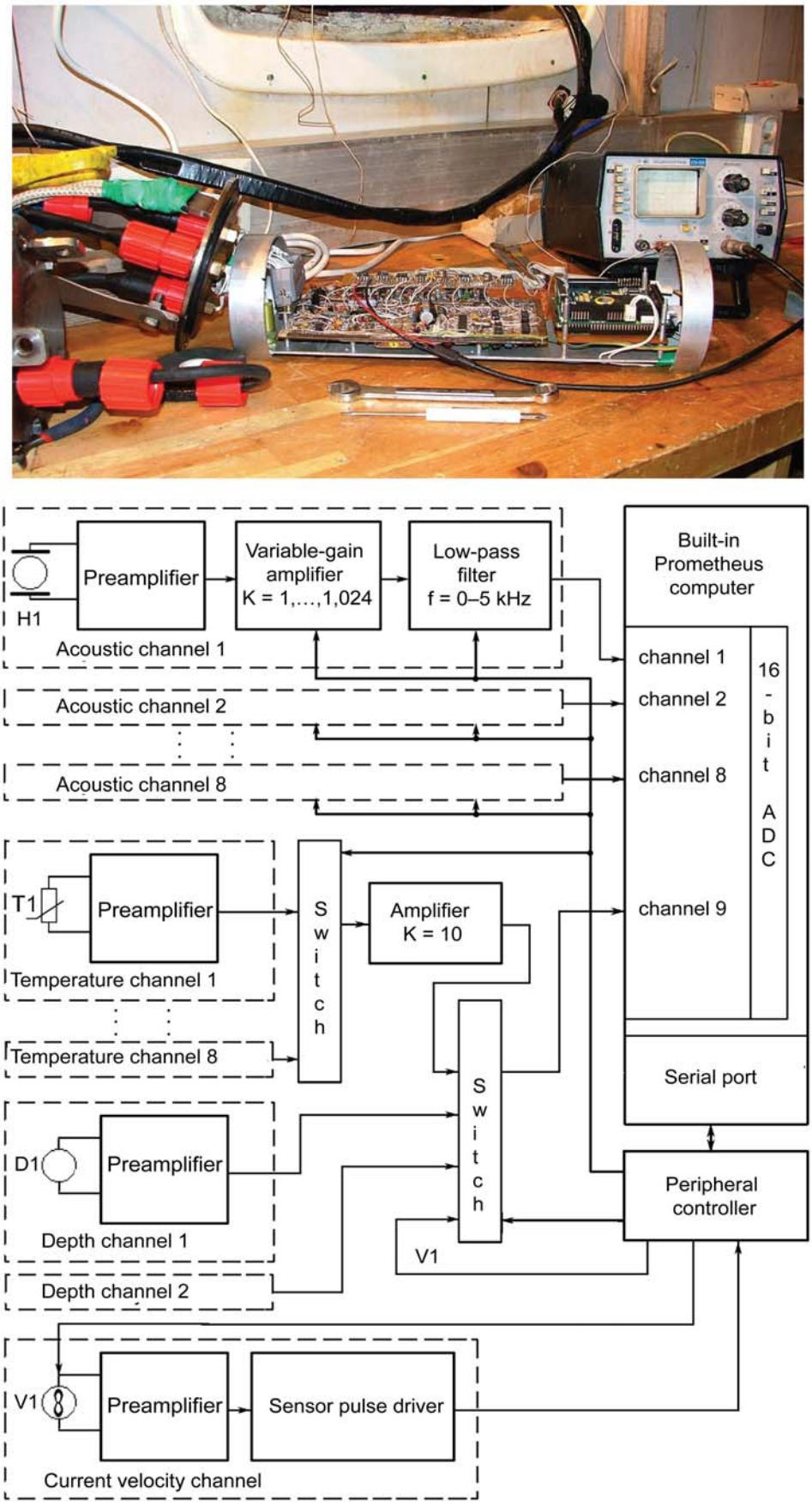

Figure 2.12 – Photograph of the basic electronic components and a system schematic of the Mollusk-07 autonomous vertical acoustic and hydrologic recording system.

The acoustic signals are input to identical analog channels; a control program is used to modify the system parameters to fulfill the goals of the experiment. The gain factors (K) and the low frequency cutoff (f_0) of the eighth-order low-pass elliptical filter are set prior to deployment. After amplification and low-pass filtering, the analog voltages corresponding to the acoustic signals measured by the eight hydrophones are input to the analog input sub-module of the Prometheus board.

Multiplexing and digitization of the acoustic signals, as well as buffered recording to the hard drive, are also controlled by this board. The system can record frequencies up to 5 kHz. A single hydrophone and preamplifier from the Mollusk-07 was calibrated up to 5 kHz at the All-Russian Scientific Research Institute of Physico-technical and Radio-technical Measurements (VNIIFTRI) in 2007.

Figures 2.13 and 2.14 show the results of the instrument testing of the acoustic channels of the Mollusk-07. Dynamic range measurements (Figure 2.14) were made using a dummy equivalent hydrophone. The preamplifier electronics in the shielded housing of the equivalent hydrophone is identical to that of the corresponding hydrophone except that a piezoceramic capacitor with the same capacitance as the hydrophone piezoceramics is connected to its input.

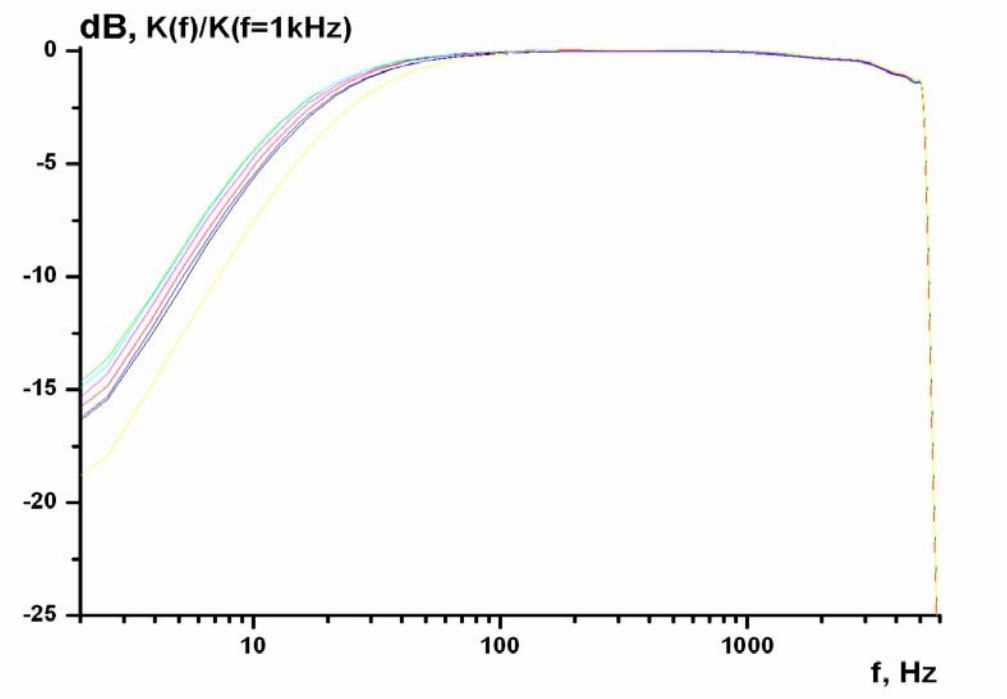

Figure 2.13 – Frequency response of the Mollusk-07 analog acoustic channels.

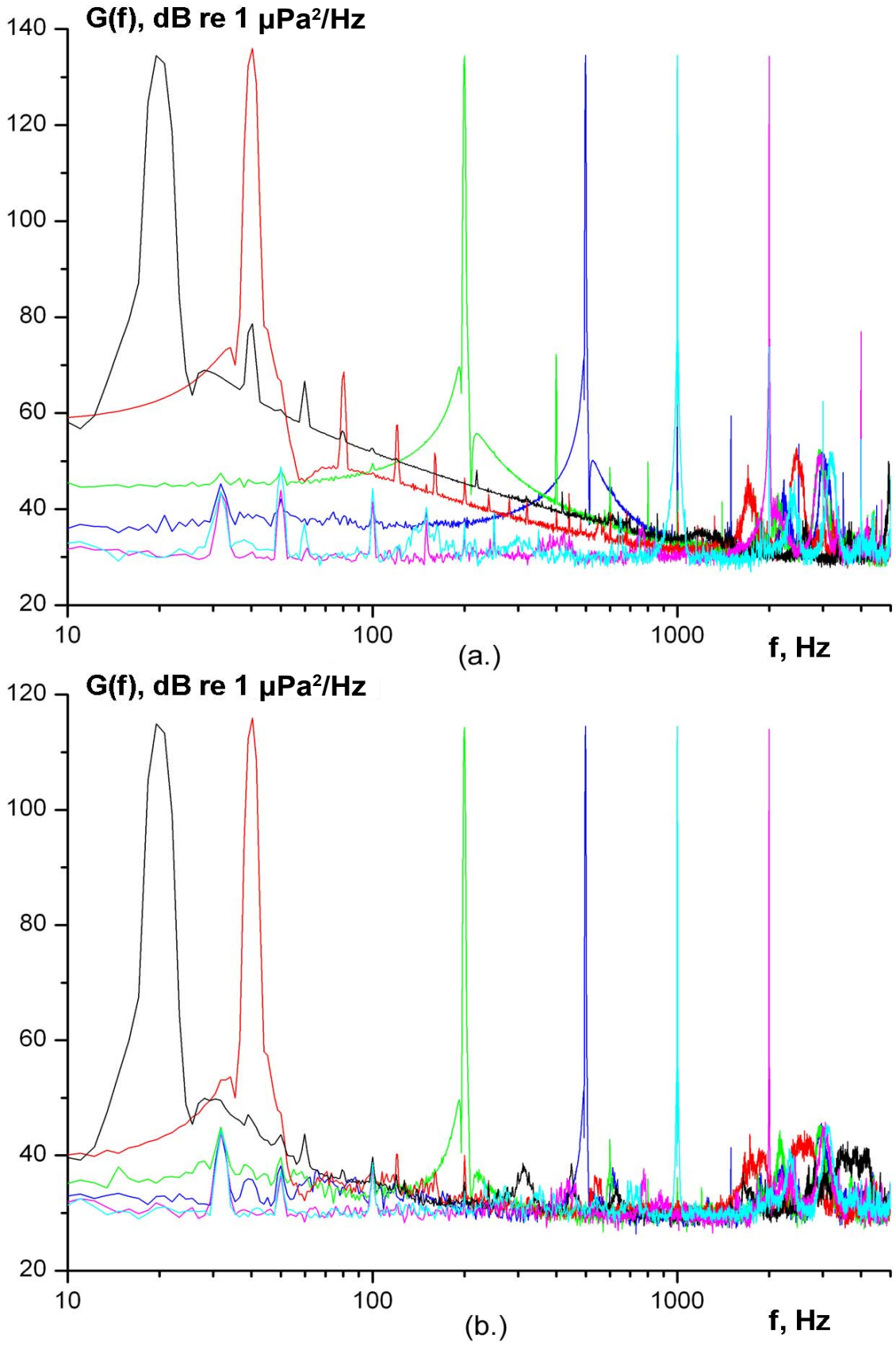

Figure 2.14 - Spectral results of the dynamic range test for the acoustic channels of the Mollusk-07 for input signals with a level of (a) 135 dB; and (b) 115 dB.

Figure 2.14 shows that when the signal levels are close to the maximum input level for this hydrophone (10 Pa); the dynamic range of the analog channel for acoustic signals is limited by the second harmonic at a level of -70 dB; and for weaker signals, by the third harmonic at a level of -75 dB. To evaluate crosstalk between the acoustic channels a 1 kHz sinusoidal signal was input via the dummy hydrophone replacing the signal from hydrophone H.5; crossfeed between channels did not exceed –90 dB in this test.

The temperature sensors used in the Mollusk-07 are AD22100KT chips made by Analog Devices, Inc. These sensors have a integrated preamplifier that coverts temperatures in the range from -50 to +50 °C to voltages of +0.25 to +4.75 V. After multiplexing and amplification, a voltage corresponding to the temperature range from -5 to +25 °C is input to a 9-channel ADC. For the temperature range from -10 to +30 °C, the absolute error does not exceed 0.4 °C; this error can be reduced by calibrating the sensors. The ADC resolution is 153 μV, which, after compensating for the gain of the buffer amplifier, corresponds to an instantaneous temperature measurement accuracy of 0.00068 °C. Averaging reduces the effect of electrical noise and crossfeed on the instantaneous measurement. The temperature sensor sample interval is 160 ms, each of these values being the average of 40 samples of a signal sampled at 10.5 kHz.

The Mollusk-07 measures depth with two PDCR 1830 D hydrostatic pressure sensors manufactured by GE Druck (England), these sensors are located near the fourth and eighth hydrophones (Figure 1.5). The sensors are calibrated for depths from 0 m to 100 m, with an absolute depth accuracy of 0.1 m. The sensor is completely sealed; the housing and membrane being constructed from titanium; and the pressure module silicon. Experience has shown that the sensitivity and speed of the sensors are sufficient for recording variations in pressure caused by internal waves. Figure 2.15 shows synchronous variations in hydrostatic pressure at two depths recorded by the Mollusk-07's pressure sensors while deployed on the NE Sakhalin shelf.

On the voyage the Mollusk-07 hydrophones were cross-calibrated with GI-50 reference hydrophone No. 038 and the depth sensors with the Valeport SVXtra hydrologic sonde (Figure 2.16). To simplify the cross-calibration operation, the Mollusk-07 electronics were placed in a standard mini-AUAR housing.

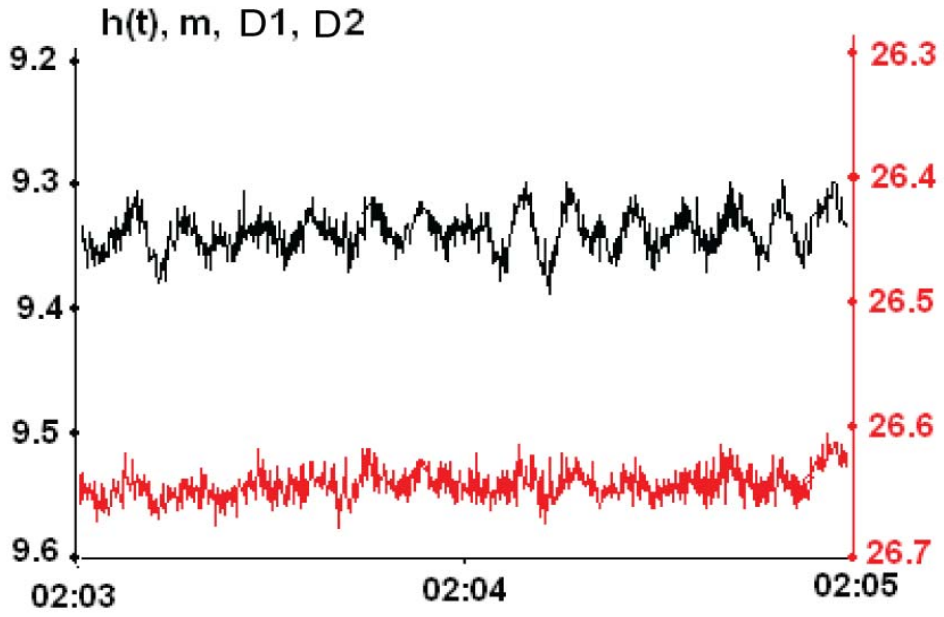

Figure 2.15 - Variations in hydrostatic pressure measured by the two Mollusk-07 depth sensors (Figure 2.11).

Figure 2.16 - Cross-calibration of the hydrophones and hydrostatic pressure sensors of the Mollusk-07 with GI-50 reference hydrophone No. 038 and Valeport SVXtra hydrologic sonde).

Figure 2.17 shows the cross-calibration results for the acoustic channels. Analysis of the cross-calibration data gives a less than 2 dB difference in the measured levels of the acoustic field for the frequency band from 10-1,000 Hz.

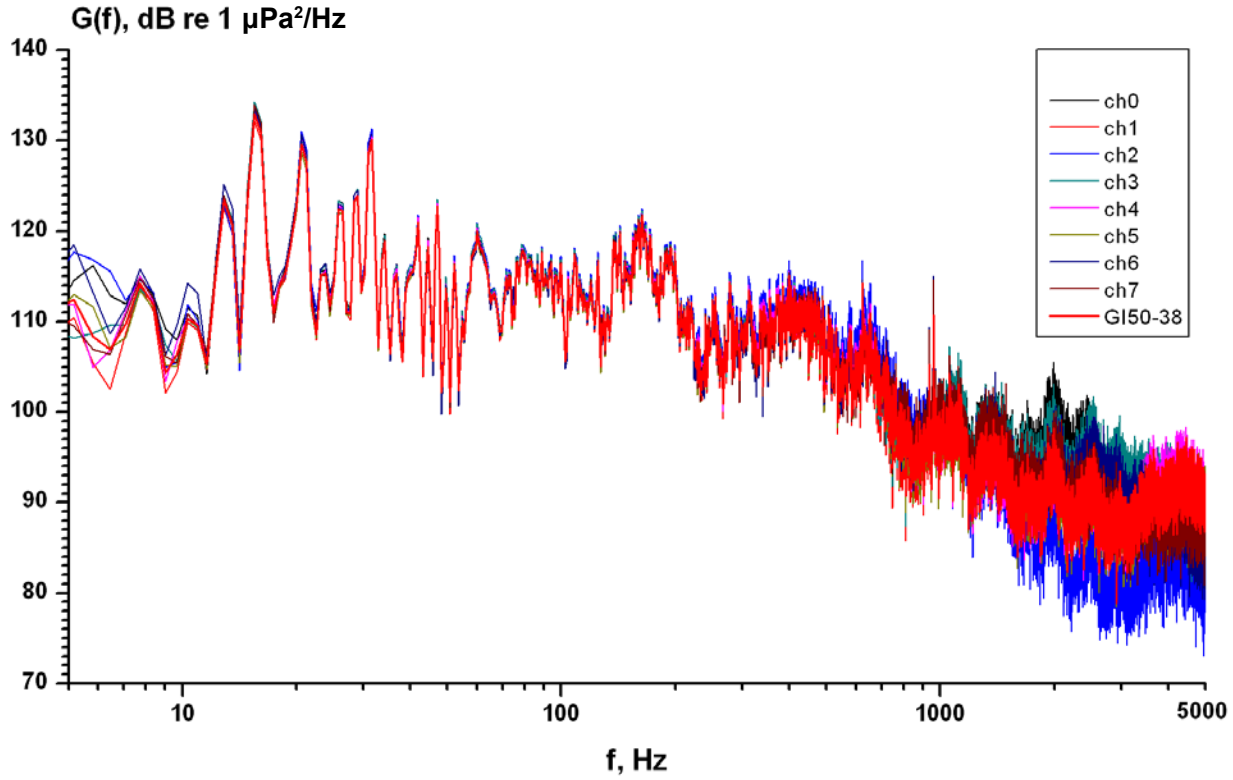

Figure 2.17 - Results of the cross-calibration of the Mollusk-07 hydrophones and GI-50 calibrated hydrophone No. 038.

Figure 2.18 gives the cross-calibration results for the eight temperature sensors of the Mollusk-07 and the temperature sensor of the Valeport SVXtra sonde. This figure shows that there is good agreement between the Mollusk-07 temperature sensors and that of the Valeport SVXtra sonde, and although they have a noticeably slower response time, they are suitable for their design objectives.

Figure 2.19 gives the cross-calibration results for the depth sensors, synchronous recordings of hydrostatic pressure were made with the Mollusk-07 pressure sensors and the Valeport SVXtra sonde at eight different depths, the vibration of the ship's hull can be clearly seen on the figure. The cross-calibration results showed good agreement, with the difference in depth readings for the Mollusk-07 sensors not exceeding 1 cm, and the difference from the SVXtra sonde depth sensor being no more than 5 cm, these values correspond to the actual position of the sensors during the cross-calibration (Figure 2.16).

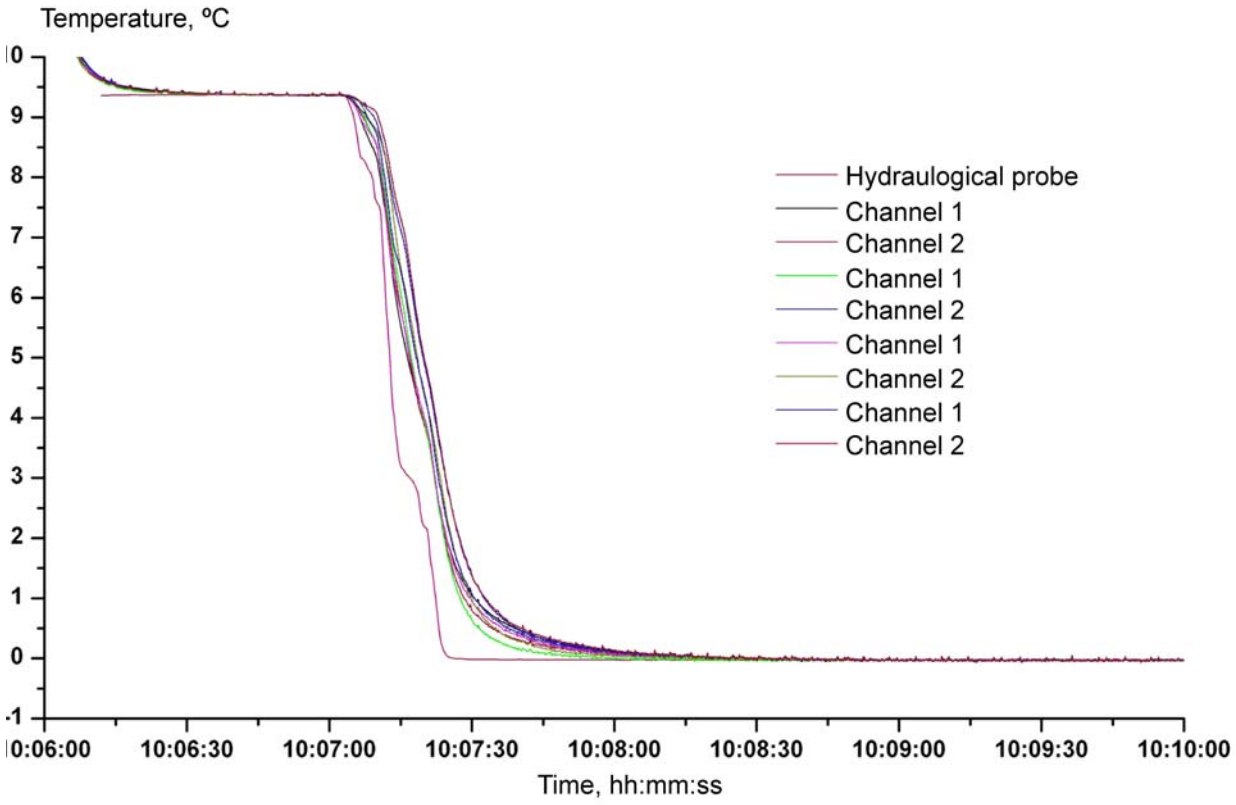

Figure 2.18 - Results of the cross-calibration of the Mollusk-07 temperature sensors with the Valeport SVXtra sonde temperature sensor.

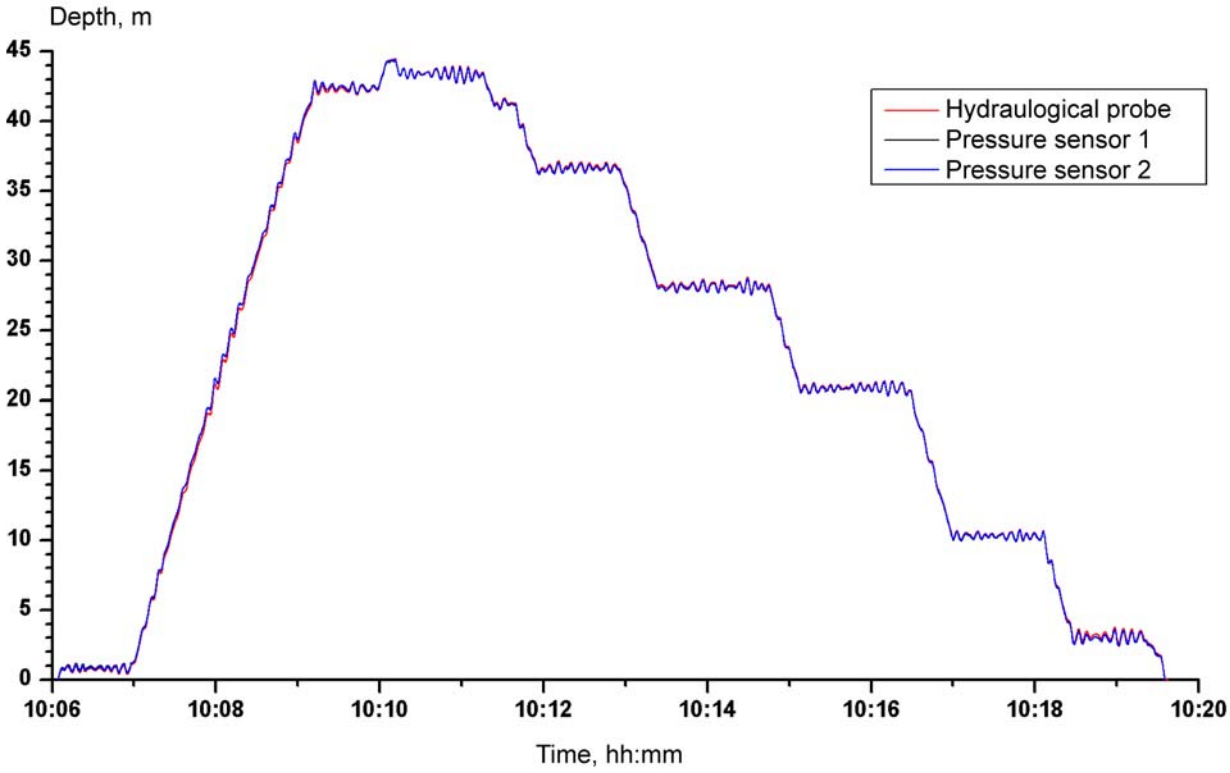

Figure 2.19 - Results of the cross-calibration of the two Mollusk-07 pressure sensors with the Valeport SVXtra sonde pressure sensor.

The endurance of the Mollusk-07 when powered by a battery compartment with two 65 ampere-hour batteries is at least seven days.

Figure 2.20 – Rapid reponse current velocity sensor.

For the last experiment conducted on the NE Sakhalin shelf and for a special experiment conducted in the Sea of Japan at the beginning of October 2007, the Mollusk-07 was additionally equipped with a current velocity sensor (Figure 2.20). The sensor operates on the change in resistance of the seawater in a gap in the sensor when the blade of a rotor passes through it. The sensor operates on alternating current, which is generated by a peripheral controller. After initial analog processing, the signal is sent in the form of voltage pulses, with frequency proportional to the current velocity, to an external interrupt input on the controller. The data is then converted to a format convenient for input, through one of the multiplexer inputs, to the 9-channel ADC Prometheus board; the data update time is 0.8 s. Measurements made with this sensor showed a correlation with short term variations in water temperature (Figure 2.21). This analysis indicates that the estimates of current velocity due to tides and the rotational motion of water particles in internal waves made by this sensor are satisfactory. POI is investigating ways to improve the accuracy of the sensor by adding an orientation sensor.

Figure 2.21 shows acoustic and hydrologic results of recorded by the Mollusk-07 in the Sea of Japan; these illustrate the type of data available using the Mollusk-07.

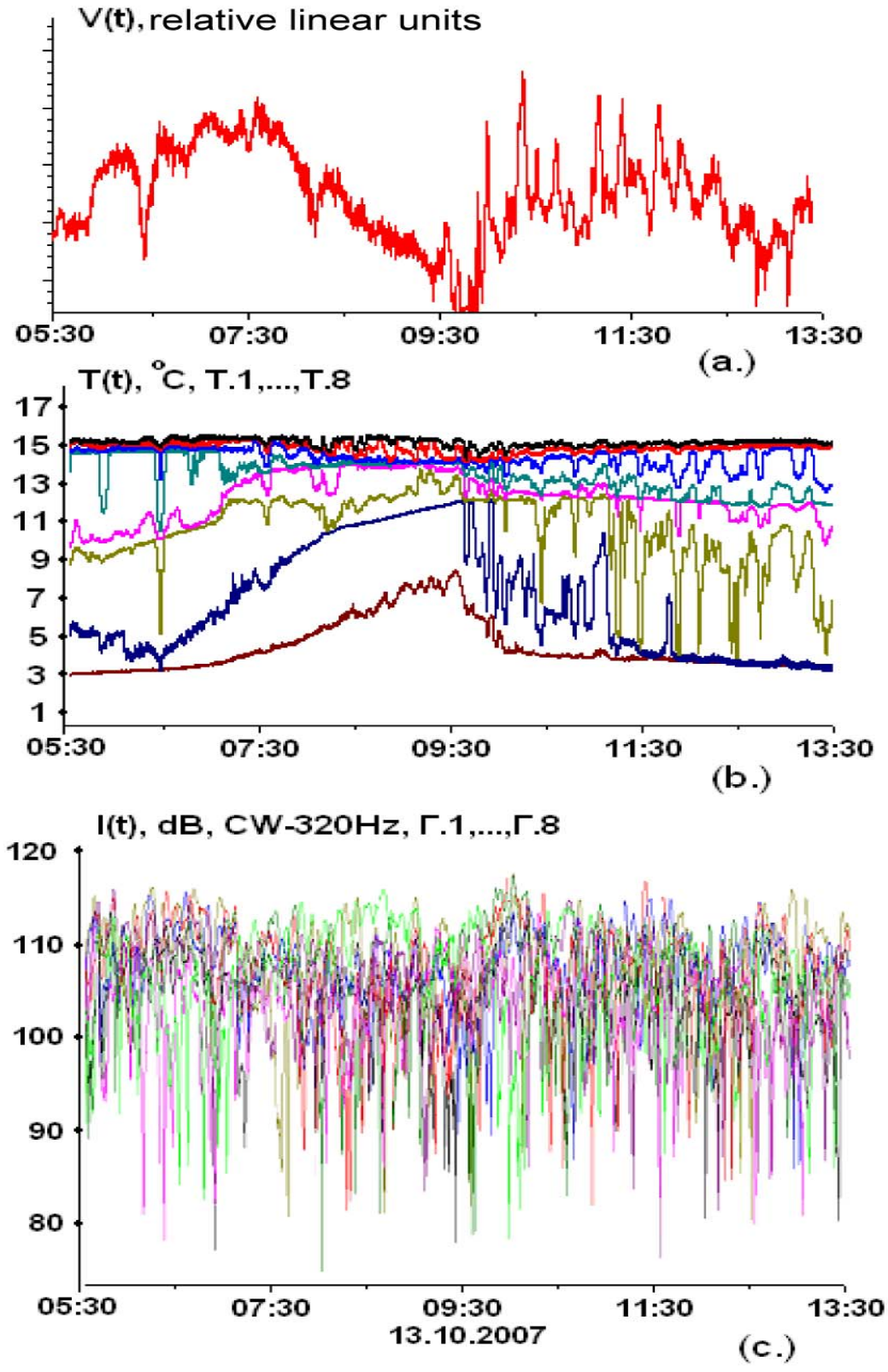

Figure 2.21 – Plot of: (a) current velocity; (b) temperature and (c) intensity of 320 Hz CW tonal signal measured synchronously by the Mollusk-07 in the Sea of Japan.

2.4 Low Frequency and High Frequency transducers and hydrological sonde

A low frequency (LF) resonant electromagnetic transducer (Figure 2.22) and high frequency (HF) piezoelectric broadband transducer (Figure 2.23) deployed from the *Professor Bogorov* were used for sound propagation and TL studies at frequencies from 15 Hz -15 kHz. The acoustic level of signals generated by these transducers was monitored using a calibrated hydrophone and recorded on the *Professor Bogorov*[29].

Figure 2.22 - Low frequency resonance transducer and calibrated monitor hydrophone.

[29] While the transducers were operating the acoustic signal levels were measured using a calibrated hydrophone located 1 m away from the transducer.

The LF transducer used in 2007 has slight structural differences from the one used in 2003-2006 [Borisov et al., 2007]. The rigidity of the piston suspension was increased, enabling the zeroing induction circuit to be removed and power to be supplied through a two-wire cable. This modification also decreased the effect of fluctuations in the hydrostatic pressure within the body of the transducer, caused by the rolling of the vessel, on the amplitude of the radiated signal. When the LF resonance transducer was deployed at a depth of 10 m from the anchored *Professor Bogorov* in water 25 m deep, the level of the 27 Hz acoustic signal generated by the transducer was ~180 dB re 1 $\mu Pa^2/Hz$ at 1 m distance from the transducer.

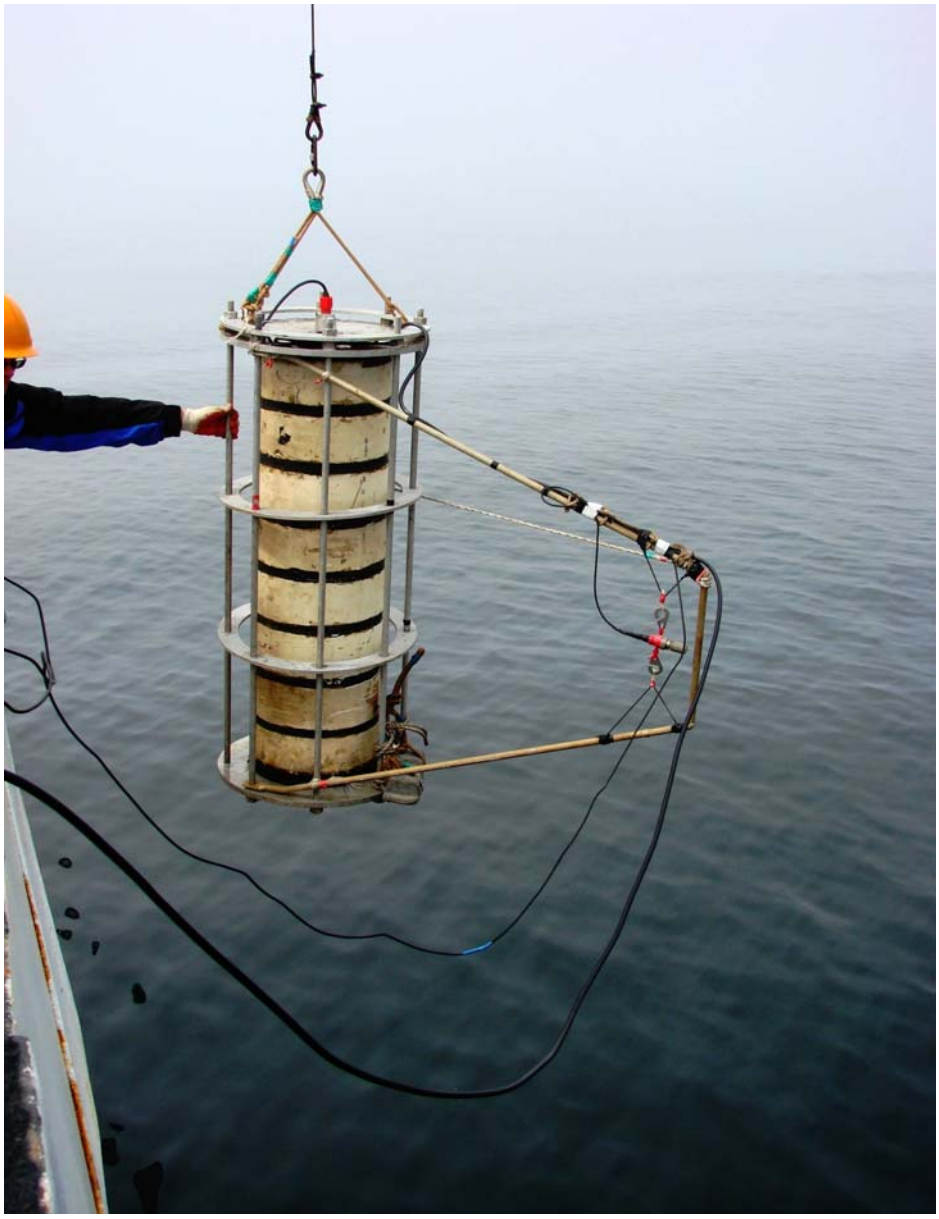

Figure 2.23 - High frequency broadband piezoelectric transducer and calibrated monitor hydrophone.

The 2007 expedition used a new, more powerful HF broadband piezoelectric (ceramic) transducer, this transducer is cylindrical[30] and consists of eight piezoelectric rings connected in parallel coated with a composite material and sealed at the ends with metal flanges (Figure 2.23). To prevent the transducer being damaged from impacts against the side of the vessel while being deployed and recovered, a reinforced cage was manufactured around the transducer. A calibrated reference hydrophone was suspended by rubber straps from a frame attached to the cage at a distance 1 m from the surface of the transducer. This attachment method controls the position of the reference hydrophone relative to the transducer in currents and as the ship rolls, significantly improving the accuracy of reference measurements of the source level of the transducer.

In 2007 a more powerful amplifier was used to power the transducer (Eurosound PWR-2000). The amplifier has an output voltage of 300 V, and a maximum power output of 5 kW. Tonal and swept FM signals were generated by an Istek GFG-3015 signal generator. This signal generator has an external control function through a standard RS-232 interface, allowing its operation to be programmed from a computer, enabling the signals coming from the reference hydrophones of the LF and HF transducers to be synchronously recorded. The program can automatically controls the operation of the generator without an operator, changing the frequency, amplitude and signal type according to a pre-programmed schedule.

Simultaneous operation of the two transducers when deployed from two different cranes and automation of the operation of the signal generator and power amplifier reduced the time taken on a source location by almost half when acquiring acoustic TL profiles.

In 2007, as in 2006 [Borisov et al., 2007], low-frequency (24–30 Hz) propagation and transmission loss was studied for onshore profiles and for profiles from the shore out to sea, using a land electromagnetic seismic resonance source that was developed and manufactured at POI. Ground vibrations are generated by a rectangular steel plate[31] buried horizontally in the ground to a depth of ~0.7 m (Figure 2.24(a)). The plate is excited by an electromagnetic source which is connected to it by two tubular stilts 1.5 m high. The upper

[30] Dimensions are diameter 60 cm, height 150 cm, weight ~100 kg in air, and ~15 kg in water.
[31] Plate size 2.2 by 1 m, 8 mm thick, weight 80 kg,

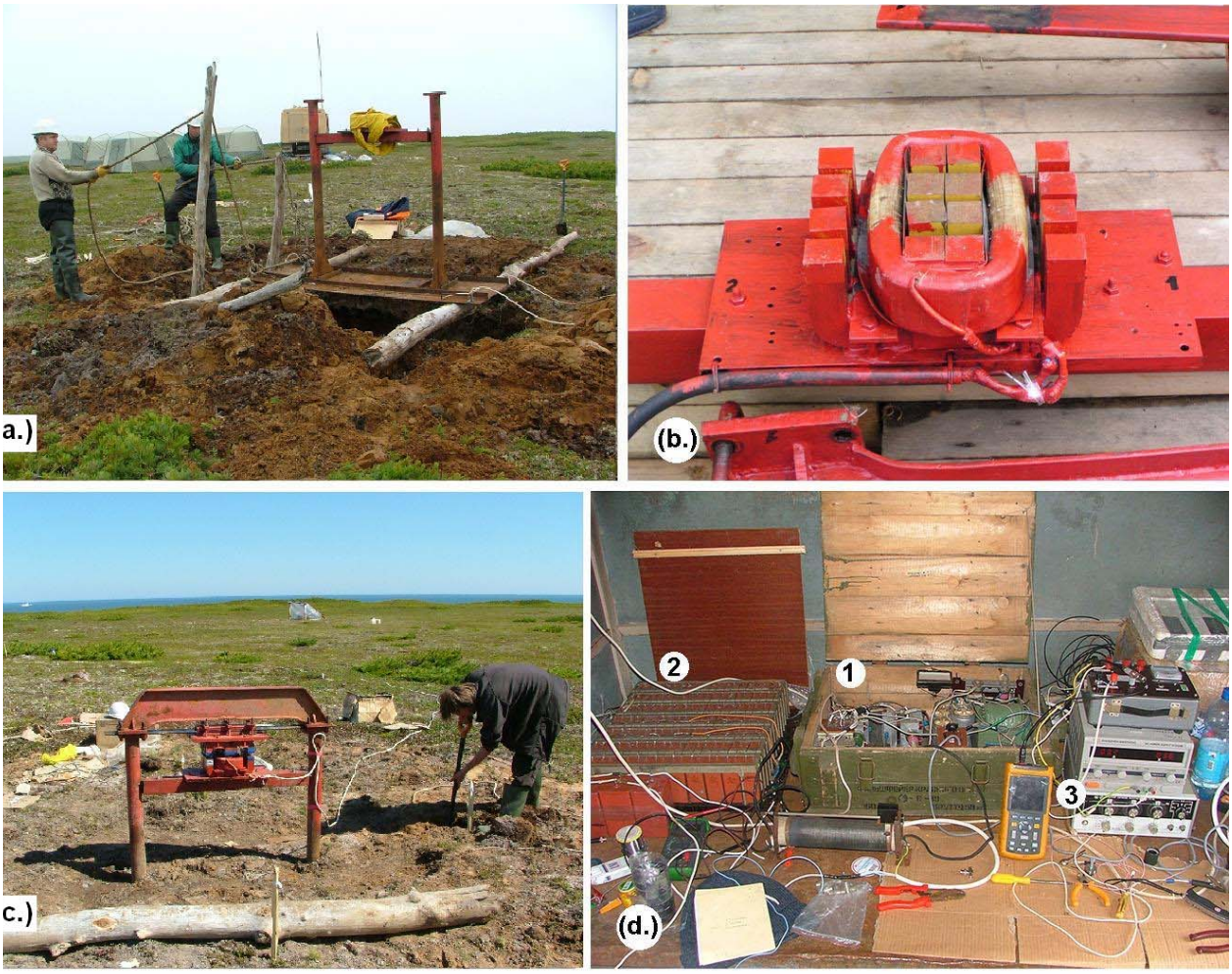

Figure 2.18 – Low frequency resonant land vibratory source: (a) Steel plate with stilts; (b) Lower core of the electromagnet with inductance coil; (c) assembled source installed onshore; (d) electronic devices supporting the operation of the source: (1) Bridge thyristor inverter; (2) Capacitor unit; (3) G3-118 master oscillator.

core of the electromagnet is connected to an elastic steel spring, the ends of which are attached to the upper part of the stilts. The lower core of the electromagnet, with the coil (Figure 2.24(b)), is mounted on a horizontal beam supported between the stilts. The weight of the upper core (35 kg), together with the elasticity of the spring, forms a mechanical vibrator with a resonant frequency of ~27 Hz. The resonant frequency of the system can be varied during assembly by inserting spacers into the attachment points to the stilts. When a voltage is applied to the electromagnet, the upper core vibrates vertically, and the force at the spring's attachment points is transmitted through the stilts to the steel plate. At the resonant frequency of ~27 Hz, if the electromagnet coil is excited by an AC voltage of 100 V, the amplitude of the vibration in the upper core reaches 10 mm, and the force transmitted to the plate is ~2 metric tons.

A bridge thyristor inverter (Figure 2.24(d)), similar to the inverter used in the marine LF transducer, is used to power the electromagnet. The inductance of the coil of the electromagnet and the capacitance of the isolation capacitor form a series oscillatory circuit, the electrical resonance frequency of which coincides with the mechanical resonance of the vibrator. When the power supply delivers 100 V from the inverter, the current consumed by the vibrator is 15 A at the mechanical resonance frequency. The power for the source and associated electronic equipment was provided by a 2 kW portable generator.

Figure 2.25 - Sensors used to record low-frequency vibrations on land: (a) A0515 geophone (1), G-33 hydrophone (2); (b) Self-contained field recording system based on TASCAM DA-P1 digital tape recorder (3).

A G3-118 precision oscillator serves as the master oscillator for the excitation frequency. Low-frequency energy generated by both the marine and land LF transducers was recorded on land using a G-33 calibrated hydrophone placed in a water-filled plastic container buried in the ground[32] and a A0515 low-frequency, single-component geophone which measured velocity (V_z). The geophone was manufactured by CJSC Geoakustika[33] (Figure 2.25).

Signals from the hydrophone and geophone, as well as signals transmitted by the digital sonobuoys, were acquired using a special recording unit (Figure 2.26). This unit was based on National Instruments equipment, and was housed in a power chassis[34]. The output from

[32] One of these G-33 reference hydrophones, with a sensitivity of 10 mV/Pa, was placed at a distance of 1 m from the center of the plate to measure the sound pressure level generated by the source.
[33] This geophone has the following basic specifications: Sensitivity (at 4 Hz): 72 $V \cdot s^2 m^{-1}$; frequency range: 0.1 to 100 Hz; maximum spectral error in the frequency range 0.25 to 50 Hz: 1 dB; maximum measurable sinusoidal acceleration: 0.02 m/s^2.
[34] National Instruments SCXI-1000DC.

each active sensor or radio receiver was connected to an eight channel terminal block[35] with BNC connectors and from there input to a low pass filter module[36] containing eight preamplifiers and elliptic filters with a user-selectable filter response. These filters were used to limit the frequency range of the input signal to within the Nyquist frequency for the sample rate of the Analog to Digital Converter (ADC). The data from all sensors or active receivers was then simultaneously converted to digital data by a multi-channel gain ranging 16 bit ADC data acquisition card[37] housed in a notebook computer. A two-channel digital tape recorder (TEAC TASCAM DA-P1)[38] was used to record signals from the hydrophone and the geophone at greater distances from the source point (Figure 2.25(b)).

Figure 2.26 - Field recording system based on National Instruments equipment.

[35] National Instruments SCXI-1305.
[36] National Instruments SCXI-1342.
[37] National instruments DAQCard-6036E.
[38] This unit records analog signals on magnetic tape in a digital format and has the following basic specifications: Analog-to-digital conversion: 16-bit line; sampling frequency: 48 kHz or 44.1 kHz; frequency range: 20 Hz to 20 kHz; variation in frequency response: 0.5 dB maximum; minimum signal-to-noise ratio: 90 dB; minimum dynamic range: 90 dB; Harmonic distortion: <0.007 %; crosstalk: maximum -85 dB (at 1 kHz).

Calibration with empirical TL data is used to enhance numerical modeling along the TL profiles. To calibrate the model along an acoustic profile, the bathymetry and hydrological characteristics (velocity, temperature and salinity) of the water layer along the profile must be known. Thus, to complement the TL measurements, the bathymetric profile was obtained using the ship's echo sounder and hydrological data was acquired using a hydrological sonde (Figure 2.27). The sonde is powered by a set of D cell batteries, providing approximately 180 hours of continuous operation. 7,200 km of bathymetric data and 634 vertical hydrologic profiles were acquired in 2007.

Figure 2.27 - SVXtra Hydrologic sonde being deployed from the *Professor Bogorov*.

3 Real-Time Acoustic Data Acquisition

This chapter discusses the implementation of a real-time acoustic monitoring program, developed to monitor anthropogenic sound generated by SEIC offshore construction operations[39]. The sections below contain a description of the objectives and methodology for the real-time acoustic monitoring program, plots of the real-time acoustic data recorded in the field and a comparison of the 10 Hz to 5 kHz transmitted data with the data over the same frequency range, recorded on the T-AUARs, and processed after the field season.

3.1 Objectives of real-time acoustic monitoring program

The objective of the real-time acoustic monitoring program was to monitor any sound propagating from the operations associated with the top-sides installation and engineering work at the PA-B and Molikpaq platforms. This real-time monitoring was designed to measure the sound from construction operations so as to minimize the impact on the western gray whale population. This program had three main goals:

1. To record the acoustic field at four monitoring stations located at the eastern edge of the Piltun feeding area[40] while construction and development activities were underway nearby. These broad band acoustic records will be used to identify any anthropogenic sounds associated with SEIC offshore construction activities. This data will be correlated with concurrent western gray whale behavioral and distribution studies to further understand any reaction to these sounds and to assist in the design and planning of future offshore development and production operations.
2. To determine the degree to which the received sound levels at monitoring points at the outer edge of the Piltun feeding area agree with predicted sound levels. These predictions were made during the design and planning phase of offshore construction activities, using an acoustic model calibrated with TL measurements [SEIC, 2006][1];
3. To ensure that sound levels reaching the feeding ground are below SEICs predefined action criteria [SEIC, 2006][2] and take appropriate mitigation measures if necessary;

3.2 Methodology for the real-time acoustic monitoring

In order to monitor the acoustic field on the eastern edge of the Piltun feeding area, a radio receiving station was set up at Piltun lighthouse (Figure 1.5). This station received radio transmissions from a total of four acoustic monitoring T-AUARs (and sonobuoys) deployed

[39] The real-time received sound levels at the edge of the feeding area were considered to be the most reliable and quantifiable indicator of disturbance, as they are independent of environmental conditions such as reduced visibility and high sea states. However, field data of gray whale behavior, distribution and abundance were also considered important in determining the potential impact on a whale on a near real time basis. For this reason daily and weekly maps of whale distribution were generated and evaluated in an effort to assess real-time impacts, bearing in mind the high variability and other limitations of these data. Also, close communications between the biological and acoustic teams were established, so as to obtain feedback on whale behavior and distribution and correlate it with data on received sound levels.

at the locations shown on Figure 3.1 and Table 3.1. The sound levels recorded by the monitoring equipment and transmitted to the Piltun lighthouse radio station were monitored 24 hours a day. The data was received and evaluated in near real-time to ensure that the sound levels at the outer edge of the Piltun feeding area did not exceed the SEIC real-time action criteria agreed before the start of the construction season[41].

The operational required the four members of the POI acoustic team to install the receiving equipment and prepare the monitoring station at Piltun lighthouse starting on 13 June. The ice conditions this early in the season precluded the deployment of acoustic equipment at the edge of the Piltun feeding area until 22 June. Due to mechanical problems the research vessel *Professor Bogorov*, the main platform for the deployment and maintenance of the AUARs and sonobuoys, was delayed in Vladivostok. The initial deployment of two analog sonobuoys with double battery packs at the monitoring stations Piltun and Odoptu-PA-B was made on 22 June from the crew change vessel *Miss Sybil*, the supply vessel *Neftegaz-51* deployed two T-AUARs at locations PA-B-20 and Molikpaq on 23 June, and two T-AUARs at locations PA-B-20[42] and Piltun on 3 July.

3.2.1 Locations of the monitoring stations

The locations of the acoustic stations used for the monitoring program are plotted in Figure 3.1 and their coordinates are given in Table 3.1. Station PA-B-20 (T-AUAR) was closest to the construction activity around the PA-B CGBS and was located to record the highest sound levels generated by these operations. Monitor stations Odoptu-PA-B, Piltun and Molikpaq (T-AUAR) were deployed to monitor sounds generated from other development activities (e.g. near Molikpaq).

3.2.2 Real-time monitoring equipment

The T-AUARs and analog sonobuoys (ASB) were both secured to the sea floor using anchors; data from a stationary hydrophone on the sea floor was connected to radio transmitters in a surface float. The main features of these systems were:

- **T-AUAR**: These are radio-enabled AUARs and are capable of both continuously recording full bandwidth (1 Hz to 15 kHz) acoustic data on the hard drive and

[40] These broad band acoustic recordings will be as continuous as operationally feasible during the construction season.
[41] SEIC representatives were in communication with both the POI Acoustics team at Piltun lighthouse and the construction operations to ensure that the action criteria were maintained.
[42] Two T-AUARs were placed at monitoring location PA-B-20 to ensure continuity and data integrity at this station, which was the closest to the PA-B topsides installation and therefore where the highest construction noise level was expected.

transmitting analog data (bandwidth 10 Hz to 5 kHz) on a pre-programmed schedule to the radio station at Piltun lighthouse. The transmission schedule was selected to optimize battery life; in 2007 data was transmitted continuously, and additional batteries were installed into the T-AUARs, thus increasing the longevity of continuous recording and transmission to 18 days.

- **Analog sonobuoy:** These sonobuoys have no on-board storage capabilities; they transmit analog data (bandwidth 10 Hz to 5 kHz) continuously to the radio station at Piltun lighthouse.

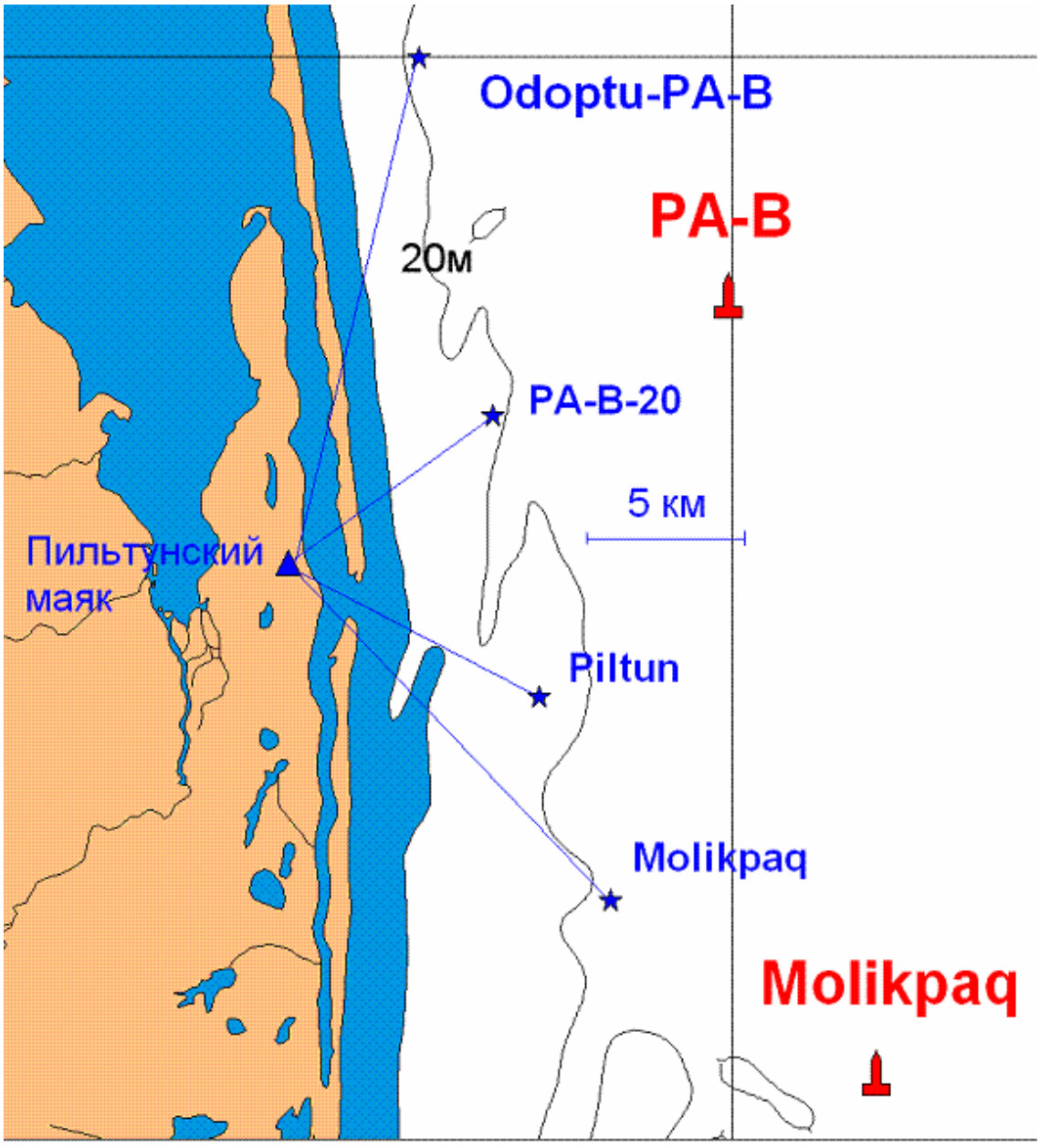

Figure 3.1 - Map of the monitor station locations as well as the PA-A (Molikpaq) and PA-B platforms. The red dots are T-AUAR stations Odoptu-PA-B, PA-B-20, Piltun, and Molikpaq.

Table 3.1 - Locations of the real-time monitoring stations.

Station	Latitude	Longitude
ODOPTU-PA-B	53°00'00"	143°21'18"
PA-B-20	52°54'04"	143°23'22"
PILTUN	52°49'19"	143°24'54"
Molikpaq	52°45'22"	143°25'04"

Use of these two recording systems provided the following primary benefits:

- Analog sonobuoys provided continuous real-time acoustic data that could be used for detailed real-time analysis during the critical construction periods. They were also used to complement the data transmission when a T-AUAR was being replenished.
- T-AUARs record nearly continuous acoustic data on its hard drive; this is not subject to radio system noise and interference. This broader bandwidth data is available for post processing after T-AUAR retrieval, and to satisfy the third goal of the acoustic monitoring program.

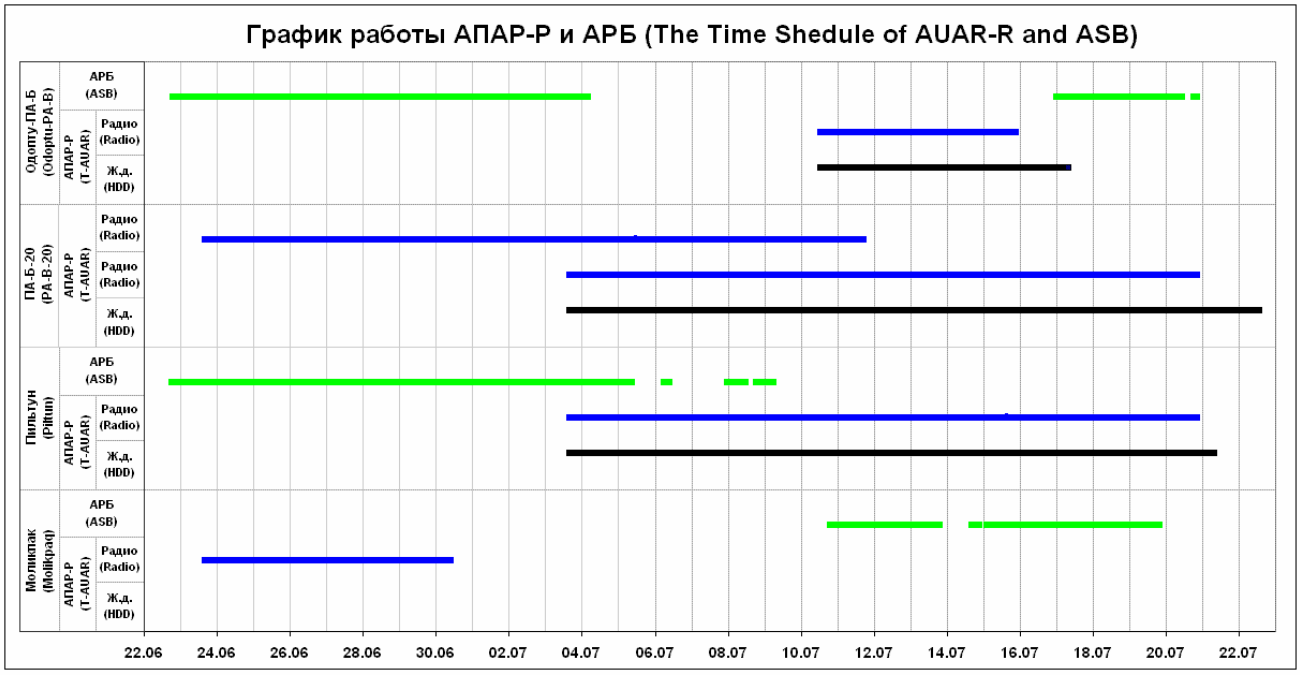

Figure 3.2 - Schedule of real-time construction monitoring in 2007.

Figure 3.2 is a graphic that displays the schedule of sound monitoring at four monitoring stations. After 22 July the T-AUARs were converted to AUARs and continued to record until the end of the season without transmitting the data.

3.3 Comparison of real-time and post processed sound levels

As a quality control check the data recorded on the hard disk of the four T-AUARs was compared to the data transmitted to the Piltun lighthouse radio station. Since the data received at Piltun lighthouse and the data on the AUAR were recorded using equipment that had been calibrated to an absolute acoustic standard the data should be almost identical. There were expected to be small differences between the two data sets due to:

- The data recorded on the AUAR was not subject to the radio system noise and interference that is present on the data transmitted from the T-AUAR and received at Piltun lighthouse. Since the dynamic range of the radio channel is approximately 35 dB and the system gain was set to record sound pressure levels of up to 140 dB re 1 $\mu Pa^2/Hz$, sound pressure levels below 105 dB re 1 $\mu Pa^2/Hz$ would not be correctly recorded. Also sound pressure levels above 140 dB re 1 $\mu Pa^2/Hz$ would be clipped while the AUAR hard drive can record sound pressure levels of up to 154 dB re 1 $\mu Pa^2/Hz$ without distortion. The dynamic range of the analog radio-telemetry channel depends on the level of radio interference.
- Strong weather and currents can have a mechanical influence on the hydrophone and thus the data, generating spikes and high amplitude, low frequency flow noise. These can strongly bias the half-hour average power spectral density estimates as the maximum input level of the radio-telemetry channel is 14 dB lower than that of the T-AUAR hard drive. Consequently, the acoustic level recorded on the T-AUAR hard drive may exceed that recorded at Piltun lighthouse. A similar effect could also be observed when a vessel passes near the station. The data must therefore be quality controlled before comparison.
- The half-hour average acoustic level estimated when a vessel passes near the station may be higher when it is estimated using data recorded on the T-AUAR hard drive than when calculated from data transmitted over the radio channel if the T-AUAR stopped during the half-hour analysis interval to write data from the flash drive to the hard drive, while transmitting data continuously via the radio channel. Figure 3.3 illustrates this effect when the average acoustic level is estimated from 18:00-18:30 recorded on the T-AUAR hard drive; we are calculating it for only an 8-minute interval. So, if the noise level decreased significantly in the remaining 22 minutes (the vessel left), then, as can be see in Figure 3.3, the half-hourly sound pressure levels calculated from the data on the hard drive will be higher than those calculated from the data recorded at Piltun lighthouse.

Figures 3.4 to 3.7 display an analysis of the data acquired at the acoustic monitoring locations during the 2007 field season. Where possible the results compare the acoustic level (over the frequency range from 10 Hz to 5 kHz) recorded on the hard drive of the T-AUAR and that transmitted over the T-AUAR radio channel and recorded at Piltun lighthouse. The comparison between post-processed and real-time data has shown that the data received at Piltun lighthouse is a good representation of the sound levels recorded at

the monitoring stations during offshore construction. Differences were seen due to de-synchronization during analysis and the gaps in the disk data, but these differences did not substantially change the recorded and interpreted variations in the level of anthropogenic sound.

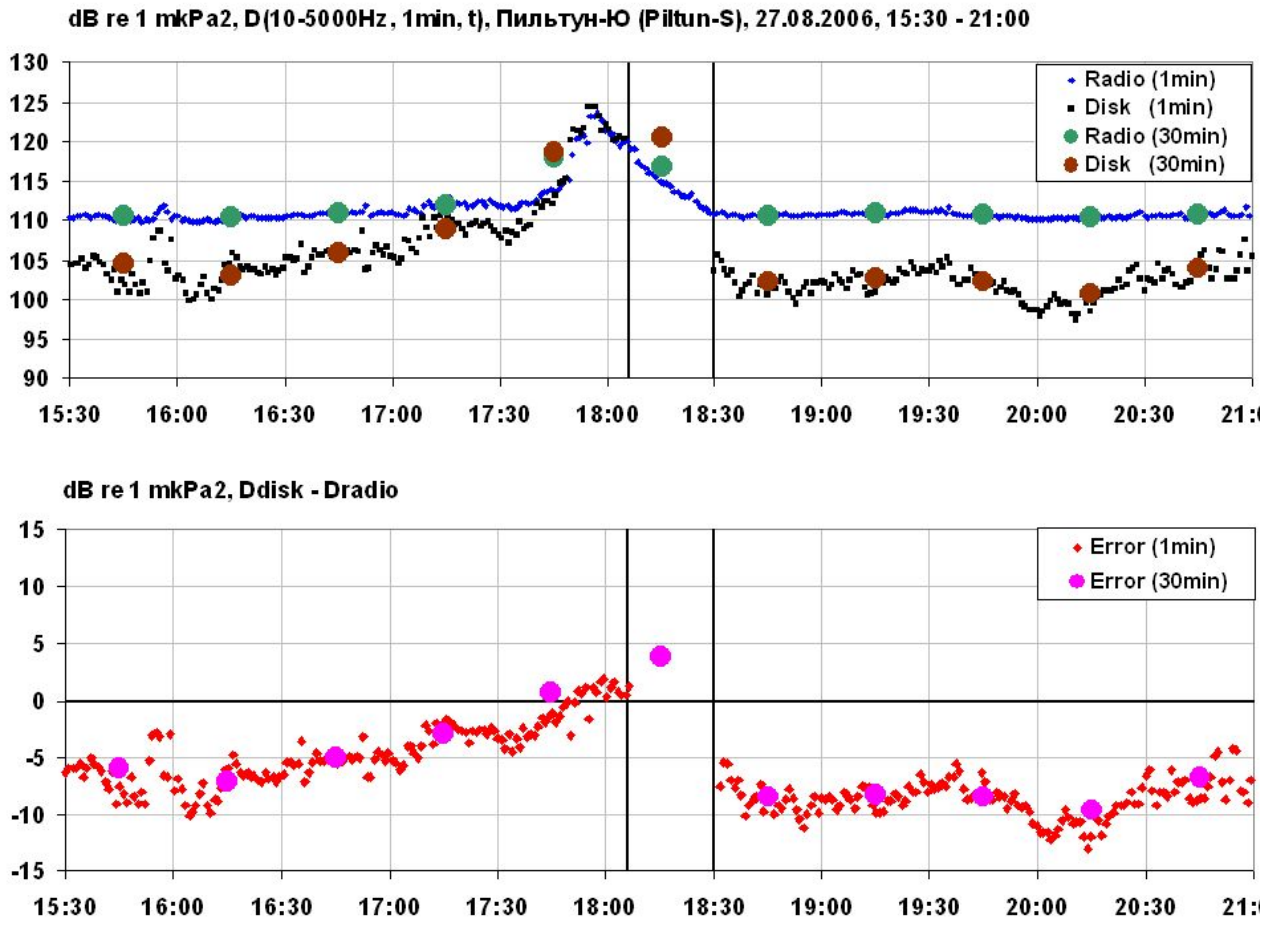

Figure 3.3 – Comparison of half-hour average acoustic levels obtained from data recorded on a T-AUAR hard drive and that transmitted by radio. The higher half-hour estimate between 18:00 and 18:30 was caused by a vessel passing by as the T-AUAR was stopped for 22 minutes (18:08 - 18:30) to write data from the flash drive to the hard drive, while the data were continuously transmitted over its radio channel.

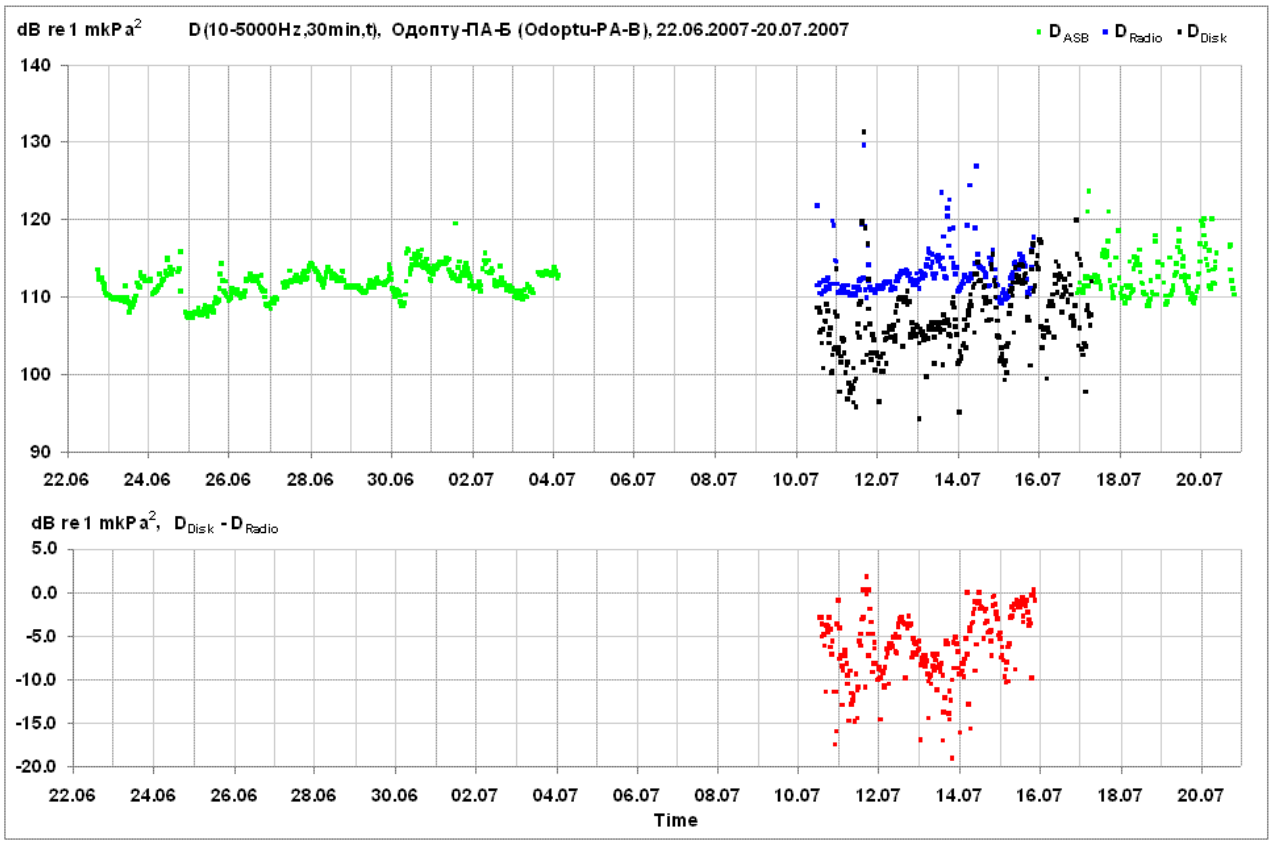

Figure 3.4 - Plot showing the average half-hour broadband (10 Hz to 5 kHz) received level transmitted by the Odoptu-PA-B T-AUAR and received at the Piltun lighthouse radio receiving station from 22 June to 20 July.

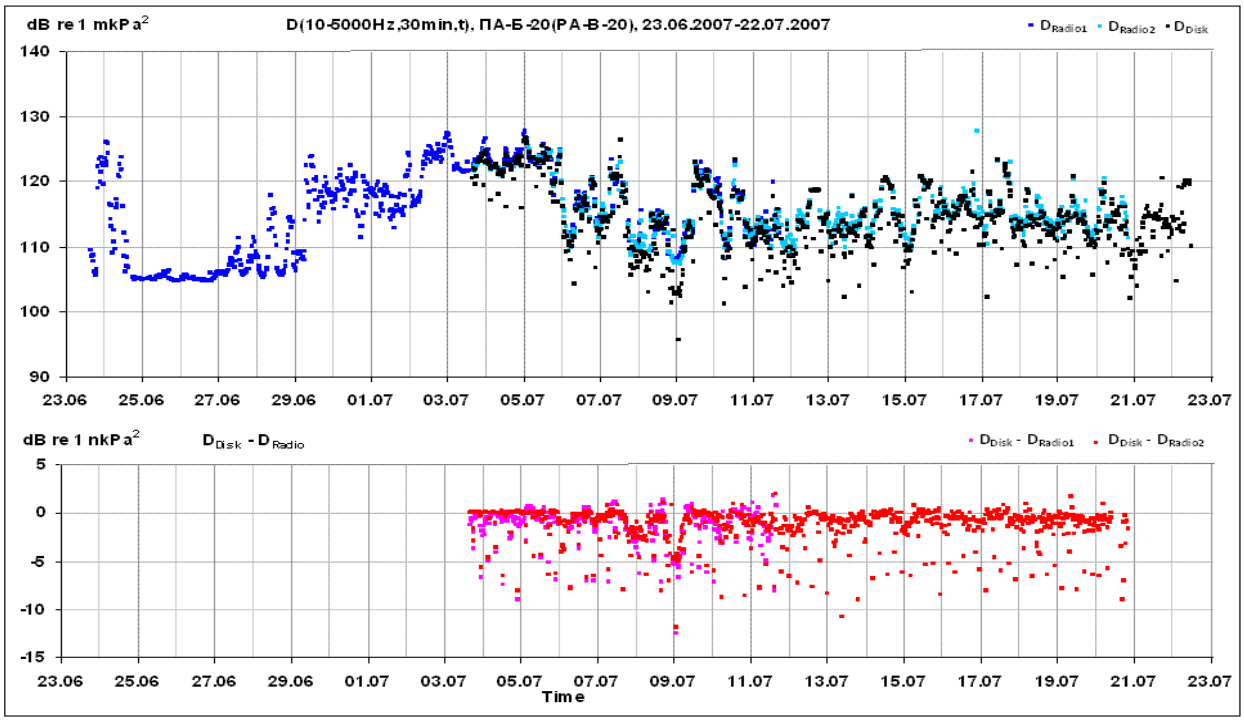

Figure 3.5 - Plot showing the average half-hour broadband (10 Hz to 5 kHz) received level transmitted by the PA-B-20 T-AUAR and received at the Piltun lighthouse radio receiving station from 23 June to 22 July.

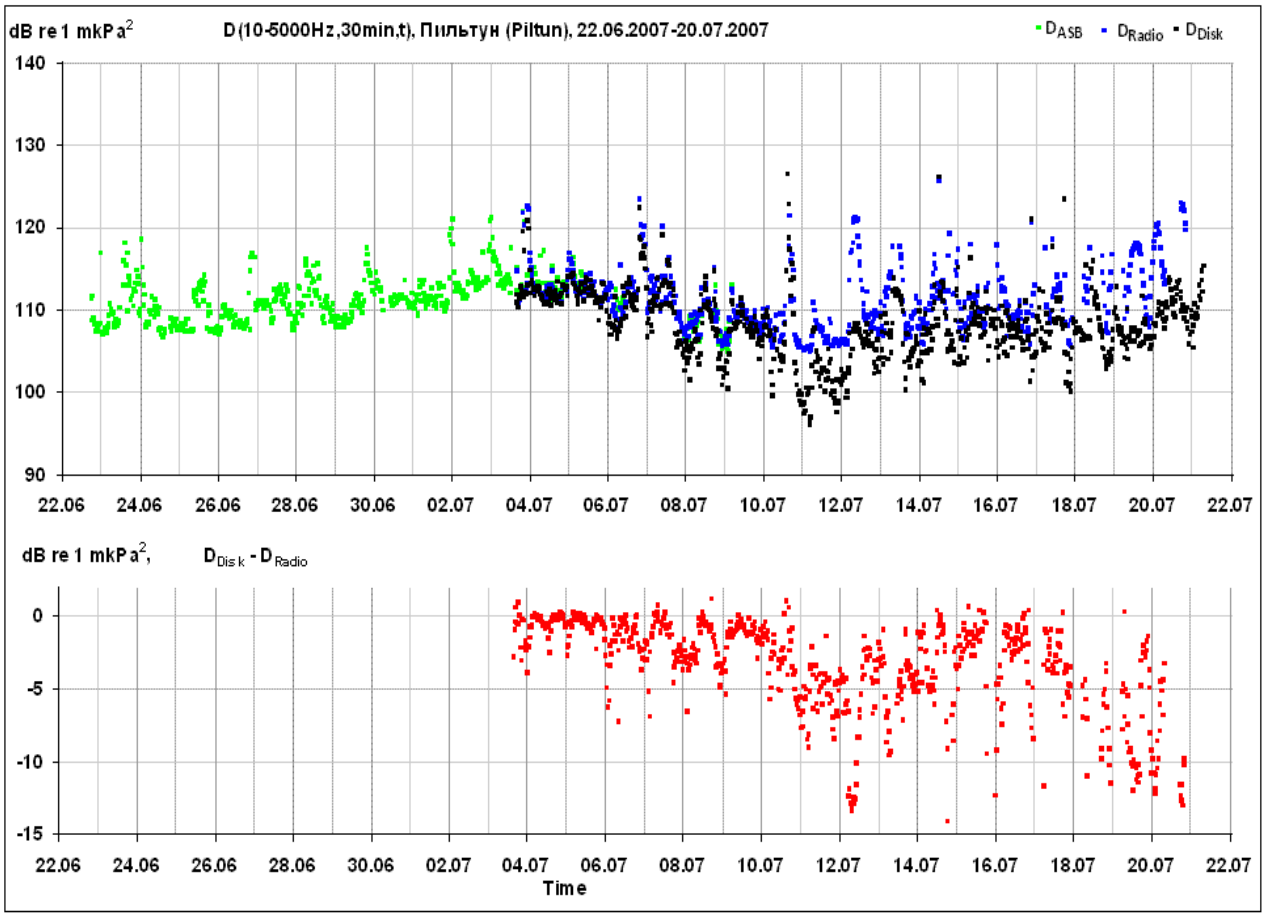

Figure 3.6 - Plot showing the average half-hour broadband (10 Hz to 5 kHz) received level transmitted by the Piltun T-AUAR and received at the Piltun lighthouse radio receiving station from 22 June to 20 July.

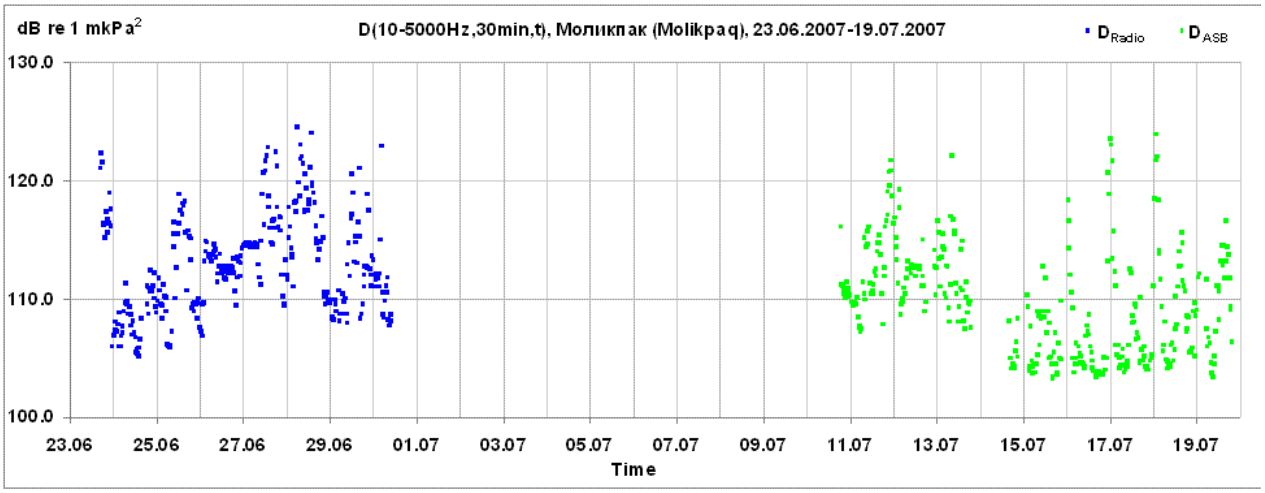

Figure 3.7 - Plot showing the average half-hour broadband (10 Hz to 5 kHz) received level transmitted by the Molikpaq T-AUAR and received at the Piltun lighthouse radio receiving station from 23 June to 19 July.

3.4 Analysis of the acoustic monitoring data

Figure 3.8 displays the average 30-minute integrated broad band (20 Hz to 5 kHz) sound level values for each of the four real-time monitoring stations, calculated from data recorded directly on the T-AUARs and analog sonobuoys in June and July 2007. Table 3.2 gives the start and end dates of offshore construction activities conducted by SEIC in 2007. The major part of the offshore construction in 2007 was related to installation of the PA-B platform topsides on the CGBS deployed in 2006, tying it to the subsea pipeline and engineering start-up of the platform.

Figure 3.8 demonstrates that broadband acoustic levels measured in real-time in the frequency range 10 Hz – 5 kHz during SEIC offshore construction at the four monitoring locations at the eastern edge of the Piltun feeding area did not exceed the thresholds defined by SEIC for triggering noise mitigation measures [Racca 2008].

Table 3.2 – Start and end dates for the Piltun area offshore construction phases monitored in real-time in 2007.

Phase	Offshore construction activity	Start	Finish
1*	**PA-B Float over:**		
	Installation barge preparation	29-jun	3-jul
	Topsides barge placement and ballasting	4-jul	5-jul
	Anchor retrieval	6-jul	8-jul
2	**Bristolia Accommodation Support Vessel (ASV) at PA-B:**		
	ASV arrival in field	29-jun	30-jun
	ASV run anchors at stand by position 1.5nm to SE from PA-B	29-jun	30-jun
	ASV ballast down at standby - 30th from 05:00hrs to 18:00hrs	30-jun	30-jun
	Flotel placement alongside the PA-B platform and ballasting	9-jul	11-jul
3	**PA-B Spool tie-in:**		
	Platform construction and PA-B Tie-in	13-jul	11-aug

* at the same time during phase 1 preliminary spool tie-in activities were taking place.

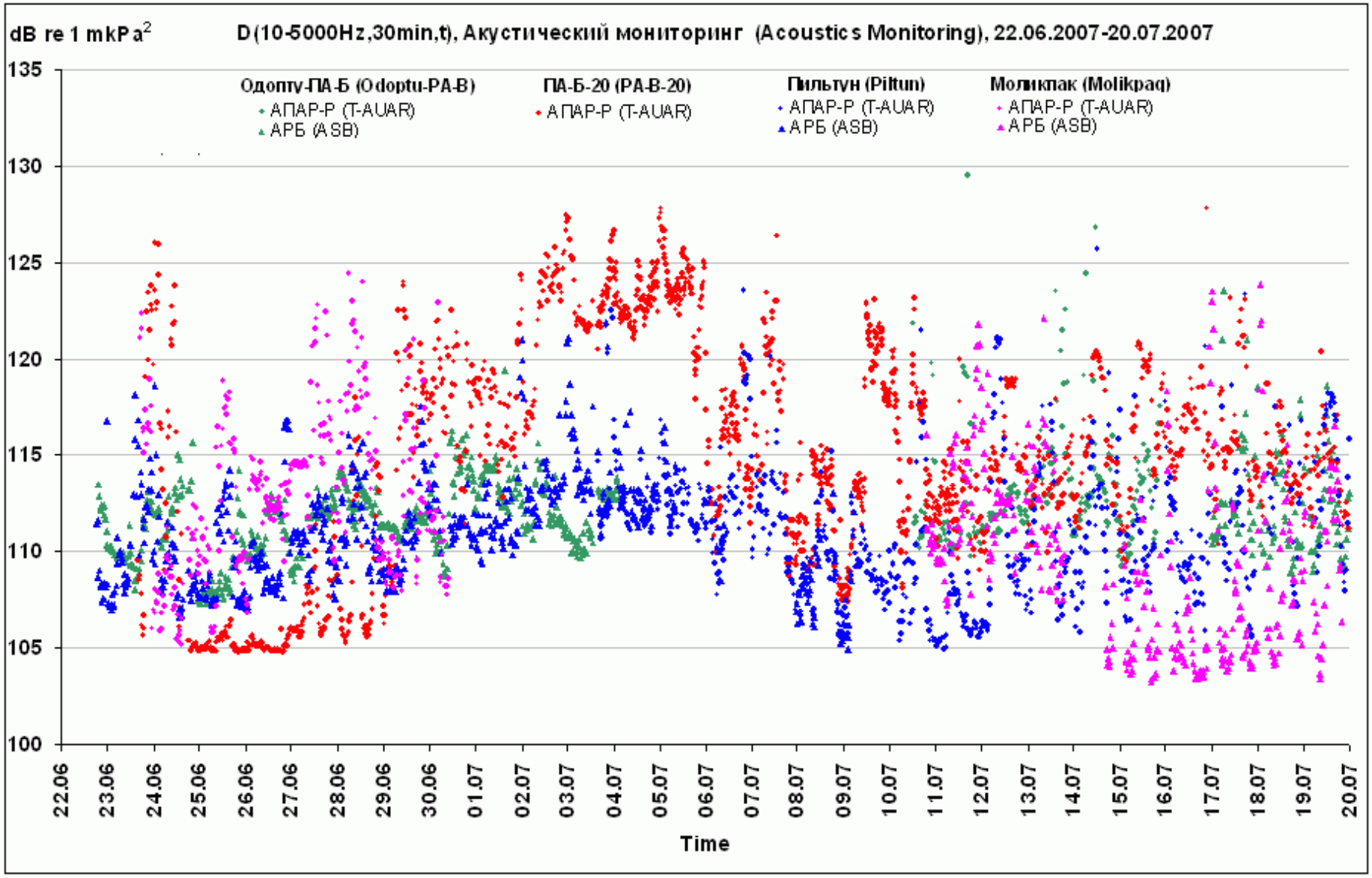

Figure 3.8 - Plot showing the average 30-minute broadband (10 Hz to 5 kHz) received level recorded on the disc of the four T-AUARs and two analog sonobuoys in June and July.

4 Impact of weather conditions on the ambient acoustic field of the NE Sakhalin shelf

This section analyzes the ambient noise measurements recorded in 2007 and discusses the variation in ambient noise with meteorological conditions and Sea State. In 2007, as in the previous two years, acoustic data was recorded using AUARs, and ambient noise data was acquired at monitoring stations across the area (Figure 1.13).

Previous reports have discussed the variation in ambient noise due to wind, surface waves and rain. For example, the broadband noise level near Chayvo rose by 12 dB when the sea state increased from 1 (calm) to 4 (moderate) [Borisov et. al. 2003]. A rainstorm with strong wind squalls pushed the ambient noise level an additional 16-18 dB higher. For frequencies above 2.5 kHz the spectral level of ambient noise recorded during a storm had a peak value of ~64 dB re 1 μPa^2/Hz (56 dB re 1 μPa^2/Hz for a storm without rain). Spectral analysis of the data acquired in 2003 showed that the sound field in the frequency band from 200-800 Hz generated by an approaching storm had the clear interference structure resulting from waveguide propagation on the shelf [Borisov et. al. 2004]. The data showed that noise produced by wind and surface waves is much lower for shallow water (10 m) than for areas outside the 20 m contour. The highest ambient sound level was recorded in the frequency band from 200-1000 Hz. The ambient noise in this frequency band had a peak value of 71 dB re 1 μPa^2/Hz during a storm and 46 dB re 1 μPa^2/Hz in calm weather (no rain).

Figure 4.1 displays sonograms of noise synchronously recorded at three monitor stations which are approximately 62 km apart. The Figure shows that twice a day tidal currents cause intense flow noise at frequencies below 15 Hz[43]. Rotational water movement in surface waves during a storm could lead to even higher flow noise and may even move a hydrophone deployed at 10-20 m[44]. Data recorded during low current periods should be used when analyzing acoustic data below 20 Hz (infrasonic).

Figures 4.1 and 4.2 are sonograms *G(f,t)* that illustrate the frequency and spatial characteristics of ambient noise generated by a prolonged cyclone as it traverses the Sea of Okhotsk.

[43] Flow noise is not a real ambient noise measurement, but an artifact caused by vibration of, and turbulent flow around, the hydrophone.
[44] During the peak of the storm this mechanical motion caused clipping of the data.

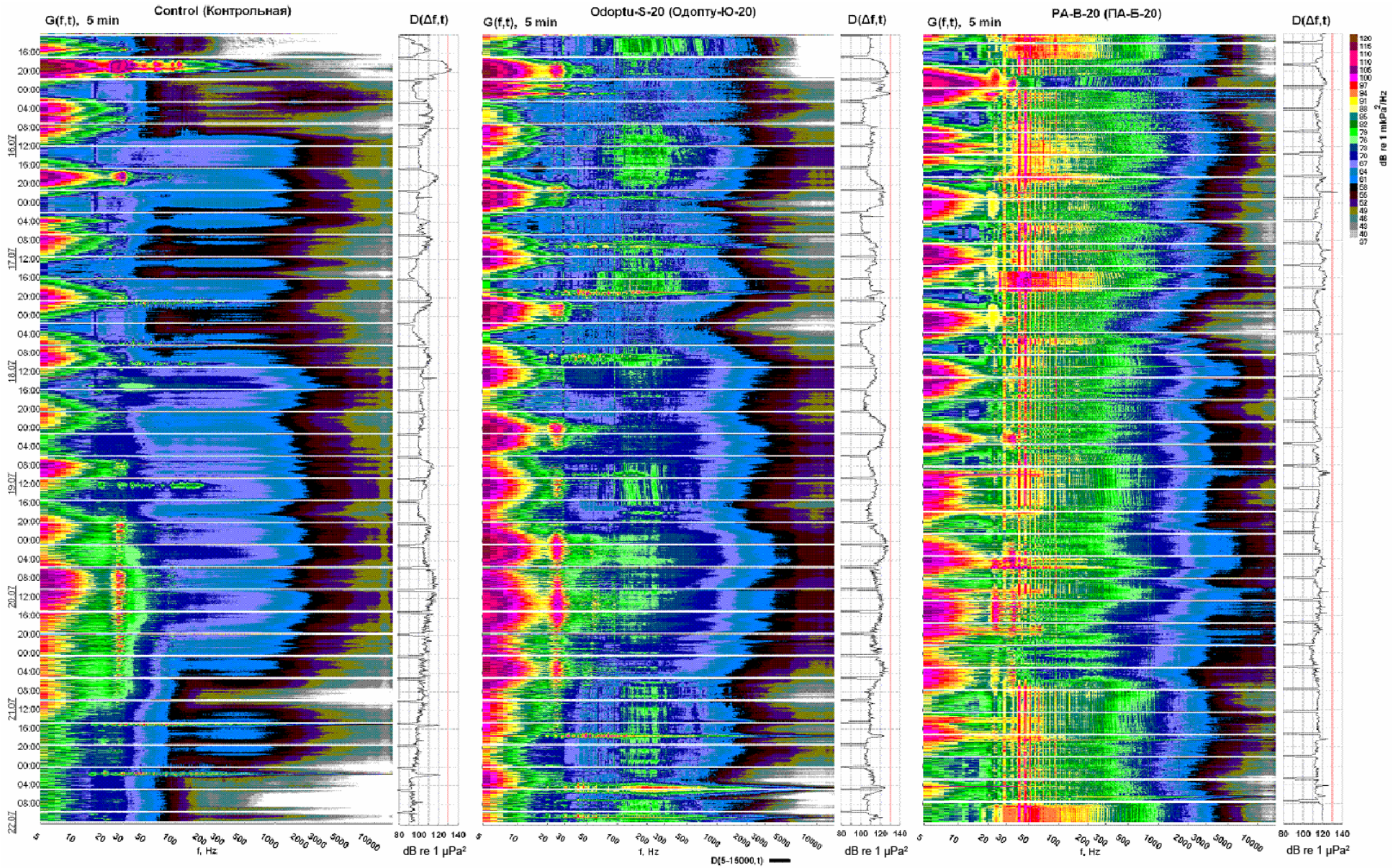

Figure 4.1 - Sonograms *G(f,t)* and plots of sound pressure level for data recorded synchronously at monitor stations Control, Odoptu-S-20 and PA-B-20 during the passage of a cyclone (18 to 20 July 2007).

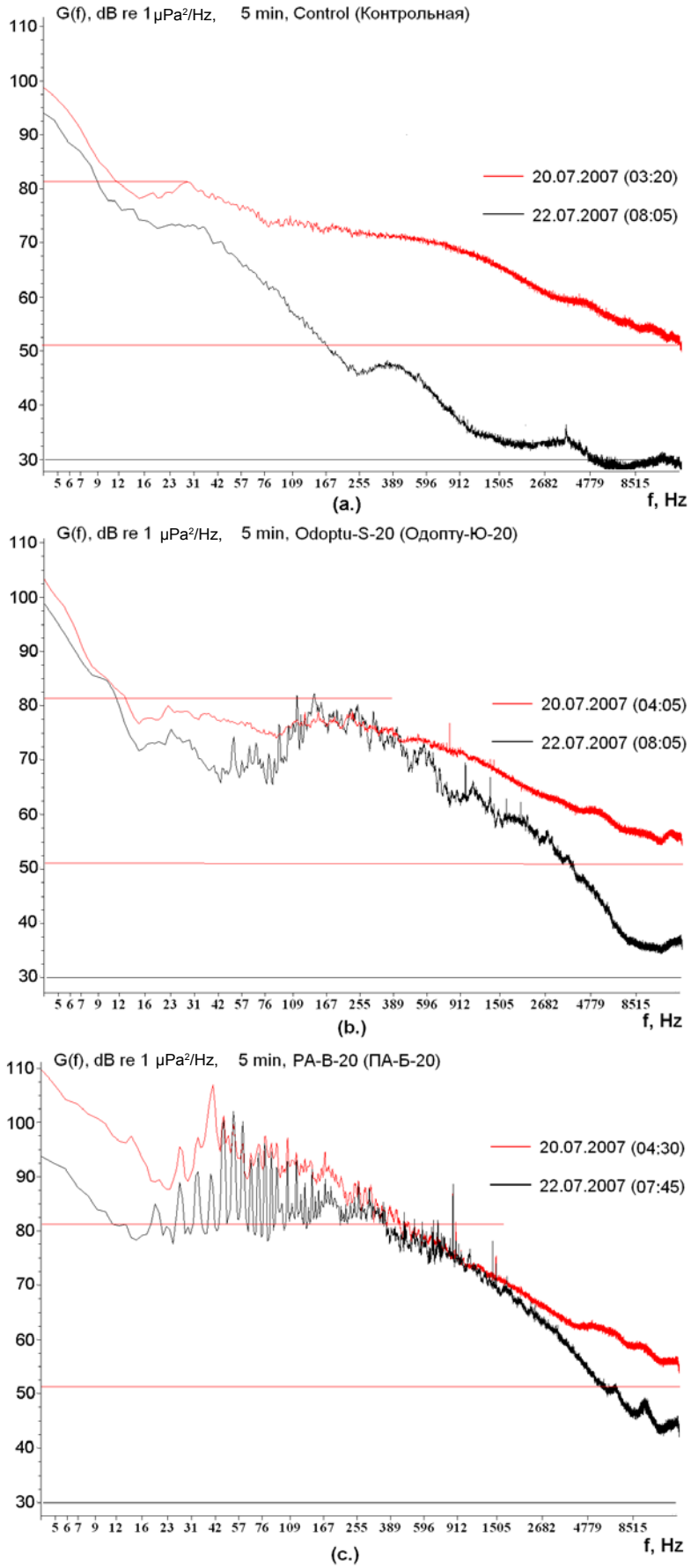

Figure 4.2 - Spectra *G(f)* of ambient noise recorded at the control, Odoptu-S-20 and PA-B-20 monitor stations during and after a storm.

Figure 4.1 gives plots of synchronous acoustic measurements made at the Control station, which is ~40 km from the closest planned ENL and SEIC production operations; this location was specially selected as a control for the annual ambient noise monitoring studies. The PA-B-20 monitor station is located on the eastern edge of the Piltun gray whale feeding area, 8 km from the PA-B platform; at this time the commissioning of the topsides for the PA-B platform and the tie in to a sub sea pipeline were actively underway. The Odoptu-S-20 monitor station is also located on the eastern edge of the inshore feeding area approximately 18 km from the PA-B platform. Figure 4.1 shows that anthropogenic sound generated by one or more of the vessels involved in the construction was constantly observed at the PA-B-20 station. During this construction phase, the level of anthropogenic sound measured in the frequency band from of 5 Hz to 15 kHz reached 120 dB re 1 μPa^2/Hz; this level is approximately equivalent to the ambient noise recorded during the peak of the storm (as seen in Figures 4.1 and 4.2).

Figure 4.2 gives a quantitative comparison of the spectra *G(f)* of acoustic noise measured at the three stations both during and after the transit of the a cyclone. The spectra were calculated in windows where the data was not contaminated by hydrophone motion. The black spectra *G(f)* correspond to measurements made in calm weather conditions. Figure 4.2 shows that during calm weather conditions anthropogenic noise can be seen in the spectral density plot *G(f)* for PA-B-20 and is noticeable at the Odoptu-S-20 station, but not at the Control station which is 60 km from the platform. The red spectral density plots *G(f)* illustrate the ambient noise levels during the peak of the storm. At the control station the ambient noise level at frequencies above 200 Hz is almost 30 dB greater than the noise level in calm weather. At the PA-B-20 and Odoptu-S-20 stations, the difference between the broadband ambient and anthropogenic noise levels is not very great in the frequency range from 70-400 Hz, but increases significantly at higher frequencies. At frequencies above 6 kHz it reaches 15 and 20 dB, respectively.

Figure 4.3 displays spectra *G(f)* of ambient noise data recorded at acoustic station A.5, located at the SE border of the Piltun feeding area (20 m depth) before (31 August 2004) and during (1 September 2004) a strong tropical cyclone. The spectral density plot *G(f)* for 6:53 (Figure 4.3: 31.08 - 6:53) corresponds to good weather conditions, however the vessel *Trias* was close to acoustic station A.5. The broadband sound level above 7 kHz has

dropped below the internal noise level of the AUAR (~35 dB re 1 μPa^2/Hz). As the typhoon approached most vessels sailed to the NE to find shelter from the storm. The spectral density plots *G(f)* for the interval between calm weather and a storm (Figure 4.3: 31.08-17:48 and 1.9-03:34 and 13:10) illustrate the increase in the acoustic levels due to wind and surface waves. These plots show that the broadband spectral levels increased by more than 20 dB (for the frequency band from 100 Hz-15 kHz) during a heavy storm (Figure 4.3: 03.34 and 13:10 relative to 06:53). At 13:10 the spectral density values for frequencies between 500-2000 Hz even exceed the levels predicted for Sea State 6 (SS-6: wind -17.5-20.6 m/s, waves - 4-6 m) [Knudsen et. al. 1948; Richardson et. al. 1995]. Comparison of the spectral density plots *G(f)* of Figures 4.2 and 4.3 indicates that the acoustic spectra of typhoons in these areas are quantitatively and qualitatively similar.

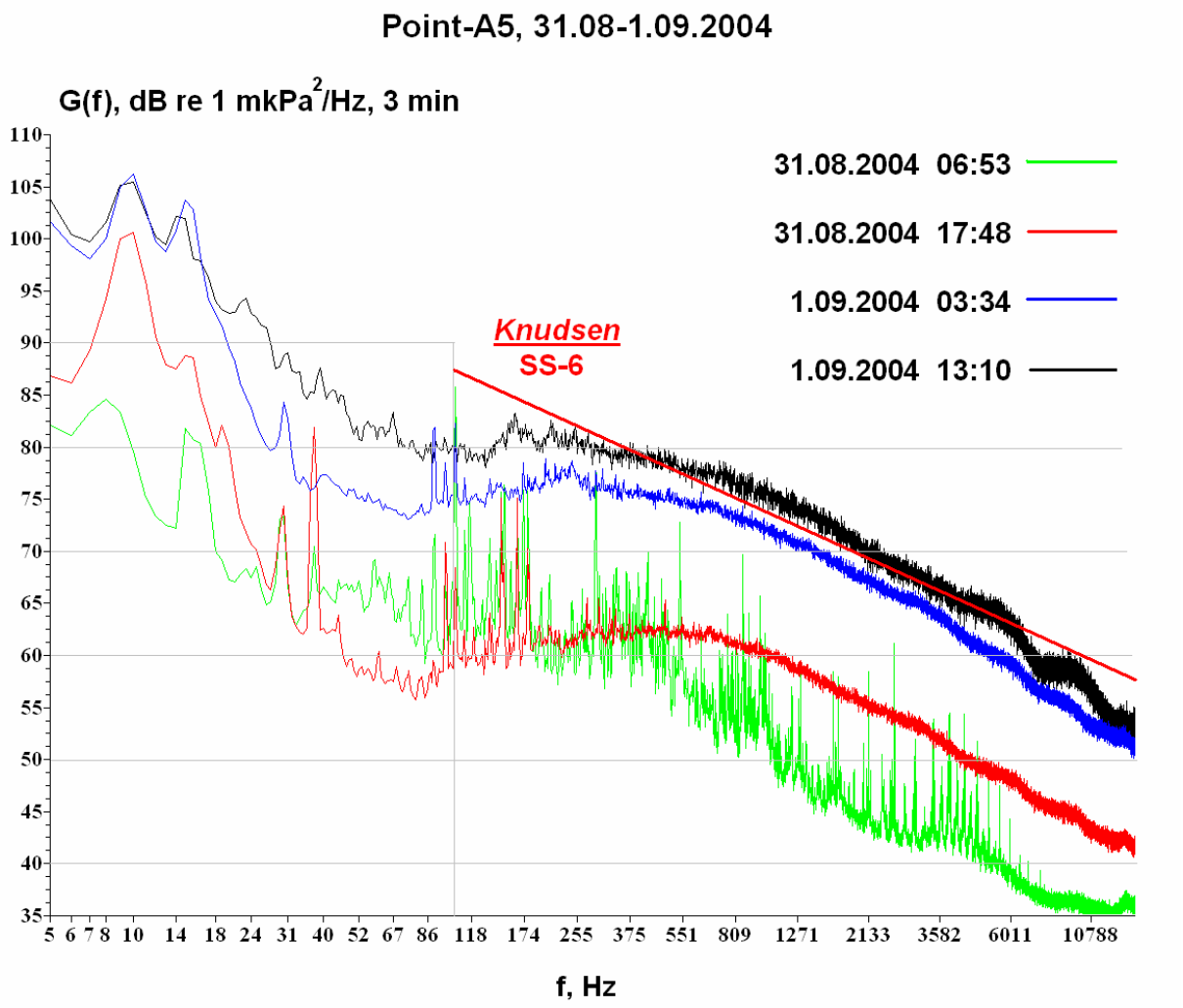

Figure 4.3 - Spectra *G(f)* of ambient noise recorded at acoustic station A.5 before and during a typhoon (Sakhalin Island 2004).

5 Analysis of Transmission Loss *TL(f,r)* experiments on the Sakhalin shelf

The first part of this section discusses the key factors influencing the variation of TL with frequency and range (*TL(f,r)*) along a shallow waveguide with uneven bathymetry. This includes the waveguide parameters as well as the influence of sea surface waves on TL. The later section presents the experimental analysis of sound propagation and TL along profile TLP-6; the results from seismo-acoustic studies from the Odoptu-FSP along profile TLP-18_L are presented in chapter 6.

5.1 Discussion of the factors controlling TL(f,r) in shallow water

The main characteristics of sound propagation on the NE Sakhalin shelf were discussed in a previous report [Kruglov and Rutenko 2004]. This showed that the main factors controlling sound propagation in a waveguide were the bathymetric and acoustic properties of the waveguide. Tidal internal waves were shown to cause up to 16 dB variation in the acoustic intensity of 320 Hz signals propagating along profiles oriented approximately parallel the shore. Scattering by sea surface waves was also shown to have a significant impact on sound propagation when the acoustic wavelength (λ) was less than the sea surface wave height (h) (usually frequencies above 2 kHz)[45]. Figure 2.21 shows short-period intensity variations of a tonal CW-320Hz acoustic signal (as measured by the 8 Mollusk-07 hydrophones). These variations in acoustic signals propagating along a fixed 5 km profile could exceed 30 dB, due to spatial and temporal variations in the acoustic properties formed in the seasonal thermocline by internal waves.

Acoustic propagation and TL data from the oil and gas production facilities to the western gray whale feeding areas are important when estimating the change in the anthropogenic noise levels in the feeding areas due to construction and development activities. Industrial sources can generate acoustic wavelengths longer than ~50 m (<30 Hz). For these wavelengths the profiled waveguides are shallow (10-50 m) and irregular and the main factors contributing to the variation in frequency dependent TL with range *TL(f,r)* are the bathymetric profile and the elastic parameters of the sub-bottom. Spatial variations in the hydrology do not have a significant impact on propagation in this frequency range.

[45] For example, at a frequency of 3 kHz the wavelength λ =50 cm, therefore surface waves with height of greater than 0.5 m can effectively dissipate its acoustic energy and increase the TL at that frequency. The effect was approximately proportional to sound frequency and profile length.

Figure 5.1 gives acoustic spectra synchronously recorded at the PA-B-20 and Odoptu-S-20 monitor stations during PA-B topsides installation (14:00: 17 July 2007). The PA-B-20 station is 8 km, and the Odoptu-S-20 station is 18.5 km from the PA-B platform. The data was recorded using four AUARs deployed along a line perpendicular to the coast. The power spectral density plots *G(f)* shown on Figure 5.1 illustrate both the acoustic source spectrum generated by these operations and the frequency dependent TL along a 18.5 km profile parallel to the shore. These spectra show that there is a narrowband component (23-100 Hz), and tonal components from 850-2000 Hz. The broad-band acoustic level for frequencies greater than 100 Hz decreases at a rate of approximately –0.0038 dB/Hz.

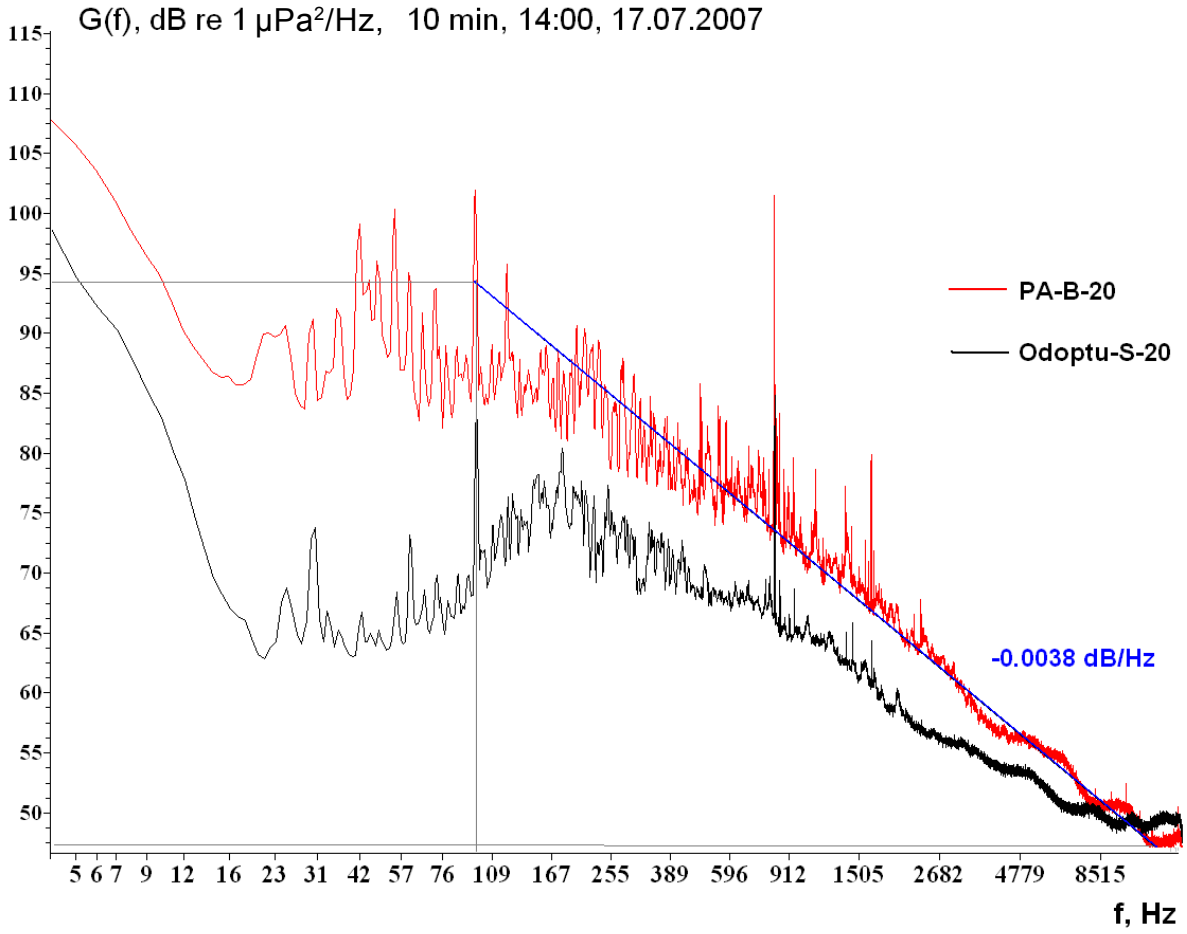

Figure 5.1 – Power spectral density plot *G(f)* showing sound generated by the operations at the PA-B platform during the topsides installation. Data was synchronously recorded at the PA-B-20 and Odoptu-S-20 stations 8 km and 18.5 km from the platform respectively.

Two plots in Figure 5.1 suggest that broadband acoustic energy in the frequency range from 170-1,500 Hz generated near the PA-B platform is propagated along the shelf with relatively low transmission loss, however, these losses increase at lower frequencies due to absorption in the bottom (mode stripping). Figure 5.1 shows that the relative

transmission losses from the PA-B platform to the PA-B-20 station (8 km) and to the Odoptu-S-20 station (18.5 km) are 17 dB for 30 Hz narrow-band sound, and ~10 dB for broad-band acoustic energy in the frequency range from 170-1,500 Hz.

Reflections from an irregular bathymetric profile lead to an uneven distribution of acoustic energy in the water layer. The spatial distribution of the sound velocity field *C(z,r)* and variations caused by tidal currents and internal waves affect acoustic propagation because the velocity field affects the spatial-interference structure of the acoustic field in the waveguide (Figure 2.21). In certain conditions the estimated transmission losses may change due to resonance interaction of the propagating sound field with spatial acoustic inhomogeneities formed by internal waves [Rutenko 2006].

The Mollusk-07 vertical autonomous acoustic and hydrologic recording array and a 320 Hz autonomous bottom CW transducer (CW-320 Hz) were used on several TL profiles in 2007. These experimental TL studies measured the variations in intensity *I(t)* of the acoustic field generated by the CW-320 Hz transducer synchronously at eight depths. Since the source was stationary, and the spatial position of the Mollusk-07 hydrophones was practically unchanged (as confirmed by the two depth sensors). The variations in *I(t)* were mostly due to slow tidal changes in the water depth and spatial and temporal acoustic inhomogeneities generated by subsurface waves propagating along the seasonal thermocline. Figure 5.2 shows plots of *I(t)* for two time intervals when the variations of *I(t)* were in phase on all eight hydrophones covering, these hydrophones cover a depth range of 31.5 m in water 43 m deep. These plots show up to 12 dB variations in TL within approximately 6 minutes (Figure 5.2(a)) and 25 min (Figure 5.2 (b)) for 320 Hz acoustic energy propagating along a profile 14 km long. Therefore, when estimating TL from experimental measurements, even using a broad-band signal, the TL values for a specific frequency band may vary by up to 12 dB, due to the resonance interaction of the sound with spatial acoustic inhomogeneities created by internal waves.

The frequency and range dependent transmission loss *TL(f,r)* can be estimated from experimental measurements if calibrated signals are transmitted and recorded using AUARs [Borisov et. al. 2005]. Spatial and frequency interference caused by intermodal interference and multi-path propagation was eliminated from the *TL(f,r)* estimates by transmitting from the *Professor Bogorov* as it drifted and averaging in one-third octave

bands. The results of these experiments can be refined with modeling. Thus for a TL profile the frequency and range dependent variation in acoustic level with velocity *C(z,r)* can be estimated for a known anthropogenic sound source.

One of the key objectives of the experimental TL measurements is to calibrate theoretical acoustic models; the acoustic and hydrologic measurements were therefore acquired to

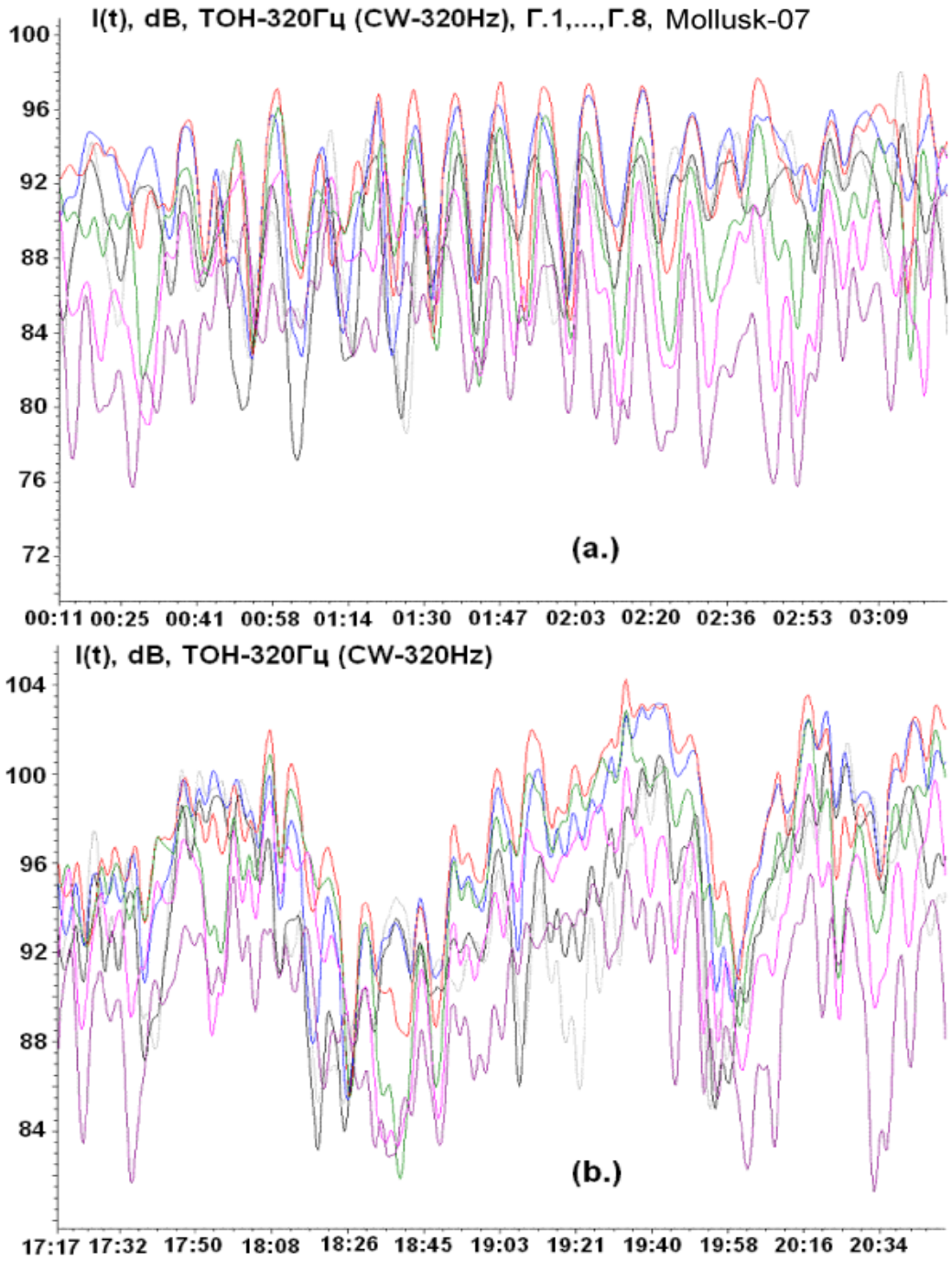

Figure 5.2 – Plots of the variations in intensity of a CW-320 Hz acoustic signal, measured by the 8 hydrophones on the Mollusk-07 along a stationary profile 14 km long acquired on the NE Sakhalin shelf in August 2007.

ensure the hydrology did not vary significantly during the experiment. A bathymetric profile, a vertical hydrologic profile at the receiver location, and at each source location, as well as at intermediate points if required, was acquired for each TL profile. This hydrologic sampling allowed the velocity distribution *C(z,r)* to be obtained along each TL profile.

5.2 Analysis of the range dependent TL (*TL(r,f)*) profiles acquired in 2007

Figure 5.3 is a map of the study area showing the profiles along which the TL experiments were conducted in 2007. The main objective of the analysis was to experimentally estimate the TL along a number of profiles for a range of frequencies. Data was acquired along profiles: TLP-1, TLP-2, TLP-3, TLP-6, TLP-15, TLP-16, TLP-18, TLP-18_L and ADP-A, B, C and D. This describes the procedure used for analysis of the field data and estimating frequency dependent TL *TL(r,f)* using profile TLP-6 as an example. The procedure for constructing TL estimates from experimental data is described in greater detail in [Borisov et. al. 2007][46].

In order to estimate the TL along a profile AUARs are deployed at the specified monitoring stations for each profile (e.g. the Piltun-S and A11 stations for TLP-6). Tonal and broadband acoustic signals are then transmitted from the source locations for each profile. At the beginning or on completion of the transmission, hydrologic measurements were taken with the sonde. The profile was sailed by the *Professor Bogorov* with bathymetric and hydrologic measurements being taken along the profile from the TL source locations to the recording station locations. Measurements were conducted according to a schedule specifically designed for each profile; this methodology ensured that the hydrological measurements were acquired as close to the acoustic measurements as possible.

One drawback with this methodology is that the sensitivity of the AUARs is high[47] and the acoustic level of the *Professor Bogorov* or the transducer when it was nearby could exceed the dynamic range of the system. Mini-AUARs were therefore additionally deployed at each station.

[46] Transmission Loss profiles are designed to better characterize the TL from a proposed facility and have multiple source points allowing a range dependent function to be estimated.
[47] The gain of the AUARs was set to record low level ambient or anthropogenic acoustic signals.

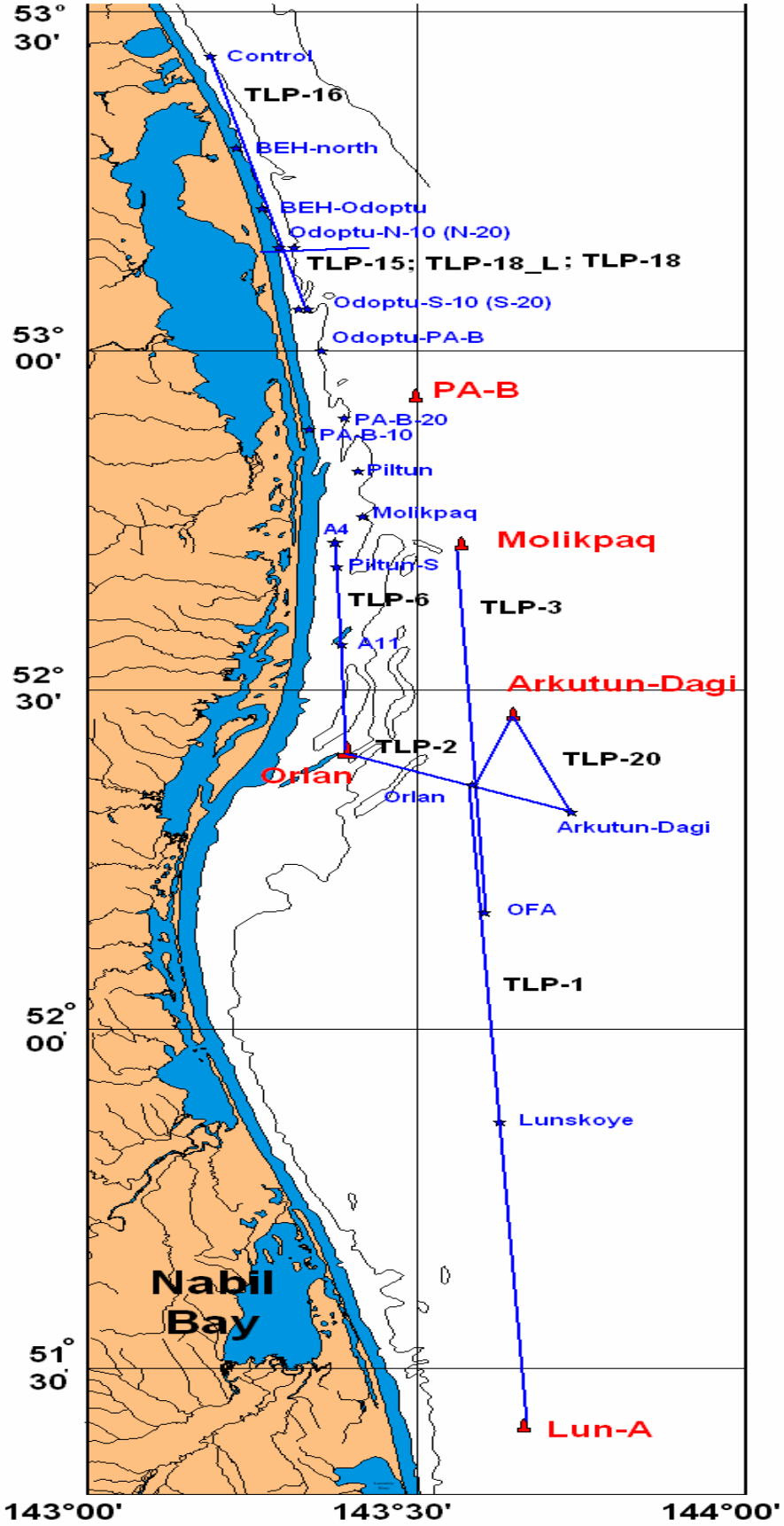

Figure 5.3 - Map of the study area showing the major facilities as well as the AUAR deployment locations for the TL experiments and the profiles surveyed in 2007.

Due to their lowered sensitivity, these mini-AUARs provided accurate measurements when the source was less than 4 km from the station[48]. When using the mini-AUARs for near-field measurements the following methodology was employed. The mini-AUAR was deployed and the GPS coordinates of its hydrophone were logged. The *Professor Bogorov* anchored 1 or 2 km from the mini-AUAR hydrophone, allowing for the length of the anchor chain and changes in the current direction and deployed its LF and HF transducers at a depth of 10 m generating signals with a signal generator according to a pre-programmed schedule. The distance from the transducer to the hydrophone was tracked over time using GPS, as accurate estimation of range is important for estimating TL, especially for distances up to 2 km.

5.3 Analysis of range dependent TL (*TL(r,f)*) along profile TLP-6

Experimental TL profile TLP-6 is 34 km long starting at the Orlan platform location and ending at station A4 at the southern edge of the Piltun feeding area (see Figure 5.3). Figure 5.4 shows the bathymetry and the spatial distribution of hydrology along the profile during the acoustic measurements. There are 12 source locations (A, B, C, D, E, F, G, H, I, J, K and L (1.5 km from the Orlan platform)) along the profile. The source locations are 1.06 km, 2.05 km, 4.2 km, 5.65 km, 6.7 km, 9.3 km, 13.3 km, 18.5 km, 19.5 km, 22.7 km, 25.1 km and 32.6 km respectively from the A4 location. Both an AUAR and a mini-AUAR were deployed at the A4, Piltun-S and A11 locations, recording while signals were transmitted at the six source locations. Figures 5.5(a-c) presents the TL results obtained from the analysis of the data, acquired using the procedure described above over the frequency range from 10 Hz to 15 kHz. The absence of experimental data in the frequency range from 100 Hz to 1 kHz for source locations I, J, K and L is explained by the relatively high level of ambient acoustic noise and the low signal levels of HF signals generated at the longest ranges.

To smooth the effect of spatial and frequency interference, the experimental *TL(f)* data was averaged in one third octave frequency bands. Figure 5.6(a-c) presents the results of this frequency averaging. This *TL(f, 1/3 octave)* data was used to construct plots of range dependent TL (*TL(f,r)*).

[48] Distances of less than 1 km are of special interest for TL at infrasonic (below 20 Hz) frequencies.

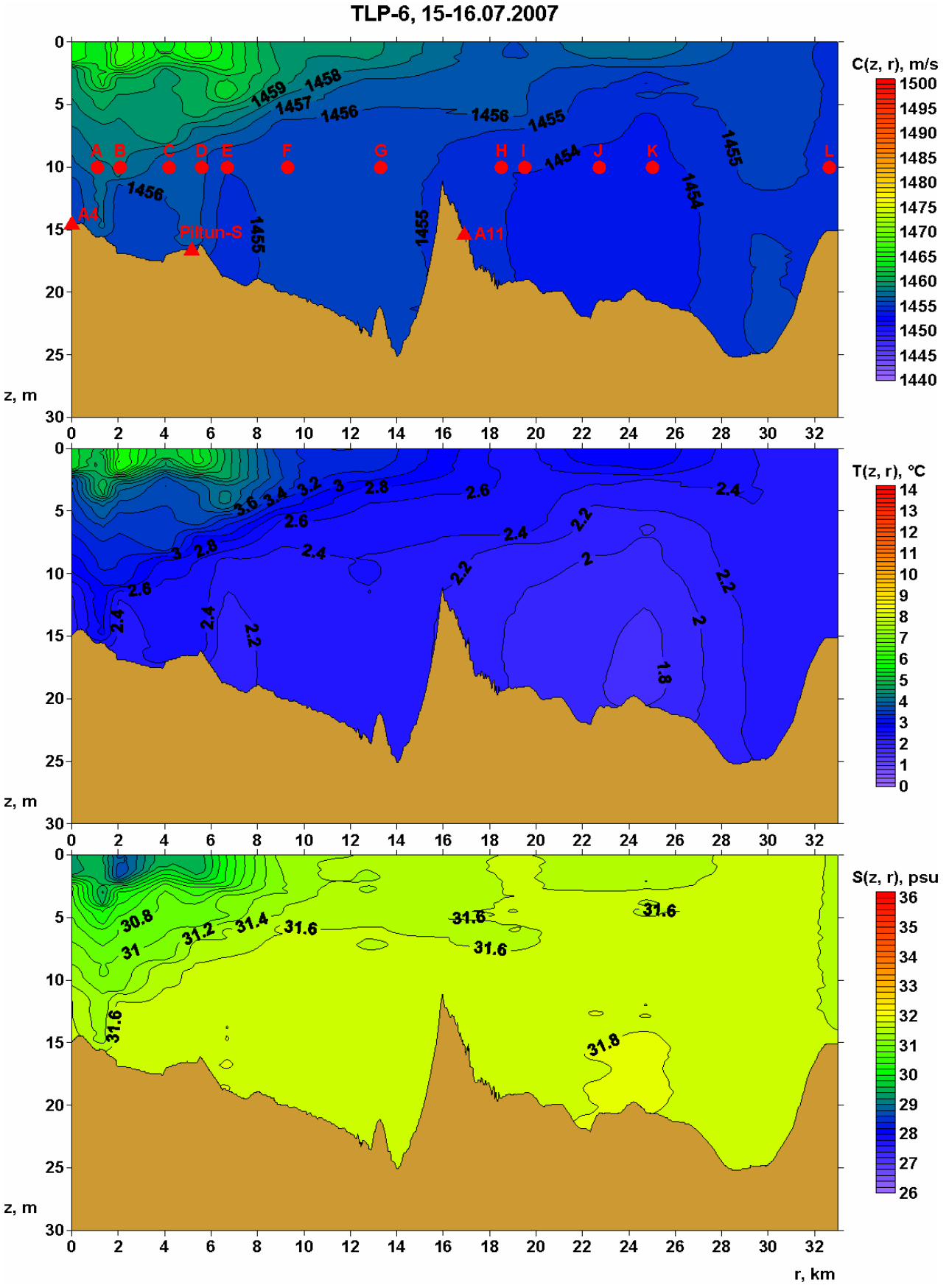

Figure 5.4 - TLP-6: Bathymetry and hydrologic parameters (velocity *C(z,r)*, temperature *T(z,r)*, and salinity *S(z,r)* acquired on 16 July 2007.

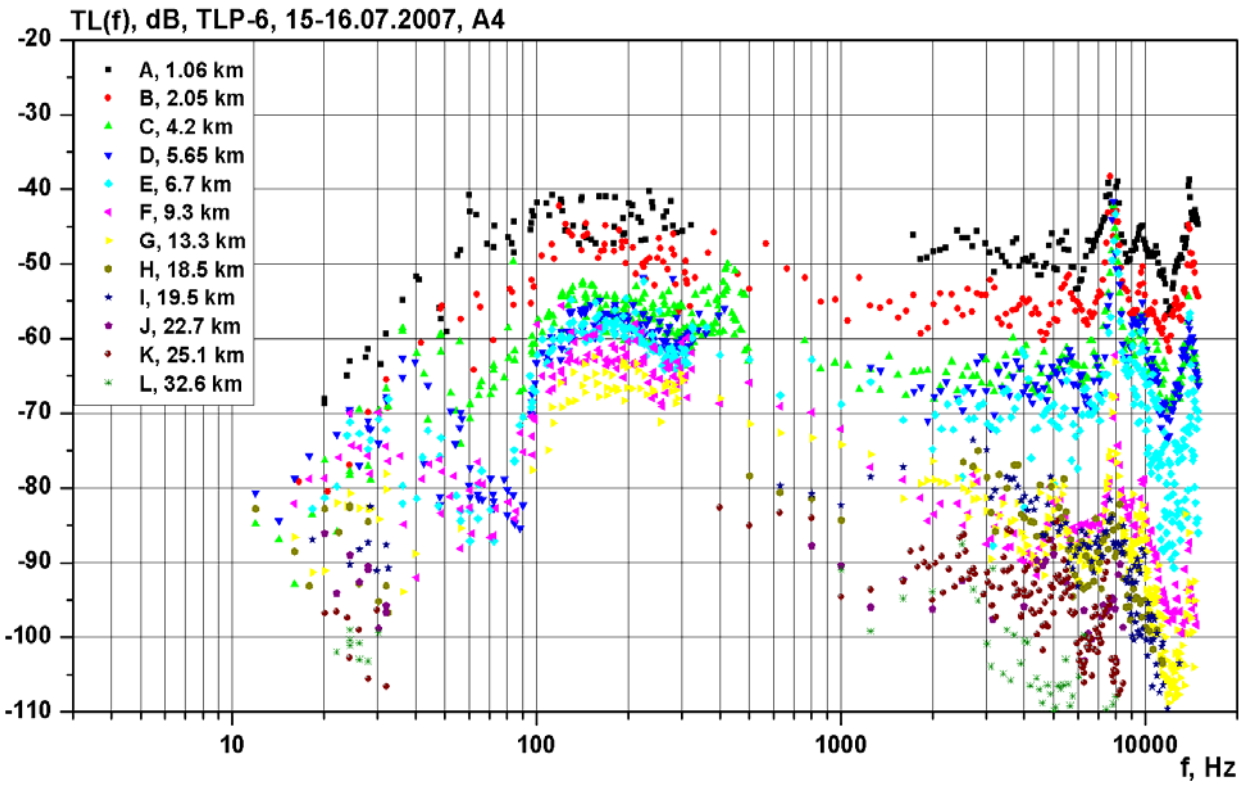

Figure 5.5(a) - TLP-6: Frequency dependent TL plot showing the results for all the source locations and the distance from the source location to the A4 location.

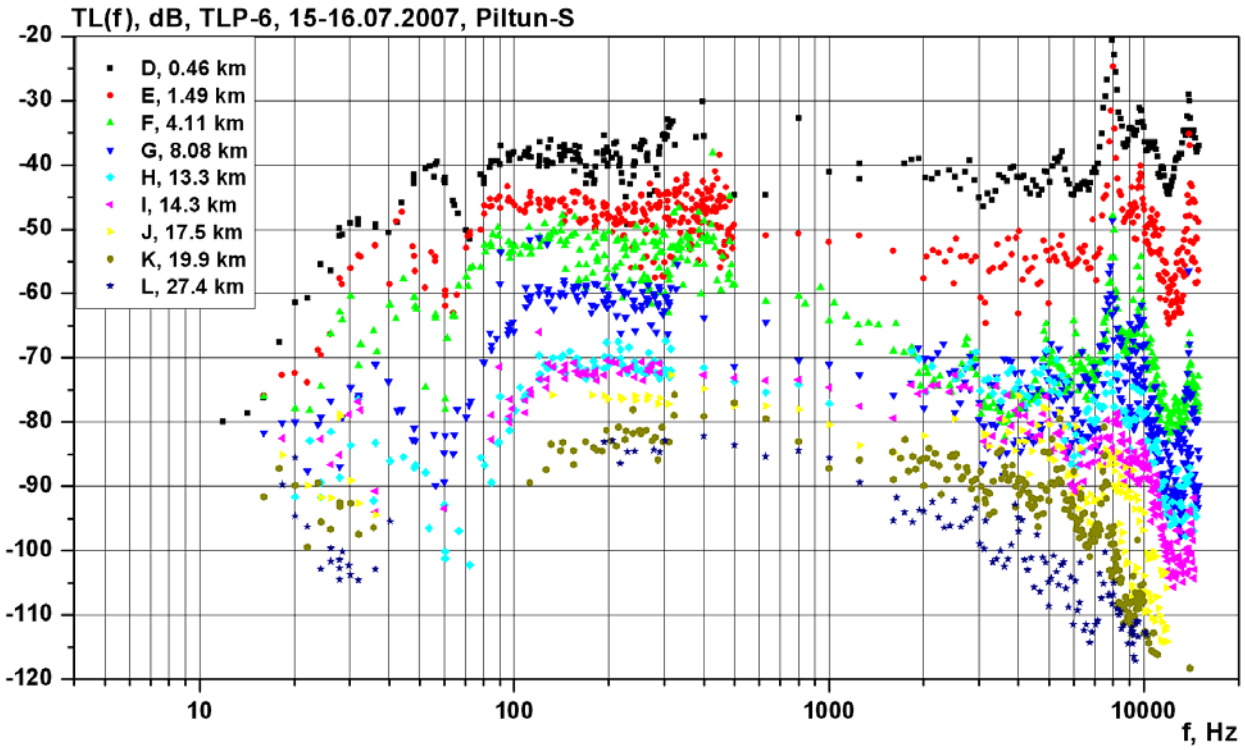

Figure 5.5(b) - TLP-6: Frequency dependent TL plot showing the results for all the source locations and the distance from the source location to the Piltun-S location.

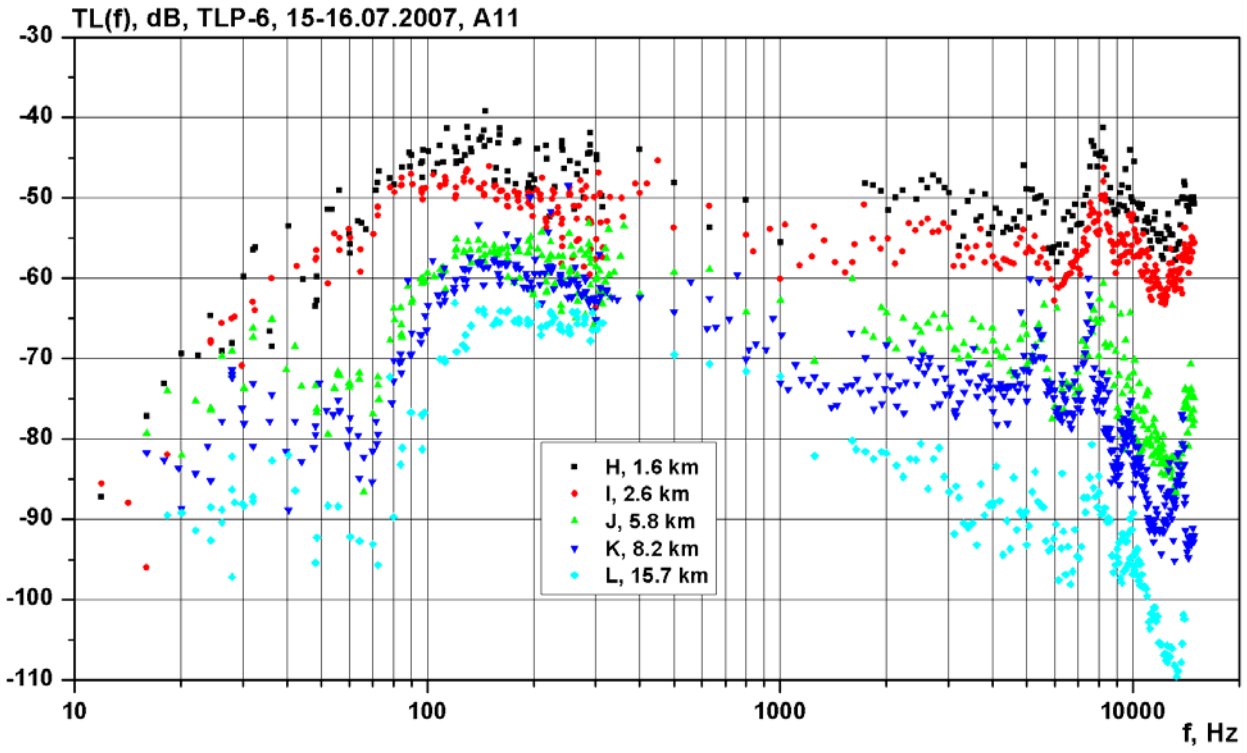

Figure 5.5(c) - TLP-6: Frequency dependent TL plot showing the results for all the source locations and the distance from the source location to the A11 location.

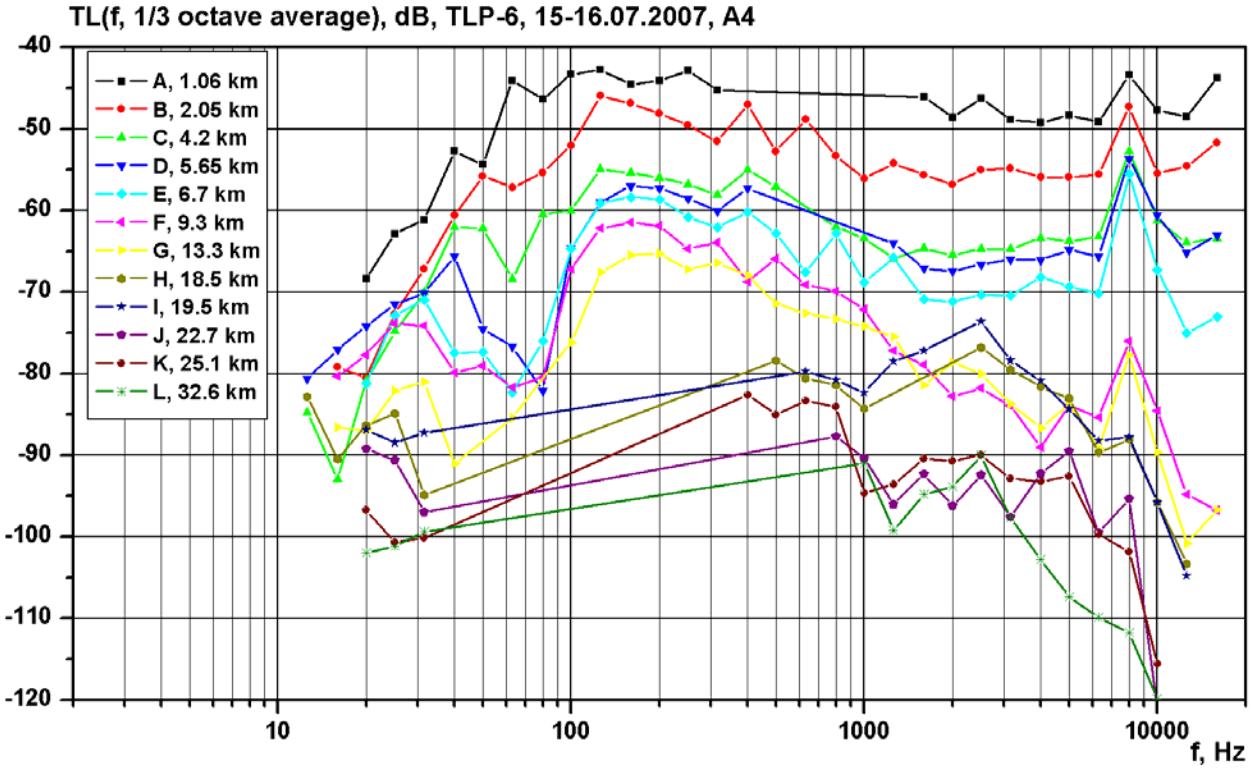

Figure 5.6(a) - TLP-6: One third octave averaged frequency dependent TL plot showing the results for all the source locations and data in Figure 5.5(a).

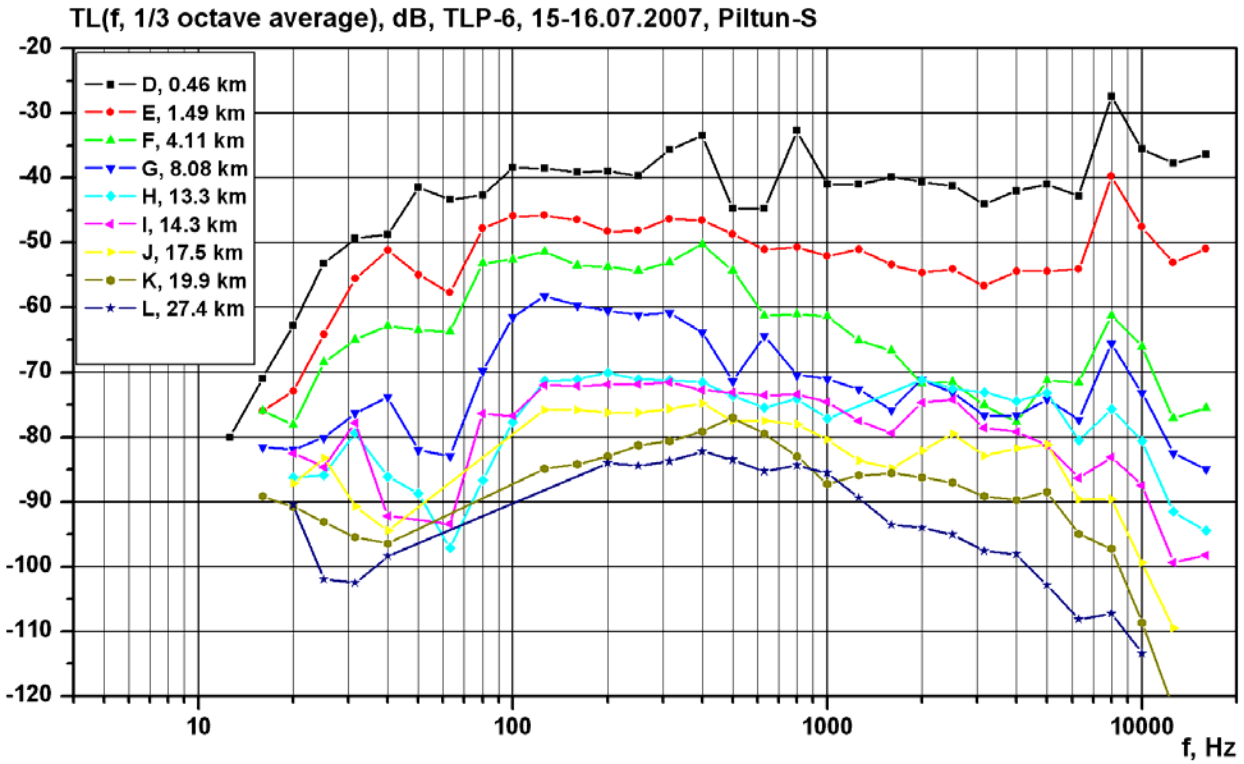

Figure 5.6(b) - TLP-6: One third octave averaged frequency dependent TL plot showing the results for all the source locations and data in Figure 5.5(b).

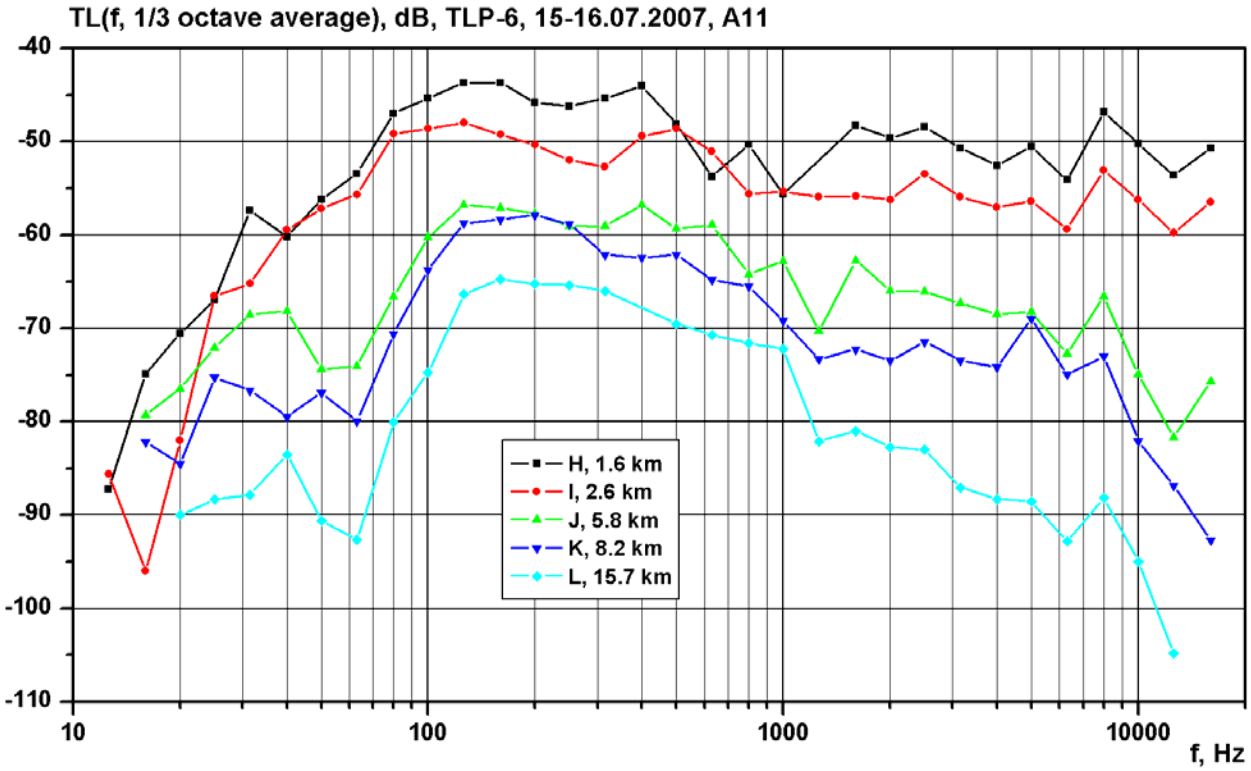

Figure 5.6(c) - TLP-6: One third octave averaged frequency dependent TL plot showing the results for all the source locations and data in Figure 5.5(c).

Figure 5.7(a-c) shows these plots for frequencies of 25 Hz, 126 Hz, 3.15 kHz and 12.6 kHz. The dotted line on this plot is the empirical *TL(r)* plot constructed using the empirical function given in Equation 5.1.

$$TL = \begin{cases} -20\log(r) & ;0 < r \le 100m \\ -10\log(r) - 20\log(100m) & ;100m < r < 800m \\ -15\log(r) - 10\log(800m) - 20\log(100m) & ;r > 800m \end{cases} \qquad (5.1)$$

Figures 5.6(a) and 5.6(b) illustrate that in the 1.5-4 kHz frequency range, the TL is less for sound generated at locations H and I and received at station A4, than for sound generated at locations F and G, while for the Piltun-S station the TL is approximately equal for all four source locations. Figure 5.4 shows that the distance between source locations H and I is 1 km, and that they are 18 km from station A4 and approximately 13 km from the Piltun-S station. The bathymetry along this profile shows a distinct bank between locations G and A11 (Figure 5.4), these TL differences may be due to the effect of this bathymetric high on the propagation of sound at these frequencies.

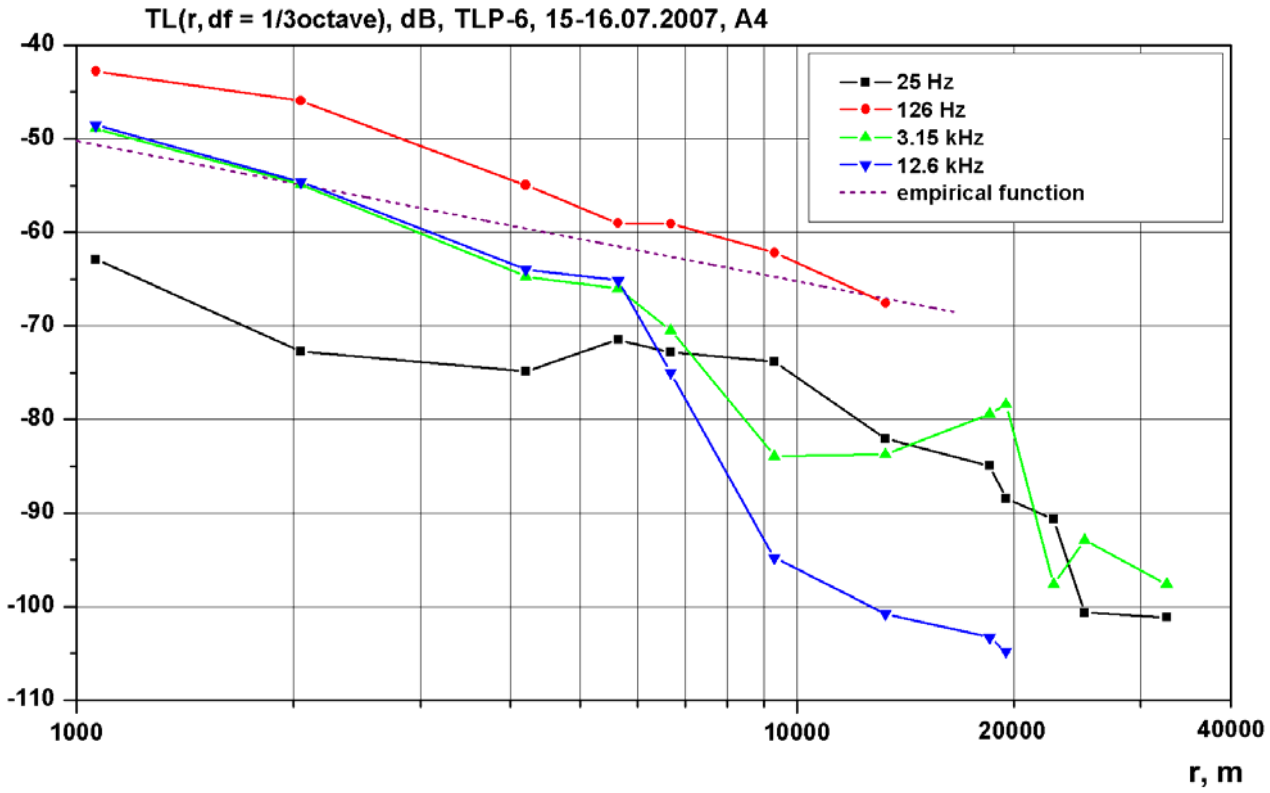

Figure 5.7(a) - TLP-6: Range dependent one third octave averaged frequency dependent TL plot showing the results for four one third octave frequency bands for station A4.

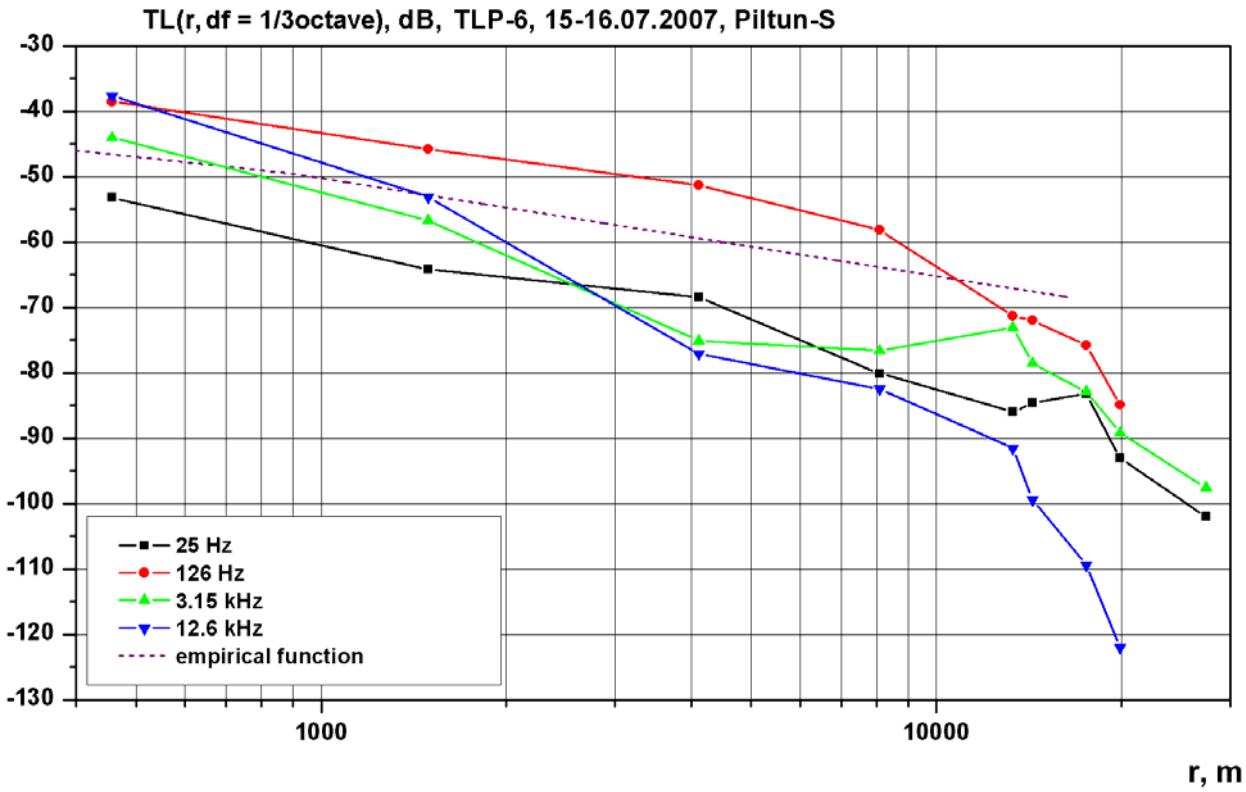

Figure 5.7(b) - TLP-6: Range dependent one third octave averaged frequency dependent TL plot showing the results for four one third octave frequency bands for station Piltun-S.

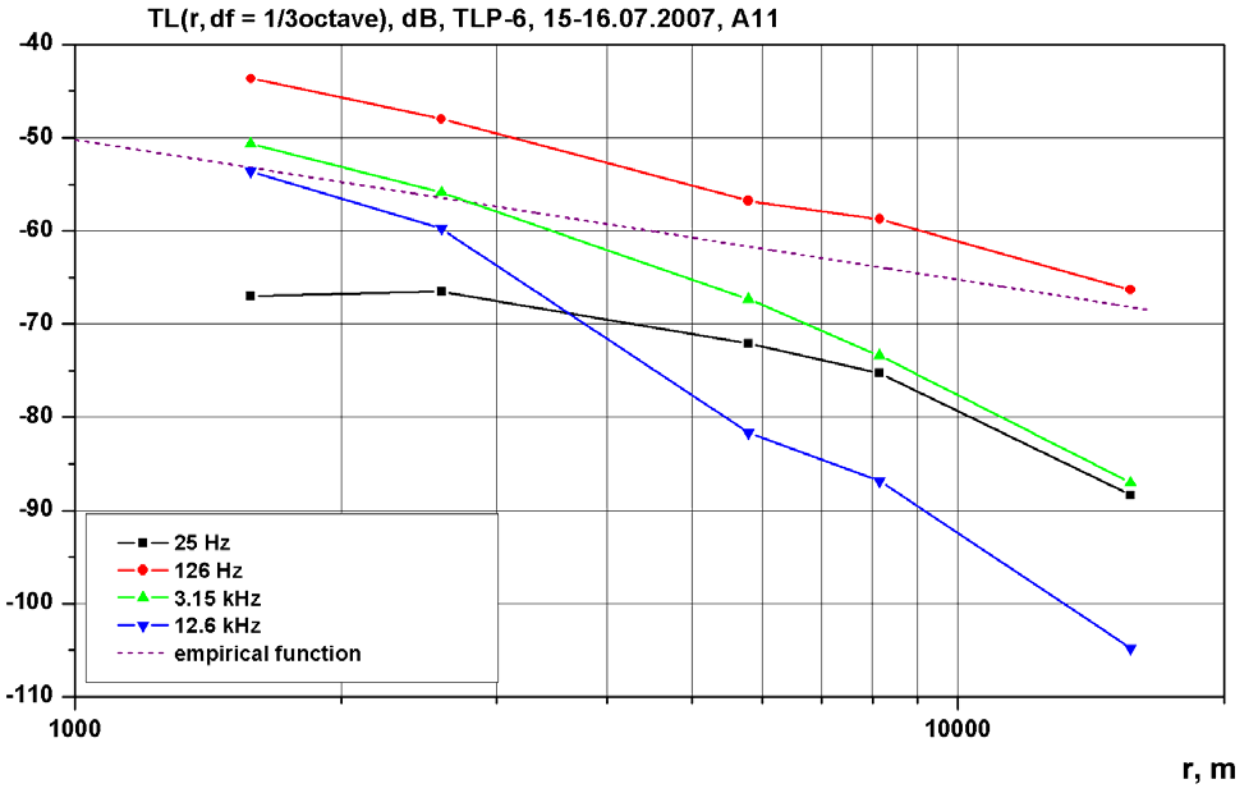

Figure 5.7(c) - TLP-6: Range dependent one third octave averaged frequency dependent TL plot showing the results for four one third octave frequency bands for station A11.

6 Analysis of acoustic propagation of seismic waves generated onshore

The current development plan is to develop the Odoptu field from onshore using directional drilling, one of the objectives for the 2007 program was therefore to study the propagation and transmission losses for low-frequency waves generated onshore and propagating offshore. For these studies, POI designed and constructed a seismic low frequency resonant electromagnetic transducer (SLFT). A detailed description of the transducer is given in [Borisov et. al., 2007] and in section 2.4 (Figure 2.24). The first combined onshore and offshore experiments on integrated seismo-acoustic profiles were conducted in 2006 on seismo-acoustic profiles TLP-17 and TLP-18. The analysis of the field data and preliminary numerical modeling were presented in [Borisov et. al., 2007]. In 2007 further, more detailed field studies were conducted on a longer seismo-acoustic profile using the Mollusk-07 vertical autonomous acoustic and hydrologic recording array and the SLFT seismic source. These studies were conducted at the Odoptu-FSP (Odoptu First Stage Production area)[49]. In Figure 6.1 and all future diagrams and maps in this section the location of the SLFT is designated as p.0.

Figure 6.1 - Seismic low frequency resonant transducer (SLFT) deployed at p.0.

[49] The Odoptu-FSP includes the North Well Site (Odoptu-NWS), non-process facility and process facility areas.

Figure 6.2 – Installation and removal of SLFT.

Figures 6.3 to 6.5 show photographs of the Odoptu-FSP and its surrounding area. Figure 6.3 shows that the Odoptu-FSP is an approximately horizontal plateau, with an elevation ~7 m above sea level. The western edge of the plateau drops off steeply to the marshy flood plain and shoreline of Piltun Bay. Figure 6.6 shows the locations at which an autonomous recording system (section 2.4 and Figure 2.25), based on a two-channel digital tape recorder, along with a hydrophone placed in a buried, water-filled plastic container, and a geophone, V_z, was deployed. The recording system measured low-frequency tonal signals (CW-27 Hz) generated onshore by a seismic source installed at location p.0 and offshore by a LF transducer (section 2.4 and Figure 2.22) deployed at a depth of 10 m from the anchored *Professor Bogorov*. Figure 6.7 shows photographs of a

number of the recording locations. The acoustic experiments that are described and analyzed in this section were conducted from 1 August through 8 August 2007.

Figure 6.3 (Left) – Eastern edge of Odoptu-FSP Figure 6.4 (Right) – Eastern edge of Odoptu-FSP showing two of the stations where LF signals generated offshore and onshore were received.

Figure 6.5 – Western and Southern edges of the Odoptu-NWS.

6.1 Procedure for recording the seismo-acoustic signal and estimating TL

Two types of transducers were used for the seismo-acoustic measurements, hydrophones and a geophone. The single-component (vertical) piezoelectric geophone, converts integrated acceleration in the principal direction to a proportional analog voltage; the sensor was carefully deployed to maintain a vertical orientation. The hydrophones were placed in buried, water-filled plastic containers to create a uniform impedance contact medium (Figure 2.25(a)). The signals were either fed directly into a computer through cables and a National Instruments ADC or recorded on a two-channel DAT recorder (Figure 2.25(b)) and later transferred to a computer.

Figure 6.6 - Location of the onshore recording stations where measurements were taken of low-frequency energy generated by the SLFT installed at point p.0.

Figure 6.7 – Photographs of a number of the onshore recording stations where measurements were taken of low-frequency energy generated by the SLFT installed at point SSW - p.0.

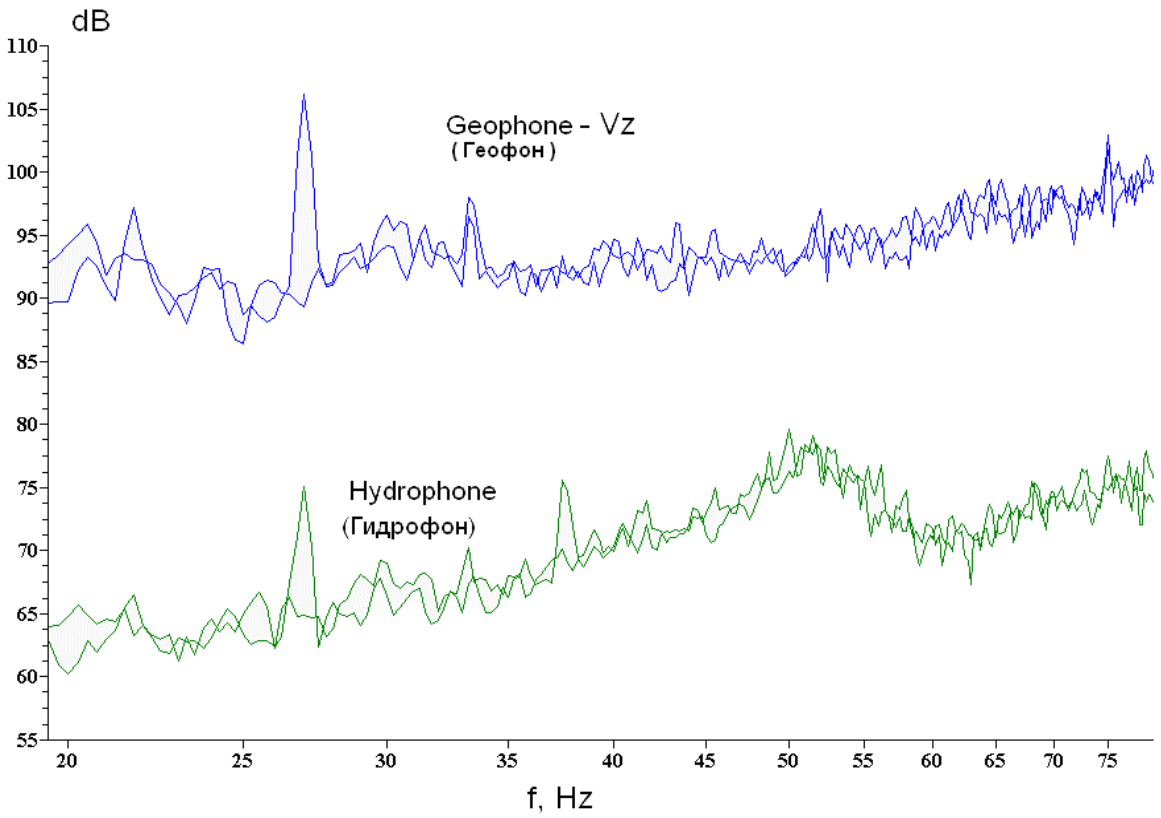

Figure 6.8 - Estimates of the level of a 27 Hz seismic signal measured onshore by a geophone and hydrophone at a point 515 m from the SLFT.

The combination of a standard geophone (single-component V_z) with a hydrophone placed in a buried, water-filled plastic container allowed the quality of the hydrophone measurements to be evaluated. The onshore hydrophone and geophone were used to synchronously record 27 Hz tonal vibrations generated onshore and offshore. The geophone was deployed adjacent to the hydrophone and the data were input synchronously into a computer or a DAT recorder. Since the impedance of the ground was not known, measurements made with the vertical geophone (V_z) must be given in relative units, as no absolute calibration of the geophone data were possible. The data from the hydrophone and geophone cannot therefore be directly compared, but can be used to quality control the onshore hydrophone measurements. Figure 6.8 displays power spectral density plots of the signals recorded synchronously by the hydrophone and geophone at a location 515 m from the SLFT both while it was operating, transmitting a 27 Hz signal, and while it was not operating. Figure 6.8 shows that the signal-to-noise ratio is ~17 dB for the geophone and ~14 dB for the hydrophone. These results showing that both the geophone

and hydrophone can resolve the signal is typical of the data acquired, and indicate the stability of onshore seismo-acoustic measurements with hydrophones deployed in buried, water-filled plastic containers.

The high sensitivity of the geophone did not allow measurements close to the source, the SLFT reference signal level for estimating TL along land profiles could therefore not be determined directly. The reference level for velocity was determined by least-squares extrapolation of all the data from the N-S and E-W profiles. First-order regression on logarithmic axes of amplitude vs. range was used to estimate a reference level of 180 dB at a distance of 2 m from the center of the source.

Figure 6.9 gives estimates of signal level measured with a hydrophone P and geophone V_z on North-South and East-West oriented onshore seismic profiles. They indicate that the results of observations made with hydrophones and geophones correlate well.

Additional experimental measurements estimated the effect of the sensor deployment conditions on onshore seismic signal reception. Data from a hydrophone placed in a buried, water-filled plastic container was compared with the same hydrophone when lying on the ground, lowered to various depths in a shallow water-filled borehole or placed in a puddle. Additional measurements were performed at locations with different ground characteristics but close proximity. Table 6.1 gives the results of these measurements and shows that differences are observed for measurements with geophones and hydrophones. These differences are determined not only by the location of the sensor, but also by the near surface soil properties.

These measurements show a significant spread in the signal levels recorded during the experiment. To minimize this measurement variability the hydrophones were deployed using the same method at each station and locations with extreme readings due to the near surface conditions were eliminated.

Figure 6.10 is a spectral *G(f)* plot of data from a hydrophone placed in a buried, water-filled plastic container, which was located at station E2, 1.9 m from the center of the operating SLFT.

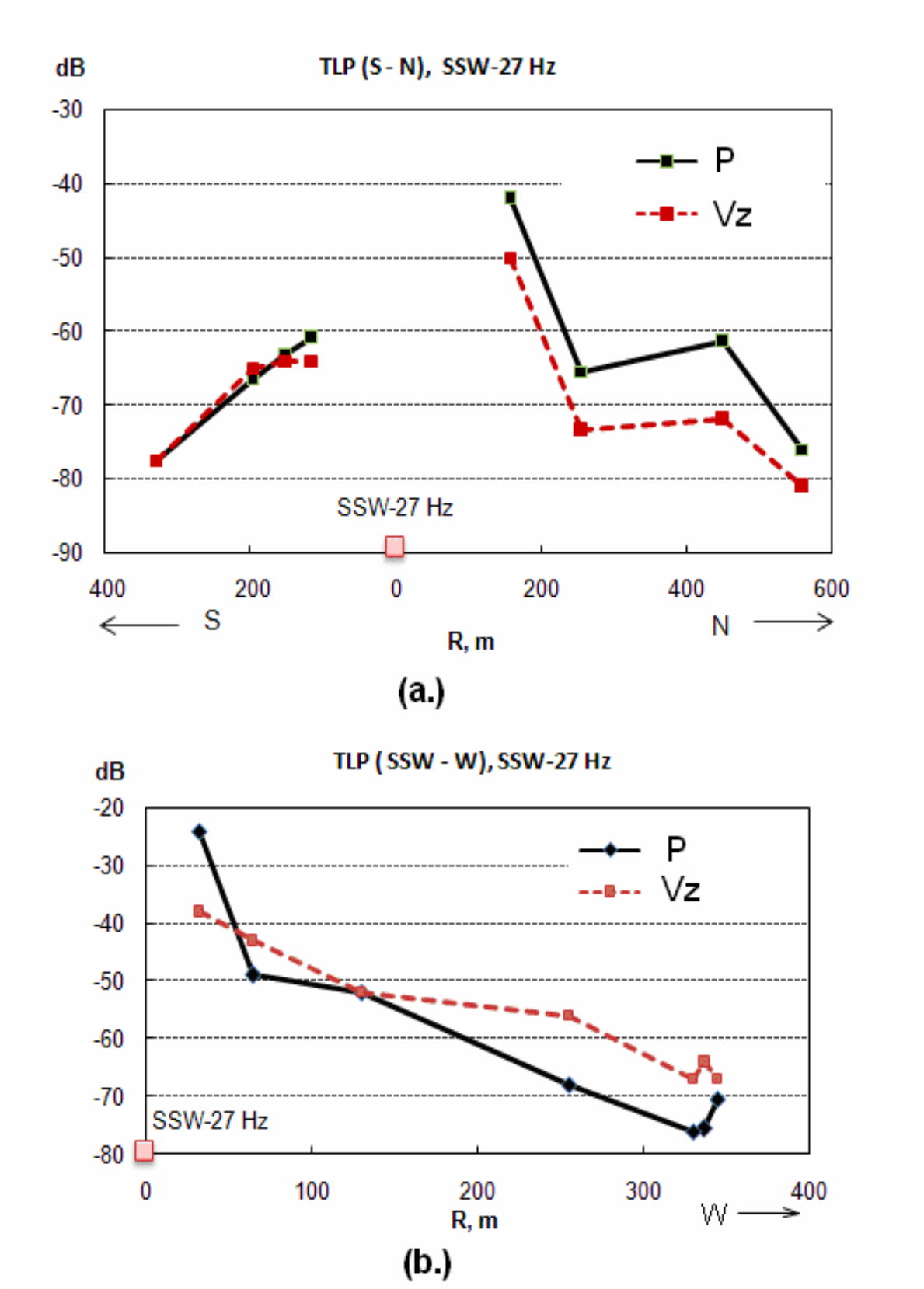

Figure 6.9 - Comparison of measurements conducted using a hydrophone P and geophone V_z in the: (a) North-South; (b) East-West direction.

Table 6.1 - TL values for conditions in which the recording devices were deployed.

Points	Distance to source in m	TL, dB (27 Hz)	Comment
S165	165	-74	In container
S165	165	-58	In puddle
S165	165	-44	In borehole at depth of 1м
S165	165	-49	In borehole at depth of 2м
S155	155	-61	In container
S155	155	-62	In borehole
S145	146	-76	In container
S145	146	-78	In borehole No. 1
S145	146	-63	In borehole No. 2
S200	197	-67	In container
S200	197	-73	In borehole
S330	330	-78	In puddle
S165	164	-71	Puddle
S165	164	-72	Geophone on ground
S165	164	-68	Geophone in puddle
E80	80	-59	At edge of hill on top
E84	84	-51	Middle of slope
E88	88	-47	Bottom

Spectral analysis was performed with a frequency resolution of 0.25 Hz to increase the signal-to-noise ratio, but the spectral density values were reduced to a 1 Hz band. For a sinusoidal signal this difference in frequency resolution will cause a -6 dB variation in the spectral density estimates; if the frequency resolution of the source and received signals was different this error was compensated for in estimating TL. It is assumed that since the hydrophone is in water its calibration is valid, therefore the power spectral density values of the signal measured by it can be given in dB re 1 $\mu Pa^2/Hz$.

In order to estimate the reference level of the SLFT, a series of measurements were taken at a constant distance (2.1 m) from the center of the SLFT baseplate. The polar plot given in Figure 6.11 illustrates the results of these measurements. The mean value of the signal strength at a frequency of 27 Hz is 154.1 dB, although the SLFT exhibits significant frequency dependent directivity in the near field.

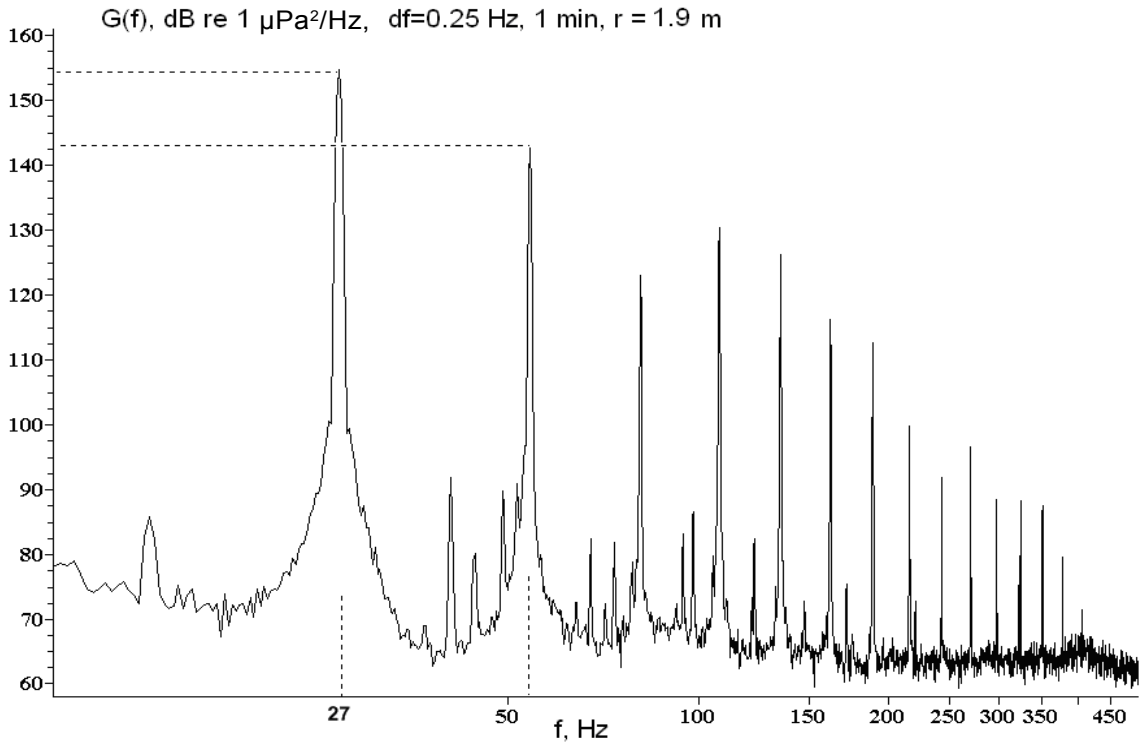

Figure 6.10 – Spectral estimate of a seismic signal measured by a reference hydrophone at location E2, a distance of 1.9 m from the center of the SLFT.

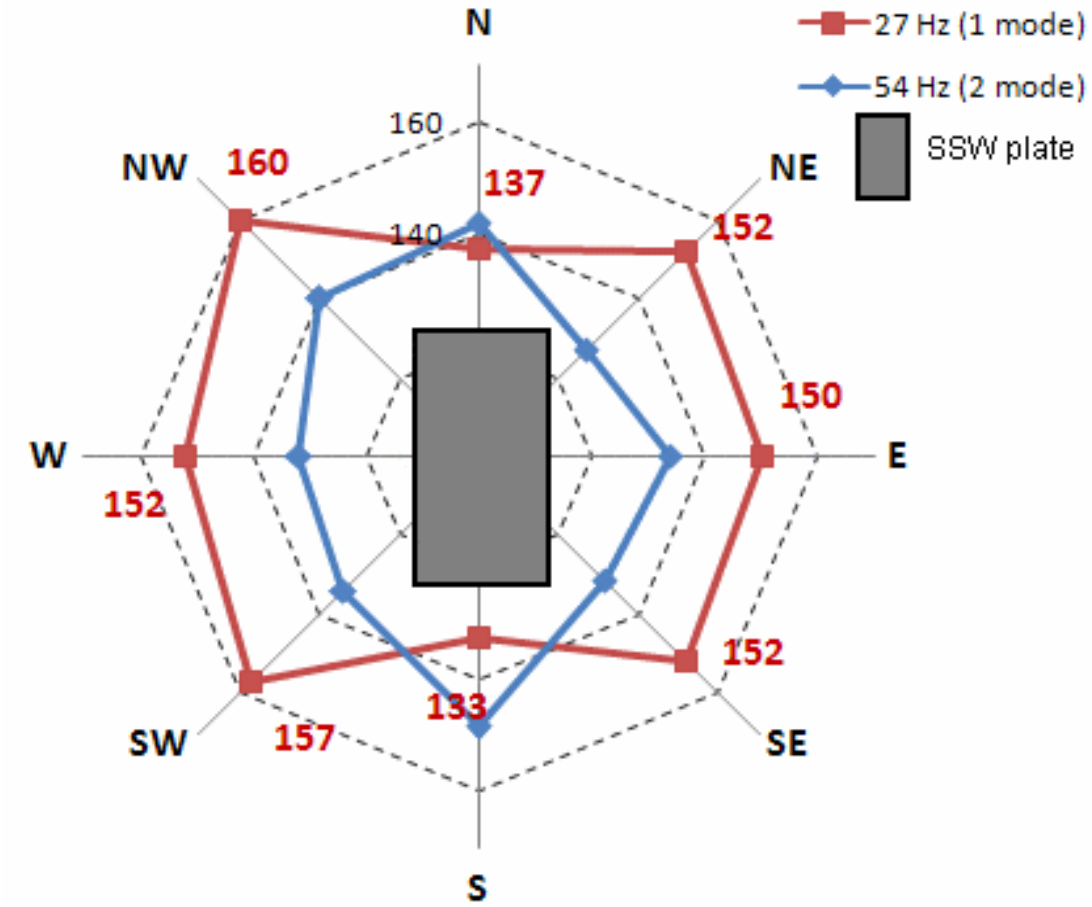

Figure 6.11 – Polar plot of the level of the signal at a specified frequency in dB received at a distance of 2.1 m from the SLFT when operating.

Whenever the SLFT was in operation the received level of a 27 Hz signal measured by a hydrophone at location E2, which is 1.9 m east of the SLFT was 154 dB. This location was therefore selected as a reference station for TL estimates. This stability was confirmed by measurements conducted practically throughout the entire operation at location E88.

Spectral analysis of these near-field measurements enabled POI to detect the second harmonic of the seismo-acoustic signal and to estimate its level and range dependent attenuation. Analysis of this data showed that the second and higher harmonics of the seismo-acoustic signal attenuate to the background noise level at distances of 100-150 m from the source. The propagation characteristics of the signal and the received signal levels are mainly determined by the local geology and topography. Figure 6.12 shows plots of the level of the first and second harmonics of the generated signal at a distance up to 10 m east of the source.

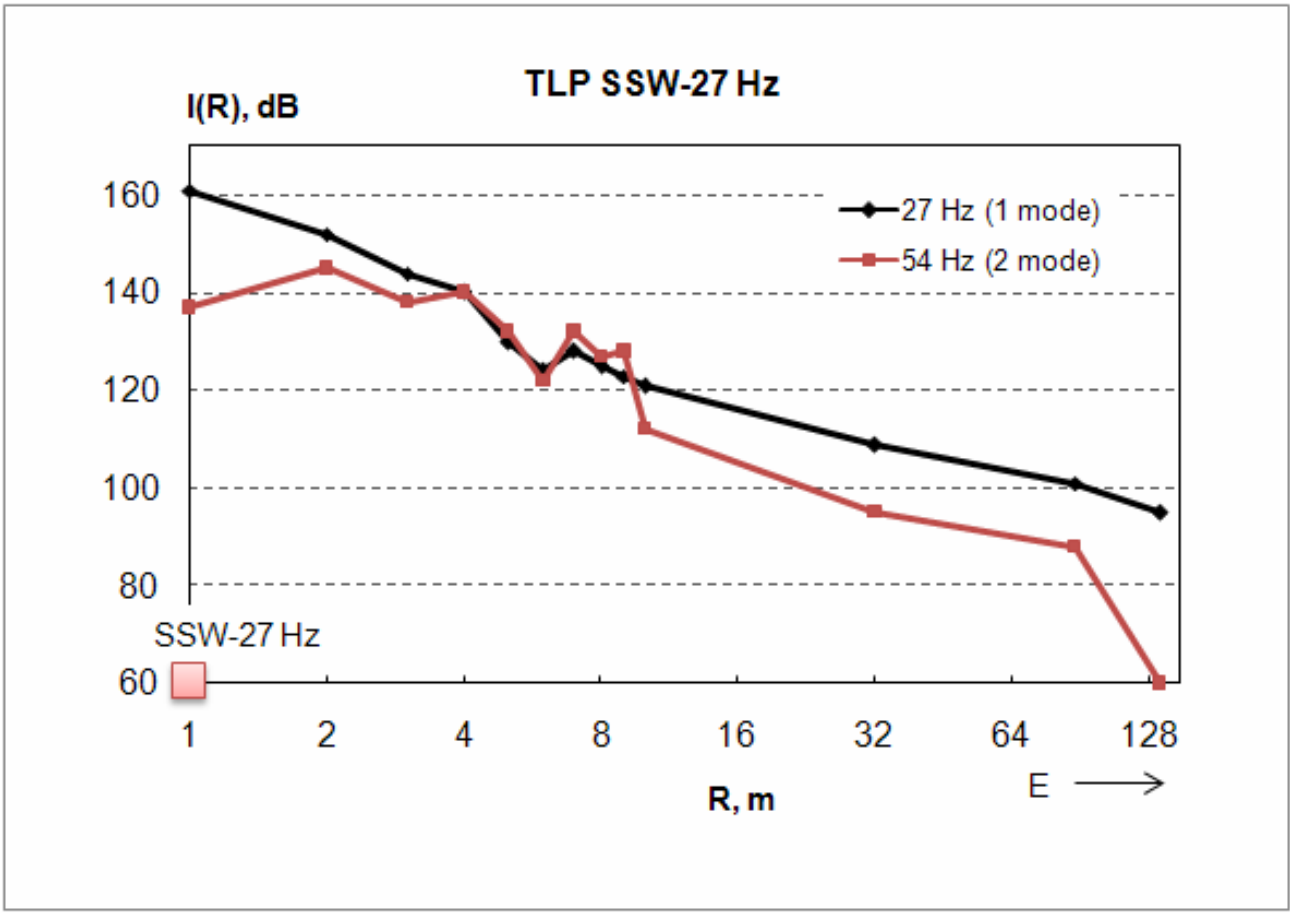

Figure 6.12 – Intensity level of the first and second harmonics (modes) of the seismo-acoustic signal in the near field of the SLFT.

Four main onshore profiles from the SLFT (SSW) were selected according to the local topography and the geographic orientation of the study area: north (N), east (E), south (S) and west (W). In order to improve their stability, measurements along the selected profiles were supplemented by measurements at the characteristic points shown in Figure 6.6. For the eastern profile data was recorded both onshore and offshore, using AUARs, mini-AUARs and DSBs located on the stations along the two versions of seismo-acoustic profile TLP-18_L, which are shown in Figure 6.13. The Mollusk-07 vertical autonomous acoustic and hydrologic recording array (Section 2.3) was deployed at the easterly end of TL profile TLP-18L2.

6.2 Analysis of range dependent TL along onshore profiles at the Odoptu-NWS

To study the propagation characteristics and transmission losses for low frequency propagation at the Odoptu-NWS, data was acquired on four profiles oriented to be orthogonal within the topographic limitations of the area. Figures 6.6 and 6.7 shows the stations at which data was acquired; the station names show the primary direction and range to the SLFT (SSW) (e.g. N450 is a station 450 m north (N) and SE515 is a station 515 m southeast (SE) of the SLFT).

The local topography allowed TL profiles to be laid out in two primary directions, north-south and east-west. The north-south direction is characterized by a minor elevation difference. The near surface layer varies from boggy, saturated peat to tightly compacted sandy-clay soil along this profile. Figure 6.14 shows the TL analysis along this north-south profile (TLP(S-N)) and an estimate of the elevation at each station. The X-axis shows the range north or south of the SLFT, the left Y-axis is the estimated TL (dB); the right Y-axis shows the estimated elevation above sea level (m).

The higher valued outlier in the TL estimates at station N160 is related to the properties of the near surface; in this area a denser, higher velocity layer outcrops at the surface and more efficiently transmits signals from the SLFT. Since the near-surface structure of the area is characterized by layers with different elastic parameters there is a natural dependence between the TL estimate and the elevation of the station.

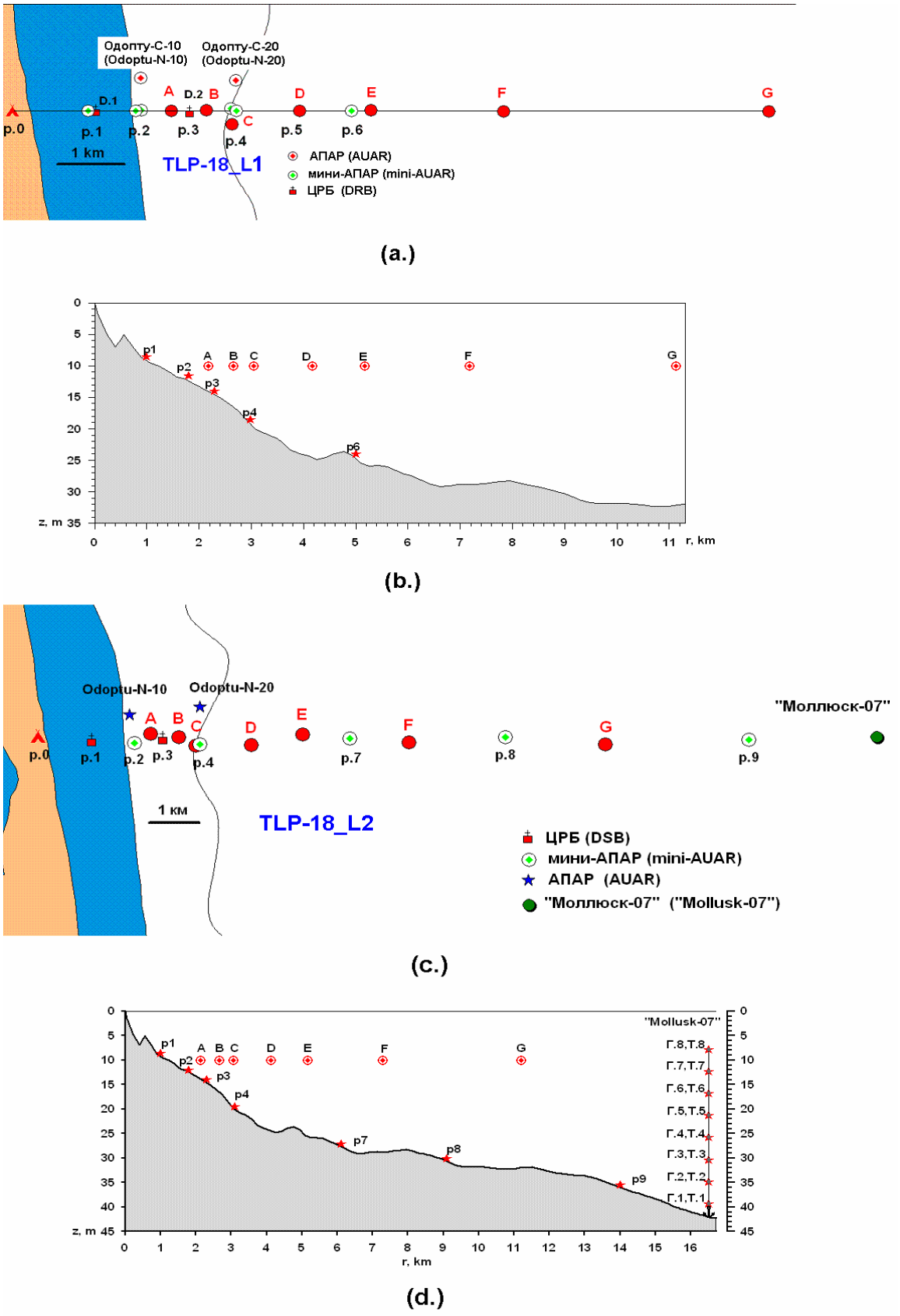

Figure 6.13 - Map of the area showing the locations where the acoustic recorders were deployed, the acoustic signal was generated, and the bathymetry along seismo-acoustic profiles TLP-18_L1 and TLP-18_L2.

The east-west profile is characterized by a greater variability in the elevation and the near-surface elastic properties. As discussed previously these differences lead to a significant irregularity in the TL estimates due to station to station differences. Figure 6.15 shows a significant variability in the TL estimates to the east, which is related to elevation differences along the profile, Figure 6.16 shows eastern part of the profile with a linear horizontal axis.

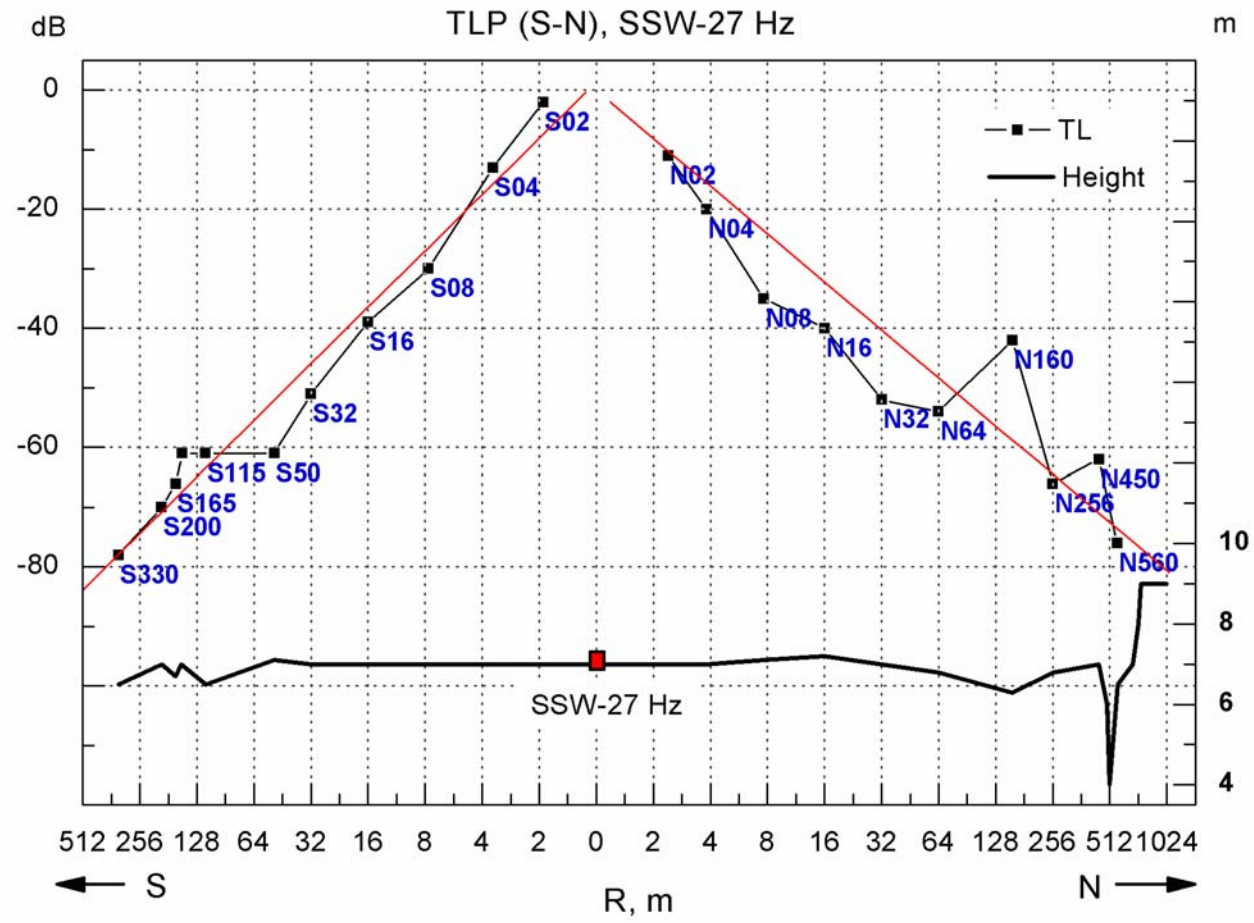

Figure 6.14 – Estimated TL and elevation along onshore TL profile TLP(S-N).

The significant difference in estimated TL at locations E80 and E88 which are at the top and bottom of a hill respectively illustrate this; station E80 is loose soil with surface water, while station E88 is on a dense, competent layer. Station E88 can be easily accessed using a cabled hydrophone, and is protected from the wind, allowing it to be used as an additional monitor for the signal stability of the SLFT (variations < 1 dB).

6.3 Analysis of range dependent TL along seismo-acoustic profile TLP-18_L

Figure 6.13 is a schematic of the area showing the locations where the acoustic equipment was deployed during TL studies on profile TLP-18_L, which were conducted from 2 to 8 August 2007. Figure 6.17 displays the bathymetric and hydrologic (temperature, salinity and velocity) profiles acquired on 6-7 August 2007 for the offshore section of profile TLP-18_L2.

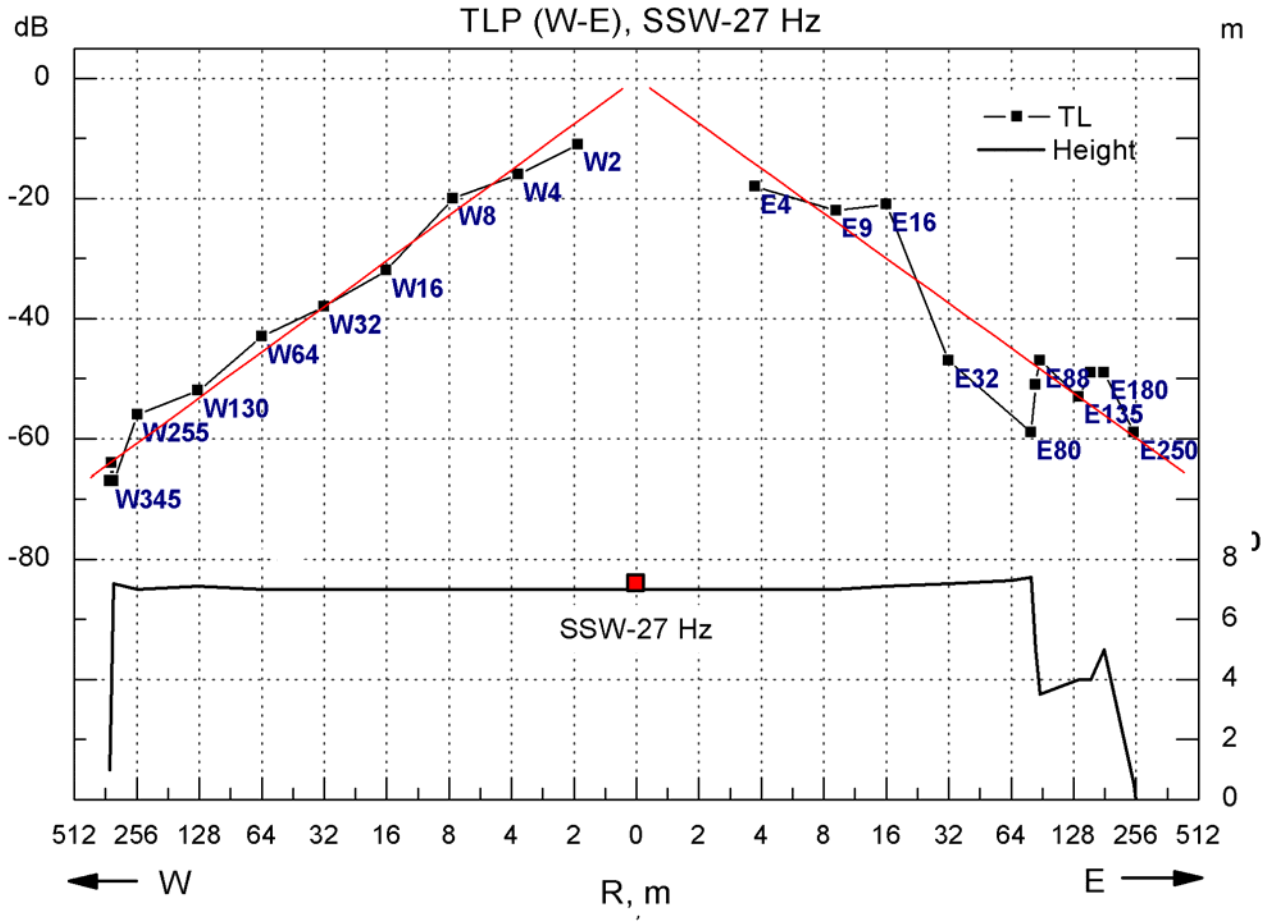

Figure 6.15 – Estimated TL and elevation along onshore TL profile TLP(W-E).

Figure 6.13 shows that synchronous acoustic measurements were taken at six locations (p.1-p.6) in the offshore section of seismo-acoustic profile TLP-18_L1, and seven on profile TLP-18_L2; the Mollusk-07 autonomous vertical acoustic and hydrologic recording system was deployed at station p.7. Station p.7 is 16.5 km from shore and the Mollusk-07 enabled synchronous acoustic and temperature measurements at eight depths (Figure 6.13(d)). Low frequency signals at frequencies of 25-31 Hz were generated onshore by the SLFT at location p.0, which was 260 m from the shoreline, and offshore by an LF transducer lowered to a depth of 10 m from the anchored *Professor Bogorov*, the offshore source

locations are marked with red dots and letters in Figure 6.13(a) and 6.13(c). The low-frequency signals generated onshore and offshore were also received by hydrophones deployed offshore and onshore. This experimental design generated extensive field data, allowing analysis of the propagation characteristics of 25-31 Hz seismo-acoustic signals in the shallow-water section of the NE Sakhalin shelf.

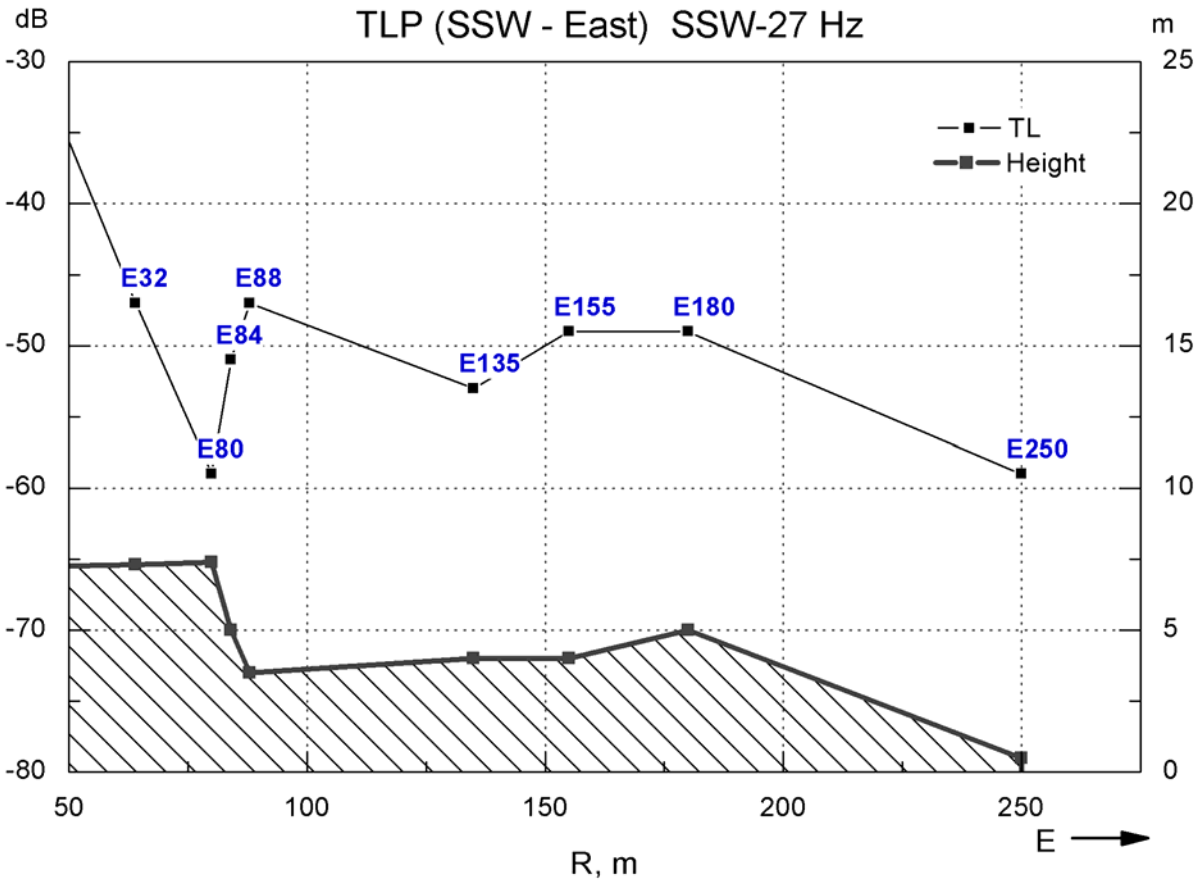

Figure 6.16 – Estimated TL and elevation along eastern onshore TL profile.

Figure 6.18 gives the transmission losses estimated from field measurements of tonal seismo-acoustic signals with frequencies from 25 to 31 Hz generated at point p.0. Figure 6.18(a) displays the entire TLP-18_L2 seismo-acoustic profile with a logarithmic distance axis; Figure 6.18(b) shows the offshore part in greater detail, with a linear distance axis. It should be noted that the data at points p.1–p.9 was acquired with hydrophones deployed ~0.3 m from the sea floor, so transmission losses were estimated using the lowest hydrophone, H.1, of the Mollusk-07 (see Fig. 13d). This hydrophone is approximately 2 m above the sea floor; the TL estimate at this location is therefore expected to be an overestimate.

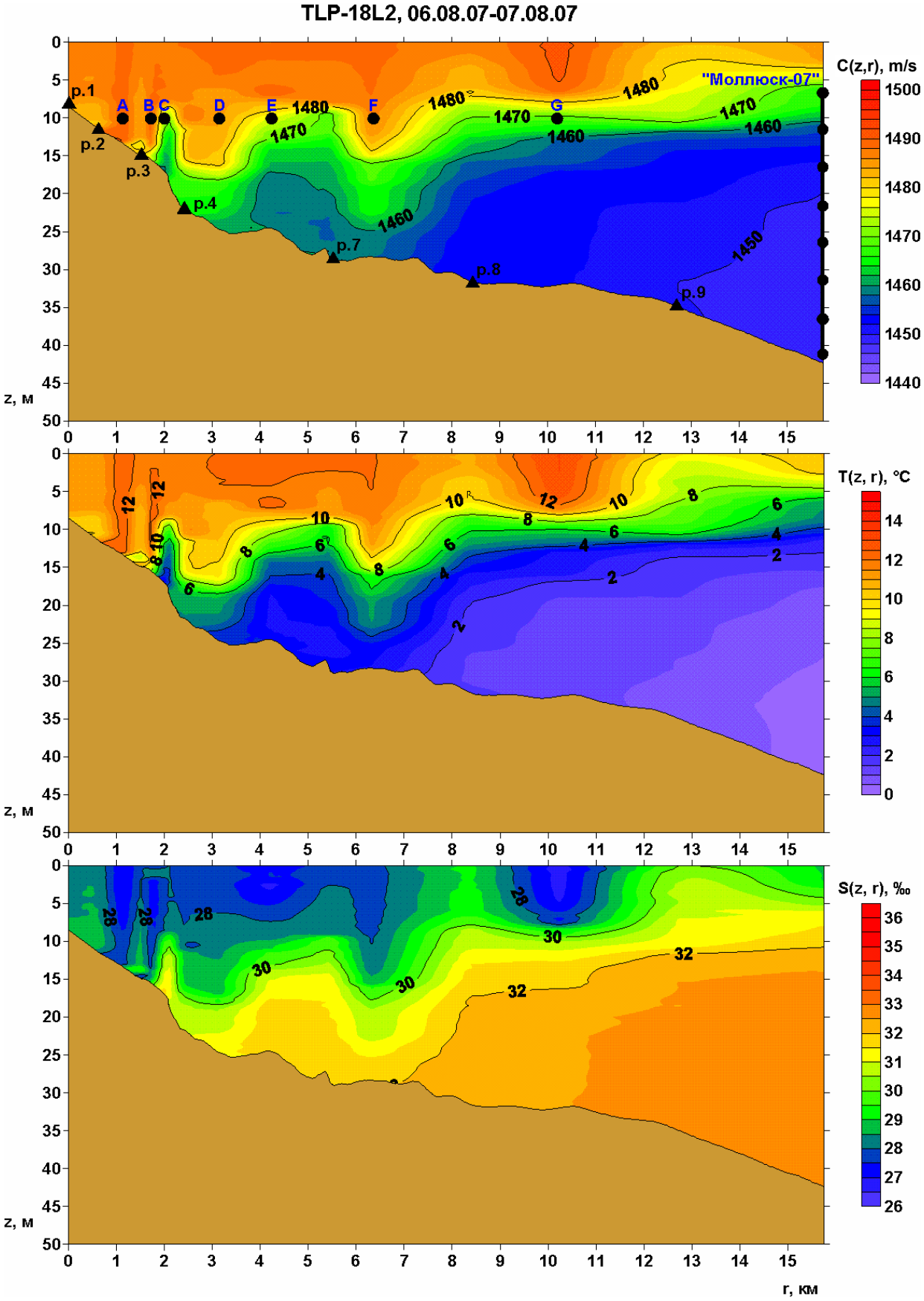

Figure 6.17 – Spatial distribution of velocity C(z,r), temperature T(z,r), salinity S(z,r) and bathymetry along seismo-acoustic profile TLP-18_L2.

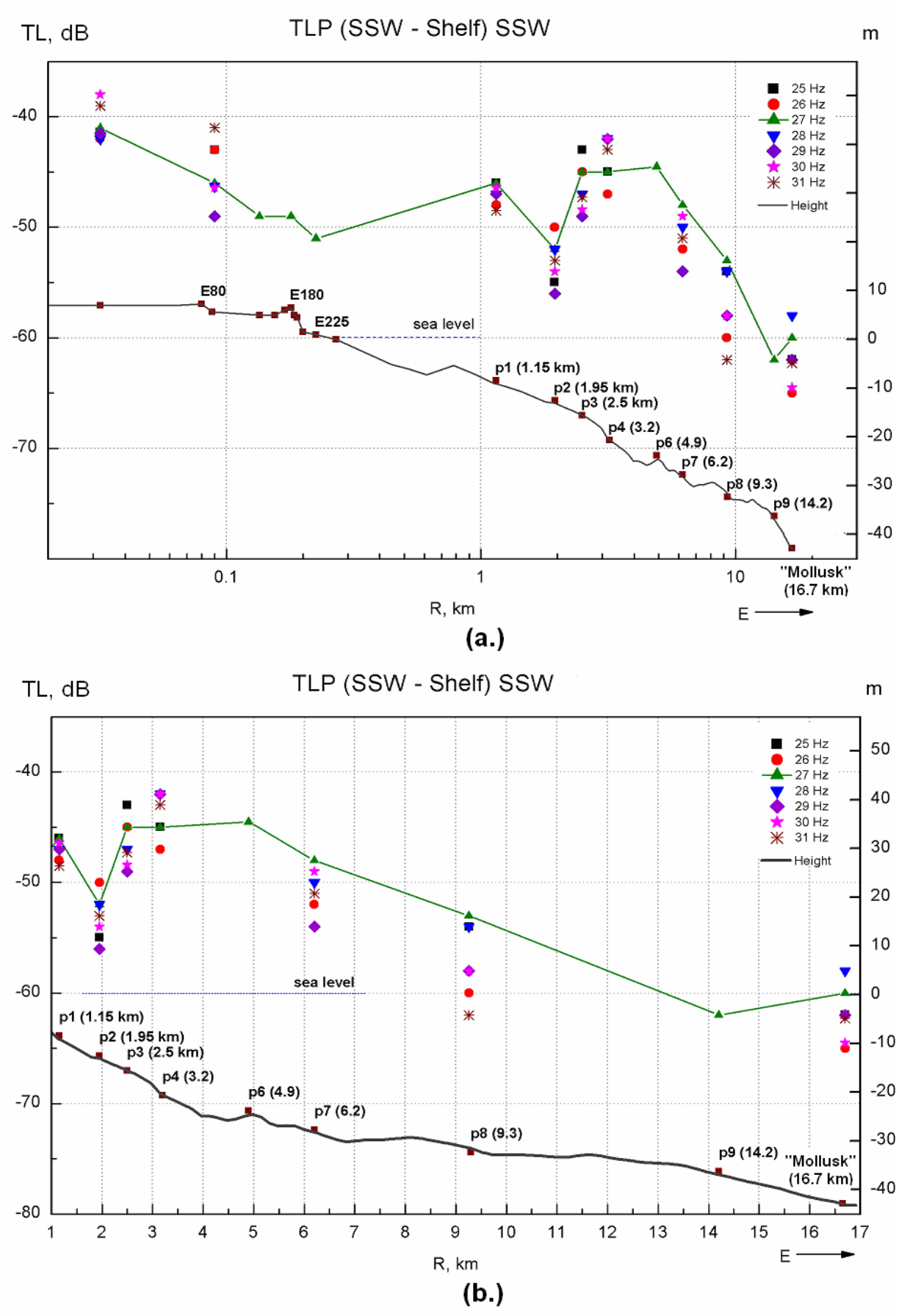

Figure 6.18 – Estimated TL along seismo-acoustic profile TLP-18_L2.

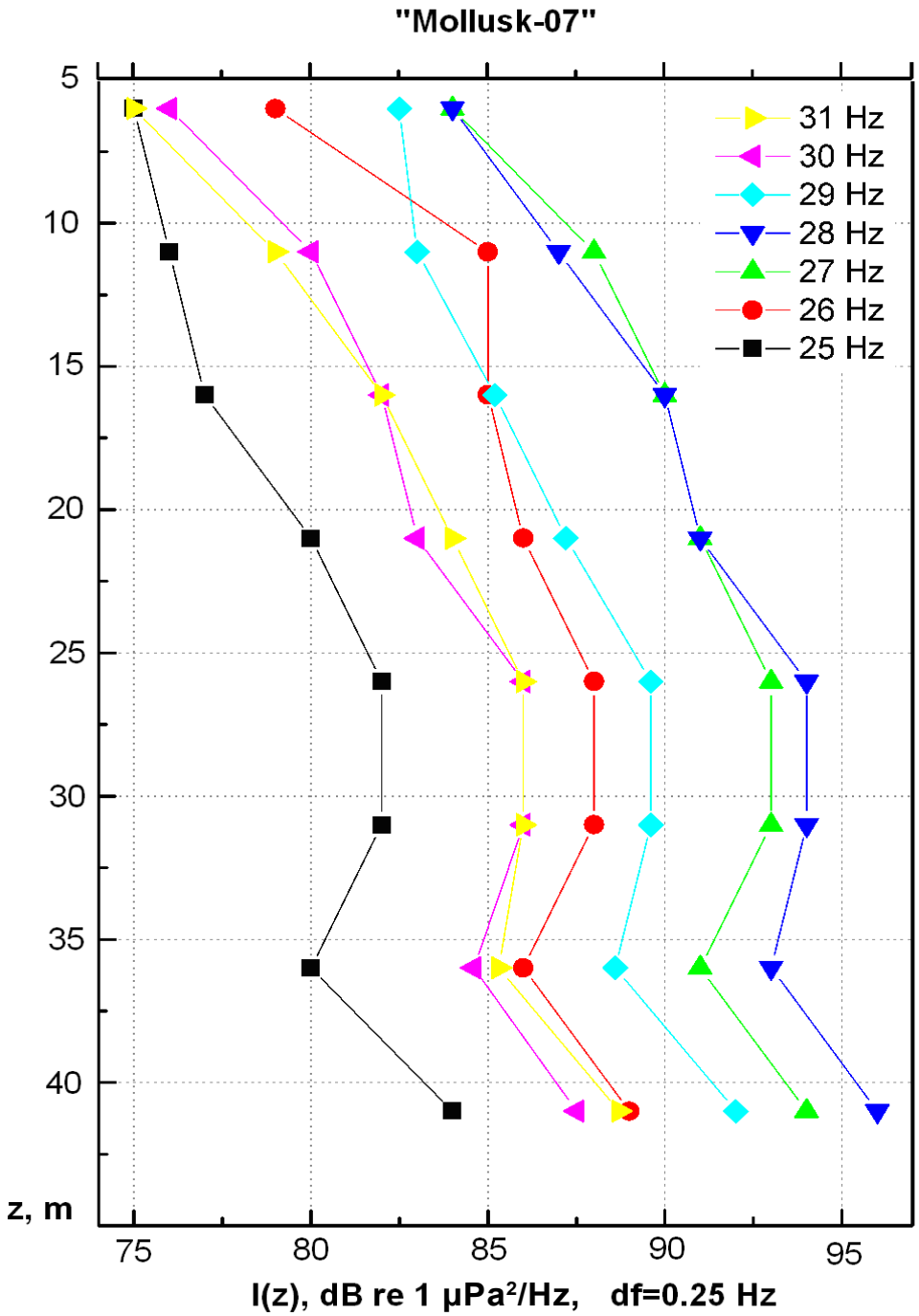

Figure 6.19 - Vertical distribution of seismo-acoustic energy generated onshore at station p.0 and received by the 8 hydrophones of the Mollusk-07.

Figure 6.19 shows the variation in the received level with depth of different frequency signals generated onshore by the SLFT; the data was acquired by the eight hydrophones of the Mollusk-07 in 43 m of water 16.7 km from location p.0. The shape of the plots of *I(t)* in Figure 6.19 and the estimated TL values displayed in Figure 6.18, indicate that the seismo-acoustic energy generated onshore mainly propagates as seismic waves in more competent sediments and attenuates rapidly with distance from these layers. The 7 dB

decrease in TL at station p.3 (range 2.5 km, depth 16 m) relative to station p.2 (range 1.95 km, depth 12 m) suggest the presence of an attenuating surface sediment layer at station p.2, while at station p.3 denser sedimentary layers are close to the surface, low frequency energy propagates along these layers with relatively lower transmission loss. When the water depth is greater than 25 m, seismic waves may excite the first normal acoustic mode in the water layer when reflecting and scattering on acoustic inhomogeneities in the sea floor sediments. This mode can transmit low frequency energy in the water layer with even smaller losses.

Figure 6.19 illustrates that the received level of seismo-acoustic signals in water 43 m deep is greatest at the maximum hydrophone depth (2 m from sea floor) for all frequencies and decreases by more than 10 dB at a depth of 36 m, possibly due to interference between the first and second normal modes in the water layer, which propagate when the water depth is greater than 40 m. Since the level of the acoustic field in the water layer is a maximum at the bottom for all of the studied frequencies (Figure 6.19), it is reasonable to conclude that the low-frequency energy (25-31 Hz) generated onshore by the SLFT propagates mainly in the sea floor sediments.

Table 6.2 - TL values for seismo-acoustic signals recorded by the Mollusk-07.

Hydrophone	Depth (m)	Frequency of SSW in Hz						
		25	26	27	28	29	30	31
H-1	40	–62	–64.6	–60	–57.4	–61	–64.5	–62.3
H-2	35.5	–66	–67.6	–63	–60.4	–64.4	–67.4	–65.7
H-3	31	–64	–65.6	–61	–59.4	–63.4	–66	–65
H-4	26.5	–64	–65.6	–61	–59.4	–63.4	–66	–65
H-5	22	–66	–67.6	–63	–62.4	–65.8	–69	–67
H-6	17.5	–69	–68.6	–64	–63.4	–67.8	–70	–69
H-7	13	–70	–68.6	–66	–66.4	–70	–72	–72
H-8	8.5	–71	–74.6	–70	–69.4	–70.5	–76	–76
mean		**–66.5**	**–67.9**	**–63.5**	**–62.3**	**–65.8**	**–68.9**	**–67.8**

Table 6.2 presents TL levels estimated for each of the hydrophones of the Mollusk-07 and their mean. From this table, we can see that the transmission loss function *TL(f)* is at a minimum for a frequency of 28 Hz (-62.3 dB), while at frequencies of 25 and 31 Hz they are -66.5 dB and –67.8 dB respectively (almost a factor of 2). This is probably due to the characteristics of low-frequency propagation in shallow water, as the transmission losses of

energy in the sea bottom sediments are approximately directly proportional to frequency, while in the water layer they are inversely proportional to frequency. For this region of the relatively shallow-water NE Sakhalin shelf, the TL is a maximum for 28 Hz seismic signals.

Stations A-G, coloured red in Figure 6.13, are the source locations at which low-frequency signals, including 28 Hz signals, were transmitted by a LF transducer deployed at a depth of 10 m from the anchored *Professor Bogorov*. These signals were synchronously received onshore and offshore, using two digital sonobuoys (DSB) and hydrophones deployed at onshore stations E88 (Figure 6.16) and E2. Table 6.3 presents the results of the analysis of these measurements. The higher signal level received onshore at station E2 compared to station E88 may be explained by denser near surface conditions at E2. Figure 6.2 shows that following the prolonged operation of the seismic source, the soil near it was compacted and the surface water present when the unit was deployed had disappeared. This compaction may also have effected the reception of the 28 Hz signal at station E2, which is ~2 m from the center of the SLFT.

Table 6.3 - TL values for a 28 Hz signal generated on the *Professor Bogorov*.

Receiver location		**Source location (see Fig. 6.13)**						
		A	**B**	**C**	**D**	**E**	**F**	**G**
p.0, (E2)	**TL, dB**	**–99**	**–101**	**–101**	**–98**	**–97**	**–103**	**–112**
	r, km	2.2	2.8	3.1	4.3	5.2	7.3	11.3
E88	**TL, dB**	**–108**	**–114**	**–115**	**–111**	**–108**	**–114**	
	r, km	2.1	2.7	3	4.2	5.1	7.2	
p.1, (DSB-1)	**TL, dB**			**–67**	**–63**	**–68**	**–76**	**–87**
	r, km			2	3.2	4.2	6.3	10.2
p.3, (DSB-2)	**TL, dB**					**–70**	**–70**	**–73**
	r, km					2.8	4.9	8.8

Table 6.3 shows that the transmission loss for an acoustic signal generated offshore and received onshore at stations E88 and E2 is at a minimum for signals generated at source location E, which is approximately 5.2 km from them: –97 dB for station E2. Note that the losses were –99 dB for source location A which is 2.2 km from E2, and -101 dB for source locations B and C. This value, -101 dB, is approximately equal to the loss when this signal is generated at source location F, 7.3 km from E2. The TL is therefore determined not only by the range to the source location, but also by the acoustic properties of the sea floor sediments at the source location. There is a good agreement between the stations for

which the TL values for signals generated both onshore and offshore are at a minimum (Table 6.3 and Figure 6.18). Offshore source location E is close to station P.6 (water depth 24 m) (Figure 6.13(a)), there is a 53 dB difference in TL between a 27 Hz signal generated by a source (deployed at 10 m depth) at location E and received onshore at p.0 (E.2) (-97 dB - Table 6.3) and a signal generated at P.0 and received offshore at p.6 (-44 dB - Table 6.4). For source location A and station p.3 (Figure 6.13(b)), the difference is 54 dB, and for source location G and station p.8 the difference is 56 dB (although G and P.8 are further apart).

6.4 Analysis of TL studies in the Odoptu area

Figure 6.20 is a map of the Odoptu area showing the stations at which 27 Hz seismo-acoustic signals were received. Table 6.4 gives the estimated TL values for acoustic data acquired during studies of a CW-28 Hz signal at station p.0 (Figure 6.1). The TL estimates computed for stations whose signal level exceeded the ambient noise level at the station by at least 4-6 dB. Figure 6.21 displays spectral estimates of acoustic data recorded at stations farthest from the source while the SLFT was generating a CW- 27 Hz signal and immediately after it was turned off. Comparison of the estimated TL values in Table 6.4 and in Figures 6.14 and 6.15 shows that the TL is significantly higher for signals propagating onshore than those propagating offshore. For example, a TL level of 78 dB was obtained for onshore stations S330 and N550 (less than 600 m from the SLFT), while offshore this level was estimated at the Odoptu-S-10 and Odoptu-S-20 stations, which are 10.2 km and 11 km from the source, respectively.

Measurements conducted on TL profile TLP-15 in 2006 [Borisov et al., 2007], indicated that for the profile from source location G to Odoptu-N-10, which is 9.7 km long and parallel to TLP-18_L2, but approximately 500 m farther north, the TL for an acoustic signal generated by an LF transducer at a depth of 10 m is 82 dB. In 2007, for a signal generated onshore at p.0 by the SLFT, the TL to location G (averaged between p.8 and p.9) is approximately 57 dB (Figure 6.18); Table 6.4 gives the TL to station p.9 (range 14.2 km) as 63 dB. Table 6.4 also shows that for seismo-acoustic profiles oriented approximately parallel to the shore (Figure 6.20) the TL is significantly greater (e.g. BEH-Odoptu station (range 7 km, TL=70 dB); Odoptu-S-20 station (range 11 km, TL=78 dB); and Odoptu-PA-B station (range 17.4 km, TL=82 dB)).

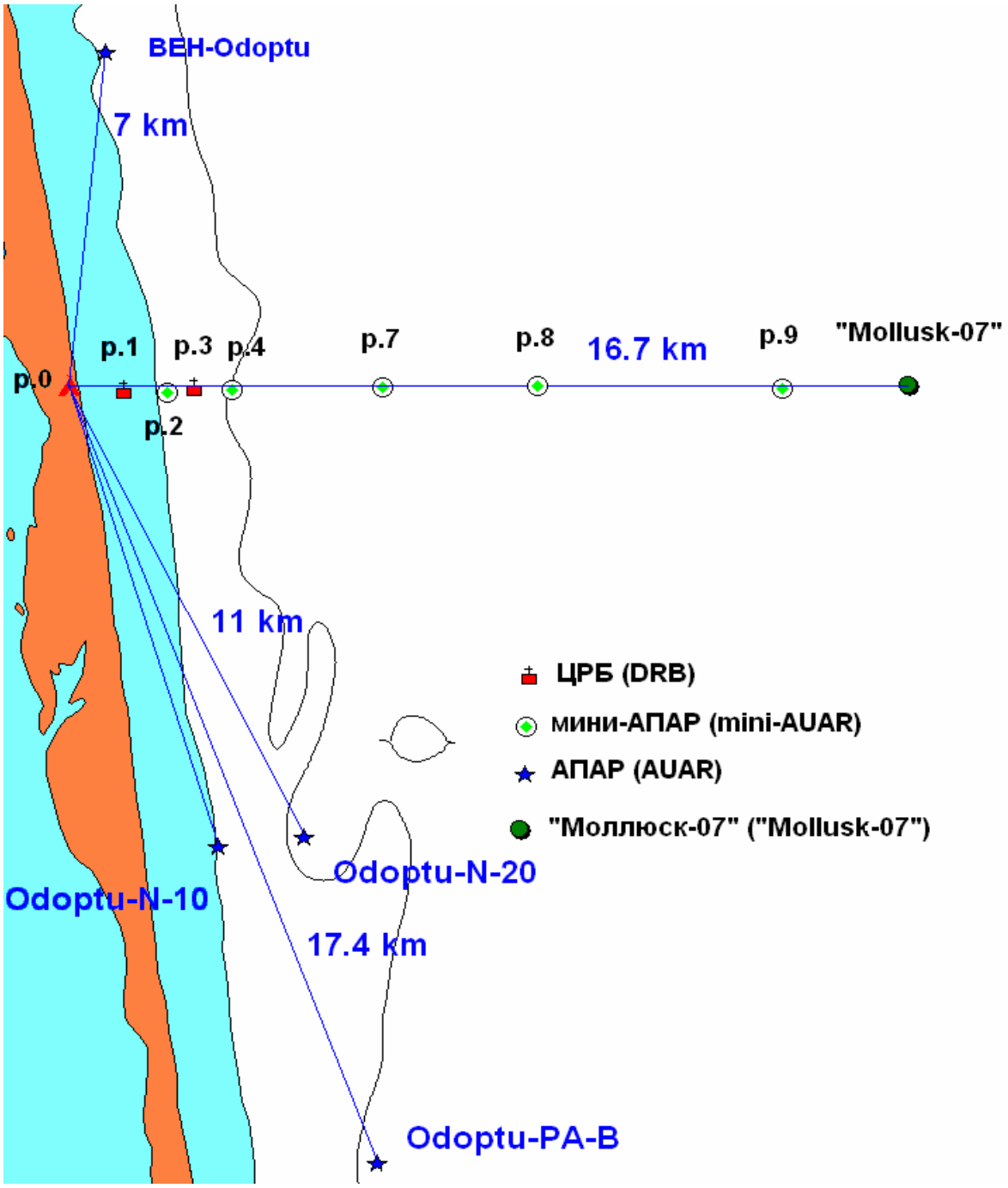

Figure 6.20 – Map of the Odoptu area showing the locations at which the signals from the SLFT were received.

6.5 Comparative analysis of 2006 & 2007 seismo-acoustic studies

The seismo-acoustic measurements presented in this report are a continuation of 2006 studies in the same area [Borisov et al., 2007]. In 2006 studies were conducted on seismo-acoustic profiles TLP-17 and TLP-18. In 2006, the seismic source was deployed on a sandy beach close to the sea, while in 2007 it was deployed on an elevated plateau

7.5 m above sea level and 260 m from the waterline. Seismo-acoustic profile TLP-18 was acquired along a profile parallel to and 500 m north of TLP-18_L. During 2007 more comprehensive onshore studies were conducted covering the Odoptu-FSP area and offshore, the coastal area out to the 43 m bathymetry contour. The Mollusk-07 autonomous vertical acoustic and hydrologic recording array was successfully used on the seismo-acoustic profile in 2007.

The near surface conditions at the locations where the SLFT was deployed were fundamentally different: fine, wet sea sand in 2006 and clay in 2007, the locations of the source (a beach and a plateau 7 m above sea level) were also very different. The different near surface structure of the area must also be taken into account when interpreting the data. Table 6.5 compares the conditions and results of the observations from the different source locations in 2006 and 2007.

Table 6.4 - TL values for a 27 Hz seismic signal generated at point p.0.

Odoptu SLFT *(27 Hz)*	**August 2007**								
Name	**p.1**	**p.2**	**p.3**	**p.4**	**p.6**	**p.7**	**p.8**	**p.9**	**"M-07"**
r, km	1.15	1.95	2.5	3.2	4.9	6.2	9.3	14.2	16.7
H, m	8	12	16	21	24	28	32	36	43
TL, dB	–48	–51	–45	–45	–45	–48	–53	–63	–62

Odoptu SLFT *(27 Hz)*	**August 2007**				
Name	**"M-07"**	**BEH-Odoptu**	**Odoptu-S-10**	**Odoptu-S-20**	**Odoptu-PA-B**
r, km	16.7	7	10.2	11	17.4
H, m	43	12	12	20	22
TL, dB	–62	–70	–78	–78	–82

Comparing the near field TL (from 2 to 10 m) for a 27 Hz tonal signal, the TL at 10 m was 121 dB in 2007 and 148 dB in 2006; the source of this difference is probably the near surface conditions at the SLFT deployment locations. The 2006 and 2007 analysis results for the onshore profiles give a similar variation in TL with range. When the different source location conditions are considered, the two data sets give similar results.

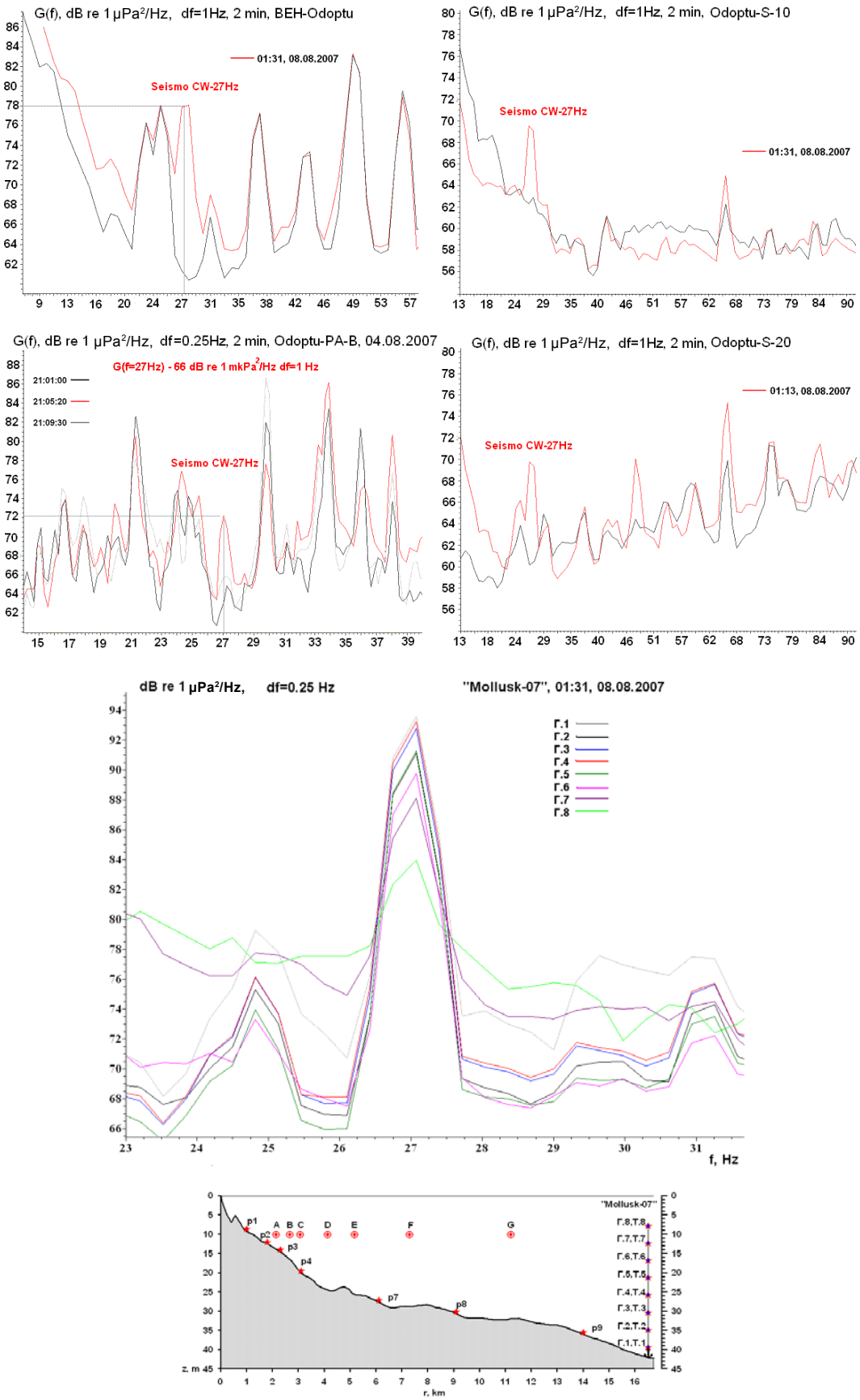

Figure 6.21 – Spectra of the acoustic field measured at the locations in Figure 6.20, both when the SLFT was operating and when it was not.

Table 6.5 - Comparison of the 2006 & 2007 deployment conditions and results.

	2006	2007	Comment
Source			
Installation site	Beach, 50 m from shoreline, Sea level	Plateau, 260 m from shoreline, 7 m above sea level	
Deployment conditions	Fine wet sand	Compacted clay, probably underlying sedimentary or permafrost layers	
SLFT - 27 Hz signal strength in the near field			
2 m from source	Measurements made only to the east 158 dB	152-160 dB. Depending on azimuth angle.	Figure 6.11.
10 m from source	Measurements made only to the east in wet sand - 148 dB	Wet clay - 121 dB	
Onshore measurements - TL for a CW-27 Hz signal generated by SLFT			
250 m from source	At range of 238 m to W: -71 dB	To W: -62±3 dB; To N & S: -70±3 dB	See Figures 6.14 and 6.15
Offshore - TL for a CW-27 Hz signal generated by SLFT			
1.8 km from source	-59 dB	At 1.95 km range: -52 dB	
5 km from source	-58 dB	-50±3 dB	

When the TL estimates for the offshore section of the seismo-acoustic profile are compared (Table 6.5) the results show similar values for a distance of 1.8 km: –59 dB in 2006 (Table 6.1 in the 2006 report) and –52 dB in 2007 (Fig. 6.18); and at 5 km: –58 dB and –50 dB in 2006 and 2007, respectively. The differences between the 2006 and 2007 TL estimates can be seen at other ranges and are probably due to the different location of the source during the two experiments. The wet beach sand transmits seismic vibrations less efficiently than compacted wet clay soil with underlying competent layers.

Thus, the 2007 measurements extended the results from the previous season and enabled some important refinements to be made to the model. The elevated plateau where the Odoptu-FSP will located is more efficient than wet beach sand at propagating low-frequency seismo-acoustic signals due to the underlying near surface characteristics. The estimated TL along the offshore section of profile TLP-18 (2007) is –50 dB at a distance of ~1 km from

the source, remaining at approximately the same level out to ~6.5 km except for a decrease of ~6 db at approximately 12 m water depth. This variability in estimated TL is probably due to the sub-surface characteristics of the area, the more efficient transmission of seismic energy along competent sub-surface layers and the locations where these layers get close to, or outcrop at, the seabed, generating an acoustic field in the water column.

6.6 Signal propagation analysis using a modal model of the acoustic field

To understand the characteristics of low-frequency propagation from the Odoptu-FSP area offshore, a modal model can be used to analyze the effect of continuously deepening bathymetry on the formation of an acoustic field. For the shallow water near the Odoptu-FSP, the most significant contribution to the acoustic field generated by an onshore source is the first mode (eigenfunction). Figure 6.22 displays plots of eigenfunctions calculated for a two-layer model of water and fluid sediments with four different water layer thicknesses H.

The shape of the eigenfunction plots indicates that the water layer propagation efficiency for a 27 Hz acoustic tone differs sharply for varying water depths. For a water layer with a depth less than 20 m, most of the energy in the acoustic field propagates in the seabed, resulting in a large TL. As the water depth increases, the eigenfunction maximum moves into the water layer, indicating more efficient acoustic propagation in the waveguide for that water depth. The practical effect of this is to cause a decrease in TL for a waveguide with a water depth greater than 20 m relative to the shallower water section. Seismic waves propagating in competent subsurface layers can form an acoustic field in the sea when the layers approach the sea floor and the depth is conducive to acoustic wavefield formation. These mode model studies can provide a basis for further theoretical studies and numerical modeling, but require further data on the elastic properties and subsurface structure along seismo-acoustic profile TLP-18_L.

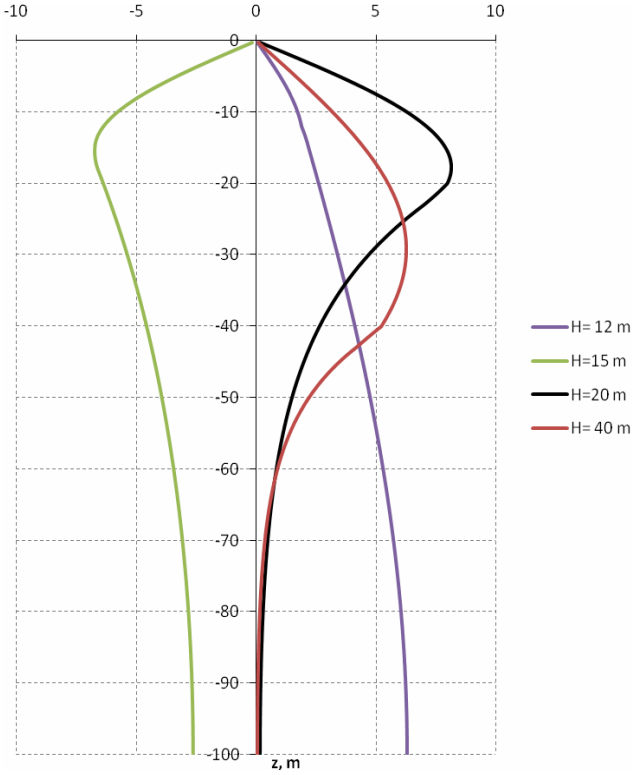

Figure 6.22 - Plots of eigenfunctions (modes) for a 27 Hz acoustic field and models with a water layer with depth (H) of 12, 15, 20 and 40 m.

7 Bathymetric and Hydrologic Studies on the NE Sakhalin Shelf

This section presents the analysis of bathymetric and hydrological measurements performed during the 2007 field season. Bathymetric and hydrological measurements conducted during the 2004, 2005 and 2006 field seasons are also used to explain the spatial distribution and variation in the temperature *T(r,z)* and salinity fields *S(r,z)* observed in the study area. In addition, the results of studies by other authors in the area are included. This data will be used to build acoustic models which will be used to model the acoustic fields generated by known sources and analyze the impact of bathymetry and hydrology on the propagation of these fields. The data will also be used to investigate the impact of temperature and salinity variations on benthos development.

Previous studies have shown that the following factors have the greatest influence on the hydrologic and acoustic properties as well as the biological productivity of the shallow waters of the NE Sakhalin shelf, especially the waters near Chayvo and Piltun bays:

- Wind mixing, especially under the influence of southerly and northerly winds, which cause upwelling downwelling respectively, along the coast;
- The intensity of vertical and horizontal mixing associated with tidal events;
- The dimensions and dynamics of the Amur River discharge lens, in which the water temperature is higher and the salinity lower than in the waters of the shelf of the Sea of Okhotsk, and on the edges of the front separating this lens and the waters of the Sea of Okhotsk; and
- The dynamics of the near-bottom layer of high-density water formed on the shelf in the winter season due to convection and salinization (brine discharge) during ice formation;

The hydrological program continued during the 2007 field season and was devoted to the study of these factors. For the last four years, hydrological work on the NE Sakhalin shelf was performed with the Valeport SVXtra sonde[50] (Figure 2.27) which is equipped with temperature, conductivity and sound velocity sensors. At the end of July the board with the temperature and pressure sensors failed due to a leak in the unit's housing. The leak was repaired, the temperature and pressure sensors were replaced, and there were no further operational problems with the sonde.

[50] A detailed description of the sonde and its specifications is given in [Borisov et. al., 2006]; the calibration certificates are on the DVD in the back of this report.

7.1 Spatial and temporal variation of the key hydrological characteristics of the area

Oceanological studies were performed in an area from 51.4°N to 53.6°N and 143.1°E to 144.0°E (Figure 7.1). Overall, these observations extended over an area stretching from Lunskoye Bay to Urkt Bay along the NE coast of Sakhalin Island; this area of the Sea of Okhotsk extends approximately 250 km from its northern to southern edge.

Three full hydrologic surveys and 15 individual transects, both perpendicular and parallel to the coastline were performed in 2007. One hundred and eighty-three (183) vertical hydrologic profiles were acquired during acoustic work on several of TL profiles. The *Professor Bogorov* sheltered from storms in Severny and Sakhalin Bays on the north of the island, six transects were performed while transiting to, and daily observations were made while anchored in Sakhalin Bay. The measurements were made under different tidal and meteorological conditions. In total 634 vertical hydrologic profiles were acquired (comprising sound velocity, temperature and salinity). Two Potok autonomous current and water temperature meters (belonging to POI) were deployed in 43 m of water at a location east of Chayvo Bay. The units were operational from 23 July to 5 September. The units were recovered using a buoy submerged to a depth of 10 m from the station and equipped with an acoustic release.

The hydrologic surveys, which consist of six-nine transects each, were performed on days when the tidal effects were minimal (neap tides). Three surveys were performed in July; from these surveys the change in the water temperature and salinity at the sea surface during the month (Fig. 7.2) could be estimated. Around 10 July a relatively uniform temperature (9-11 °C) and salinity (27-29 psu) (practical salinity units) distribution was observed at the sea surface. Only along the coast near Piltun Bay was the surface temperature slightly lower (8 °C). In mid-July there was a constant moderate to strong southerly wind in the study area, as a result an upwelling zone formed along the coast, stretching at minimum along Chayvo and Piltun bays and extending 25-30 km out to sea. The water temperature in this zone did not exceed 5 °C, and the salinity was 30 psu. During the latter part of July, after the passage of a strong low-pressure system, slight northerly winds were mainly observed. This allowed mixed Amur waters to once again approach Piltun Bay. The surface water temperature rose to 9-11 °C, and the salinity

decreased to 27–29 psu. At the same time a temperature (8-6 °C) and salinity (29-31 psu) front was noted near Chayvo Bay. Another front, caused by nascent upwelling, was noted north of the mouth of Piltun Bay.

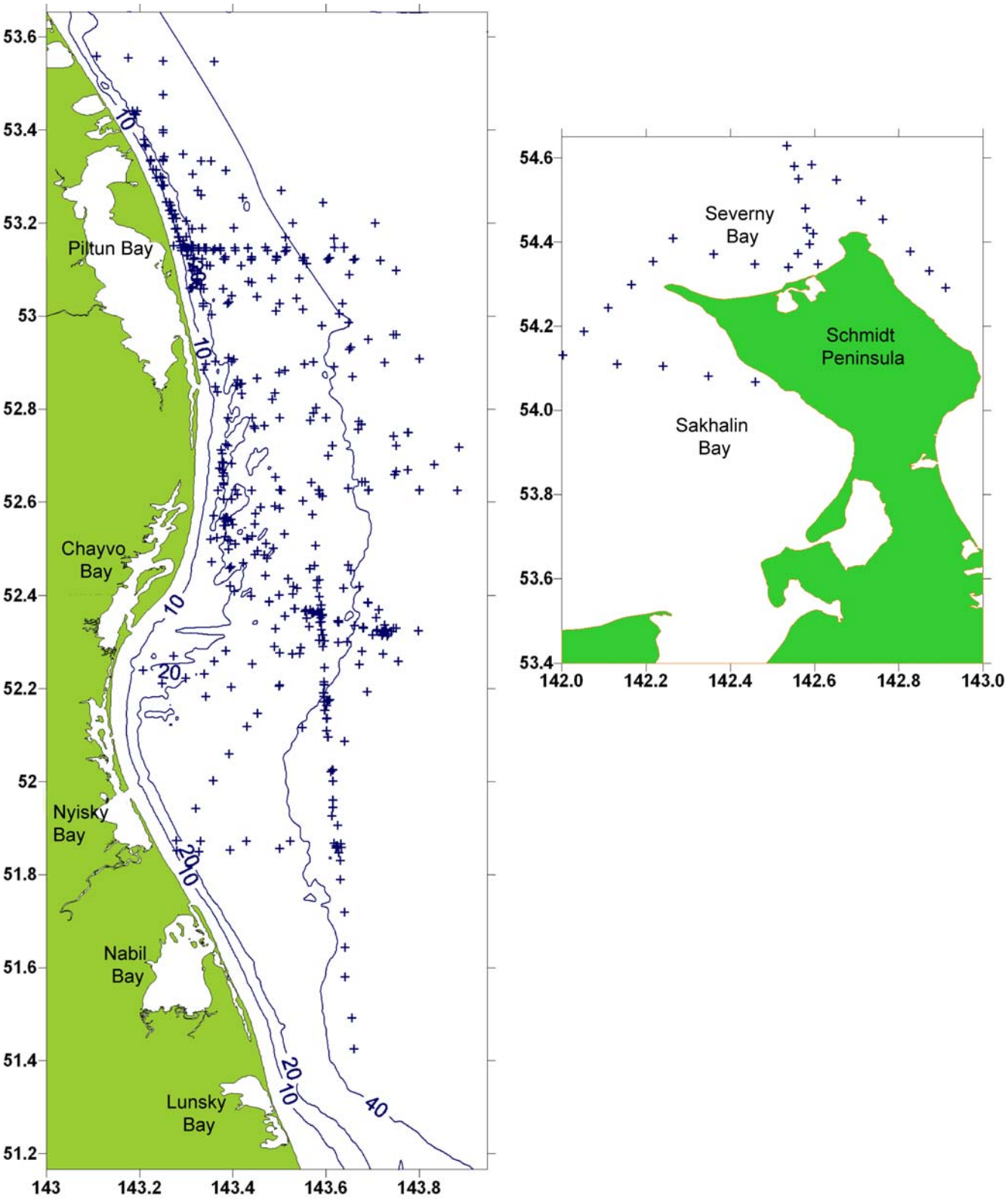

Figure 7.1 - Map of the NE Sakhalin Shelf showing (a) the bathymetry of the study area and (b) locations where vertical hydrologic profiles were acquired.

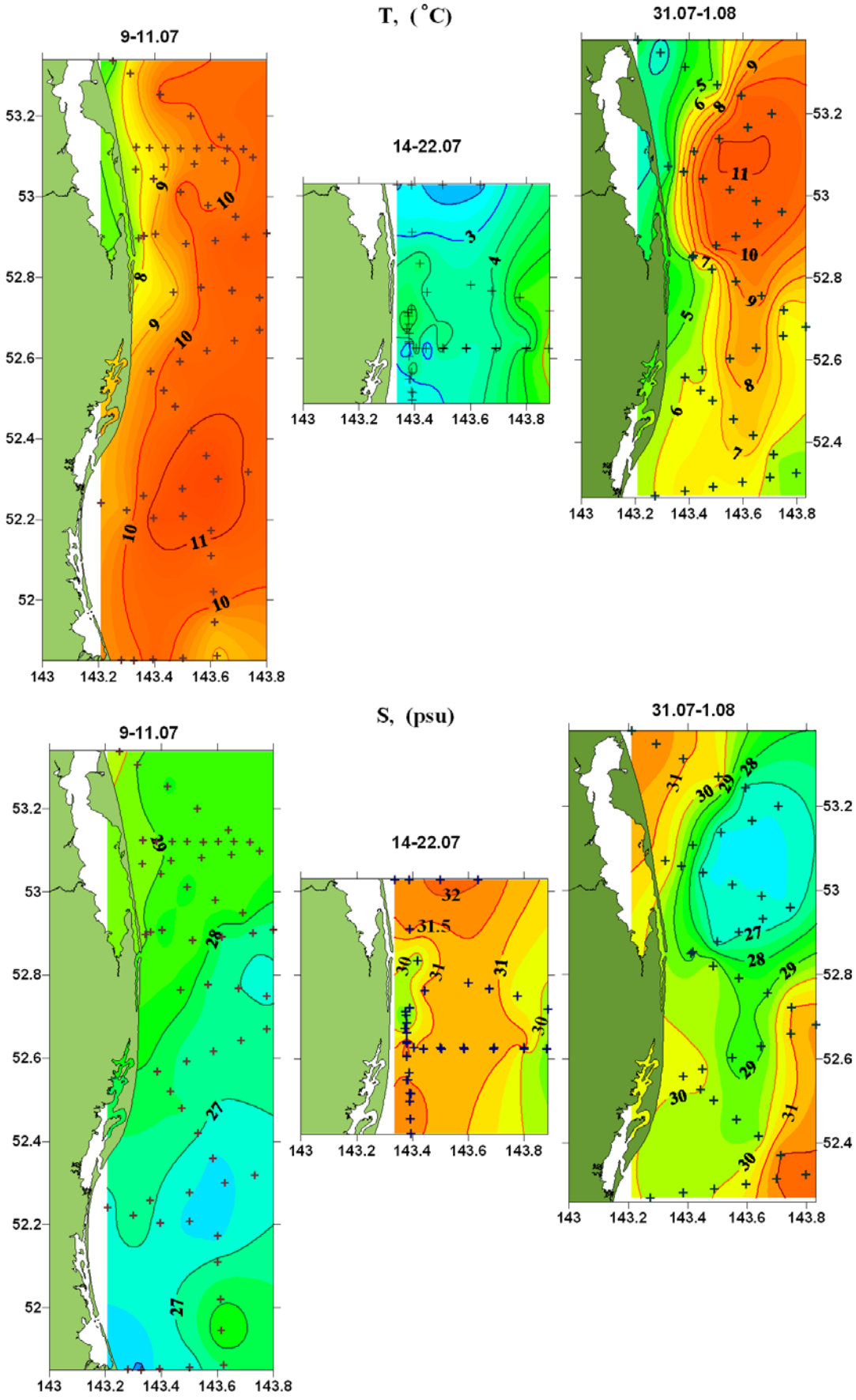

Figure 7.2 – Variability of sea-surface Temperature *T(r,z)* and salinity *S(r,z)* in July.
(values inside the lagoons are a plotting artifact and are not correct)

In 2007 the maximum sea surface water temperature was 5 °C lower, and the minimum temperature was almost a degree lower than in July 2006 [Borisov et al., 2007], while the range of salinity variation was practically the same. From 6 to 8 August, warmer and less saline water arrived once again.

In the middle of August the weather over the Sea of Okhotsk once again created a constant moderate to strong southerly wind in the study area. As a result an upwelling zone formed once again along the coast, stretching from Nyisky Bay to the middle of Piltun Bay, and the coastal zone was once again filled with cold (less than 5 °C) and saline (more than 31 psu) waters. As a result of the upwelling a new north-south temperature (5-10 °C) and salinity (32-39 psu) front formed. The coldest and most saline waters were seen near the coast, north of the mouth of Piltun Bay (Figure 7.3).

In the second half of August 2007, during the passage of a cyclone (21-22 August) and later, there were strong winds from the north and northeast and mixed Amur River waters once again approached the area; by the end of the month they had reached Nabil Bay (Figures 7.4 and 7.5). The sea surface water temperature and salinity were higher than at the end of July (up to 14.5 °C and 28.5–29.5 psu), and the uniform surface layer thickened to 10-15 m. A similar pattern was seen at the beginning of September.

Thus, in August 2007 the hydrologic conditions differed significantly from those at the same time in 2006. Within a month two extensive upwelling events were noted in the area, lasting from a few days at the beginning of the month to a week in the middle of the month. During the first period there was a spot of cold water along Piltun Bay; during the second it extended along Piltun and Chayvo bays all the way to Nyisky Bay.

At the end of August and beginning of September the uniform surface layer in the coastal zone expanded to 10-15 m, with a water temperature of 10-14°C and salinity less than 30 psu; the thermocline and halocline were found at a depth 5-10 m deeper than at the same time in 2006. The thickness of this uniform layer was still significantly dependent on the tidal stage. During this time no water was found with temperature below zero.

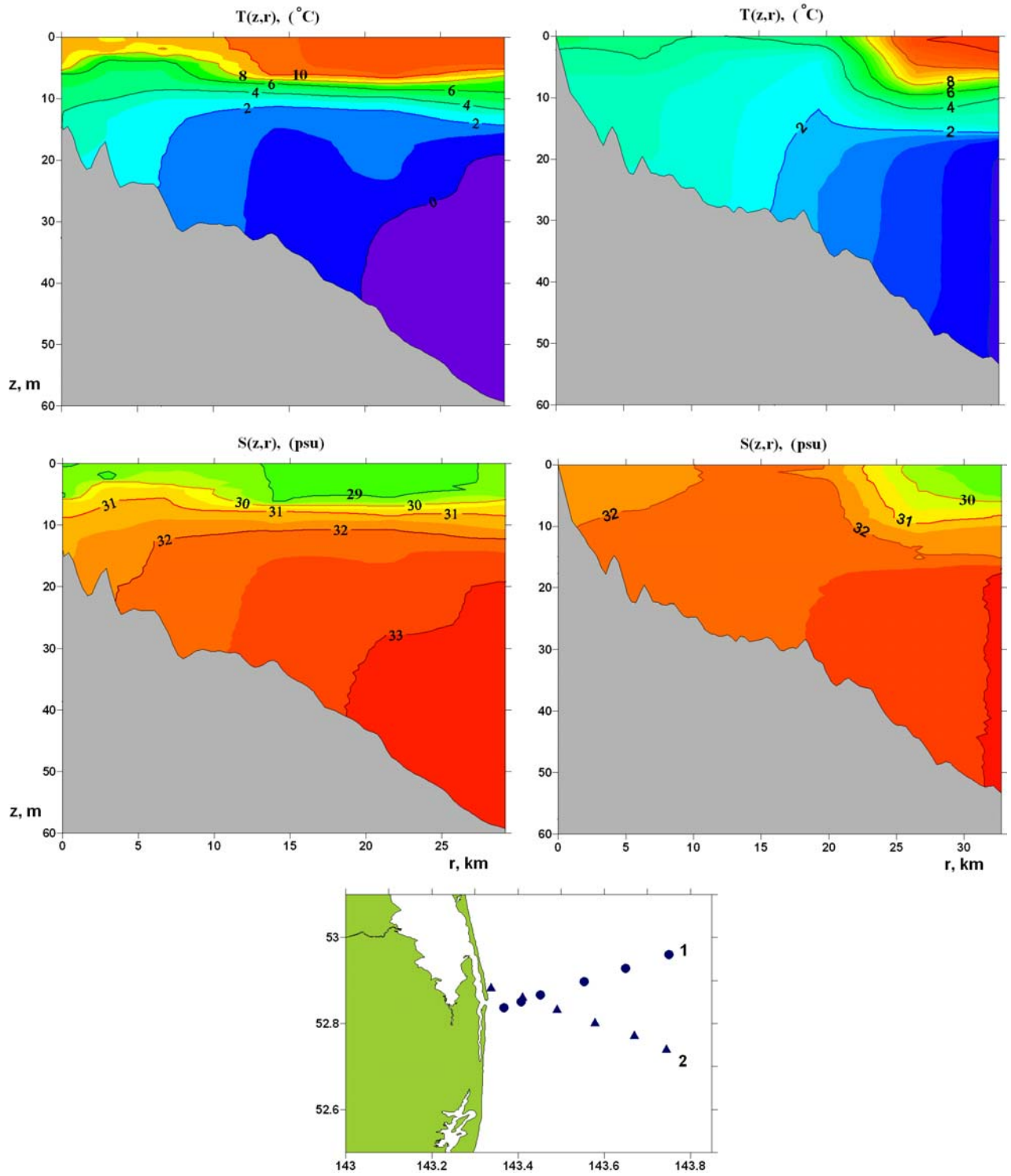

Figure 7.3 - Distribution of Temperature *T(r,z)* and salinity *S(r,z)* and the location of the sampling stations for a hydrologic transect east from the mouth of Piltun Bay acquired on 9 and 15 August 2007.

Thus, as in previous years, considerable spatial and temporal hydrologic variability was present in the area. In contrast to 2006, the maximum sea surface water temperature variability along the coast was noted in August: from 2 to 14.8 °C, while salinity varied from

27 to 32 psu. At the sea floor the temperature varied from 1 to 6 °C; and salinity, from 29 to 33 psu. In the middle of the month, the water temperature was lower than 0 °C for water depths greater than 40 m, and salinity was greater than 32.5 psu.

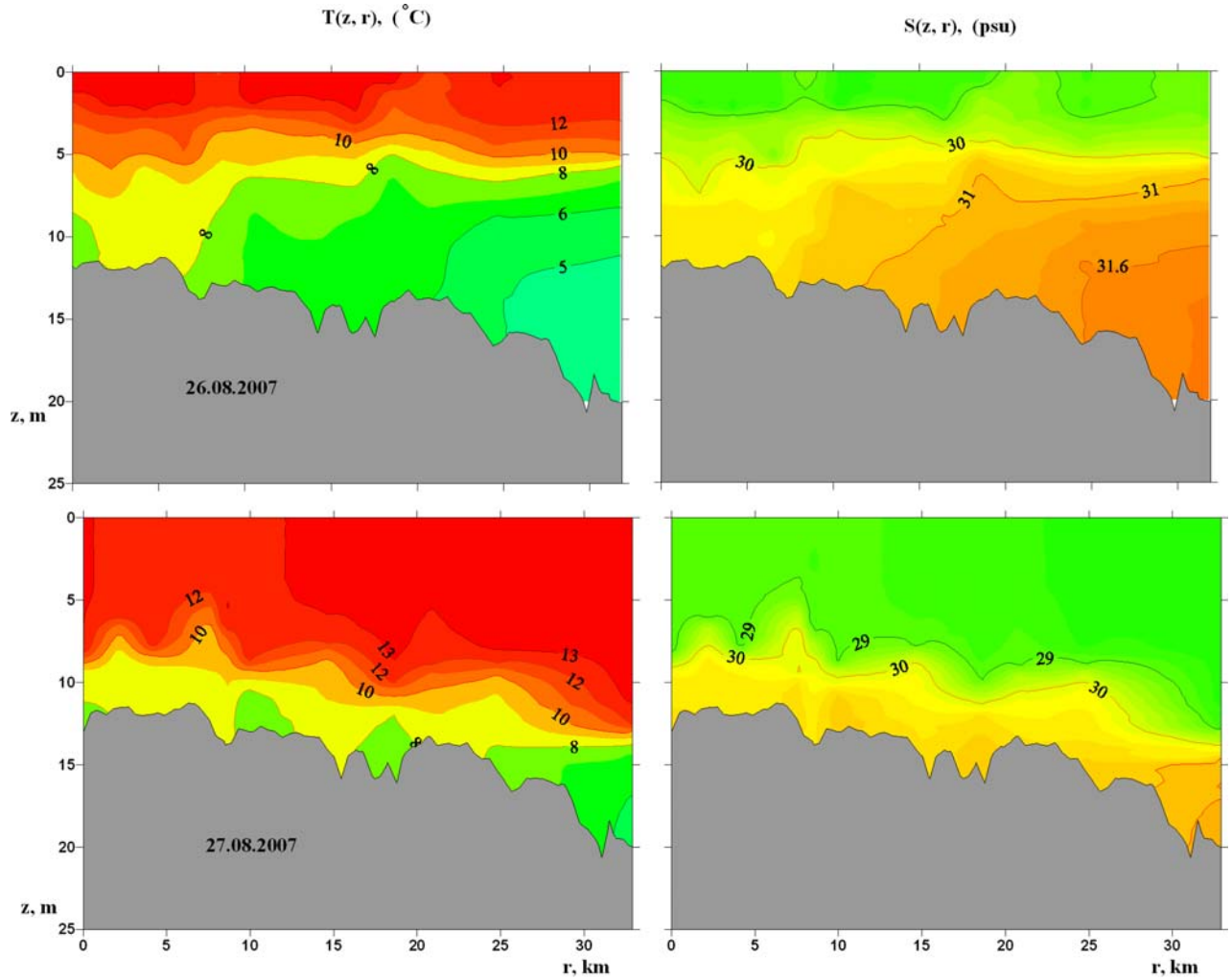

Figure 7.4 - Distribution of Temperature *T(r,z)* and salinity *S(r,z)* along a hydrologic transect along the shore opposite the northern section of Piltun Bay acquired on 26 and 27 August 2007.

For the entire time from July to September, upwelling formed frontal zones (in the 0-10 m layer) with significant water temperature and salinity gradients near Chayvo and Piltun bays.

7.2 Impact of tides and inter-annual variability of water temperature

As discussed in previous reports, the opposing directions of the sea surface and sea floor currents and vertical water flow near the coast when the tide is coming in, form surface patches of water with higher salinity and lower water temperature. The rate of vertical mixing depends significantly on the tidal phase and intensifies during syzygial (spring) tides,

when complete disruption of water stratification is possible. The report for 2006 [Borisov et al., 2007] described the effect of the flood tide in calm weather. The inflow of saline (>32 psu) and cold (<3.5 °C) waters towards the coast and their rise to the sea surface is evident in these conditions. At the same time, warm surface waters (>10 °C) were driven from the coast.

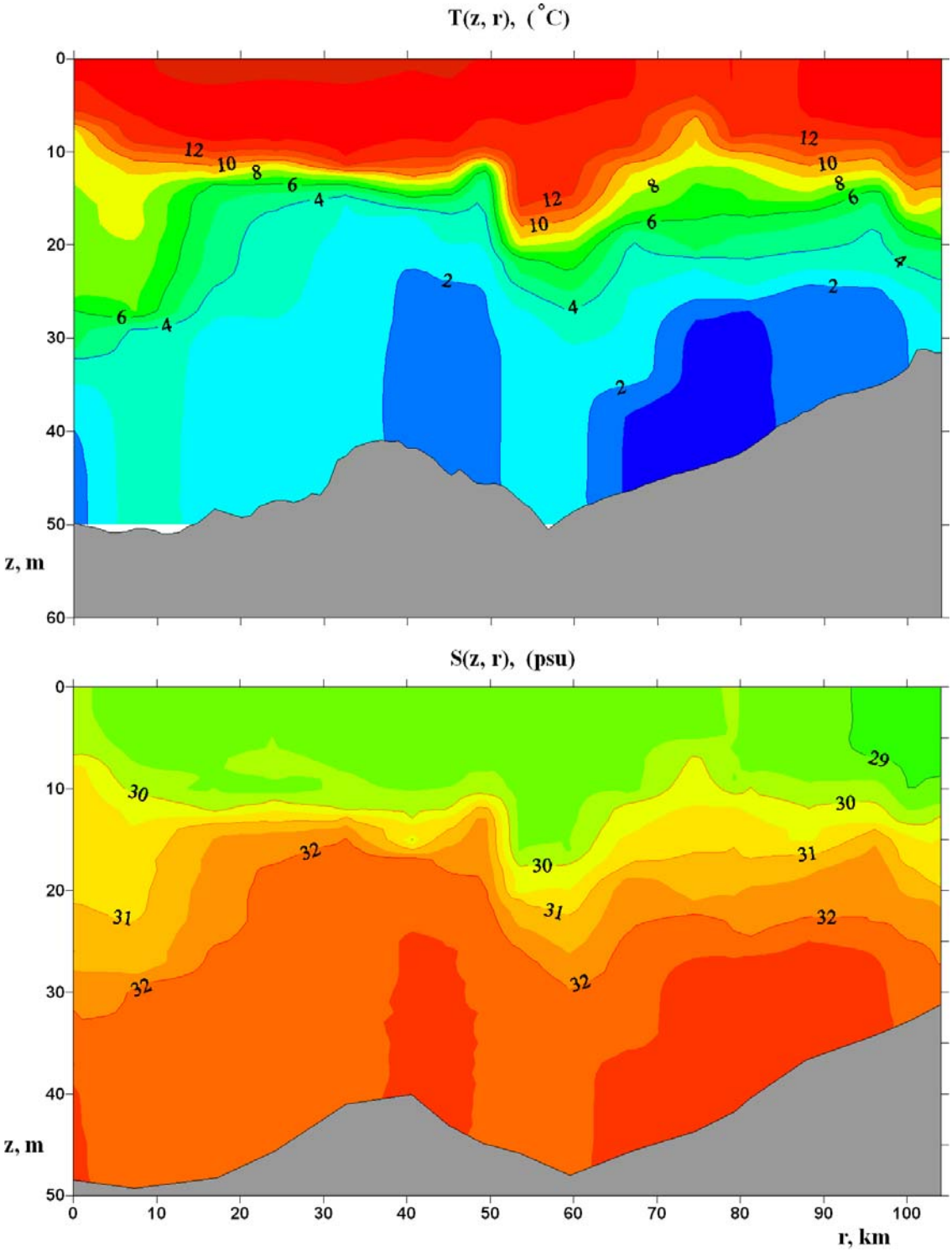

Figure 7.5 - Distribution of Temperature *T(r,z)* and salinity *S(r,z)* along a north-south hydrologic transect from the LUN-A platform to the Orlan monitor station, acquired on 31 August 2007.

On 11 and 12 July 2007, three transects were acquired at different tidal stages, with moderate to strong southeasterly winds, when upwelling started along the coast. Figure 7.6 shows that, at least in this case, the flood tide only affects the uniform surface layer. The warmer (greater than 8 °C temperature) water recedes approximately 5–7 km from shore after the flood tide and returns during the ebb tide.

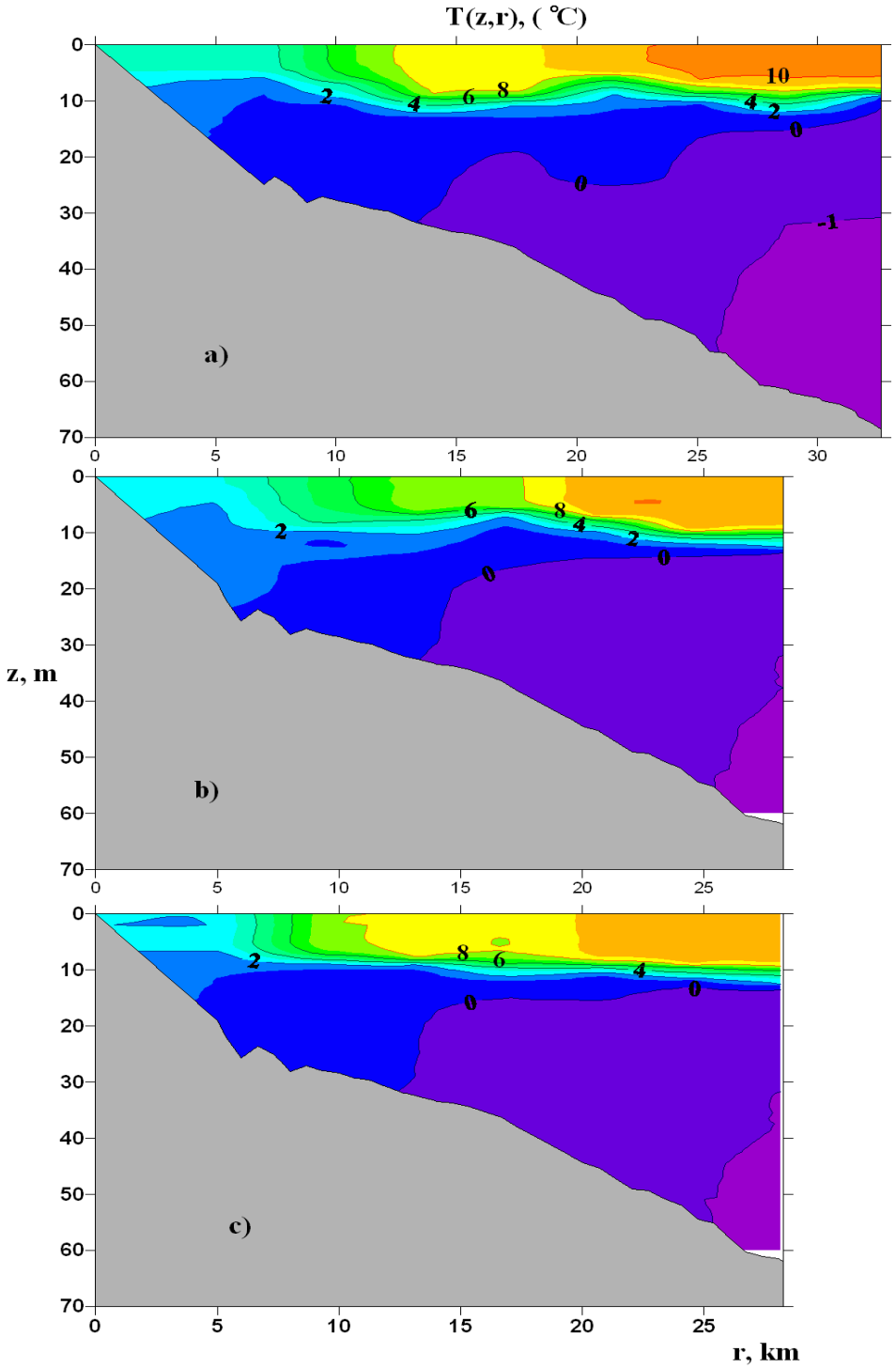

Figure 7.6 – Spatial distribution of water temperature in transects seawards from Piltun Bay acquired on 11-12 July 2007:(a) flood tide; (b) high tide; (c) ebb tide.

As previously noted [Kruglov et al. 2006], water temperature is one of the most important factors influencing the summertime benthos development on the Sakhalin shelf as it has a stimulating or restricting effect on biological productivity, the spawning time and spatial extent of various species, the maturation of eggs and larvae and the growth rate of young fish. This is especially true of the water temperature in the near bottom layer. The waters of the near-bottom layer are transported to the shallow coastal zone and rise to the surface during upwelling and as a result of tidal movements. Figure 7.7 shows the temperature distribution in the near-bottom water layer generated from data acquired from the first ten days of July until the middle of August 2007.

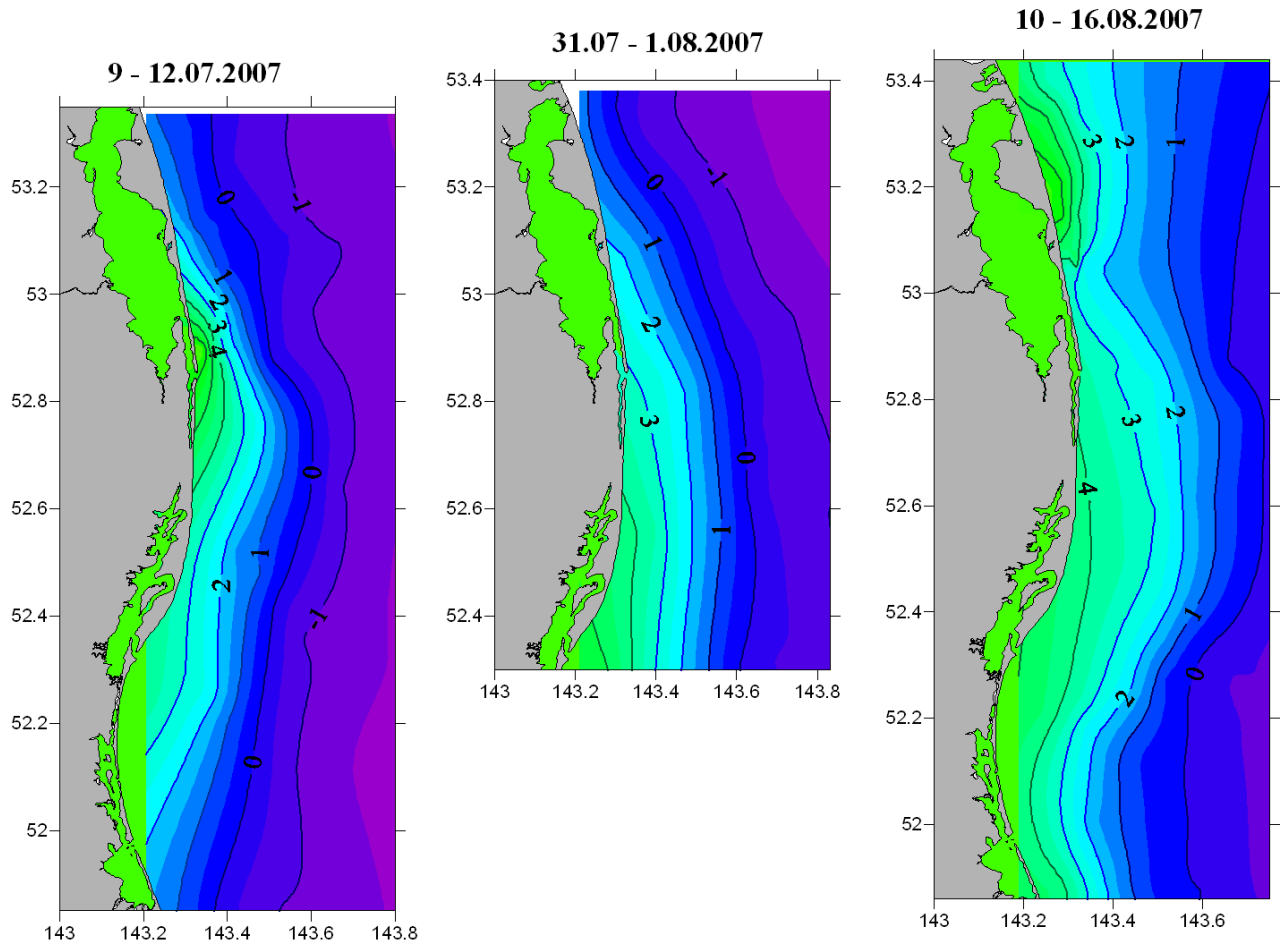

Figure 7.7 - Spatial distribution of water temperature at the sea floor constructed from vertical hydrologic profiles acquired in July and August 2007.

The figure shows that by the middle of August 2007 the bottom water temperature was similar to the same period in 2006 [Borisov et al., 2007]. In the second half of July water temperatures of 1-0 °C were found along Piltun Bay, creating favorable conditions for the spawning of sand lances, which were observed at the sea surface in large numbers at that

time. In the middle of August, water with bottom temperatures below zero receded from shore to beyond the 40-50 m bathymetry contour, moving even farther at the end of the month.

7.3 Upwelling on the NE Sakhalin shelf and on the N and NE end of Sakhalin Island

Upwelling phenomena have been recorded in the shallow waters of the NE Sakhalin shelf on previous expeditions. This year the phenomenon was seen multiple times during hydrologic studies. In July and August, five instances of upwelling were noted: 11-14 July, 22 July, 3-4 August, 9 August, and 15 August.

Because the hydrologic measurements are not continuous it is not currently possible to fully describe the phenomenon. Later, with further analysis, possibly with the use of satellite photos and independent data on the wind field, more specific conclusions may be able to be drawn for each instance of upwelling. Each of the upwelling phenomena persist for different lengths of time and have different surface water temperature and salinity. Depending on the phase of their development, they have (from our data), different spatial dimensions and extend out from the coast for distances from 5 to 40 km. A typical size of a fully developed upwelling with a surface water temperature of 2 °C is on the order of 25 km. Since abnormally cold water rises to the sea surface near the coast during an upwelling event, they are usually accompanied by the formation of dense fog near the coast. Figure 7.8 shows the spatial temperature and salinity distribution immediately after a southerly gale; the plots are constructed from measurements made on 22 July 2007, on transects 1 and 2 (also shown on the figure) and is an example of pronounced upwelling.

Upwelling near the shores of Sakhalin is relatively short-lived, since immediately after the wind dies down the upwelling is broken up by diurnal tidal currents bringing higher temperature and lower salinity water into the coastal area. To a certain extent the dynamics of this replacement is demonstrated by successive hydrologic surveys conducted on seismo-acoustic profile TLP-18L from 3 August to 7 August 2007 (Figure 7.9).

The full hydrologic survey acquired from 10 to 16 August 2007, gives a sense of the spatial scale of an upwelling event observed at that time from Nyisky Bay to the middle of Piltun Bay (Figure 7.10). Figure 7.10 shows that the upwelling zone stretches more than 120 km along the coast and has a width of about 30 km.

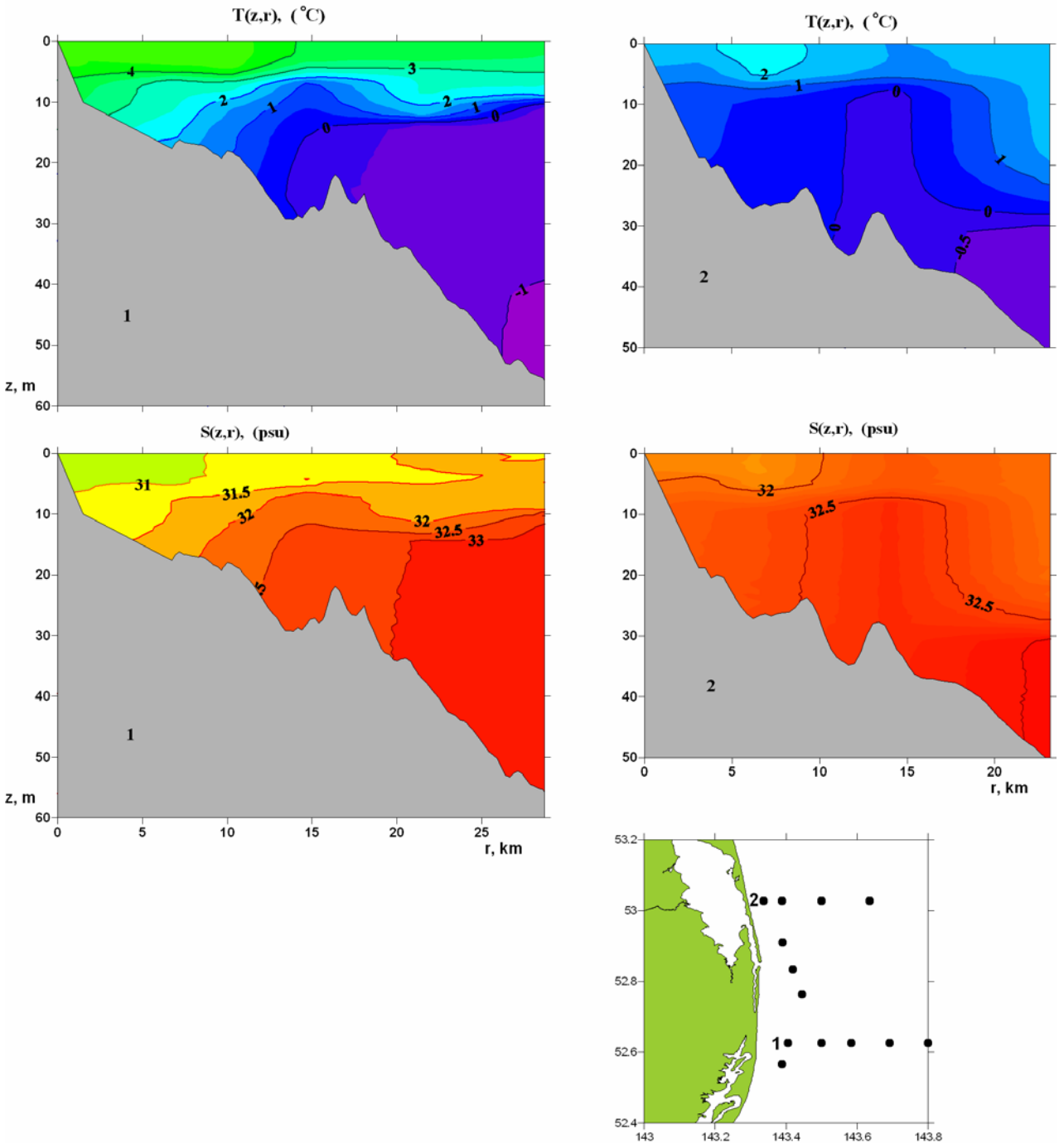

Figure 7.8 - Distribution of Temperature *T(r,z)* and salinity *S(r,z)* and the location of the sampling stations for 2 hydrological transect acquired on 22 July 2007.

Repeat transects acquired in the vicinity of Piltun Bay on 9 and 15 August (Figure 7.3), allow the dynamics of the intensification of the upwelling phenomenon to its maximum development to be analyzed. Examination of the wind field during this time should give a full picture of the development of this phenomenon.

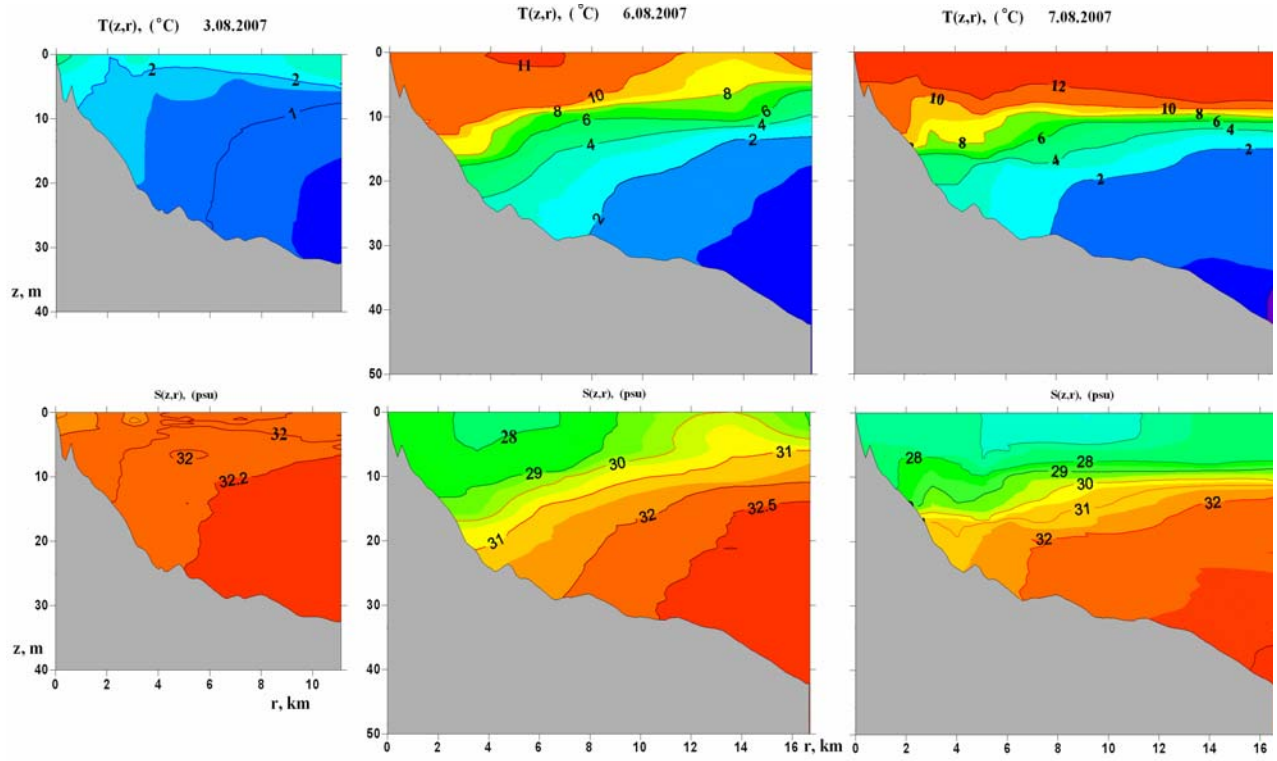

Figure 7.9 - Distribution of Temperature *T(r,z)* and salinity *S(r,z)* along a hydrologic transect TLP-18L, acquired on 3, 6 and 7 August 2007.

During the summer upwelling was also recorded in the shallow offshore waters of northern (Severny Bay) and northwestern (Sakhalin Bay) Sakhalin. While sheltering from a storm in Severny Bay on 17-21 July 2007, daily hydrologic measurements taken while the vessel was at anchor; these measurements showed that the surface water temperature in the bay was close to 0 °C, and the salinity was close to 33 psu. Thus, with the strong southerly wind prevailing at the time, upwelling was observed for three days in Severny Bay, disappearing as the wind direction and strength changed. The time when the upwelling ended and warm, fresh water from Sakhalin Bay replaced the cold, saline water was clearly recorded, as the front between the dark warm waters and the greenish cold waters was highly visible (Figure 7.11).

The fresher water front moved to the east, this less dense fresher water gives a choppy character to the sea, with accumulations of vegetation from the Amur River. The movement of the front, which was tracked on the vessel's 3 cm radar, had a velocity of 1.5 knots.

The movement of warm waters began at the initial tidal stage (data from the Kuegda Bay station). Within about an hour fresher and relatively warmer water arrived at the monitor

station (anchorage, 22 m deep) in a surface layer up to 6 m thick. During the next hour this warm water filled the surface layer to a depth of 17 m. Following this the volume of incoming water decreased somewhat, and the thickness of this warm upper layer was about 12 m and remained until the end of observations (Figure 7.12). In this surface lens the salinity dropped to 23 psu or less.

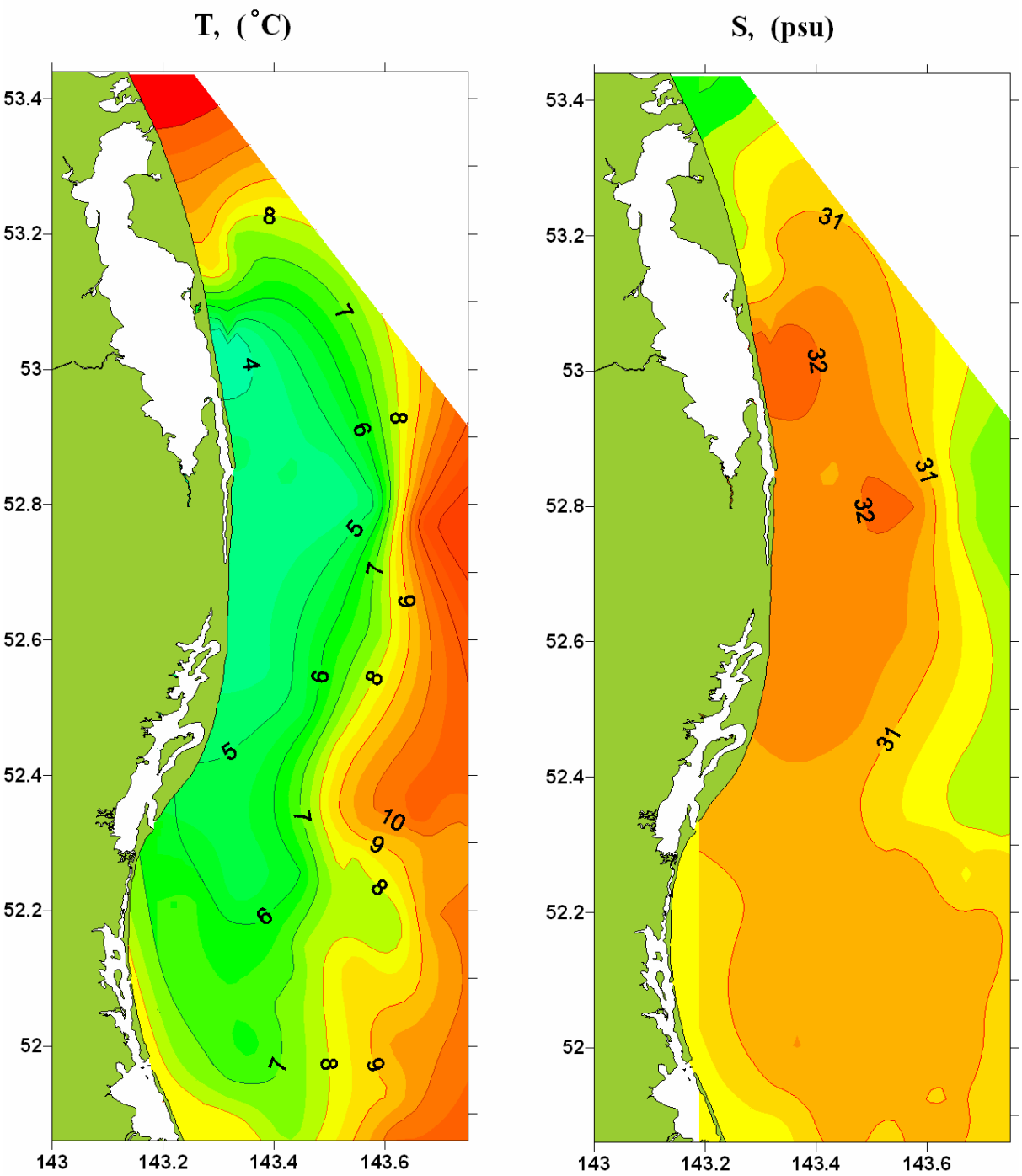

Figure 7.10 - Spatial distribution of water temperature and salinity at the sea surface constructed from vertical hydrologic profiles acquired between 10th and 16 August 2007.

Figure 7.11 – The front between the fresh warm waters from Sakhalin Bay and the colder more saline upwelling waters.

The extent of this fresher water at the north end of Sakhalin is illustrated by two transects performed near Cape Elizaveta on 21 August 2007. They show that the fresh water lens stretched 30-35 km north from Cape Elizaveta. The salinity of the surface waters in the lens did not exceed 24 psu. Thus, upwelling at the northern end of Sakhalin Island inevitably ends with the formation of another lens of warmer, fresher water coming from Sakhalin Bay.

Upwelling was also recorded in Sakhalin Bay itself. On 23 August 2007 after several days of stormy weather and easterly winds, a backward surge, induced by strong winds, led to lower surface water temperatures on the leeward shore south of Cape Maria (down to 3 °C), and about 33‰ salinity. A transect acquired in Sakhalin Bay showed that the upwelling was about 10–20 miles across (Figure 7.13).

Thus, our data shows that upwelling is observed in the summer around the north end of Sakhalin Island in when there are southerly and easterly winds. For the NE Sakhalin shelf

upwelling is observed when there are southerly winds. The process of upwelling and the backward surge of warm and fresher water away from shore into the open sea does not depend on the tidal stage.

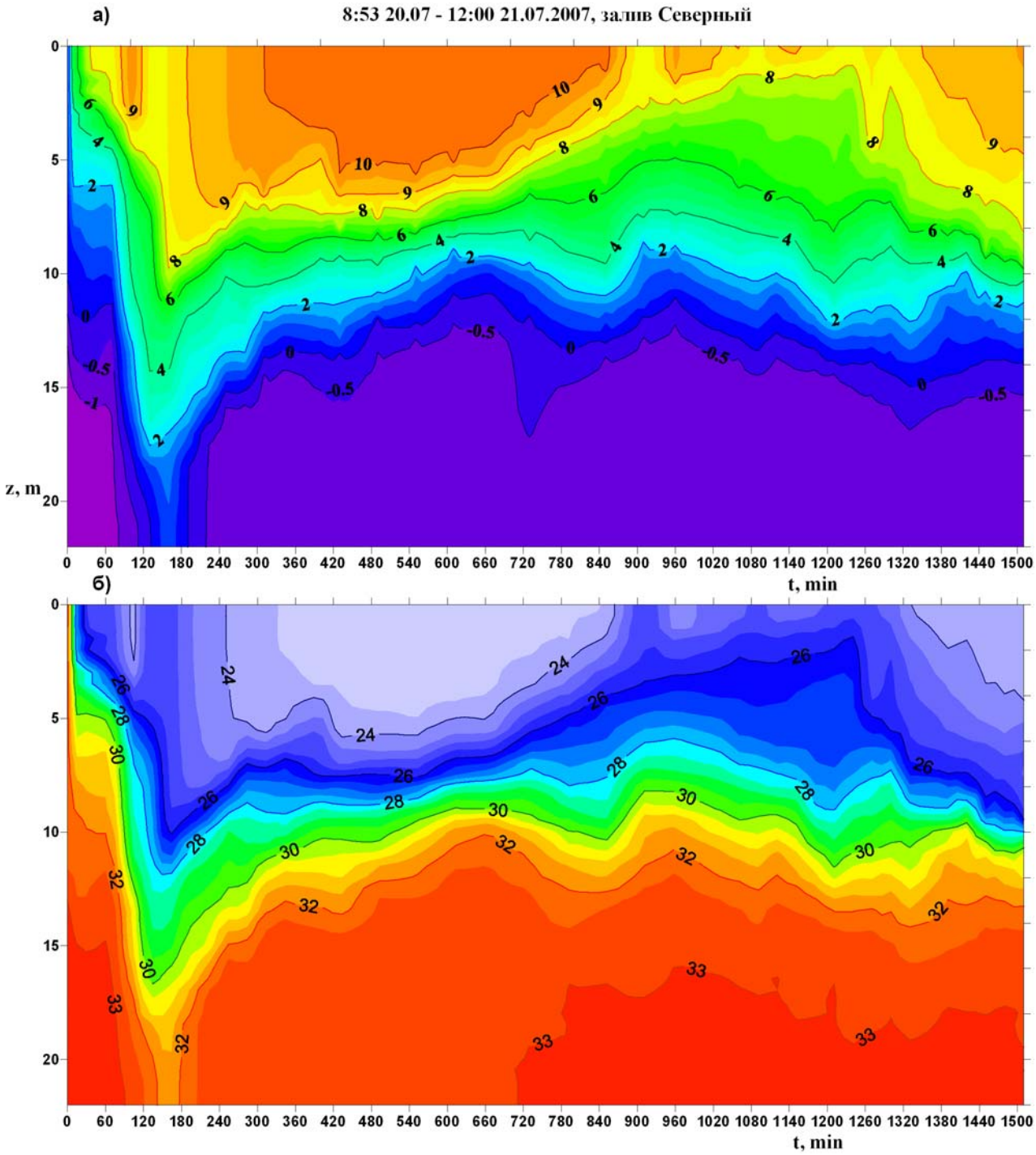

Figure 7.12 – Temporal distribution of: (a) water temperature; and (b) salinity at a hydrologic station in Severny Bay acquired between 20 and 21 July 2007;
(sampling was increased during periods of rapid change).

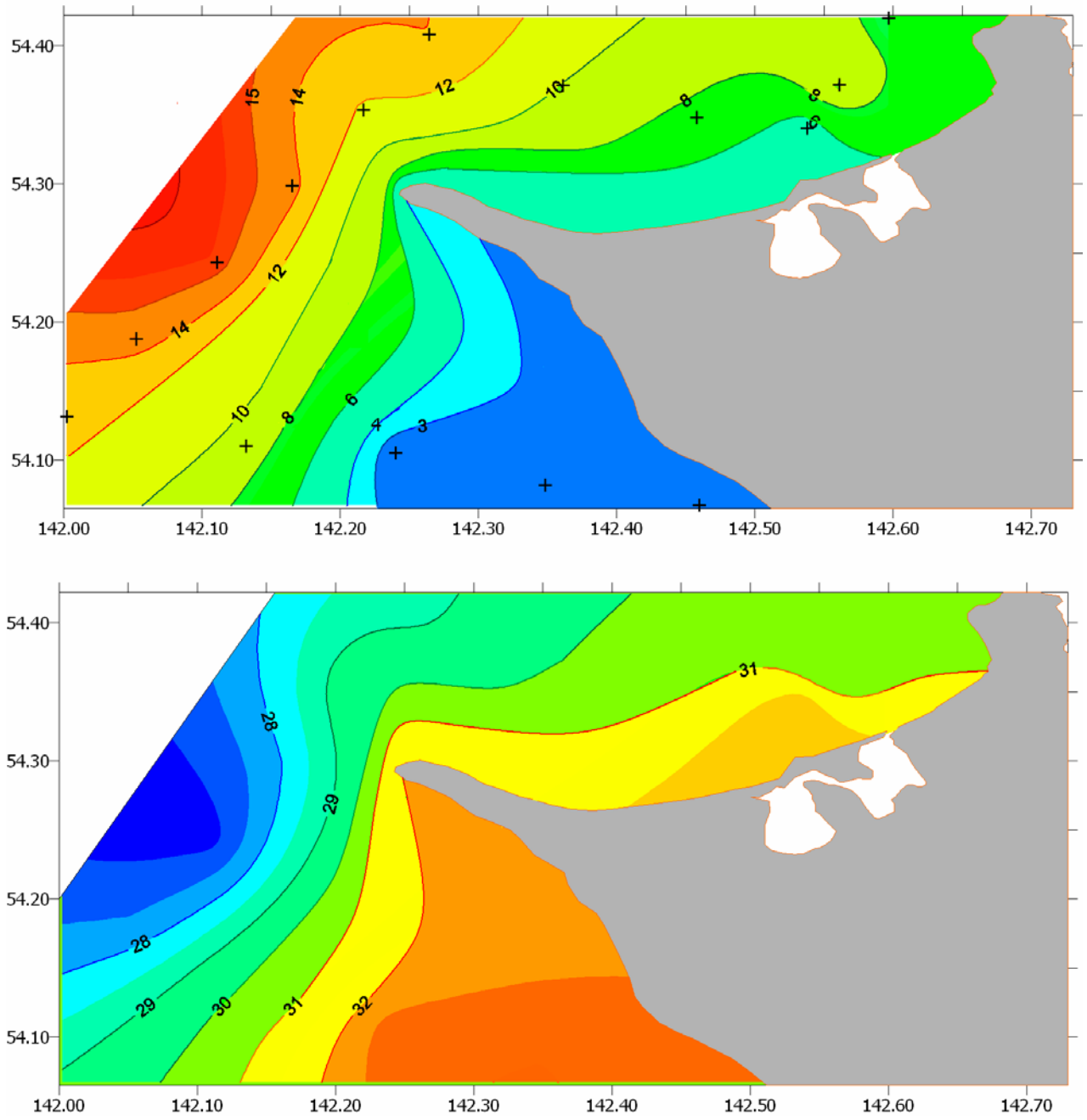

Figure 7.13 - Spatial distribution of water temperature and salinity at the sea surface of Sakhalin and Severny Bays, constructed from vertical hydrologic profiles acquired on 23 August 2007.

7.4 Analysis of data from 2 Potok autonomous current and water temperature meters

During the 2007 expedition, an oceanological station with two Potok autonomous current and water temperature meters was deployed at a location east of the Orlan platform in 43 m water depth; and operated there from 23 July to 5 September. An oceanological buoy submerged to a depth of 10 m, controls the position of a vertical string consisting of an

anchor (240 kg) that can be disconnected by an acoustic release, and two Potok meters positioned at depths of 38 m and 13 m.

The Potok digital integrating current and temperature meter is designed to measure and record the current velocity vector and water temperature as part of an autonomous oceanological station. The basic technical characteristics of the unit are:

Range of velocity measurements:	3.0-150 cm/s
Velocity measurement error:	Greater of: 3.0 cm/s or ±2% of measured V
Measures the velocity vector direction (0-360°) at intervals of not more than 5°	
Range of temperature measurements:	-2°C to +32°C
Temperature measurement error :	±0.05°C
The recording period can be selected from:	1, 1/2, 1/4, 1/8, 1/16, 1/32, 1/64, 1/128 hour (measured values averaged over entire period)
Accuracy of the programming device:	$\pm 2 \cdot 10^{-4}$ s
Endurance:	60 days with a recording period of 1/8 hour
Maximum depth:	6,000 m
Weight:	56 kg
Dimensions (assembled):	1,200 x 655 x 300 mm

Both of the instruments operated for the entire deployment period; however abnormal measurement results, which were greater for the Potok deployed at 13 m depth, were noted. Figure 7.14 shows plots of water temperature and the current velocity constructed from measurements made throughout the observation period. Preliminary analysis of the observation data showed that in the layer near the bottom the water temperature was mostly below zero, with 0.5 °C amplitude fluctuations until 23 August, it then varied by 2 °C in a week, with an increase in the amplitude fluctuations to 3 °C, after which the water temperature and amplitude fluctuations decreased again.

The upper meter was in the thermocline, and the water temperature fluctuations there were significantly greater. Prior to 15 August, they did not exceed 7 °C (from values below zero). In the second half of August, the average water temperature gradually rose to 8 °C, and the amplitude fluctuations increased to 10 °C. In this case, when the tidal currents were at a minimum the average water temperature increased, with a decrease in the amplitude

fluctuations, and when the tidal currents were at a maximum the water temperature amplitude fluctuations increased, with a decline in the average temperature (Figure 7.14).

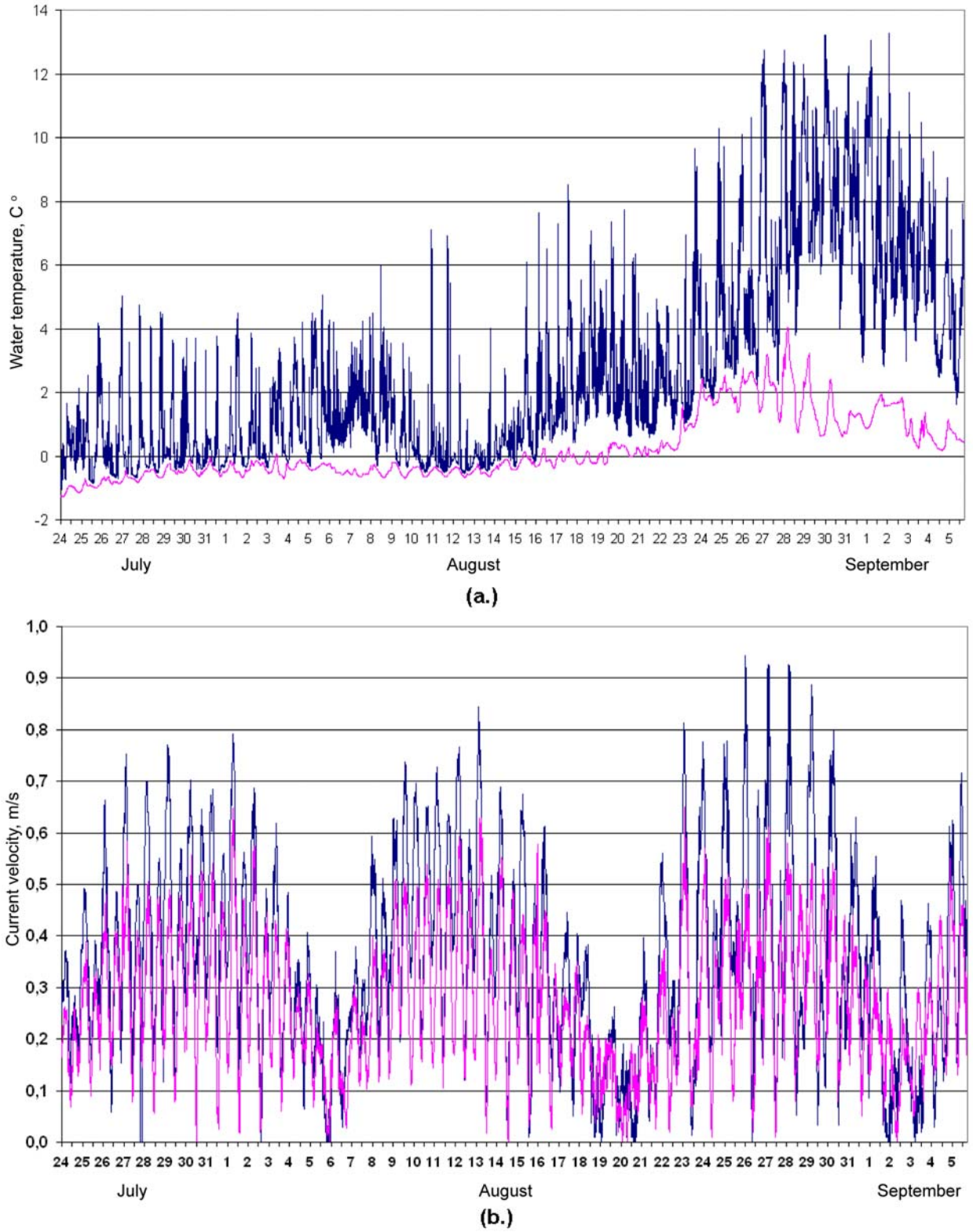

Figure 7.14 – Variations in water temperature and modulus of current velocity measured synchronously at depths of 13 m (blue) and 38 m (pink).

The values of the current velocity at a depth of 13 m varied from 0 to 0.95 m/s. During flood tides the direction of the current was to the south, and its velocity was 0.1-0.2 m/s greater than during an ebb tide, when the current ran north. In the layer near the bottom the current velocity was somewhat lower and did not exceed 0.65 m/s, but the difference in the current velocity and direction during flood and ebb tides at the two depths was maintained.

On individual days with gale force winds, currents in different directions were observed at the two depths (e.g. during gale force winds on 20 to 22 August - Figure 7.15). The difference in current direction in the thermocline and the layer near the bottom varied from 90° to 180°. On the night of 21 and 22 August during a flood tide, the difference in current directions fluctuated in the same range, going to the southwest in the thermocline and to the northwest near the bottom (i.e. shoreward), this led to the arrival of cold bottom water at the coast and development of upwelling near Chayvo and Piltun bays. At the same time the water temperature at the upper depth (13 m) decreased from 5-6 °C to 1-2 °C, while at the

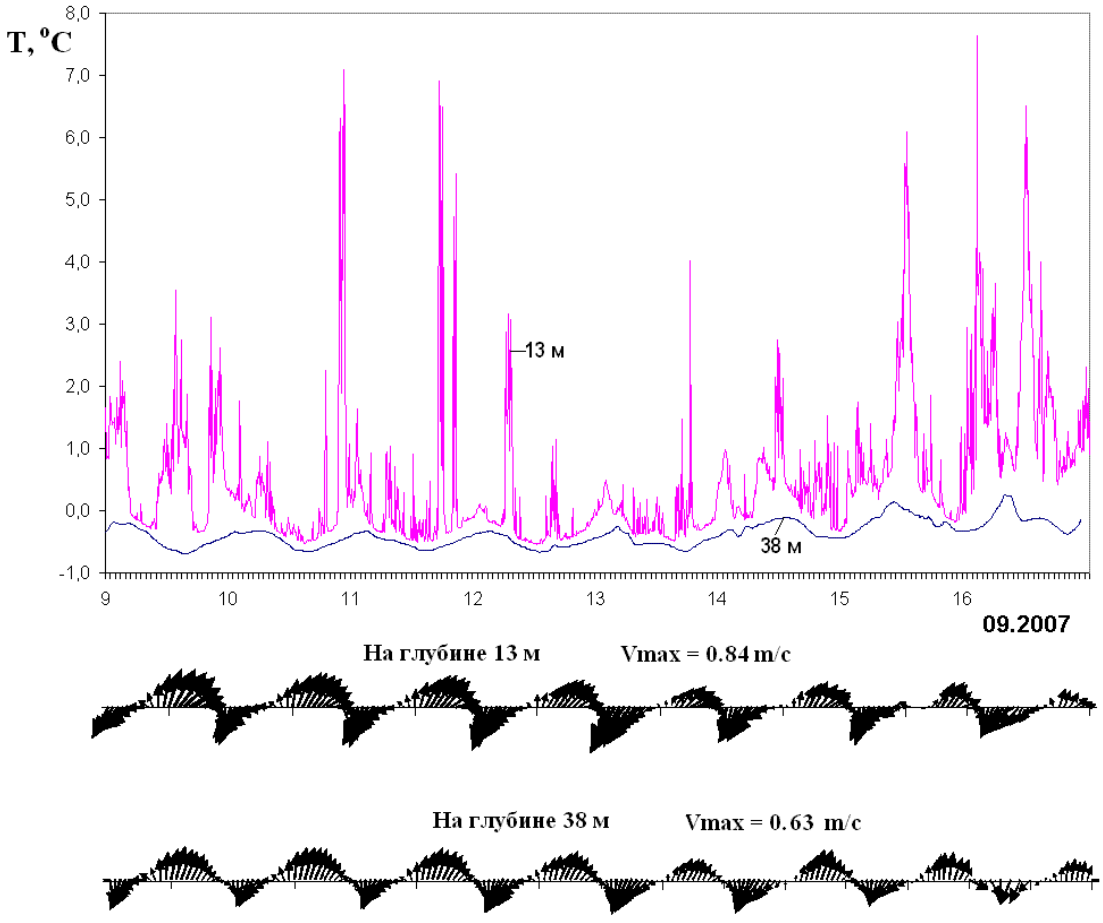

Figure 7.15 – Variations in water temperature and current velocity vector measured synchronously at depths of 13 m (blue) and 38 m (pink) on 20-22 August.

8 Main Results

1. One new AUAR was built by POI in 2007 and 15 AUARs were upgraded, bringing the total to 16 (one AUAR was lost in 2006); ten had an endurance of 28 days, and six 18 days. Five of these were equipped with a radio-telemetry channel (T-AUAR) giving them a real-time transmit capability for a bandwidth of 10 Hz to 5 kHz, these T-AUARs (and sonobuoys) were used in the real-time acoustic monitoring program.
2. Ten acoustic releases (the same model as the eight units purchased in 2006) were acquired in 2007. Therefore all of the AUARs were deployed without a surface float, significantly reducing the possibility of unauthorized retrieval. During the 2007 expedition, for the first time, not a single AUAR was lost.
3. An additional three mini-AUARs with a 3-day operational endurance were constructed for short term TL or source level measurements in 2007 bringing the total to six. All the AUARs (T-AUAR, AUAR and mini-AUAR) recorded high fidelity data for frequencies from 1 Hz to 30 kHz (1 Hz to 15 kHz unaliased).
4. The Mollusk-07 vertical autonomous acoustic and hydrologic recording array was manufactured and operated effectively during the 2007 expedition (three deployments). This system allows stationary synchronous measurements at eight depths, of variations in sound pressure (frequency range 10 Hz to 15 kHz) and water temperature (resolution 0.006°C). Two pressure sensors record the depth of the top and center hydrophones, and a micro-rotor measures current velocity. The Mollusk-07 is designed to be deployed at depths of up to 100 m, using an anchor and acoustic release. An onboard computer is used to control the data acquisition and storage schedules. The system has an endurance of 7 days.
5. The low frequency (24-28 Hz) electromagnetic resonance Seismic Low Frequency Transducer (SLFT) (built in 2006) was used for TL studies at the Odoptu-FSP location and the adjacent offshore waters. The SLFT generated signals that were received offshore at ranges of up to 17 km.
6. A new, more powerful, HF broadband piezoceramic transducer and a new power amplifier allowed the time spent transmitting at TL source locations to be significantly reduced by the use of broadband acoustic signals. A computer program to control the operation of the signal generator that creates the signals was developed and used in 2007. Two electric winches were installed on the *Professor Bogorov* to allow both the LF transducer (right side) and HF transducer (left side) to be deployed together, when the

transducers were operated in parallel it significantly reduced the time transmitting at TL source locations.

7. The Zodiac purchased in 2006, with its rigid plastic bottom, steering console and Yamaha-55 engine was equipped with a hand-operated winch for recovering the AUARs from greater depths in 2007, making this operation considerably easier and safer.
8. The AUARs designed and developed at POI recorded 19,249 hours (802 days) of acoustic data. Acoustic monitoring was conducted almost continuously from 9 July to 7 September 2007. All the data acquired in 2007 is displayed, as daily sonograms (2 Hz to 15 kHz, 60 1-second spectral averages) and plots of sound pressure level for five frequency bands (2 Hz - 15 kHz, 20 Hz - 15 kHz, 10 - 100 Hz, 100 - 2000 Hz, 2 - 15 kHz) are on a DVD in the back of this report.
9. Real-time acoustic monitoring was conducted from 22 June (immediately after the waters were clear of ice) until 20 July, using T-AUARs, and (periodically) sonobuoys, deployed at at four points on the eastern edge of the inshore feeding area. This report presents the results of the analysis of the acoustic data received at Piltun lighthouse over the radio-telemetry channels and recorded on the T-AUAR hard drives.
10. The source level of a transducer at 1 m is a critical parameter for TL studies. Experimental and theoretical studies of the near acoustic field generated by the LF and HF transducers used for TL studies were conducted using a consistent methodology. The goal of these experiments was to estimate the corrections that had to be applied to *TL(f)* estimates along different TL profiles to compensate for near-field effects including the location of the reference hydrophone with respect to the transducer and the water depth at the transmission point. Experimental studies were conducted in water depths of 25 m (the 2006 experiment was repeated) and an average water depth of 15 m.
11. Range and frequency dependent transmission loss studies were acquired on 12 profiles[51] for frequencies from 15 Hz to 15 kHz and on one seismo-acoustic profile[52] for frequencies of 25-31 Hz (and harmonics). The TL studies included bathymetric profiling and sampling of the hydrology at the transmitting and receiving locations and at locations in between if the distances were greater than 7 km. The TL was estimated for known sound velocity profiles - *C(r,z)*. Frequency dependent transmission loss estimates *TL(f)*, were averaged in one-third octave bands *TL(f {1/3 octave})* to improve

[51] Profiles TLP-1, TLP-2, TLP-3, TLP-6, TLP-15, TLP-16, TLP-18, TLP-20, ADP-A, ADP-B, ADP-C and ADP-D.
[52] Profile TLP-18_L.

the statistical stability of the TL measurements, smooth the frequency and spatial interference effects and enable a better comparison with numerical model studies. The variation in these frequency dependent TL measurements with range were also studied *TL(r, f {1/3 octave})*.

12. Three full hydrologic surveys and 15 individual transects, both perpendicular and parallel to the coastline were performed in 2007. The *Professor Bogorov* sheltered from storms in Severny and Sakhalin bays on the north of the island, six transects were performed while transiting to, and daily observations were made while anchored in Sakhalin Bay. In total, 634 vertical hydrologic profiles were acquired (comprising sound velocity, temperature and salinity).
13. Two Potok autonomous current and water temperature meters (belonging to POI) were deployed in 43 m of water at a location east of Chayvo Bay. The units were operational from 23 July to 5 September. The units were recovered using a buoy submerged to a depth of 10 m from the station and equipped with an acoustic release.
14. The Mollusk-07 vertical autonomous acoustic and hydrologic recording array and an autonomous 320 Hz tonal transducer (CW-320 Hz) were used to investigate the internal waves characteristic of the summer hydrologic conditions in the study area and their effect on the TL of low-frequency sound.
15. Seven thousand, two hundred (7,200) km of bathymetry data and 634 vertical hydrologic profiles were acquired in 2007. All the bathymetric data acquired from 2004 to 2007 was tide-corrected, and, together with hydrology data is available on the DVD at the back of this report.

9 Conclusions

1. Real-time monitoring of the anthropogenic sound levels at four locations on the southern and eastern boundaries of the Piltun feeding area showed that from 22 June to 20 July 2007, the sound pressure levels (10 Hz - 5 kHz) did not exceed the pre-defined action criteria [SEIC 2006] (Figure 3.9).
2. Anthropogenic sound measurements were continuously observed at monitor station PA-B-20 (which is 8 km from the PA-B platform) while construction work was being performed on the PA-B platform. In the most active construction phases, the anthropogenic sound pressure level in the frequency range from 5 Hz to 15 kHz never exceeded 130 dB re 1 μPa^2.
3. Spectral analysis of the acoustic energy generated by wind and surface waves during typhoons in 2004, 2006 and 2007 showed their quantitative and qualitative similarity and again showed a good correlation between the relationship between noise and sea state proposed by Knudsen and data from the NE Sakhalin shelf.
4. The ambient and anthropogenic acoustic data acquired in the offshore feeding area (Lunskoye, OFA, Orlan and Arkutun-Dagi stations) from 9 July to 8 September 2007 was periodically distorted by input overloads to the AUAR analog channel when seismic operations were being conducted in the area (Figure 1.15). The AUAR sensitivity was not set to record such powerful seismo-acoustic signals, the effects of this clipping must be evaluated when using these acoustic measurements.
5. Analysis of the variations in the level of a CW-320 Hz tone measured synchronously by the eight hydrophones of the Mollusk-07 on stationary profiles 8-14 km long showed that TL can vary by more than 12 dB, due to refraction and resonance scattering of acoustic waves on spatial and temporal acoustic inhomogeneities created by internal waves propagating along the seasonal thermocline (Figure 5.2).
6. Analysis of frequency and range dependent transmission loss TL(*f,r*) along seismo-acoustic profile TLP-18_L shows that:
   - The loss function *TL(f)* between the SLFT and the Mollusk-07 deployed 16.7 km away in 43 m of water is resonant in nature. The TL is at a minimum for a frequency of 28 Hz (-62.3 dB), while at frequencies of 25 and 31 Hz it is -66.5 dB and -67.8 dB, respectively (i.e. increasing by almost a factor of 2).
   - The TL of seismo-acoustic signals are significantly higher onshore than offshore. For example for two onshore locations 330 and 550 m from the SLFT the TL was -78 dB,

while offshore this was the TL to the Odoptu-S-10 and Odoptu-S-20 stations, which are 10.2 and 11 km from the SLFT.

- There is a pronounced anisotropy in the estimated TL offshore from the Odoptu-FSP. The TL along profile TLP-18_L2 from the SLFT to station p.9 (range 14.2 km) was -63 dB, while along a seismo-acoustic profile oriented approximately parallel to the shore (Figure 6.20) the TL is significantly greater. The TL to the BEH-Odoptu station (range 7 km) is -70 dB; to the Odoptu-S-20 station (range 11 km) is -78 dB; and to the Odoptu-PA-B station (range 17.4 km) is -82 dB.
- The 7 dB decrease in TL between stations p.3 (range 2.5 km, depth 16 m) and p.2 (range 1.95 km, depth 12 m) can be explained by the presence of a higher attenuation surface sediment layer at station p.2 while at station p.3 more competent elastic layers could be closer to the sea bed. Low-frequency seismo-acoustic signals can propagate along this layer with relatively low losses. When the water layer is more than 25 m deep, seismo-acoustic waves may excite a normal acoustic wave (the first mode), due to reflections and scattering on acoustic inhomogeneities in the rocks near the sea floor. This wave can transmit low-frequency energy in the water layer with even lower TL.
- The TL values for a seismic signal and an acoustic signal were compared and showed that for source location E (Figure 6.13), which is close to station p.6 (water depth 24 m). The losses were at a minimum (-44 dB) for a 27Hz seismic signal generated onshore and received at p.6; the losses were also at a minimum (–97 dB) for a 28 Hz acoustic signal generated at point E and received onshore (Table 6.3).
- Comparing the results of seismo-acoustic studies conducted in this area in 2006 [Borisov et al., 2007] and 2007, the elevated plateau selected for the Odoptu-FSP proved to be a more efficient than the sandy sea shore for the transmission of LF (25-31 Hz) seismo-acoustic signals offshore. For example, the TL for a seismic signal to a location 1.8 km offshore was -59 dB in 2006, while in 2007 it was –52 dB. This is probably due to the sub-surface sedimentary characteristics of the study area, efficient transmission of seismic vibrations along these elastic layers and the outcropping of these layers close to the seabed, followed by generation of an acoustic field in the water column.

7. The following conclusions can be drawn from the analysis of the hydrological data acquired in 2004, 2005, 2006 and 2007:

- Just as in previous years, there is considerable spatial and temporal variability in the hydrological characteristics of the study area. In July 2007, the maximum sea-surface water temperature was 5 °C lower than in July 2006); the minimum temperature was also almost a degree lower, while the range of salinity variation was practically unchanged.
- The maximum variability in the sea surface temperature along the coast occurred in August (from 2 to 14.8 °C), the salinity varied from 27 to 32 psu. At depths to the 50 m isobath the sea floor water temperature was 0-6 °C, and salinity 29-33 psu.
- During July and August, five upwelling events were noted in the Chayvo and Piltun areas (1: 11-14 July, 2: 22 July, 3: 3-4 August, 4: 9 August and 5: 15 August). As a result of this upwelling, frontal zones with considerable horizontal water temperature and salinity gradients were formed in the 0-10 m water layer.
- This upwelling phenomenon was also observed around the northern end of Sakhalin Island with southerly and easterly winds in the summertime. On the NE Sakhalin shelf, this phenomenon is observed with southerly winds. The process of upwelling and backward surge of warm and fresher water away from shore into the open sea does not depend on the tidal stage.
- The measured current velocities at the depth of the thermocline east of the Orlan platform did not exceed 0.95 m/s; while near the bottom the current velocity did not exceed 0.65 m/s. On days with gale force winds, currents in opposite direction were observed at these depths.

10 Future plans

POI has 12 AUARs, four T-AUARs, six mini-AUARs, the Mollusk-07 vertical autonomous acoustic and hydrologic recording array, four analog (ASB) and two digital (DSB) sonobuoys, LF and HF transducers, an LF seismic low frequency transducer and a combined CTD/SVP sonde available for acoustic studies in 2008. POI also has the software needed for visualizing, recording, storing (archiving) and analysis of experimental data as well as numerical modeling of acoustic fields in shallow-water waveguides with spatial inhomogeneities in the seabed and the water layer.

Two autonomous current velocity sensors with orientation sensors will be added to the Mollusk-07 in 2008.

The comprehensive TL studies initiated in 2002 will be continued in 2008 with the main objective being the calibration of acoustic models along key profiles over the NE Sakhalin shelf. These TL and model studies will investigate sound propagation from the planned construction/development areas to the Piltun and offshore gray whale feeding areas. As in 2007 detailed hydrologic profiling using the sonde and vessel sonar will be conducted in the study area. The bathymetric and hydrologic data will be used in the construction of theoretical acoustical and hydrodynamic models and numerical experiments. These 2D acoustic models will be used to estimate the acoustic fields produced by multiple sources with known characteristics along the calibrated profiles. These models will extend the experimental TL data to other frequencies, sources and hydrology. This data will allow the impact of variations in the hydrologic field on sound propagation to be estimated (i.e. by internal waves, hydrologic fronts and tidal and eddy currents) and will improve the accuracy of the numerical modeling. The effects of these acoustic variations will be further evaluated by broadband testing in 2008.

During the multiyear western gray whale program, POI has gathered a large quantity of acoustic, hydrologic and bathymetric data. POI will continue establishing a database of field data and analysis results allowing easy access and reliable storage and backup. Again, all the data collected in 2008 will be uploaded into the database.

The integration between the acoustic and hydrologic studies and other components of the western gray whale research program will continue in 2008. Two integrated programs will be conducted in 2008, these are:

1. Recording of ambient and anthropogenic acoustic levels at the 10 m bathymetric contour offshore from the behavioral monitoring stations. Computation of the energy level in one minute windows over the frequency range from 20 Hz to 15 kHz for the monitoring period.
2. Investigation of the correlation between the spatial distribution and development of benthos and variations in the bathymetry and hydrology of the study area. The study, conducted with the benthic team will:
   - Determine the size and dynamics of the discharge lens from the Amur River, where the temperature is higher and the salinity lower than the NE coast of Sakhalin Island in the Sea of Okhotsk.
   - Determine the impact of the water discharge from Piltun lagoon on the salinity of the water in the Piltun area.
   - Study the intensity of the tide driven (especially summer) and wind driven vertical mixing on the shallow part of the shelf.
   - Determine the location and dynamics of the high density, near-bottom, biogen rich layer formed by convection during the winter.

11 Acknowledgements

The authors would like to thank the V.I. Il`icev Pacific Oceanological Institute, FEB Academy of Sciences of Russia (POI), (Тихоокеанский океанологический институт им. В.И. Ильичева ДВО РАН), for assistance in performing this work. The expedition on the *Professor Bogorov* was made possible by the efforts of Academic V.A. Akulichev (академик Акуличев В.А.) and the head of the POI marine department A.I. Botsul (Боцула А.И.).

The authors would also like to acknowledge the following personnel from POI, who while they did not contribute to the report, contributed significantly to the success of the program in the field. Sc. T.V. Soltanova (Т.В. Солтанова); engineer: V.V. Lihachev (Лихачев В.В.), and main laboratory assistant T.Y. Antipenkova (Т.Я. Антипенкова). The authors wish to thank the crew of the *Professor Bogorov* for their hospitality and assistance while conducting acoustic measurements on the NE Sakhalin shelf.

Finally the authors would like to express their gratitude to Academic V.A. Akulichev (академик Акуличев В.А.) (POI), Dr. Sc. V.G. Petnikov (д.ф-м.н Петников В.Г.) (Institute of general physics, RAS, Moscow), Dr. H.R. Melton (ExxonMobil Upstream Research Co.), as well as Dr. C.I. Malme (LGL Limited) for reviewing this report.

Our special thanks go to the investment companies, their employees and consultants, without whom the present work could not have been conducted. These include:
LGL Limited. - S.R. Johnson, S. Meier, V. Yetskalo, and I. Zhmaev.
Exxon Neftegas Ltd. - M.R. Jenkerson, H.R. Melton and E.N Kalinin.
Sakhalin Energy Investment Company Ltd. - V.E. Nechayuk and T. Sapozhkova.

12 Authors

The following members of staff from the V.I. Il`icev Pacific Oceanological Institute, Far East Branch, Academy of Sciences of Russia have contributed to the report:

Sc. S.V. Borisov (Борисов С.В.)

Sc. V. A. Gritsenko (Гриценко А.В.)

Lead engineer D.G. Kovzel` (Ковзель Д. Г.)

Dr. R.A. Korotchenko (Коротченко Р.А.)

Sc. M.V. Kruglov (Круглов М.В.)

Dr. Sc. A.N. Rutenko (Рутенко А.Н.)

Dr. A.A. Solov'ev (Соловьев А.А.)

Sc. V.G. Ushipovsky (Ущиповский)

Dr. F.F. Khrapchenkov (Храпченков Ф.Ф.)

13 Bibliography

1. Blokhin, S.A., S.A. Yazvenko, V.L. Vladimirov and S.I. Lagerev. (2002). Population Size, Distribution and Behavior of Gray Whale (*Eschrichtius robustus)* Based on Aerial Observations on the Northeast Shelf of Sakhalin Island in the Summer and Fall of 2001 // Report to the conference on Marine Mammals in Remote Regions of the Arctic, September 11–13, 2002, Lake Baikal, Russia.

   Блохин С.А., Язвенко С.Б., Владимиров В.Л., Лагерев С.И. (2002). Численность, распределение и характер поведения серого кита (*Eschrichtius robustus)* на основании авиационных наблюдений на северо-восточном шельфе острова Сахалин летом и осенью 2001 г. // Доклад на конференции Морские млекопитающие в удаленных районах Арктики, 11-13 сентября 2002 г., озеро Байкал, Россия.
2. Borisov, S.V., A.V. Gritsenko, M.R. Jenkerson, A.N. Rutenko and A,V. Hodzevich. (2002). Evaluating and Monitoring Acoustic Transmission from the Odoptu 3D seismic Survey 5 August - 9 September, 2001; Sakhalin, Russian Federation // Pacific Oceanological Institute (FEB RAS) report for Exxon Neftegas Ltd.

   Борисов С.В., Гриценко А.В., Дженкерсон М.Р., Рутенко А.Н., Ходзевич А.В. (2002). Оценка и наблюдение распространения акустических сигналов, при проведении трехмерной сейсморазведки в районе Одопту с 5 августа по 9 сентября 2001 г. на о.Сахалин, Россия // Отчет Тихоокеанского океанологического института ДВО РАН для компании Эксон Нефтегаз Лимитед.
3. Borisov, S.V., A.V. Gritsenko, A.N. Rutenko, and A.V. Hodzevich. (2003). Results of Acoustic Studies Within and Adjacent to the Piltun-Astokh License Area 1-6 August, 2001 and 17-24 September, 2001; Sakhalin, Russian Federation // Pacific Oceanological Institute (FEB RAS) report for Exxon Neftegas Ltd. and Sakhalin Energy Investment Co.

   Борисов С.В., Гриценко А.В., Рутенко А.Н., Ходзевич А.В. (2003). Результаты акустических исследований, проведенных с 1 по 16 августа 2001 г. и с 17 по 24 сентября 2001 г. в акватории Пильтунско-астохской лицензионной зоны, а также прилегающей к ней акватории на о.Сахалин, Россия / Отчет Тихоокеанского океанологического института ДВО РАН для компаний Эксон Нефтегаз Лимитед и Сахалин Энерджи Инвестмент Компани.
4. Borisov, S.V., A.V. Gritsenko, M.V. Kruglov, R.A. Korotchenko, and A.N. Rutenko. (2003). Results of Acoustic Studies between Molikpaq and Piltun and Near Chayvo Bay,

12 September to 23 September, 2002; Sakhalin, Russian Federation // Pacific Oceanological Institute (FEB RAS) report for Exxon Neftegas Ltd. and Sakhalin Energy Investment Co.

Борисов С.В., Гриценко А.В., Круглов М.В., Коротченко Р.А., Рутенко А.Н. (2003). Результаты акустических исследований, проведенных с 12 по 23 сентября 2002 г. на акваториях между платформой Моликпак и заливом Пильтун, и прилегающей к заливу Чайво, на о.Сахалин, Россия / Отчет Тихоокеанского океанологического института ДВО РАН, г. Владивосток, для компаний Эксон Нефтегаз Лимитед и Сахалин Энерджи Инвестмент Компании .

5. Borisov, S.V., A.V. Gritsenko, and A.N. Rutenko. (2004). Acoustic Studies on the North East Sakhalin Shelf, Volume 1: Equipment, Methodology and Data; 15 August to 20 September, 2003; Sakhalin, Russian Federation // Pacific Oceanological Institute (FEB RAS) report for Exxon Neftegas Ltd. and Sakhalin Energy Investment Co.

   Борисов С.В., Гриценко А.В., Рутенко А.Н. (2004). Результаты акустических исследований, проведенных с 15 августа по 20 сентября 2003 г. на северо-восточном шельфе о. Сахалин, Россия. Том 1: «Оборудование, методика и данные» / Отчет Тихоокеанского океанологического института ДВО РАН, г. Владивосток, для компаний Эксон Нефтегаз Лимитед и Сахалин Энерджи Инвестмент Компании.

6. Borisov, S.V., A.V. Gritsenko, A.V. Dmitrieva, A.A. Karnauhov, M.V. Kruglov and A.N. Rutenko. (2005). Acoustic Studies on the North East Sakhalin Shelf, Volume 1: Equipment, Methodology and Data; 30 July to 7 October, 2004; Sakhalin, Russian Federation // Pacific Oceanological Institute (FEB RAS) report for Exxon Neftegas Ltd. and Sakhalin Energy Investment Co.

   Борисов С.В., Гриценко А.В., Дмитриева А.В., Карнаухов А.А., Круглов М.В., Рутенко А.Н. (2005). Результаты гидро-акустических исследований, проведенных с 30 июля по 07 октября 2004 г. на северо-восточном шельфе о. Сахалин, Россия. Том 1: «Оборудование, методика и данные» / Отчет Тихоокеанского океанологического института ДВО РАН, г. Владивосток, для компаний Эксон Нефтегаз Лимитед и Сахалин Энерджи Инвестмент Компании.

7. Borisov, S.V., A.V. Gritsenko, R.A. Korotchenko, D.G. Kovzel, M.V. Kruglov, A.N. Rutenko and A.A. Solovyev. (2006). Acoustic Studies on the North East Sakhalin Shelf, Volume 2: Equipment, Calibration and Methodology; 7 July to 7 October, 2005; Sakhalin,

Russian Federation // Pacific Oceanological Institute (FEB RAS) report for Exxon Neftegas Ltd. and Sakhalin Energy Investment Co.

Борисов С.В., Гриценко А.В., Коротченко Р.А., Ковзель Д.Г., Круглов М.В., Рутенко А.Н., Соловьев А.А. (2006). Гидроакустические есследования, проведенные с 07 июля по 07 октября 2005 г. на северо-восточно шельфе о,Сахалин, Россия. Том 2: «Обороудование, калибровка и методика» / Отчет Тихоокеанского океанологического института ДВО РАН для компаний Эксон Нефтегаз Лимитед и Сахалин Энерджи Инвестмент Компани.

8. Borisov, S.V., A.V. Gritsenko, D.G. Kovzel, M.V. Kruglov, A.N. Rutenko, A.A. Solovyev, V.G. Ushipovsky and F.F. Khrapchenkov. (2007). Acoustic and Hydrographic Studies on the North East Sakhalin Shelf, 15 June to 5 October, 2006; Sakhalin, Russian Federation // Pacific Oceanological Institute (FEB RAS) report for Exxon Neftegas Ltd. and Sakhalin Energy Investment Co.

   Борисов С.В., Гриценко А.В., Ковзель Д.Г., Круглов М.В., Рутенко А.Н., Соловьев А.А, Ущиповский В.Г., Храпченков Ф.Ф. (2007). Акустико-гидрофизические исследования на северо-восточном шельфе о. Сахалин с 15 июня по 05 октября 2006 г.; о. Сахалин, Российская Федерация. / Отчет Тихоокеанского океанологического института ДВО РАН для компаний Эксон Нефтегаз Лимитед и Сахалин Энерджи Инвестмент Компани.
9. Brekhovskikh, L.M. and Yu.P. Lysanov. (2003). Fundamentals of Ocean Acoustics, 3rd ed. (Modern Acoustics and Signal Processing). AIP Press, Springer-Verlag.
10. Brovko, P.F. and Y.A. Mikishin. 1999. Modern tendencies in the development of the North East Sakhalin coasts // FERHRI Special Issue # 2, Vladivostok, Dalnauka, pp. 193-203.

    Бровко П.Ф., Микишин Ю.А. (1999) Современные тенденции развития берегов северо-восточного Сахалина // Гидрометеорологические и экологические условия дальневосточных морей: оценка воздействия на морскую среду. Владивосток, с. 193-203. (Тематический выпуск № 2).
11. Buckland, S.T., D.R. Anderson, K.P. Burnham, J.L. Laake, D.L. Borchers and L. Thomas. (2001). Introduction to Distance Sampling. Oxford University Press. New York.
12. Fadeev, V.I. (2006). Benthos and food supply studies in feeding areas of the Okhotsk-Korean gray whale population. // Institute of Marine Biology (FEB RAS), Vladivostok,

Russia. Final report for Exxon Neftegas Ltd. and Sakhalin Energy Investment Co. 150 p.
Фадеев В.И. (2006) Исследования бентоса и кормовой базы в районах питания охотско-корейской популяции серого кита. // Заключительный отчет Института биологии моря ДВО РАН для компаний Сахалин Энерджи и Эксон Нефтегаз. Владивосток. 150 с.

13. Fadeev, V.I. (2007). Status of benthos and food supplies studies in feeding areas of the Okhotsk-Korean gray whale population in 2006. // Institute of Marine Biology (FEB RAS), Vladivostok, Russia. Final report for Exxon Neftegas Ltd. and Sakhalin Energy Investment Co. 122 p.
    Фадеев В.И. (2006) Состояние бентоса и кормовой базы в районах питания охотско-корейской популяции серого кита в 2006 году. // Заключительный отчет Института биологии моря ДВО РАН для компаний Сахалин Энерджи и Эксон Нефтегаз. Владивосток. 150 с.
14. Fadeev, V.I. (2008). Status of benthos and food supplies studies in feeding areas of the Okhotsk-Korean gray whale population in 2006. // Institute of Marine Biology (FEB RAS), Vladivostok, Russia. Final report for Exxon Neftegas Ltd. and Sakhalin Energy Investment Co.
    Фадеев В.И. (2008) Состояние бентоса и кормовой базы в районах питания охотско-корейской популяции серого кита в 2006 году. // Заключительный отчет Института биологии моря ДВО РАН для компаний Сахалин Энерджи и Эксон Нефтегаз. Владивосток.
15. Gailey, G., O. Sychenko, and B. Würsig. 2006. Western gray whale behavior, movement, and occurrence patterns off Sakhalin Island, 2005, Prepared for LGL ecological research associates Ltd, for Exxon-Neftegas Ltd. and Sakhalin Energy Investment Company, Yuzhno-Sakhalinsk, Russian Federation.
16. Gailey, G., T. MacDonald, R. Racca, O. Sychenko, A. Rutenko and B. Würsig. 2007. Influences of Underwater Sound and Nearshore Vessel Activity on Western Gray Whale Behavior during the Installation of a Concrete Gravity Based Structure off Sakhalin Island, Summer 2005. Prepared for LGL ecological research associates Ltd, for Exxon-Neftegas Ltd. and Sakhalin Energy Investment Company, Yuzhno-Sakhalinsk, Russian Federation. 150 pp.
17. Gershanovich, D.E. and A.M. Muromtsev. (1982). Oceanological principles of the biological productivity of the world's oceans // Gidrometeoizdat, 320 pp.

Гершанович Д.Е., Муромцев А.М. (1982). Океанологические основы биологической продуктивности Мирового океана. // Гидрометеоиздат. 320 с.

18. Hooge, P.N. and B. Eichenlaub. (1997). Animal movement extension to arcview. Ver. 1.1. Alaska Science Center - Biological Science Office // U.S. Geological Survey, Anchorage, AK, USA.
19. Karnauhov, A.A., M.V. Kruglov and A.N. Rutenko. (2005). Acoustic Studies on the North East Sakhalin Shelf, Volume 2: Analysis, Conclusions and Recommendations; 30 July to 7 October, 2004; Sakhalin, Russian Federation // Pacific Oceanological Institute (FEB RAS) report for Exxon Neftegas Ltd. and Sakhalin Energy Investment Co.

    Карнаухов А.А., Круглов М.В., Рутенко А.Н. (2005). Результаты гидроакустических исследований, проведенных с 30 по 07 октября 2004 г. на северо-восточном шельфе о. Сахалин,Россия. Том 2: «Оборудование методика и данные» / Отчет Тихоокеанского океанологического института ДВО РАН, г. Владивосток, для компаний Эксон Нефтегаз Лимитед и Сахалин Энерджи Инвестмент Компании.
20. Knudsen, V.O., R.S. Alford and J.W. Emling. (1948). Underwater ambient noise // J. Mar. Res. Vol. 7. № 3, pp. 410-429.
21. Krasavtsev, V.B., K.L. Puzankov and G.V. Shevchenko. (2000). Wind driven upwelling formation on the northeast shelf of Sakhalin Island. // DVNIGMI special issue No. 3, Vladivostok, Dalnauka, pp. 106–120.

    Красавцев В. Б., Пузанков К. Л., Шевченко Г. В. (2000). Формирование апвеллинга на северо-восточном шельфе острова Сахалин под воздействием ветра. // Тематический вып. ДВНИИГМИ № 3. Владивосток: Дальнаука, С. 106-120.
22. Kruglov, M.V., and A.N. Rutenko. (2003). Transmission Loss Studies on the North east Sakhalin Shelf 2001 and 2002; Sakhalin, Russian Federation // Pacific Oceanological Institute (FEB RAS) report for Exxon Neftegas Ltd. and Sakhalin Energy Investment Co.

    Круглов М.В., Рутенко А.Н. (2003). Исследования потерь акустических шумов, проведенные в 2001, 2002 гг. На северо-восточном шельфе о.Сахалин, Россия / Отчет Тихоокеанского океанологического института ДВО РАН для компаний Эксон Нефтегаз Лимитед и Сахалин Энерджи Инвестмент Компани.
23. Kruglov, M.V., and A.N. Rutenko. (2004). Acoustic Studies on the North East Sakhalin Shelf, Volume 2: Analysis, Conclusions and Recommendations; 15 August to 20 September, 2003; Sakhalin, Russian Federation // Pacific Oceanological Institute (FEB RAS) report for Exxon Neftegas Ltd. and Sakhalin Energy Investment Co.

Круглов М.В., Рутенко А.Н. (2004) Результаты акустических исследований, проведенных с 15 по 20 сентября 2003 г. на северо-восточном шельфе о.Сахалин, Россия. Том 2: «Анализ, выводы и рекомендации» / Отчет Тихоокеанского океанологического института ДВО РАН для компаний Эксон Нефтегаз Лимитед и Сахалин Энерджи Инвестмент Компани.

24. Kruglov, M.V., A.N. Rutenko and F.F. Khrapchenkov. (2006). Acoustic Studies on the North East Sakhalin Shelf, Volume 3: Analysis, Conclusions and Recommendations; 7 July to 7 October, 2005; Sakhalin, Russian Federation // Pacific Oceanological Institute (FEB RAS) report for Exxon Neftegas Ltd. and Sakhalin Energy Investment Co.

    Круглов М.В., Рутенко А.Н., Храпченков Ф.Ф. (2006). Гидроакустические исследования, проведенные с 07 июля по 07 октября 2005 г. на северо-восточном шельфе о.Сахалин. Том 3: «Анализ, выводы, рекомендации». / Отчет Тихоокеанского океанологического института ДВО РАН для компаний Эксон Нефтегаз Лимитед и Сахалин Энерджи Инвестмент Компани.

25. Kruglov, M.V., A.N. Rutenko and R. Racca. (2006). Estimating anthropogenic sound levels at the boundaries of gray whale feeding areas during construction and production activities on the northeastern shelf of Sakhalin Island // Ocean Acoustics / Proceedings of the 11th L. M. Brekhovskikh Conference. M.: GEOS. pp. 340-343.

    Круглов М.В., Рутенко А.Н., Расчет уровней акустических шумов на границах районов кормления серых китов во время проведения строительных работ на северо-восточном шельфе о. Сахалин (2006).// Акустика океана/ Доклады на 11-ой школе-семинаре Л.М. Бреховских/ М.. ГЕОС. С. 340-343.

26. Malme, C.I., P.W. Smith Jr. and P.R. Miles. 1986. Study of the effects of offshore geophysical acoustic survey operations on important commercial fisheries in California. BBN Rep. 6125; OCS Study MMS 86-0032. Rep. from BBN Labs Inc., Cambridge, MA, for Battelle Labs, Ventura, CA, and U.S. Minerals Manage. Serv., Los Angeles, CA. 106 p.

27. Miller, J.F. and S.N. Wolf. (1980). Modal acoustic transmission loss (MOATL): A transmission loss computer program using a normal mode model of acoustic field in the ocean // Naval research laboratory, Washington.

28. Perlov, A.S. and M.K. Maminov. (2002). Population size, distribution and behavior of gray whales (*Eschrichtius robustus)* in the coastal waters of northeast Sakhalin in 2002 (Vessel Observations) // Pacific Oceanological Institute (FEB RAS), Vladivostok, report

for Exxon Neftegas Ltd. and Sakhalin Energy Investment Co.

Перлов А.С., Маминов М.К. (2002) Численность, распределение и характер поведения серого кита (*Eschrichtius robustus)* в прибрежных водах северо-восточного Сахалина в 2002 г. (судовые наблюдения) // Отчет Тихоокеанского научно-исследовательского рыбохозяйственного центра, г. Владивосток, для компаний Эксон Нефтегаз Лимитед и Сахалин Энерджи Инвестмент Компании ЛТД.

29. Pishchalnik, V.M. and V.S. Arkhipkin. (1999). Seasonal variations in the circulation of waters on the Sakhalin shelf of the Sea of Okhotsk // Hydrometeorological and Ecological Conditions of Far Eastern Seas: Assessment of Impact on Marine Environment, DVNIGMI special issue No. 2, Vladivostok, Dalnauka, pp. 193-95.

    Пищальник В.М., Архипкин В.С. (1999). Сезонные вариации циркуляции вод на охотоморском шельфе острова Сахалин. // Гидрометеорологические и экологические условия Дальневосточных морей: Оценка воздействия на морскую среду. Тематический выпуск № 2. – Владивосток. Дальнаука, С. 84-95.

30. Racca. R. (2008). Acoustic Monitoring of Piltun 2007 Offshore Construction – Summary Report Ракка и др., (2008).

    Акустический мониторинг морских строительных операций в Пильтунском районе в 2007 году - заключительный отчет.

31. Rexstad, E. and D. Borchers. 2006. Memorandum: Western gray whale detection function and gradient // University of St. Andrews. Scotland.

32. Richardson, W.J., C.R. Greene, C.I. Malme and D.H. Thomson. (1995). Marine mammals and noise. Academic Press Limited. 576 p.

33. Rutenko, A.N. (2006). Acoustic Studies on the North East Sakhalin Shelf, Volume 1: Objectives and Data; 7 July to 7 October, 2005; Sakhalin, Russian Federation // Pacific Oceanological Institute (FEB RAS) report for Exxon Neftegas Ltd. and Sakhalin Energy Investment Co.

    Рутенко А.Н. (2006) Гидроакустические исследования, проведенные с 07 июля по 07 октября 2005 г. на северо-восточном шельфе о.Сахалин, Россия. Том 1: «Цели и полученные данные». / Отчет Тихоокеанского океанологического института ДВО РАН для компаний Эксон Нефтегаз Лимитед и Сахалин Энерджи Инвестмент Компани.

34. Rutenko, A.N. (2006). Effect produced on sound propagation by an internal temperature front moving over the shelf // Acoustical Physics, Vol. 52, No. 5, pp, 613-617.

Рутенко А.Н. (2006) Влияние движущегося по шельфу внутреннего температурного фронта на распространение звука // Акустический журнал Том. 52, № 5, С. 710-715.

35. SEIC. (2006). 1000-S-90-04-P-0048-00-E#04 - Marine Mammal Protection Plan, 2006, page 52, Annex 3.

СЭИК. (2006). 1000-S-90-04-P-0048-00-R#04 - План защиты морских млекопитающих, 2006, стр. 52, приложение 3.

36. SEIC. (2006). 1000-S-90-04-P-0048-00-E#04 - Marine Mammal Protection Plan, 2006, page 43, Annex 1.

СЭИК. (2006). 1000-S-90-04-P-0048-00-R#04 - План защиты морских млекопитающих, 2006, стр. 43, приложение 1.

37. Thomas, L., J.L. Laake, S. Strindberg, F.F.C. Marques, S.T. Buckland, D.L. Borchers, D.R. Anderson, K.P. Burnham, S.L. Hedley, J.H. Pollard and J.R. B. Bishop. (2004). Distance 4.2. Research Unit for Wildlife Population Assessment, University of St. Andrews, UK. http://www.ruwpa.st-and.ac.uk/distance/

38. Thomas, L., Laake, J.L., Strindberg, S., Marques, F.F.C., Buckland, S.T., Borchers, D.L., Anderson, D.R., Burnham, K.P., Hedley, S.L., Pollard, J.H., Bishop, J.R.B. and Marques, T.A. 2006. Distance 5.0. Release 1. Research Unit for Wildlife Population Assessment, University of St. Andrews, UK. http://www.ruwpa.st-and.ac.uk/distance/.

39. Yakovlev, Yu.M. (2003). Photo-identification of the Okhotsk-Korean gray whale population *(Eschrichtius Robustus)* в 2002. // Report for Exxon Neftegas Ltd. and Sakhalin Energy Investment Co.

Яковлев Ю.М. (2003). Фотоидентификация корейско-охотской популяции серого кита *(Eschrichtius Robustus)* в 2002 г. // Отчет для Эксон Нефтегаз и Сахалин Энерджи Инвестмент Компании.

40. Zhabin, I.A., L.N. Propp, T.I. Volkova and P.Ya. Tishchenko. (2005). Variability of hydrochemical and hydrologic parameters near the mouth of the Amur River // *Okeanologiya*, Vol. 45, No. 5, pp. 703-709.

Жабин И.А., Пропп Л.Н., Волкова Т.И., Тищенко П.Я. (2005). Изменчивость гидрохимических и гидрологических параметров вблизи устья реки Амур.// Океанология, том 45, № 5, с. 703-709.

Appendix A - Daily Sonograms for AUAR Data.

July	Lunskoye	OFA	Orlan	Arkutun-Dagi	Piltun-S	Piltun	PA-B-10	PA-B-20	Odoptu-PA-B	Odoptu-S-10	Odoptu-S-20	Odoptu-N-10	Odoptu-N-20	Control	Molikpaq	BEH-Odoptu	BEH-North	Chayvo-4
#	1	2	3	4	5	6	7	8	9	10	11	12	13	14	15	A9	A10	A11
1																		
2																		
3						✓		✓										
4						✓		✓										
5						✓		✓										
6						✓		✓										
7						✓		✓										
8						✓		✓										
9	✓	✓	✓	✓		✓		✓										✓
10	✓	✓	✓	✓		✓	✓	✓	✓									✓
11	✓	✓	✓	✓		✓	✓	✓	✓		✓			✓			✓	✓
12	✓	✓	✓	✓		✓	✓	✓	✓		✓			✓			✓	✓
13	✓	✓	✓	✓		✓	✓	✓	✓		✓			✓			✓	✓
14	✓	✓	✓	✓		✓	✓	✓	✓		✓			✓			✓	✓
15	✓	✓	✓	✓		✓	✓	✓	✓		✓			✓			✓	✓
16	✓	✓	✓	✓		✓	✓	✓	✓		✓			✓			✓	✓
17	✓	✓	✓	✓		✓	✓	✓	✓		✓			✓			✓	✓
18	✓	✓	✓	✓		✓	✓	✓			✓			✓			✓	✓
19	✓	✓	✓	✓		✓	✓	✓			✓			✓			✓	✓
20	✓	✓	✓	✓		✓	✓	✓			✓			✓			✓	✓
21	✓	✓	✓	✓		✓	✓	✓			✓			✓			✓	✓
22	✓	✓	✓	✓	✓		✓		✓		✓			✓	✓		✓	
23	✓	✓	✓	✓	✓	✓	✓	✓	✓		✓	✓		✓	✓		✓	
24	✓	✓	✓	✓	✓	✓	✓	✓	✓		✓	✓		✓	✓		✓	
25	✓	✓	✓	✓	✓	✓	✓	✓	✓		✓	✓		✓	✓		✓	
26	✓	✓	✓	✓	✓	✓	✓	✓	✓		✓	✓		✓	✓		✓	
27	✓	✓	✓	✓	✓	✓	✓	✓	✓		✓	✓		✓	✓		✓	
28	✓	✓	✓	✓	✓	✓	✓	✓	✓			✓			✓		✓	
29	✓	✓	✓	✓	✓	✓	✓	✓	✓	✓	✓	✓			✓			
30	✓	✓	✓	✓	✓	✓	✓	✓	✓	✓	✓	✓	✓	✓	✓	✓		
31	✓	✓	✓	✓	✓	✓	✓	✓	✓	✓	✓	✓	✓	✓	✓	✓		

August	Lunskoye	OFA	Orlan	Arkutun-Dagi	Piltun-S	Piltun	PA-B-10	PA-B-20	Odoptu-PA-B	Odoptu-S-10	Odoptu-S-20	Odoptu-N-10	Odoptu-N-20	Control	Molikpaq	BEH-Odoptu	BEH-North	Chayvo-4
#	1	2	3	4	5	6	7	8	9	10	11	12	13	14	15	A9	A10	A11
1	✓	✓	✓	✓	✓	✓	✓	✓	✓	✓	✓	✓	✓	✓	✓	✓		
2	✓	✓	✓	✓	✓	✓	✓	✓	✓	✓	✓	✓	✓	✓	✓	✓		
3	✓	✓	✓	✓	✓	✓	✓	✓	✓	✓	✓	✓	✓	✓	✓	✓		
4	✓	✓		✓	✓	✓	✓	✓	✓	✓	✓	✓	✓	✓	✓	✓		
5	✓	✓		✓	✓	✓	✓	✓	✓	✓	✓	✓	✓	✓	✓	✓		
6	✓	✓		✓	✓	✓	✓	✓		✓	✓	✓	✓	✓	✓	✓		
7	✓	✓		✓	✓	✓	✓	✓		✓	✓	✓	✓	✓	✓	✓		
8					✓	✓	✓	✓		✓	✓	✓	✓	✓	✓	✓		
9					✓	✓		✓		✓	✓	✓	✓	✓	✓	✓		
10					✓	✓		✓		✓	✓	✓	✓	✓	✓	✓		
11					✓	✓		✓		✓	✓	✓	✓	✓	✓	✓		
12					✓	✓		✓		✓	✓	✓	✓	✓	✓	✓		
13					✓	✓		✓		✓	✓	✓	✓	✓	✓	✓		
14	✓	✓			✓	✓		✓		✓	✓		✓	✓	✓	✓		
15	✓	✓	✓	✓	✓	✓	✓	✓		✓	✓		✓	✓	✓	✓		
16	✓	✓	✓	✓	✓	✓	✓	✓		✓	✓		✓	✓	✓	✓		
17	✓	✓	✓	✓	✓	✓	✓	✓		✓	✓	✓	✓	✓				
18	✓	✓	✓	✓		✓	✓	✓		✓	✓	✓	✓	✓				✓
19	✓	✓	✓	✓	✓	✓	✓	✓	✓	✓	✓	✓	✓	✓	✓			✓
20	✓	✓	✓	✓	✓	✓	✓	✓	✓	✓	✓	✓	✓	✓	✓			✓
21	✓	✓	✓	✓	✓	✓	✓	✓	✓	✓	✓	✓	✓	✓	✓			✓
22	✓	✓	✓	✓	✓	✓	✓	✓	✓	✓	✓	✓	✓	✓	✓			✓
23	✓	✓	✓	✓	✓	✓	✓	✓	✓	✓	✓	✓	✓	✓	✓			✓
24	✓	✓	✓	✓	✓	✓	✓	✓	✓	✓	✓	✓	✓	✓	✓			✓
25	✓	✓	✓	✓	✓	✓	✓	✓	✓	✓	✓	✓	✓	✓	✓			✓
26	✓	✓	✓	✓	✓	✓	✓	✓	✓	✓	✓	✓	✓	✓	✓			✓
27	✓	✓	✓	✓	✓	✓	✓	✓	✓	✓	✓	✓	✓	✓	✓			✓
28	✓	✓	✓	✓	✓	✓	✓	✓	✓	✓	✓	✓	✓	✓	✓			✓
29	✓	✓	✓	✓	✓	✓	✓	✓	✓	✓	✓	✓	✓	✓	✓			✓
30	✓	✓	✓	✓	✓	✓	✓	✓	✓	✓	✓	✓	✓	✓	✓			✓
31	✓	✓	✓	✓	✓	✓	✓	✓	✓	✓	✓	✓	✓	✓	✓			✓

September	Lunskoye	OFA	Orlan	Arkutun-Dagi	Piltun-S	Piltun	PA-B-10	PA-B-20	Odoptu-PA-B	Odoptu-S-10	Odoptu-S-20	Odoptu-N-10	Odoptu-N-20	Control	Molikpaq	BEH-Odoptu	BEH-North	Chayvo-4
#	1	2	3	4	5	6	7	8	9	10	11	12	13	14	15	A9	A10	A11
1	✓	✓	✓	✓	✓	✓	✓	✓	✓	✓	✓	✓	✓	✓	✓			✓
2	✓	✓	✓	✓	✓	✓	✓	✓	✓	✓	✓	✓	✓	✓	✓			✓
3	✓	✓	✓	✓	✓	✓	✓	✓	✓	✓	✓	✓	✓	✓	✓			✓
4	✓	✓	✓	✓	✓	✓	✓	✓	✓	✓	✓	✓	✓	✓	✓			✓
5	✓	✓	✓	✓	✓	✓	✓	✓	✓	✓	✓	✓	✓	✓	✓			✓
6	✓	✓	✓	✓	✓	✓	✓	✓	✓						✓			
7	✓	✓	✓	✓	✓	✓	✓	✓	✓						✓			
8	✓		✓	✓					✓									
9			✓															
10																		

Appendix B - Calibration Certificates.

Hydrophones:

1. Certificate # 5/32-008-07	Hydrophone # GI-50 № 25	Type GI-50 (GI-50)
	Hydrophone # GI-50 № 28	Type GI-50 (GI-50)
	Hydrophone # GI-50 № 26	Type GI-50 (GI-50)
	Hydrophone # GI-50 № 29	Type GI-50 (GI-50)
2. Certificate # 5/32-009-07	Hydrophone # GI-50 № 41	Type GI-50 (GI-50)
	Hydrophone # GI-50 № 43	Type GI-50 (GI-50)
	Hydrophone # GI-50 № 44	Type GI-50 (GI-50)
	Hydrophone # GI-50 № 45	Type GI-50 (GI-50)
3. Certificate # 5/32-010-07	Hydrophone # GI-50 № 32	Type GI-50 (GI-50)
	Hydrophone # GI-50 № 34	Type GI-50 (GI-50)
	Hydrophone # GI-50 № 37	Type GI-50 (GI-50)
	Hydrophone # GI-50 № 38	Type GI-50 (GI-50)
4. Certificate # 5/24-006-06	Hydrophone # GI-50 №009	Type GI-50 (GI-50)
	Hydrophone # GI-50 №011	Type GI-50 (GI-50)
	Hydrophone # GI-50 №014	Type GI-50 (GI-50)
	Hydrophone # GI-50 №016	Type GI-50 (GI-50)
	Hydrophone # GI-50 №003	Type GI-50 (GI-50)
5.Certificate # 5/24-004-05	Hydrophone # GI-50 №004	Type GI-50 (GI-50)
	Hydrophone # GI-50 №006	Type GI-50 (GI-50)
	Hydrophone # GI-50 №018	Type GI-50 (GI-50)
	Hydrophone # GI-50 №010	Type GI-50 (GI-50)
	Hydrophone # GI-50 №008	Type GI-50 (GI-50)
6.Certificate # 5/24-005-05	Hydrophone # GI-50 №017	Type GI-50 (GI-50)
	Hydrophone # GI-50 №023	Type GI-50 (GI-50)
7.Certificate # 5/24-002-05	Hydrophone # Г-33 №112	Type G-33 (Г-33)

Geophone type A0515 No. 12:

1. Data sheet MGFK.402152.003FO.
2. Basic specifications and acceptance certificate

SVXtra hydrologic sonde:

1. Equipment Checklist		
2. SVXtra Calibration and Instrument build record		
3. Conductivity sensor Calibration record	SN #14083	Type 62R
4. Sound Velocity sensor Calibration record	SN #10903	Type 100 mm
5. Pressure sensor Calibration record	SN # 1599575	Type PDCR4000
6. Temperature sensor Calibration record	SN # 405	Type PRT

Copies of these calibration certificates are in the file 'Calibration certificates (Appendix B)' on the DVD at the back of this report.

Appendix C – Estimation of Western Gray Whale Core Areas[53]

In these analyses, cumulative probability contours are used to visualize areas with the greatest likelihood of encountering gray whales, and examine shifts in the 'centers of activity' of gray whales over time[54]. Probability contours of 50% and 95% are generated to visualize the distribution of gray whales. The 50% contour represents the area within which 50% of the whales sighted are expected to be found. In 2003, the probability contours were estimated from 2003 and 2004 aerial survey data that took the survey effort into account[55] using a conventional kernel density method[56]. This kernel density method employed a square-gridding process, which is robust for small sample sizes unless the variances of the north-south and east-west components of the distribution are very different, which is the case for the Piltun feeding area.

For the Piltun feeding area the distribution of whale sightings is oriented parallel to the coast with significantly greater variance in the along-shore direction than in the perpendicular-to-shore direction. For this reason, in 2004, a grid was constructed for the Piltun feeding area that was oriented along-shore and with an along-shore grid cell dimension greater than the perpendicular-to-shore dimension, (i.e. each cell was 4 km by 0.5 km). Density was then computed for each cell as the number of whales divided by the cumulative area surveyed within the cell. The same methodology was employed for the offshore feeding area except that, in this case, the conventional assumptions about distribution were satisfied and a grid of 1 km by 1 km cells was employed.

There was substantial variation among the 2003, 2004, 2005 and 2006 estimates of the western gray whale core areas. Consequently, this analysis was updated in 2007 using all available systematic survey data. These included data from the 2001 to 2005 aerial surveys, 2002 to 2006 vessel-based surveys, 2001 to 2006 shore-based behavior scan surveys, and the 2004 to 2006 shore-based vehicle scan surveys.

---

[53] This section is based on work performed by LGL Limited (Robin Tamasi, Peter Wainwright, Judy Muir, Sergei Yazvenko, Sonya Meier, and Steve Johnson).
[54] Probability contours were computed independently for the Piltun and offshore feeding areas.
[55] Density is the number of whales per unit area, multiple surveys over a grid cell can result in larger densities within that cell if the survey effort is not taken into account.
[56] The kernel density contours were mapped using the ArcView© 3.1 extension Animal Movement v2.04 [Hooge et. al., 1997]. Kernel density contours are an estimator that assesses an animal's probability of occurrence at each point in space based on a utilization distribution. It is a non-parametric estimator that has no underlying assumptions of how animals use space.

Because there are significant differences in these survey methods, it is necessary to calibrate the observations or bring them to a common standard, before performing density calculations. This was achieved by using Distance analysis [Buckland et. al. 2001] to correct for differences in the ability to detect whales, and by applying an additional correction for the probability that some whales were underwater during the survey. Details of the density calculations are as follows:

- Distance 4.2 software [Thomas et. al. 2004] was used to compute sightability functions and Effective Strip Width (ESW) for the aerial survey data set. Distance 5.0 software [Thomas et. al. 2006] was used to compute a sightability function and Effective Strip Width (ESW) for the vessel survey data. There are issues with using standard Distance analysis methodology to develop sightability functions for the shore-based surveys. In particular, the assumption that the observation stations are located randomly with respect to the whale distribution is violated because whale density is correlated with water depth. This confounds sightability functions because the variability in detections with distance may be due to effects of both changing density and sightability. The shore-based detection function was determined instead based on an analysis conducted by the University of St. Andrews that used simultaneous shore-based and ship-based sightings to estimate parameters of a shore-based detection function (Rexstad and Borchers 2006). This analysis showed that the shore-based detection function is flat (i.e. the detection probability does not decrease with increasing distance from the observation station) for up to 0.1 reticle radial distance (range 4.5 to 10.8 km) from each shore station, to a maximum of 8 km distance.
- Two grids were produced: one for the Piltun feeding area and one for the offshore feeding area.
- The Piltun feeding area grid consisted of a grid of cells oriented north/south with cell dimensions of 4-km alongshore by ½-km perpendicular to shore with an average area of 2.03 km² (standard deviation = 0.02 km²).
- The Offshore feeding area grid consisted of a grid of cells oriented north/south with cell dimensions of 1-km alongshore by 1-km perpendicular to shore with a cell area of 1.0 km² (standard deviation = 0.02 km²).
- ArcGIS v9.0 (ESRI 2005) geographic information system (GIS) software was used to construct buffers around each aerial survey transect(s) flown (1 km wide for surveys at 300m altitude and 1½ km wide for surveys at 500 m altitude) and each vessel survey transect (4.5 km wide) to represent the surveyed swathes. For shore-based stations, buffers with radius equal to 0.1 reticle radial distance (range 4.5 to 10.8 km) from each shore station, to a maximum of 8 km distance were constructed to represent the area surveyed by each station.
- These resulting buffers were then overlaid on the grid and the area of the cell within the buffer ($Area_i$) was computed. Where less than 10% of the cell area fell within the buffer it was considered inappropriate to estimate density for that cell because survey coverage was not sufficient to provide a reliable estimate of density.
- The number of whales within the buffer within each grid cell was then computed. First, the number of whales for each sighting was inflated for aerial and vessel surveys using

the appropriate sightability function to compensate for the lower probability of sighting whales at greater distances from the observer.

- Next, the inflated whale sightings were overlaid on the result of the grid/buffer overlay. This resulted in an estimate of the number of whales within the surveyed area of each grid cell ($Count_i$). Finally, density was estimated for each grid cell as the number of whales per unit area adjusted by the probability that whales were underwater during the period of the survey (*g(0)*):

$$Density = \frac{\left[\frac{Count_i}{Area_i}\right]}{g(0)} \qquad \text{(C.1)}$$

  g(0) was estimated separately for each survey type and year based on 2001-2006 western gray whale surface-respiration-dive cycle behavior data, the field of view, and the aircraft or vessel speed or the rate of scanning at shore-based observation stations.

- A weighted average of the density estimates from individual surveys was then computed to obtain an overall average estimated density for each grid cell. The weightings were based on the area of the grid cell that was sampled by the individual survey.

Kernel probability densities were then computed for the Piltun and offshore feeding areas separately as follows:

- The total of the densities of all cells in the feeding area grid was computed.
- The cell data were then sorted by density in ascending order.
- *Cumulative densities* were computed for each cell by summing the densities of all preceding cells in the sorted cell density list, i.e., summing all cells with lower estimated gray whale densities.
- Kernel probability densities were then calculated for each cell by dividing the *cumulative density* of the cell by the total of the feeding area grid densities, expressed as a percentage.
- Finally, the ArcGIS Spatial Analyst extension inverse distance weighting (IDW) method with a distance threshold of 3-km was used to compute 25%, 50%, 75% and 95% probability contours for the feeding area grid. These contours were then used in combination with the kernel probability density grid cells to manually delineate smoothed 50% and 95% probability contours for the feeding area.

Appendix D - Cross-calibration Results

At the start of the 2007 expedition a cross-calibration of all eleven AUARs, five T-AUARs, and six mini-AUARs, as well as the two digital (DSB) and four analog (ASB) sonobuoys used for the 2007 field program was conducted on the *Professor Bogorov*. The purpose of these calibrations was to confirm the absolute calibration[57] of all the recording systems by comparing the acoustic spectra of synchronously measured signals. All AUARs and sonobuoys were calibrated by comparing the synchronous spectra of broadband and tonal signals generated by the *Professor Bogorov* and the HF broadband sound transducer. All spectra were corrected for amplitude and frequency (using the instrument response of each system determined by instrument tests in the laboratory), so the absolute acoustic level of the signal was calculated for the specified frequencies.

The field cross-calibration was conducted by tying a number of hydrophones together in a bundle, and deploying them from the *Professor Bogorov* at a depth of 10-15 m while it was drifting in greater than 30 m of water. The hydrophones were divided into groups (Figure D.1) due to the large number of hydrophones being calibrated and the potential for crossfeed between the sonobuoys during cross-calibration due to the close proximity of the units. One mini-AUAR (No. 23) was used as a control for all the groups. The AUARs and sonobuoys on the *Professor Bogorov* synchronously recorded the signals from these hydrophones. The purpose was to simultaneously record the same signal on all the units, allowing the relative calibrations of the AUARs and sonobuoys to be confirmed. Data was recorded using the operational configurations for the equipment. The methodology described by Borisov [Borisov et. al., 2006, 2007] was used to calculate the relative error for each AUAR and sonobuoy. The results from these measurements are given in Figures D.2 to D.17 and Tables D.1 to D.12.

[57] These cross-calibrations allowed the amplitude response (with frequency) of the analog circuits of the AUARs and sonobuoys to be compared with the laboratory measurements. They also allowed the manufacturer's hydrophone calibrations to be confirmed.

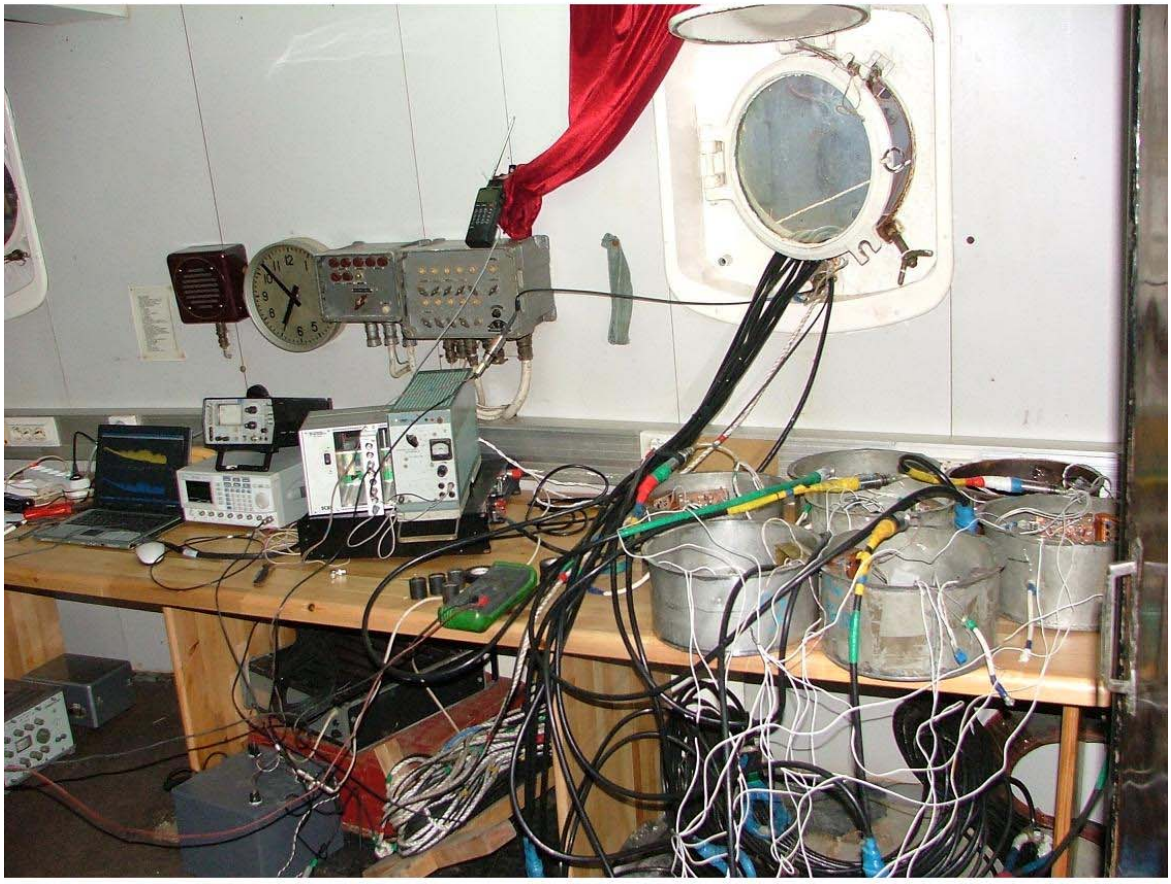

Figure D.1 – Cross-calibration of the AUARs and sonobuoys on the *Professor Bogorov.*

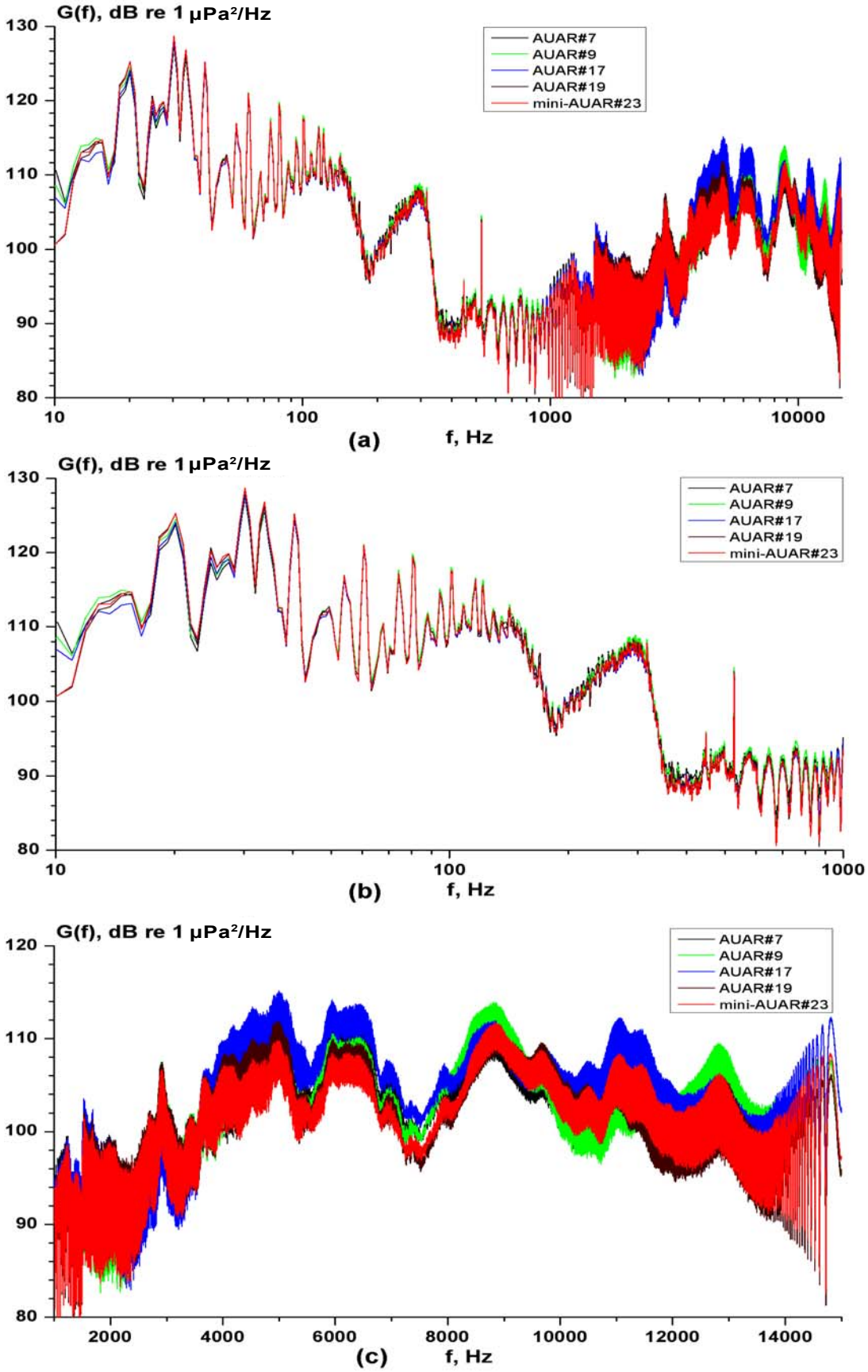

Figure D.2 - Spectra of acoustic signals synchronously measured by AUARs No. 7, 9, 17, 19 and the reference mini-AUAR No. 23 (after instrument response [amplitude-frequency] correction).
(a) 10 Hz-15 kHz; (b) 10 Hz-1 kHz; (c) 1-15 kHz.

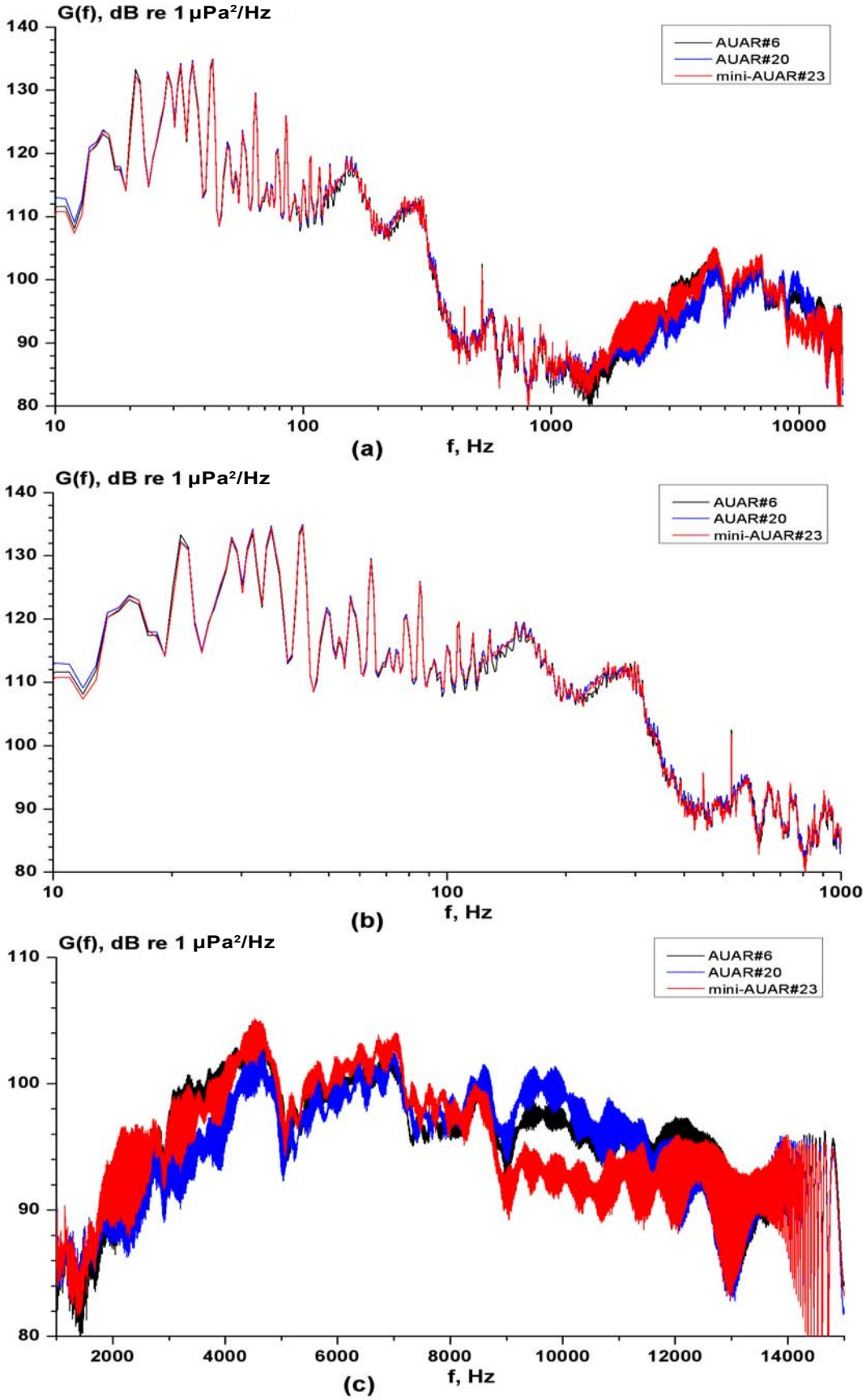

Figure D.3 - Spectra of acoustic signals synchronously measured by AUARs No. 6, 20 and the reference mini-AUAR No. 23 (after instrument response [amplitude-frequency] correction).
(a) 10 Hz-15 kHz; (b) 10 Hz-1 kHz; (c) 1-15 kHz

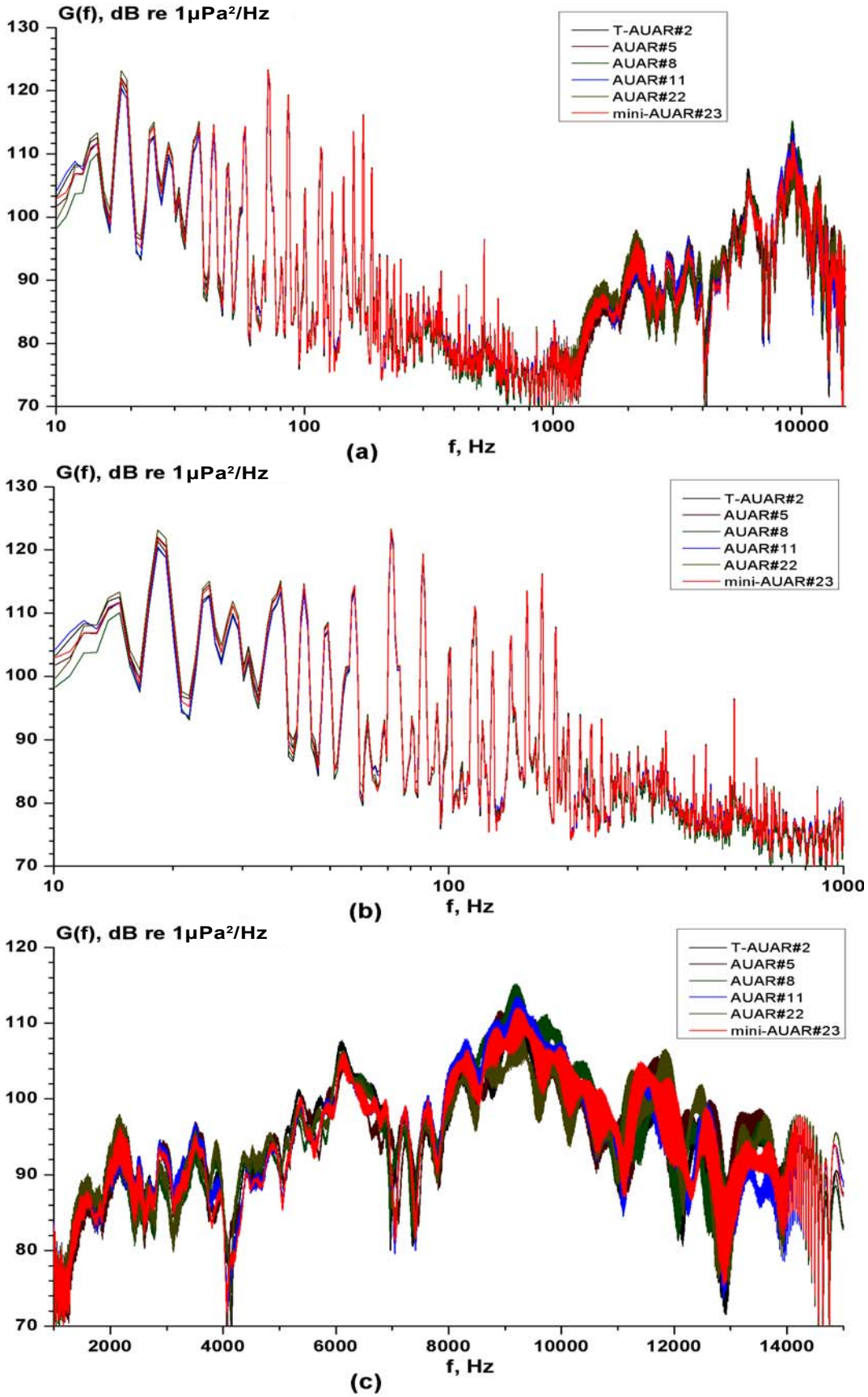

Figure D.4 - Spectra of acoustic signals synchronously measured by T-AUAR No. 2, AUARs No. 5, 8, 11, 22 and the reference mini-AUAR No. 23 (after instrument response [amplitude-frequency] correction). (a) 10 Hz-15 kHz; (b) 10 Hz-1 kHz; (c) 1-15 kHz.

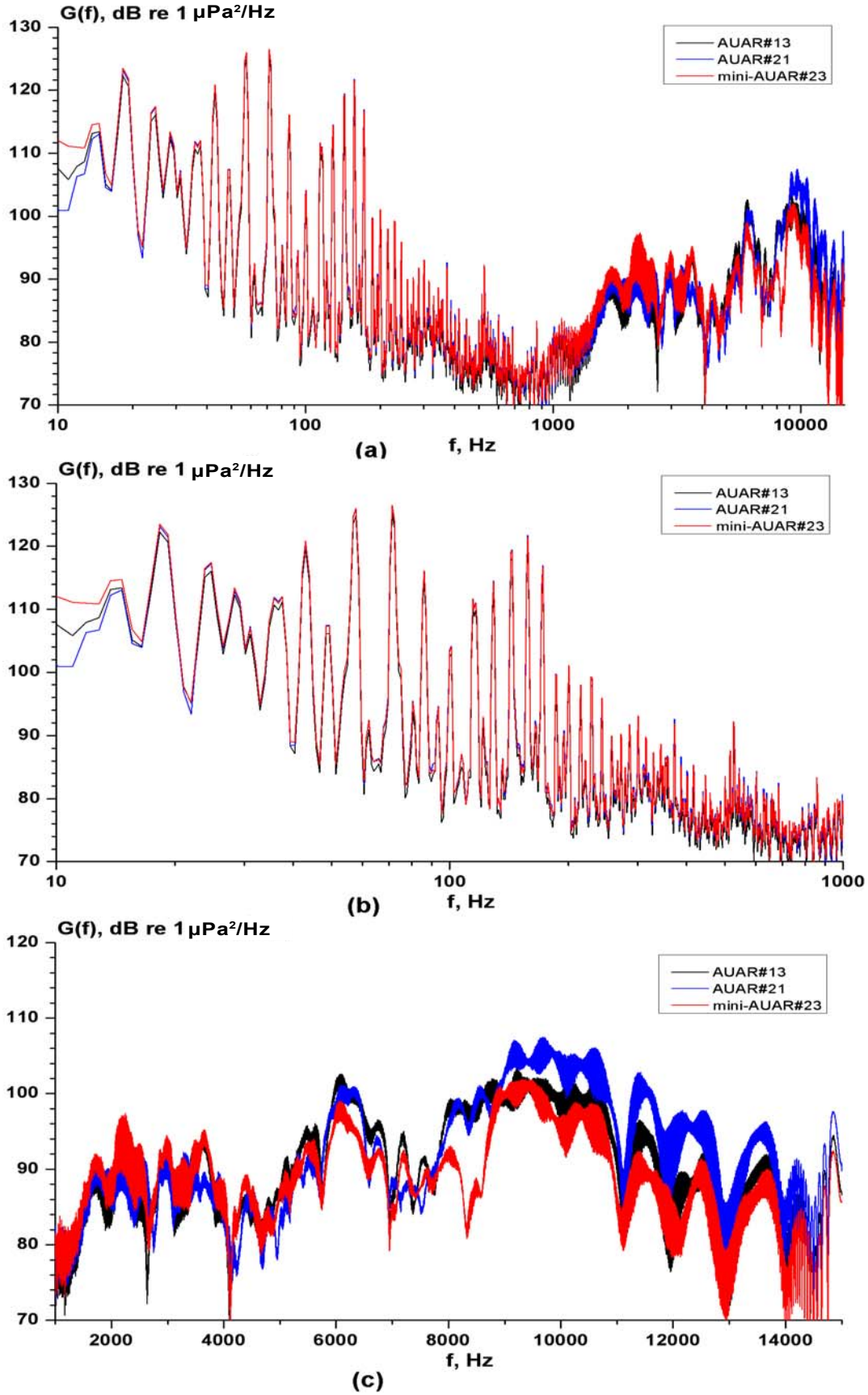

Figure D.5 - Spectra of acoustic signals synchronously measured by AUARs No. 13, 21 and the reference mini-AUAR No. 23 (after instrument response [amplitude-frequency] correction).
(a) 10 Hz-15 kHz; (b) 10 Hz-1 kHz; (c) 1-15 kHz.

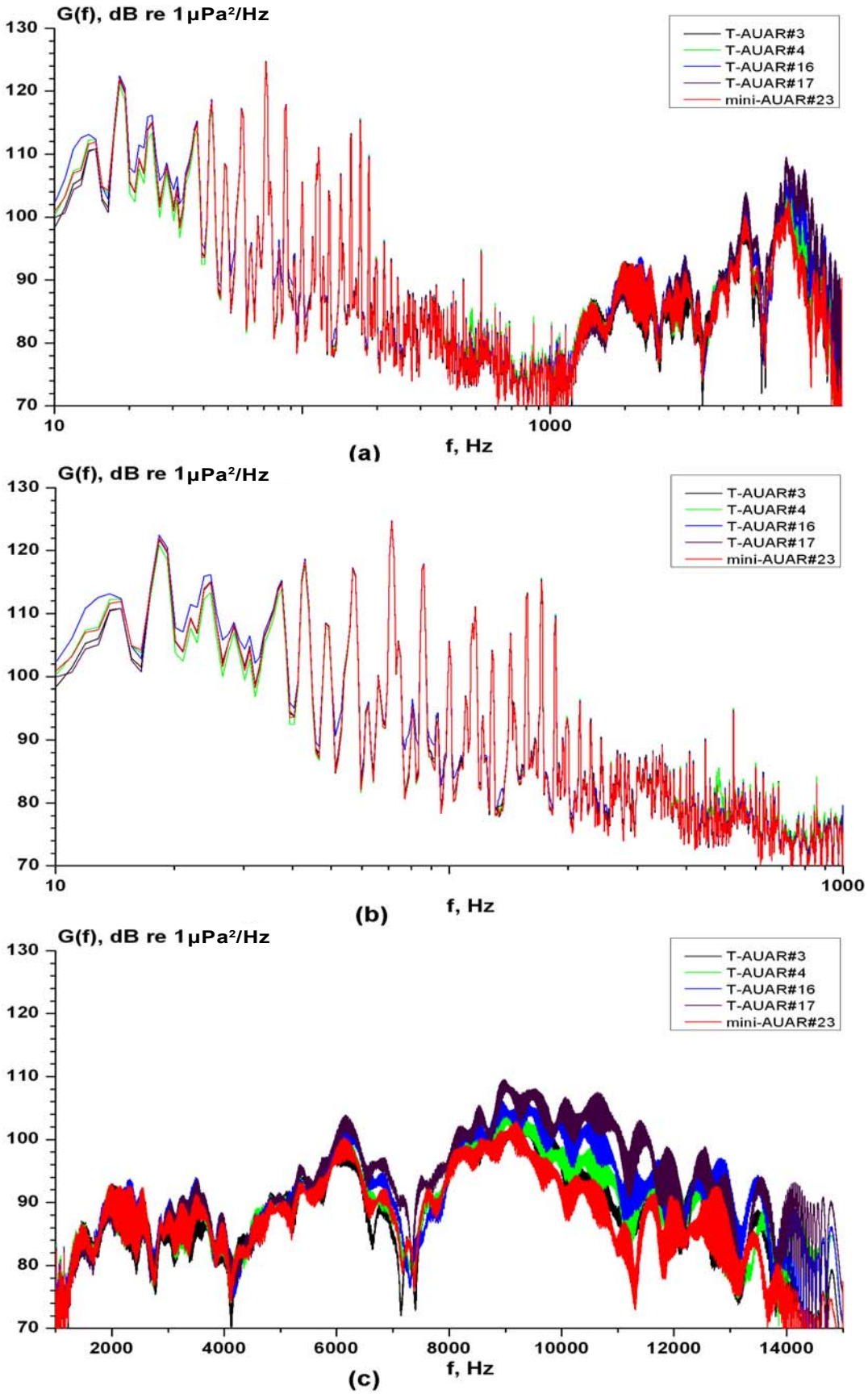

Figure D.6 - Spectra of acoustic signals synchronously measured by T-AUAR No. 3, AUARs No. 4, 16, 17 and the reference mini-AUAR No. 23 (after instrument response [amplitude-frequency] correction). (a) 10 Hz-15 kHz; (b) 10 Hz-1 kHz; (c) 1-15 kHz.

Table D.1 - Cross-calibration - statistical relative error analysis in the frequency bands 10-1000 Hz, 10 Hz to 15 kHz for AUARs No. 7, 9, 19, T-AUAR No. 17, and the reference (mini-AUAR No. 23)

AUAR #	$D(\Delta f_1)$ [dB] f_1 = 10-1000	$\sigma(\Delta f_1)$ [dB] f_1 = 10-1000	$D(\Delta f_2)$ [dB] f_2 = 10-15 kHz	$\sigma(\Delta f_2)$ [dB] f_2 = 10 Hz-15
Reference	138.3	0.3	146.4	0.9
7	137.6	0.1	146.9	0.4
9	138.1	0.3	147.5	1.2
17 (T-AUAR)	137.7	0.2	149.1	1.8
19	138.2	0.4	146.5	0.8
Mean	***138.0***		***147.3***	

Table D.2 - Cross-calibration - statistical relative error analysis in the frequency bands 10-1000 Hz, 10-15 kHz for AUARs 6, 20 and the reference (mini-AUAR No. 23).

AUAR #	$D(\Delta f_1)$ [dB] f_1 =10-1000 Hz	$\sigma(\Delta f_1)$ [dB] f_1 =10-1000 Hz	$D(\Delta f_2)$ [dB] f_2 =0.01-15 kHz	$\sigma(\Delta f_2)$ [dB] f_2 =0.01-15 kHz
Reference	145.3	0.0	146.3	0.0
6	145.1	0.2	146.1	0.2
20	145.5	0.2	146.4	0.1
Mean	***145.3***		***146.3***	

Table D.3 - Cross-calibration - statistical relative error analysis in the frequency bands 10-1000 Hz, 10-15 kHz for AUARs No. 5, 8, 11, 22, T-AUAR No. 2, and the reference (mini-AUAR No. 23)

AUAR #	$D(\Delta f_1)$ [dB] f_1 = 10-1000	$\sigma(\Delta f_1)$ [dB] f_1 = 10-1000	$D(\Delta f_2)$ [dB] f_2 = 10-15 kHz	$\sigma(\Delta f_2)$ [dB] f_2 = 10-15 kHz
Reference	131.1	0.3	142.3	0.1
2 (T-AUAR)	130.8	0.0	141.8	0.6
5	131.1	0.3	142.5	0.1
8	129.9	0.9	143.7	1.3
11	130.3	0.5	143.0	0.6
22	131.6	0.8	141.1	1.3
Mean	***130.8***		***142.4***	

Table D.4 - Cross-calibration - statistical relative error analysis in the frequency bands 10-1000 Hz, 10-15 kHz for AUARs 13, 21 and the reference (mini-AUAR No. 23).

AUAR #	$D(\Delta f_1)$ [dB] f_1 = 10-1000	$\sigma(\Delta f_1)$ [dB] f_1 = 10-1000	$D(\Delta f_2)$ [dB] f_2 = 10-15 kHz	$\sigma(\Delta f_2)$ [dB] f_2 = 10-15 kHz
Reference	135.1	0.5	127.7	1.2
13	133.9	0.7	138.4	0.6
21	134.9	0.3	140.7	1.7
Mean	***134.6***		***139.0***	

Table D.5 - Cross-calibration - statistical relative error analysis in the frequency bands 10-1000 Hz, 10-15 kHz for T-AUARs No. 3, 4, 16, 17, and the reference (mini-AUAR No. 23)

AUAR #	$D(\Delta f_1)$ [dB] f_1 = 10-1000	$\sigma(\Delta f_1)$ [dB] f_1 = 10-1000	$D(\Delta f_2)$ [dB] f_2 = 10-15 kHz	$\sigma(\Delta f_2)$ [dB] f_2 = 10-15 kHz
Reference	131.7	0.1	132.3	0.0
3 (T-AUAR)	131.8	0.0	132.3	0.0
4 (T-AUAR)	131.7	0.1	132.2	0.1
16 (T-AUAR)	131.4	0.4	132.0	0.3
17 (T-AUAR)	132.3	0.5	132.8	0.5
Mean	***131.8***		***132.3***	

Tables D.1 to D.5 give an analysis of power spectral density levels for the two frequency bands (10 Hz to 1 kHz and 10 Hz to 15 kHz) and the calibration error from the mean for the two frequency bands. As can be seen the maximum absolute error for any AUAR from the mean is 0.9 dB in the frequency band from 10 to 1000 Hz and less than 1.8 dB between 10 Hz and 15 kHz[58]. This is within the expected relative error limits for the equipment and the absolute calibration of the data was therefore confirmed.

[58] The highest errors were due to the low level of the calibration signal at low frequencies. These signals are measured approximately synchronously by the radio transmission and recording channels of a T-AUAR. Precise synchronization is not possible between acoustic data recorded by an AUAR and data arriving via its radio link. Also certain field inaccuracies are present in the cross-calibration measurements; the acoustic measurements are not synchronous (the hydrophones are in different position in the bundle and may mask each other), these errors are not large enough to invalidate the results).

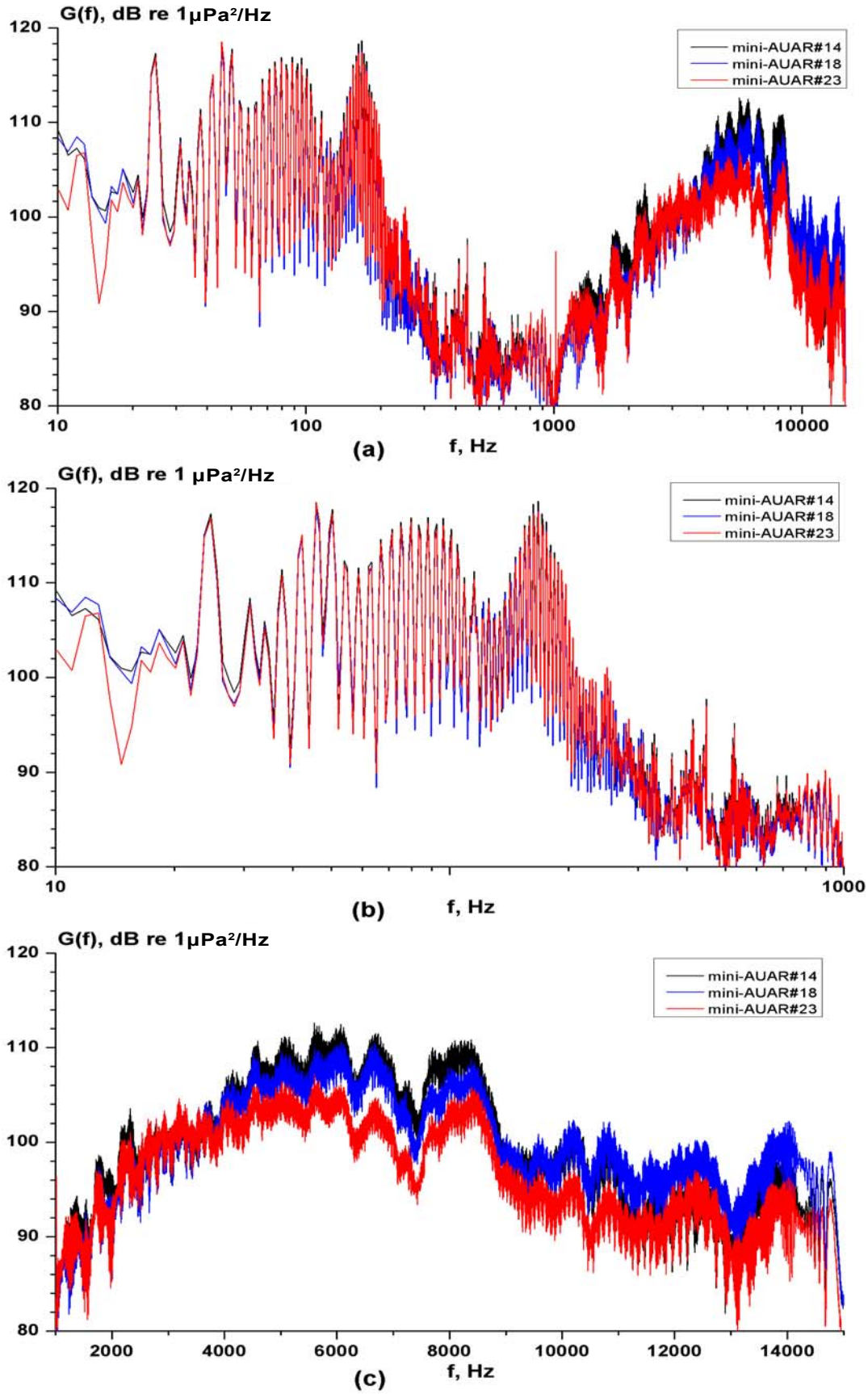

Figure D.7 - Cross calibration analysis - Spectra of acoustic signals synchronously measured by mini-AUARs No. 14, 18 and the reference mini-AUAR No. 23 (after instrument response [amplitude-frequency] correction). (a) 10 Hz-15 kHz; (b) 10 Hz-1 kHz; (c) 1-15 kHz.

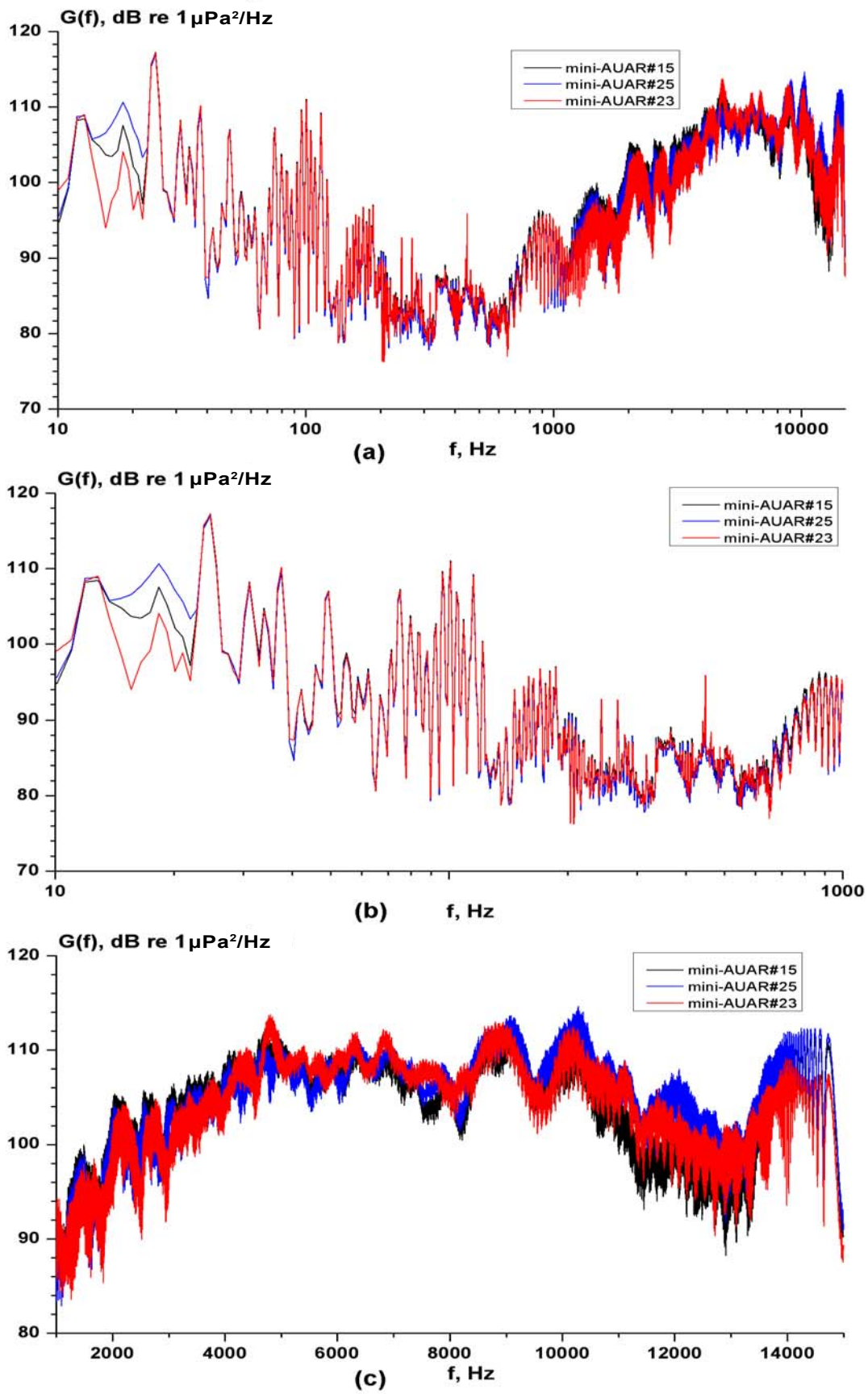

Figure D.8 - Cross calibration analysis - Spectra of acoustic signals synchronously measured by mini-AUARs No. 15, 25 and the reference mini-AUAR No. 23 (after instrument response [amplitude-frequency] correction). (a) 10 Hz-15 kHz; (b) 10 Hz-1 kHz; (c) 1-15 kHz.

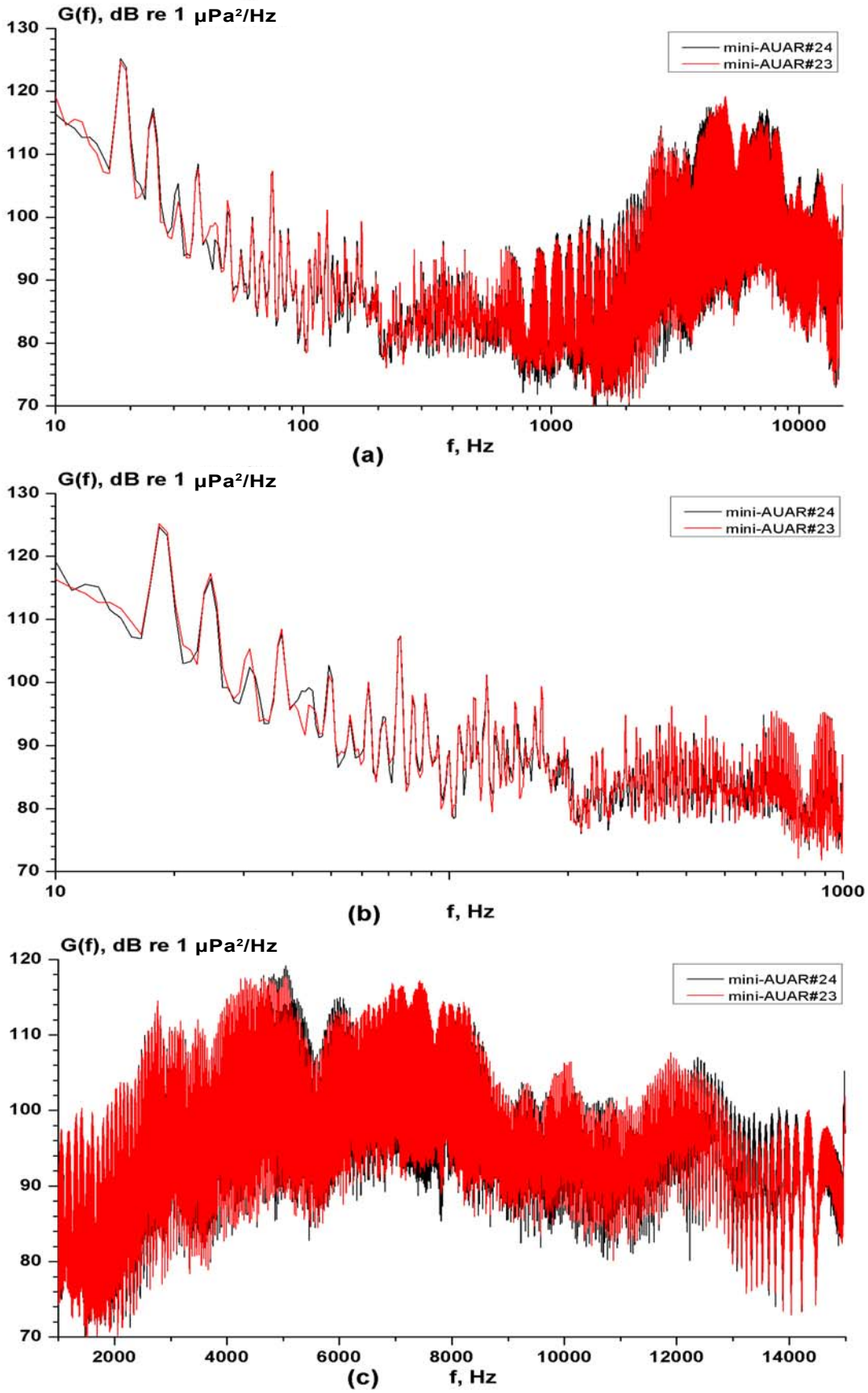

Figure D.9 - Cross calibration analysis - Spectra of acoustic signals synchronously measured by mini-AUAR No. 24 and the reference mini-AUAR No. 23 (after instrument response [amplitude-frequency] correction). (a) 10 Hz-15 kHz; (b) 10 Hz-1 kHz; (c) 1-15 kHz.

Table D.6 - Cross-calibration - statistical relative error analysis in the 10-1000 Hz, 10 Hz to 15 kHz frequency bands for mini-AUARs 14, 18, and the reference (mini-AUAR No. 23)

mini-AUAR #	$D(\Delta f_1)$ [dB] f_1 =10-1000	$\sigma(\Delta f_1)$ [dB] f_1 =10-1000	$D(\Delta f_2)$ [dB] f_2 = 10-15 kHz	$\sigma(\Delta f_2)$ [dB] f_2 = 10-15 kHz
Reference	133.1	0.2	141.8	2.3
14	133.7	0.4	145.9	1.8
18	133.0	0.3	144.6	0.5
Mean	***133.3***		***144.1***	

Table D.7 - Cross-calibration - statistical relative error analysis in the 10-1000 Hz, 10-15 kHz frequency bands for mini-AUARs 15, 25 and the reference (mini-AUAR No. 23).

mini-AUAR #	$D(\Delta f_1)$ [dB] f_1 = 10-1000	$\sigma(\Delta f_1)$ [dB] f_1 = 10-1000	$D(\Delta f_2)$ [dB] f_2 = 10-15 kHz	$\sigma(\Delta f_2)$ [dB] f_2 = 10-15 kHz
Reference	125.3	0.4	148.3	0.5
15	125.7	0.8	148.1	0.3
25	123.7	1.2	146.9	0.9
Mean	***124.9***		***147.8***	

Table D.8 - Cross-calibration - statistical relative error analysis in the 10-1000 Hz, 10-15 kHz frequency bands for mini-AUAR No. 24 and the reference (mini-AUAR No. 23).

mini-AUAR #	$D(\Delta f_1)$ [dB] f_1 = 10-1000	$\sigma(\Delta f_1)$ [dB] f_1 = 10-1000	$D(\Delta f_2)$ [dB] f_2 = 10-15 kHz	$\sigma(\Delta f_2)$ [dB] f_2 = 10-15 kHz
Reference	135.1	0.6	137.8	0.3
24	133.9	0.6	138.4	0.3
Mean	***134.5***		***138.1***	

Tables D.6 to D.8 give an analysis of power spectral density levels for the two frequency bands (10 Hz to 1 kHz and 10-15 kHz) and the calibration error from the mean for the two frequency bands. As can be seen the maximum absolute error for any mini-AUAR from the mean is 1.2 dB in the frequency band from 10 to 1000 Hz and less than 2.3 dB between 10 Hz and 15 kHz[59]. This is within the expected relative error limits for the equipment and the absolute calibration of the data was therefore confirmed.

[59] As with the AUARs the highest errors were due to the low level of the calibration signal at low frequencies.

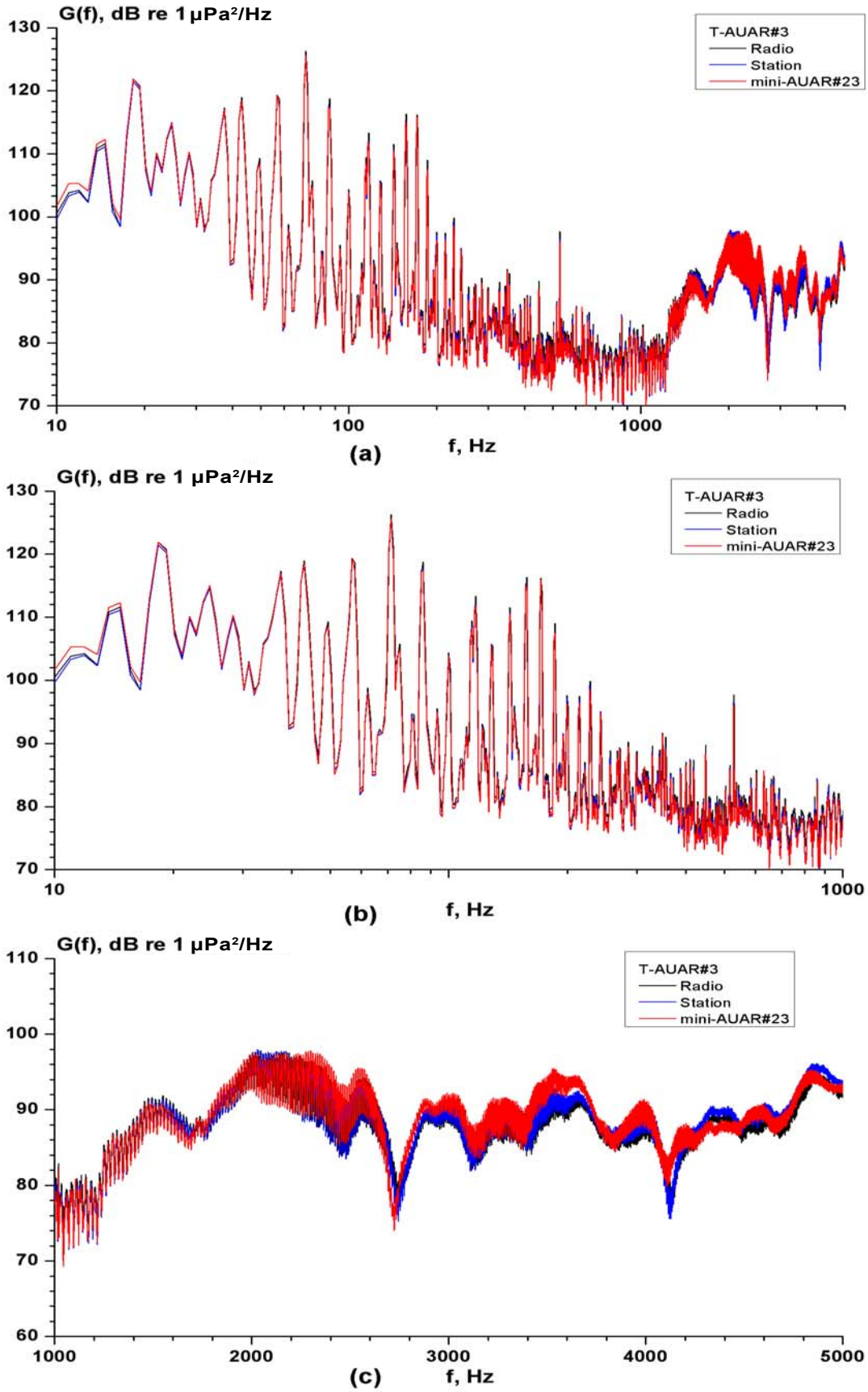

Figure D.10 - Cross calibration analysis - Spectra of acoustic signals synchronously measured by T-AUAR No. 3 and the reference mini-AUAR No. 23 (after instrument response [amplitude-frequency] correction). (a) 10 Hz-15 kHz; (b) 10 Hz-1 kHz; (c) 1-15 kHz.

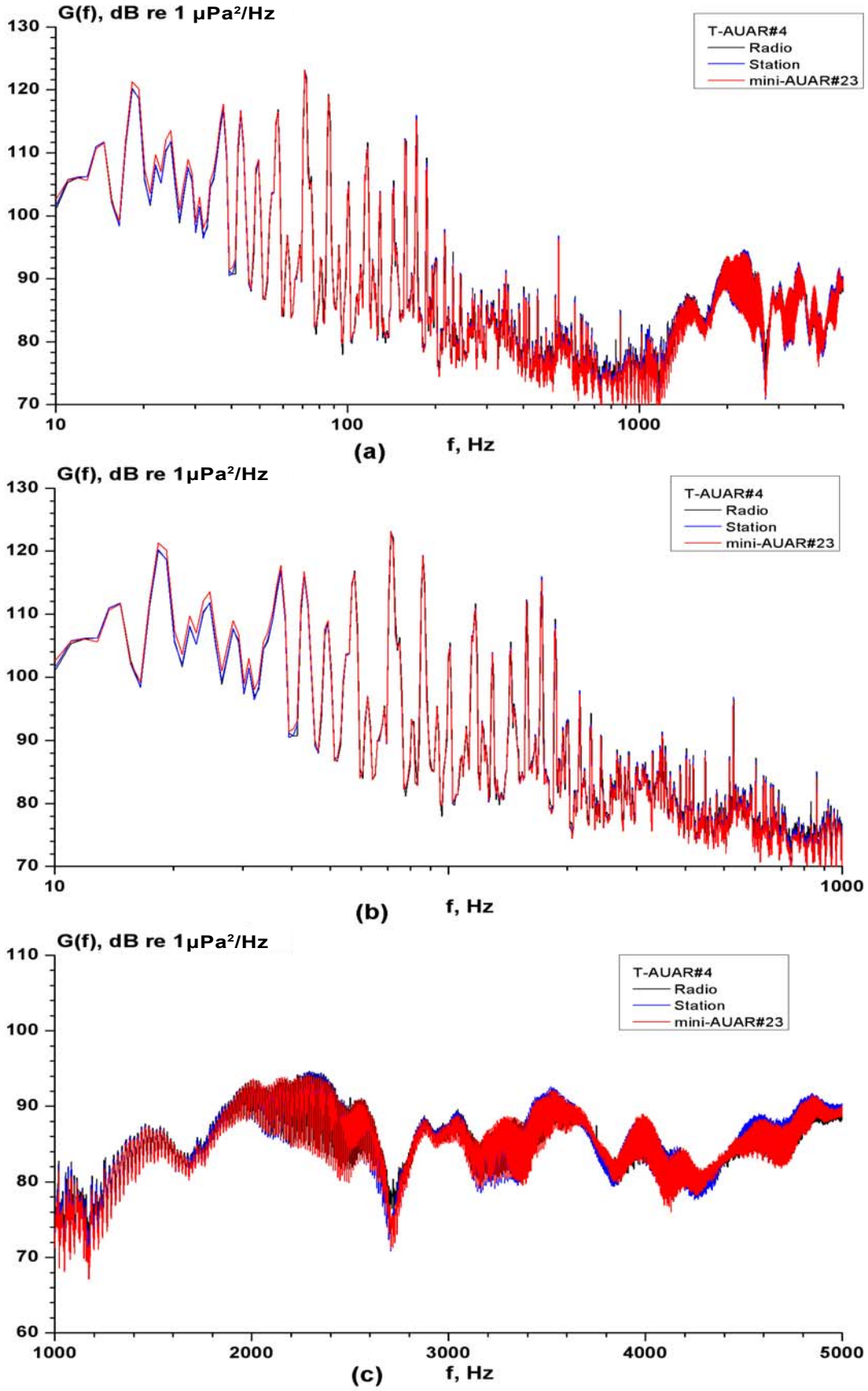

Figure D.11 - Cross calibration analysis - Spectra of acoustic signals synchronously measured by T-AUAR No. 4 and the reference mini-AUAR No. 23 (after instrument response [amplitude-frequency] correction). (a) 10 Hz-15 kHz; (b) 10 Hz-1 kHz; (c) 1-15 kHz.

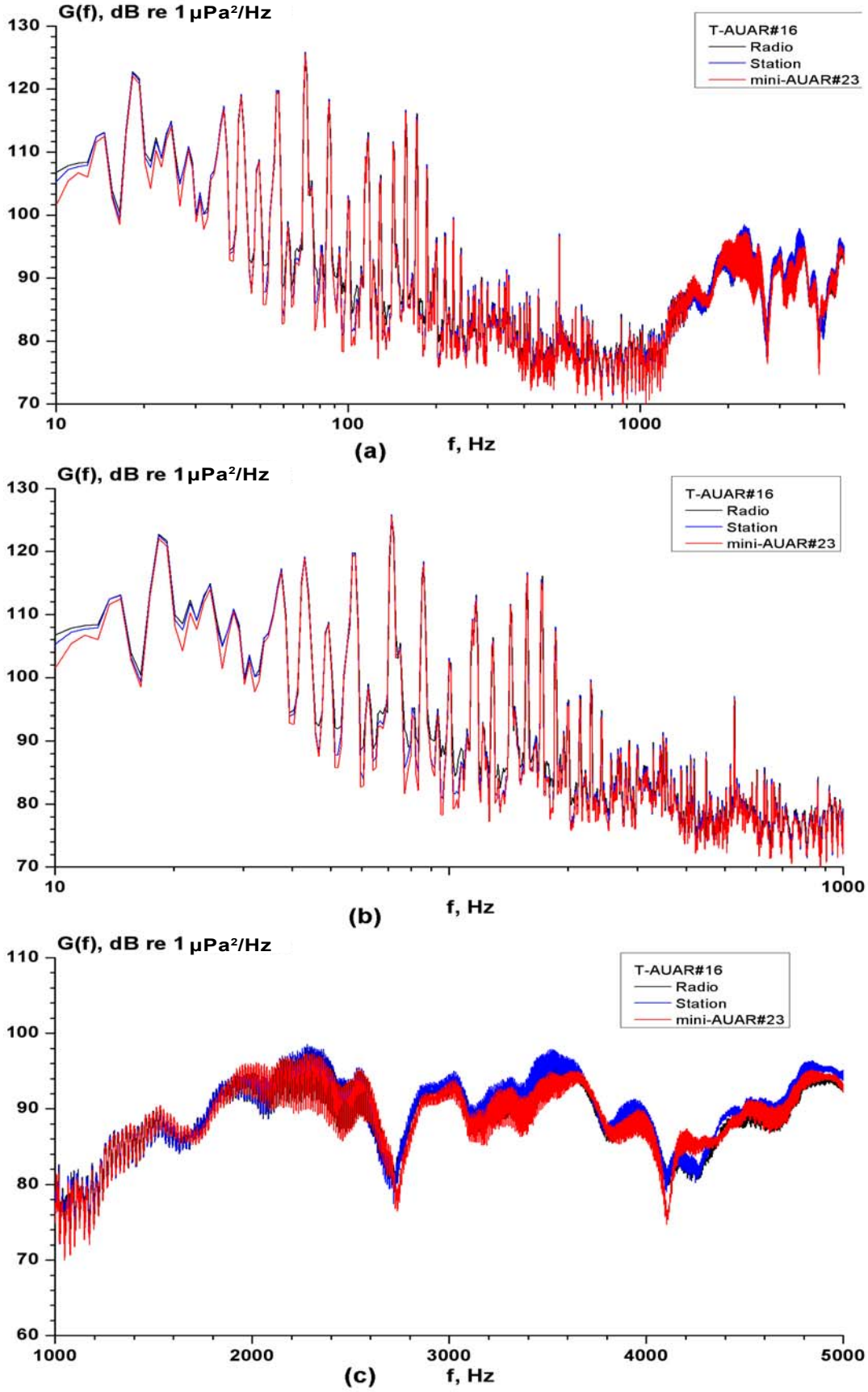

Figure D.12 - Cross calibration analysis - Spectra of acoustic signals synchronously measured by T-AUAR No. 16 and the reference mini-AUAR No. 23 (after instrument response [amplitude-frequency] correction). (a) 10 Hz-15 kHz; (b) 10 Hz-1 kHz; (c) 1-15 kHz.

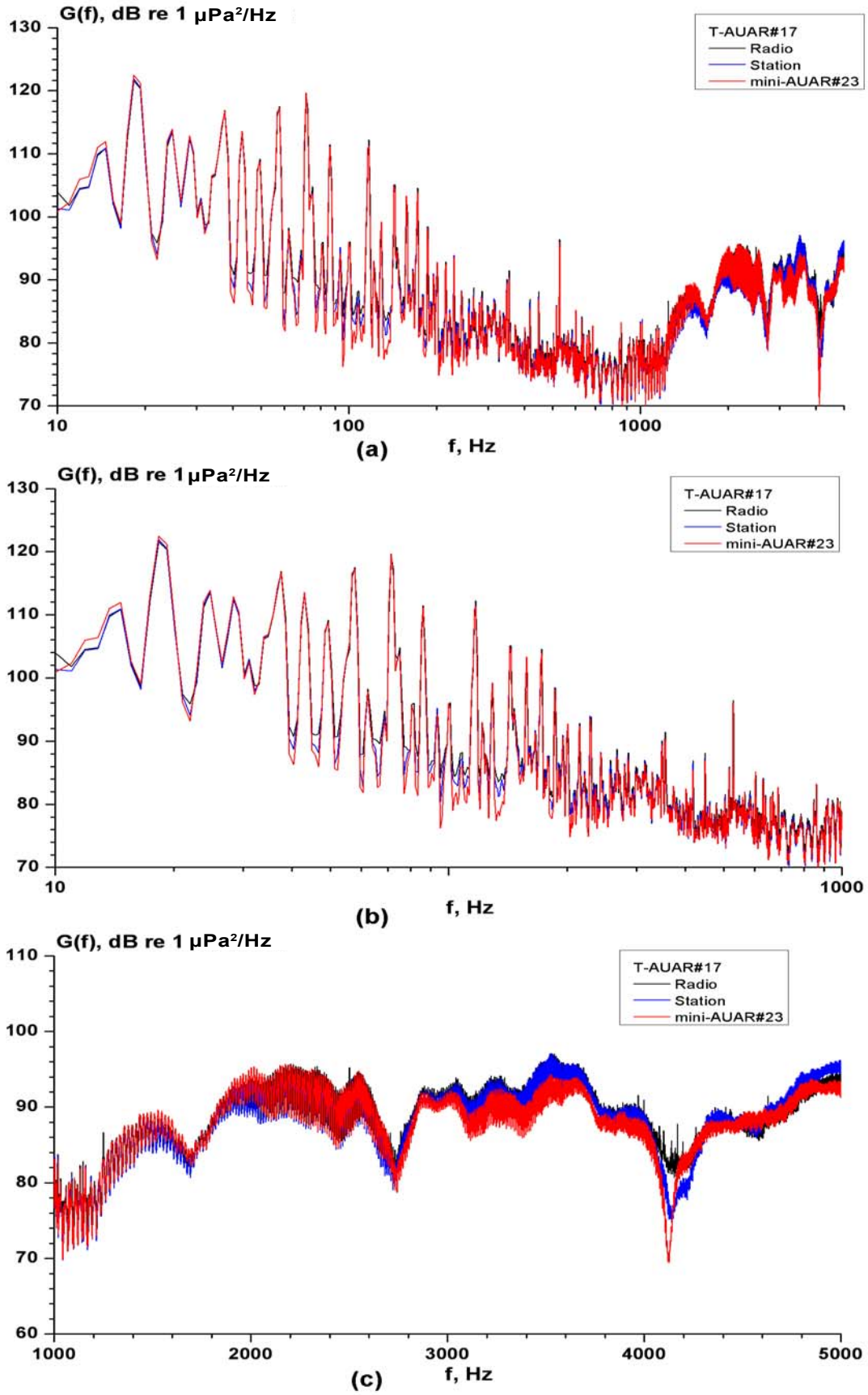

Figure D.13 - Cross calibration analysis - Spectra of acoustic signals synchronously measured by T-AUAR No. 17 and the reference mini-AUAR No. 23 (after instrument response [amplitude-frequency] correction). (a) 10 Hz-15 kHz; (b) 10 Hz-1 kHz; (c) 1-15 kHz.

Table D.9 - Cross-calibration - statistical relative error analysis in the frequency bands 10 Hz-5 kHz, for disk and radio recording for T-AUARs No. 2, 3, 4, 16, 17 and the reference (mini-AUAR No. 23).

	D(10-5000 Hz) [dB]				*ΔD*(ICOM-AUAR)
T-AUAR #	***AUAR***	***IC-R20***	***Reference***	***Mean***	***IC-R20*** **[dB]**
2					
3	133.5	133.8	133.6	133.6	0.3
4	131.7	131.7	131.9	131.8	0.0
16	134.1	134.2	133.7	134.0	0.1
17	131.4	131.4	131.4	131.4	0.0

Table D.9 shows the power spectral density levels for the frequency band from (10 Hz to 5 kHz) for signals received on the five T-AUARs and the radio signal received on ICOM IC-R20 receiver. The table also shows the error between the directly recorded acoustic data and the data transmitted over the radio-telemetry channel, this error does not exceed 0.3 dB.

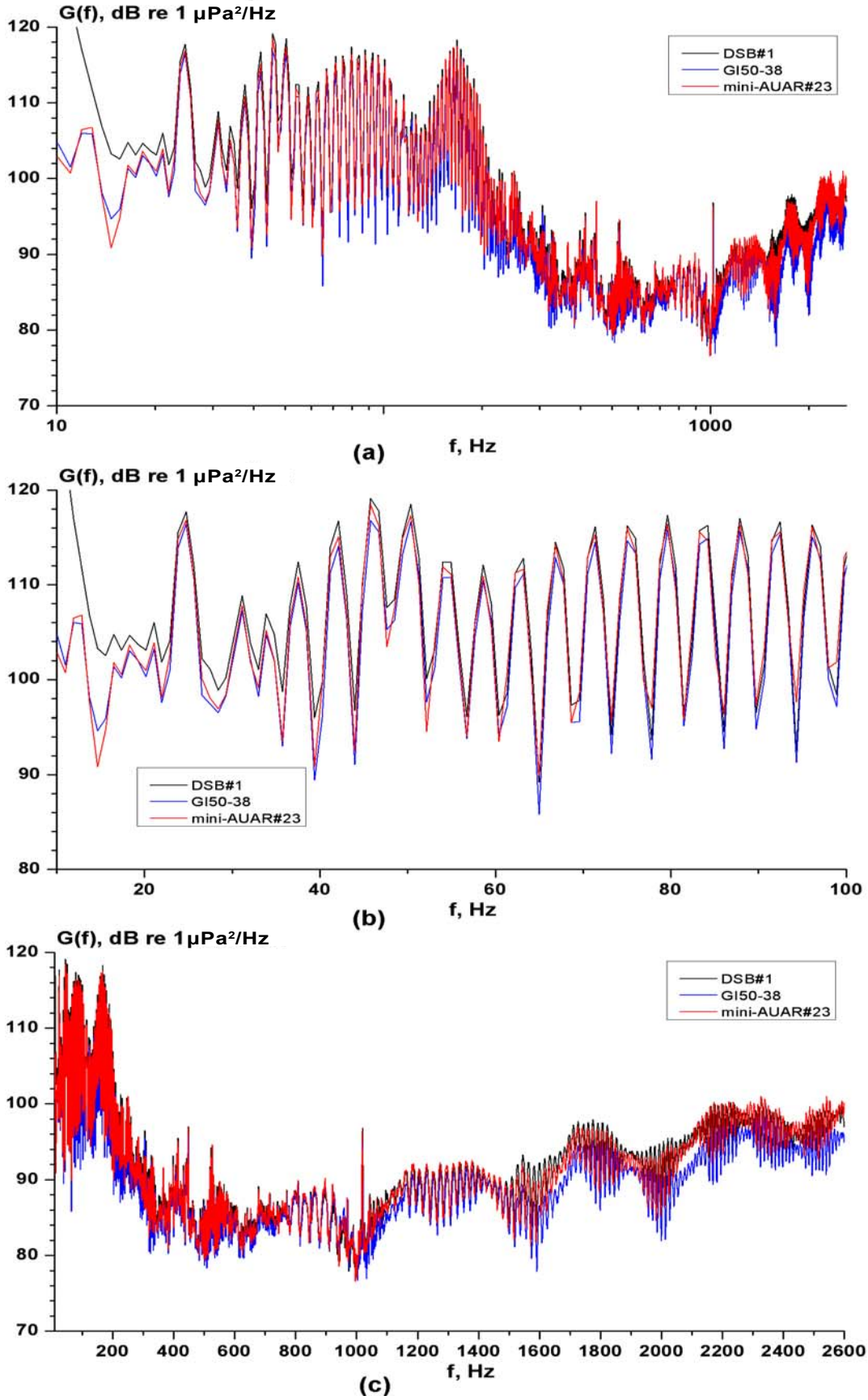

Figure D.14 - Cross calibration analysis - Spectra of acoustic signals measured synchronously by Digital sonobuoy No. DSB-1, the reference mini-AUAR No. 23 and reference hydrophone G150-38 (after instrument response [amplitude-frequency] correction). (a) 10 Hz-26 kHz; (b) 10-100 Hz; (c) 10 Hz -2.6 kHz.

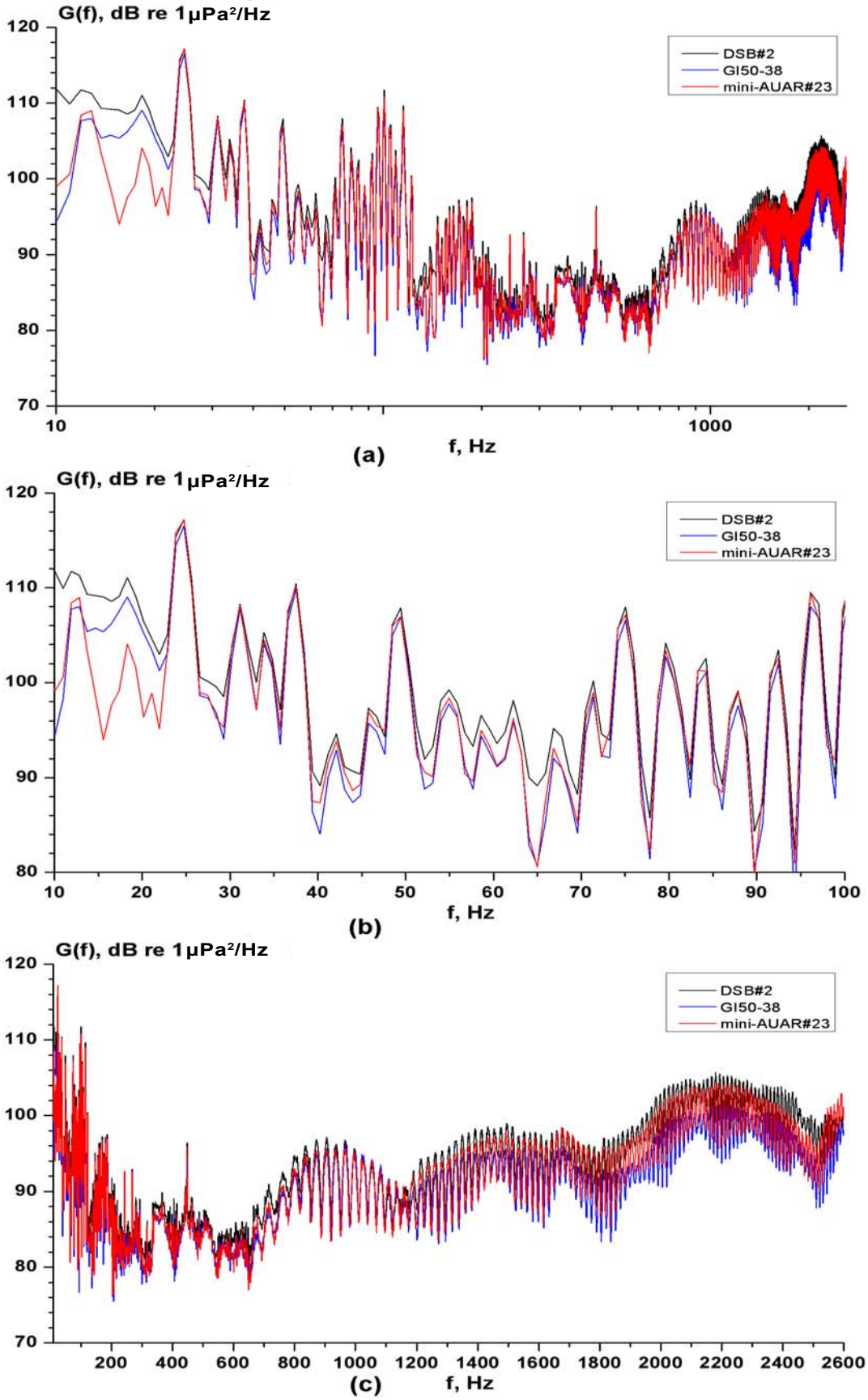

Figure D.15 - Cross calibration analysis - Spectra of acoustic signals measured synchronously by Digital sonobuoy No. DSB-2, the reference mini-AUAR No. 23 and reference hydrophone G150-38 (after instrument response [amplitude-frequency] correction). (a) 10 Hz-26 kHz; (b) 10-100 Hz; (c) 10 Hz -2.6 kHz.

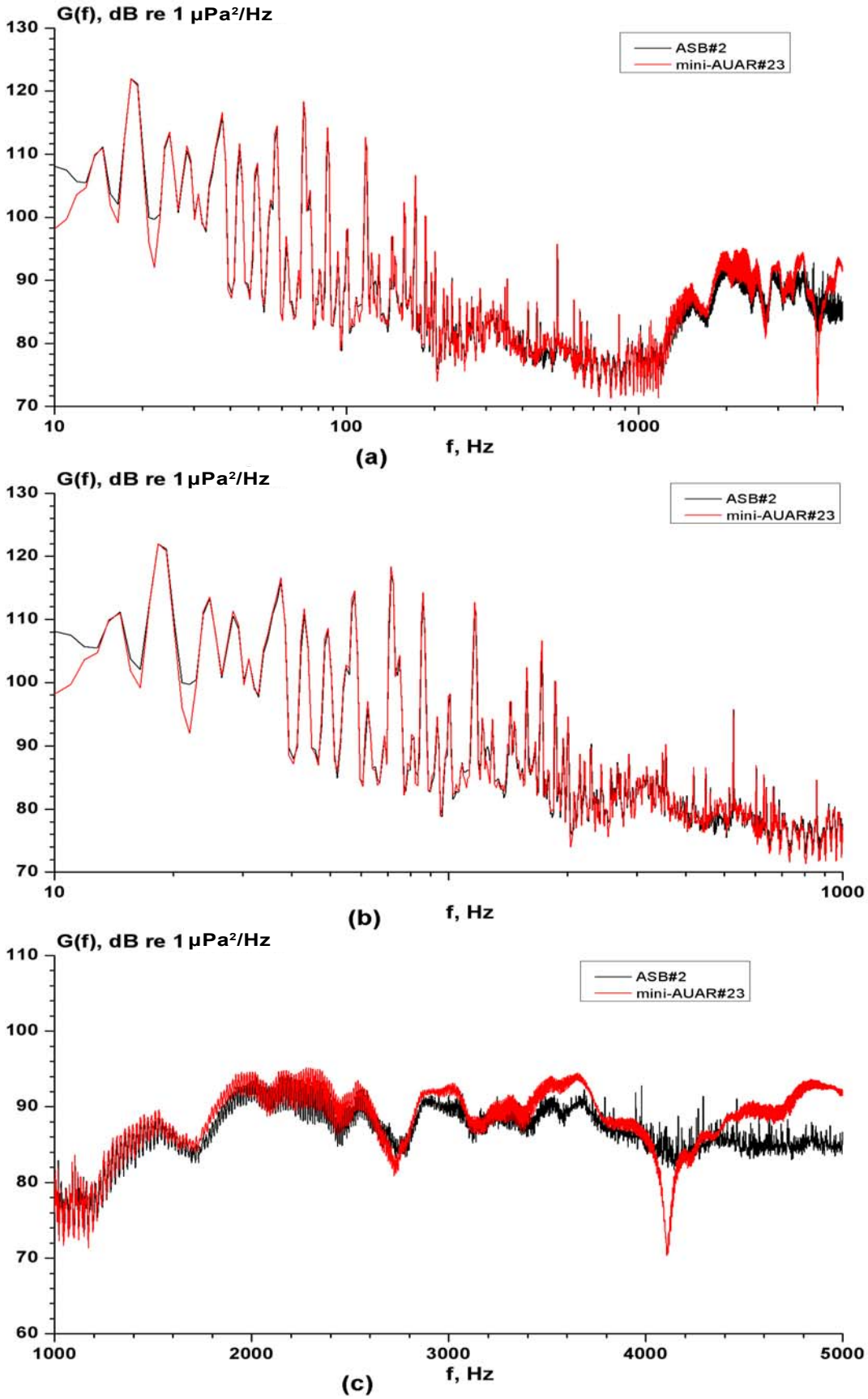

Figure D.16 - Cross calibration analysis - Spectra of acoustic signals measured synchronously by Analog sonobuoy No. ASB-2, the reference mini-AUAR No. 23 (after instrument response [amplitude-frequency] correction). (a) 10 Hz-5 kHz; (b) 10 Hz-1 kHz; (c) 1-5 kHz.

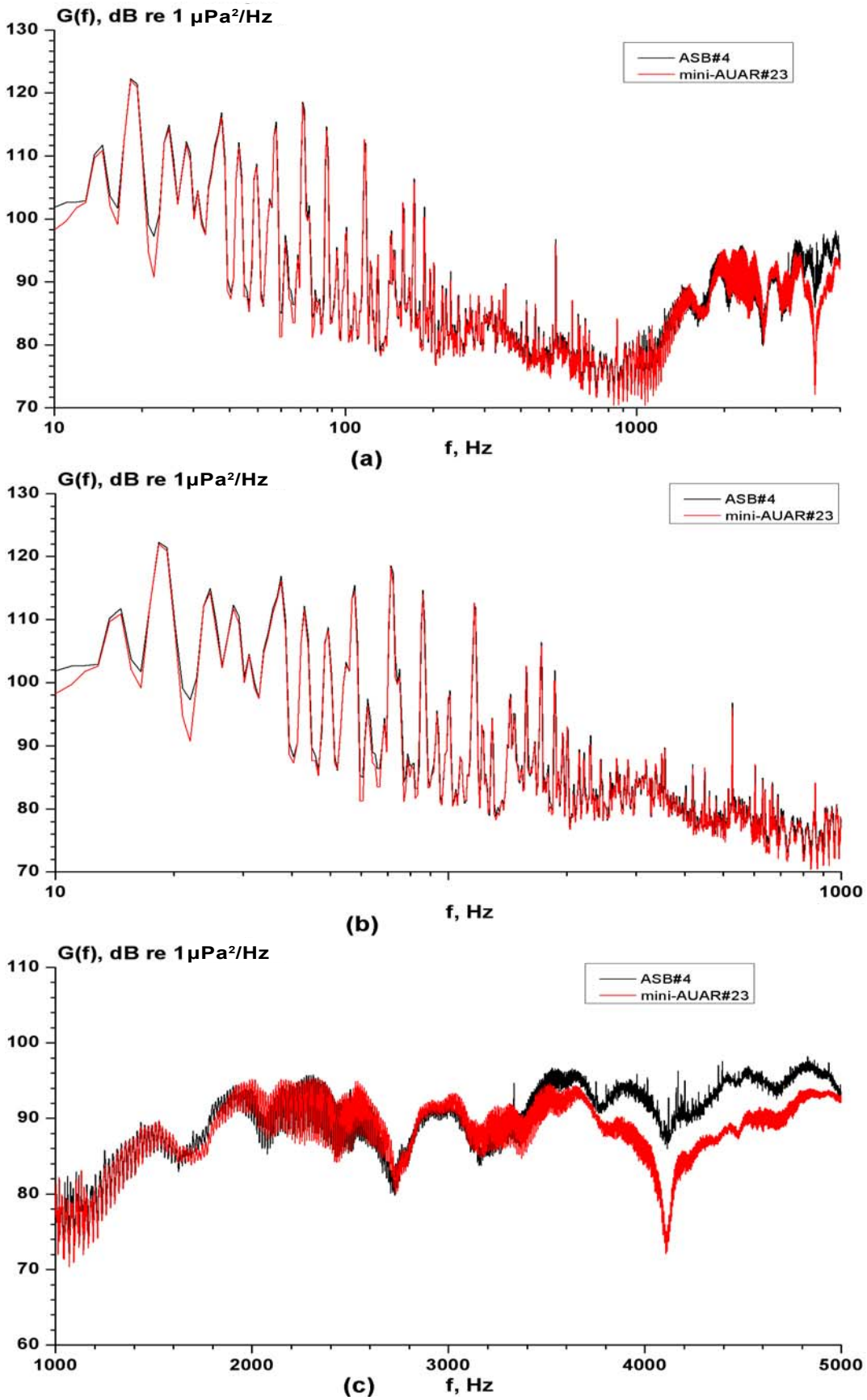

Figure D.17 - Cross calibration analysis - Spectra of acoustic signals measured synchronously by Analog sonobuoy No. ASB-4, the reference mini-AUAR No. 23 (after instrument response [amplitude-frequency] correction). (a) 10 Hz-5 kHz; (b) 10 Hz-1 kHz; (c) 1-5 kHz.

Table D.10 - Cross-calibration - statistical relative error analysis in the 10-2300 Hz frequency band for DSB No. 1, and reference (mini-AUAR No. 23).

Unit	$D(10-2300Hz)$ **[dB]**	$\sigma(10-2300Hz)$ **[dB]**
Reference	133.7	0.2
G150-38	132.7	1.2
DSB-1	135.4	1.5
Mean	***133.9***	

Table D.11 - Cross-calibration - statistical relative error analysis in the 10-2300 Hz frequency band for DSB No. 2, and reference (mini-AUAR No. 23).

Unit	$D(10-2300Hz)$ **[dB]**	$\sigma(10-2300Hz)$ **[dB]**
Reference	130.2	0.0
G150-38	128.7	1.5
DSB-2	131.6	1.4
Mean	***130.2***	

Table D.12 - Cross-calibration - statistical relative error analysis in the 10 Hz-5 kHz frequency band for analog sonobuoys No. 2, and 4 and reference (mini-AUAR No. 23).

	D(10-5000 Hz) **[dB]**				
	Reference		**ASB**		
ASB	***D*** **[dB]**	***ΔD*** **[dB]**	***D*** **[dB]**	***ΔD*** **[dB]**	**Mean**
2	127.0	1.2	125.6	0.2	125.8
4	126.7	1.2	125.4	0.1	125.5

Tables D.10 and D.11 shows the power spectral density levels for the frequency band from (10 Hz to 2.6 kHz) for signals received from the two digital sonobuoys, these results show that the error does not exceed 1.5 dB. Table D.12 shows the power spectral density levels for the frequency band from (10 Hz to 5 kHz) for signals received from two analog sonobuoys, these results show that the error does not exceed 1.2 dB[60]. These values are within the expected relative error limits for the equipment and the absolute calibration of the data was therefore confirmed[61].

[60] These cross-calibration measurements have the same synchronization & field measurement inaccuracies as the AUARs.
[61] The digital sonobuoys have been calibrated from 1 Hz to 2.6 kHz and the analog sonobuoys from 10 Hz to 5 kHz.